



Advanced estimation algorithms for connected and autonomous vehicle applications

Hichem Bessafa

► To cite this version:

Hichem Bessafa. Advanced estimation algorithms for connected and autonomous vehicle applications. Automatic. Université de Lorraine, 2024. English. NNT : 2024LORR0075 . tel-04744305

HAL Id: tel-04744305

<https://hal.univ-lorraine.fr/tel-04744305v1>

Submitted on 18 Oct 2024

HAL is a multi-disciplinary open access archive for the deposit and dissemination of scientific research documents, whether they are published or not. The documents may come from teaching and research institutions in France or abroad, or from public or private research centers.

L'archive ouverte pluridisciplinaire **HAL**, est destinée au dépôt et à la diffusion de documents scientifiques de niveau recherche, publiés ou non, émanant des établissements d'enseignement et de recherche français ou étrangers, des laboratoires publics ou privés.



UNIVERSITÉ
DE LORRAINE

BIBLIOTHÈQUES
UNIVERSITAIRES

AVERTISSEMENT

Ce document est le fruit d'un long travail approuvé par le jury de soutenance et mis à disposition de l'ensemble de la communauté universitaire élargie.

Il est soumis à la propriété intellectuelle de l'auteur. Ceci implique une obligation de citation et de référencement lors de l'utilisation de ce document.

D'autre part, toute contrefaçon, plagiat, reproduction illicite encourt une poursuite pénale.

Contact bibliothèque : ddoc-theses-contact@univ-lorraine.fr
(Cette adresse ne permet pas de contacter les auteurs)

LIENS

Code de la Propriété Intellectuelle. articles L 122. 4

Code de la Propriété Intellectuelle. articles L 335.2- L 335.10

http://www.cfcopies.com/V2/leg/leg_droi.php

<http://www.culture.gouv.fr/culture/infos-pratiques/droits/protection.htm>



Université de Lorraine

École doctorale : IAEM - Informatique, Automatique, Electronique-Electrotechnique, Mathématiques et Sciences de l'Architecture

Laboratoire : CRAN - Centre de Recherche en Automatique de Nancy

Thèse pour obtenir le grade de

Docteur de l'Université de Lorraine

Spécialité : Automatique, Traitement du Signal et des Images, Génie Informatique

présentée et soutenue publiquement par

Hichem BESSAFA

le 19 Septembre 2024

ADVANCED ESTIMATION ALGORITHMS FOR CONNECTED AND AUTONOMOUS VEHICLE APPLICATIONS

Sous la direction de Ali ZEMOUCHE et Cédric DELATTRE

Jury :

Directeurs de thèse

M. Ali ZEMOUCHE, Maître de conference (HDR) – CRAN – Université de Lorraine

M. Cédric DELATTRE , Maître de conference – CRAN – Université de Lorraine

Présidente du jury

Mme Catherine BONNET, Directrice de recherche – Inria – Saclay

Rapporteurs

M. Angelo ALESSANDRI, Professeur – DIME– University of Genoa

M. Thierry-Marie GUERRA, Professeur – LAMIH – Université Polytechnique Hauts-de-France

Examinateurs

M. Michel ZASADZINSKI, Professeur – CRAN – Université de Lorraine

M. Redouane KHEMMAR, Enseignant-chercheur – IRSEEM – ESIGELEC Rouen

Mme Zehor BELKHATIR, Enseignante-chercheuse – Department of Electronics and Computer Science – University of Southampton



Remerciements

Avant toute chose, je tiens à exprimer ma profonde gratitude à Dieu pour m'avoir accordé la santé, la patience et la force nécessaires pour mener à bien ce projet. Sans Ses bienfaits, je n'aurais pas pu surmonter les épreuves et les défis rencontrés tout au long de cette thèse.

Ce manuscrit marque l'aboutissement d'un long voyage de trois ans, durant lequel j'ai énormément appris, tant sur le plan personnel que professionnel. C'est un chapitre important de ma vie qui s'achève, et je souhaite remercier chaleureusement toutes les personnes qui ont contribué, de près ou de loin, à cette aventure.

En premier lieu, je souhaite exprimer mes remerciements à M. Angelo Alessandri et M. Thierry-Marie Guerra, pour avoir accepté d'être les rapporteurs de ma thèse. Je suis très reconnaissant pour le temps qu'ils ont consacré à l'évaluation de ce travail ainsi que pour leurs retours précieux, qui ont permis d'améliorer ce manuscrit.

Je voudrais tout d'abord exprimer mes sincères remerciements à l'Université de Lorraine, au laboratoire CRAN, et au projet ANR ArtIsMo pour le financement et les ressources qui ont permis la réalisation de cette thèse. Leur soutien constant a été indispensable pour la réussite de ce projet.

Je tiens également à remercier mes encadrants, Ali Zemouche et Cédric Delattre, pour leur accompagnement exceptionnel. Leurs conseils avisés, leur disponibilité et leur soutien, tant professionnel qu'humain, ont été essentiels tout au long de ce parcours. Leur confiance et leur bienveillance m'ont permis de m'épanouir dans mes recherches.

Mes remerciements vont également à l'ensemble de mes collaborateurs des différentes universités internationales impliquées dans le projet ANR ArtIsMo. Leurs contributions et leurs échanges ont été une source d'inspiration et ont enrichi mes travaux de recherche.

Je tiens aussi à exprimer ma gratitude à mes collègues du laboratoire et aux doctorants de l'IUT de Longwy, avec qui j'ai partagé des moments inoubliables. Un merci spécial à Hasni, Echrak, Huy, Shegnya, ainsi qu'aux docteurs Shiveraj et Dyhia pour leur soutien

et pour tous les moments de convivialité et de collaboration que nous avons vécus ensemble.

Ces trois années de thèse ne se résument pas uniquement à des recherches scientifiques ; elles représentent aussi trois années de vie, marquées par des joies, des défis, et des émotions partagées avec les personnes qui m'ont entouré. Ce travail n'aurait pas été possible sans leur présence et leur soutien.

Je suis profondément reconnaissant envers mes parents Dr. Mohammed Bessafa et Dr. Djamila Saboundji, qui ont été ma plus grande source de force et d'inspiration. Leur amour inconditionnel et leur soutien indéfectible ont été un véritable moteur tout au long de ma vie. Les mots ne suffisent pas à exprimer l'ampleur de ma gratitude pour tout ce qu'ils m'ont offert.

Je souhaite également exprimer toute ma reconnaissance à ma sœur Imene et à mon frère Abd Errahmane, qui ont toujours été présents pour m'encourager et me soutenir. Leur affection et leurs encouragements m'ont été d'un grand réconfort.

Un immense merci à mes amis, Sohaib, Sofiane, Houssem, Tima et Ouiam, pour leur amitié fidèle et leur soutien constant. Vous avez été à mes côtés dans les moments les plus difficiles, et je vous en suis infiniment reconnaissant.

Enfin, je voudrais exprimer toute ma gratitude à Yousra, dont le soutien, l'amour et la patience ont été d'une importance capitale durant ces années. Ta présence à mes côtés, dans les moments de doute comme dans les moments de réussite, m'a apporté une force inestimable. Merci d'avoir cru en moi, d'avoir partagé chaque étape de ce parcours, et d'être un véritable pilier dans ma vie. Je ne saurais exprimer à quel point ta présence a compté dans la réussite de cette thèse.

Table of Content

Introduction	16
1 State of the art	19
1.1 Introduction	20
1.2 Driver assistance systems	21
1.2.1 Adaptive Cruise Control (ACC)	21
1.2.2 Lateral and steering control	23
1.3 Vehicle modelisation	26
1.3.1 Kinematic model for the vehicle lateral motion	26
1.3.2 Vehicle lateral dynamic model	29
1.3.3 Tire Dynamic Models	32
1.3.4 Vehicle longitudinal dynamic model	34
1.4 Estimation Schemes for Vehicle State Estimation	39
1.4.1 Classical Model-Based Methods for Vehicle State Estimation	40
1.4.2 Data-Driven Based Observers	48
1.4.3 Deep Learning-based Luenberger Observers	49
1.4.4 Machine Learning for Moving Horizon Estimation	51
1.4.5 Neuro-Adaptive Observer	53
1.5 Conclusion	56
2 New Discrete Time Interval Observer	58
2.1 Introduction	59
2.2 Interval observers for discrete-time LPV systems	60
2.2.1 LPV systems	60
2.2.2 Interval relations	61
2.2.3 Interval Observer for Discrete-LPV systems	61
2.3 Exact finite-time estimation of LPV systems	64
2.3.1 System description	64
2.3.2 Finite time estimation by using two combined observers	65

2.3.3	Design of the estimator parameters	66
2.4	Finite-time interval estimator design	68
2.4.1	Problem formulation	68
2.4.2	Application of developed estimation algorithm to vehicle lateral model	72
2.4.3	Comparative study	76
2.5	Conclusion	79
3	Neuro-Adaptive Learning-based Observer for Nonlinear States and Unknown Inputs Estimation	81
3.1	Introduction	83
3.2	Neuro-Adaptive Observers	85
3.2.1	Problem Formulation	85
3.2.2	Robust Data-Driven Neuro-Adaptive Observer	85
3.3	Concurrent Learning-Based Adaptive Observation	86
3.3.1	Problem statement	86
3.3.2	Observer Design	87
3.4	Proposed Neuro-Adaptive LMI Based Observer	88
3.5	Application to vehicle longitudinal model	94
3.5.1	Vehicle Longitudinal model	94
3.5.2	Observer design	95
3.5.3	Simulation results	97
3.5.4	Comparison	98
3.6	Conclusion	100
4	Generalize High-Gain Observer with Multi Output	104
4.1	Introduction	106
4.2	Overview of High-Gain Observer	107
4.2.1	Observability canonical forms	108
4.2.2	High-Gain observer design	111
4.2.3	Limitations of High-Gain observers	113
4.3	New Multi-Output High-Gain observer Design	115
4.3.1	Preliminary tool	115
4.3.2	Callback on the standard High-Gain observer	115
4.3.3	Problem formulation and objectives	118
4.3.4	New Observer Design Methodologies	118
4.3.5	Generalized High-Gain with ISS bounds	123

4.4	Output-based dynamic extension High-Gain observer	128
4.4.1	System transformation and observer structure	128
4.4.2	Generalized High-Gain observer-based design	130
4.4.3	Simplification of the design conditions	133
4.5	Conclusion	135
5	Vehicle Applications and Simulations	136
5.1	Introduction	137
5.2	Vehicle Longitudinal Tracking	138
5.2.1	Vehicle dynamic longitudinal model	139
5.2.2	MATLAB simulation results	140
5.2.3	CARLA-based simulation scenarios and estimation results	144
5.2.4	Comparison with the Standard High-Gain Observer	147
5.3	Vehicle Motion Estimation	152
5.3.1	Vehicle kinematic model	152
5.3.2	Triangular Transformation	152
5.3.3	Observer Design for the Vehicle Model	154
5.3.4	Simulation Results	155
5.3.5	Experimental Results	158
5.4	Conclusion	166
Conclusion and perspectives		168
A	Appendix	170
A.1	LMIs	171
A.1.1	Definition of Linear Matrix Inequalities (LMIs)	171
A.1.2	Convexity of LMIs	171
A.1.3	Congruence Transformation	172
A.1.4	Schur Complement	173
A.1.5	Young Inequality	174
A.1.6	Feasibility of LMIs	175
A.1.7	Optimization with LMIs	175
A.1.8	Solving LMIs	175
A.2	Lipschitz Constant Computation for Nonlinear Functions	176
A.2.1	Definition of Lipschitz Continuity	176
A.2.2	Computing the Lipschitz Constant for Differentiable Functions	176
A.2.3	Numerical Computation of Lipschitz Constants	176

A.2.4 Lipschitz Constant for Composite Nonlinear Functions	177
A.3 Basic Artificial Neural Networks (ANNs)	178
A.3.1 Overview	178
A.3.2 Structure of an ANN	178
A.3.3 Activation Functions	179
A.3.4 Training an ANN	180
A.3.5 Examples	182
B Bibliography	183
References	184
List of publications	195

List of Figures

1.1	Platoon of adaptive cruise control vehicles [7]	22
1.2	Lane Keeping System based on a forward-facing camera	24
1.3	Yaw control system [7]	25
1.4	Kinematics of lateral vehicle motion [7]	27
1.5	Lateral vehicle dynamics	29
1.6	Vehicle longitudinal dynamics	34
1.7	Longitudinal tire force as a function of slip ratio [7]	36
1.8	Longitudinal force in a driving wheel [47]	37
1.9	The Observation general diagram (light blue is the software blocks and dark blue is a hardware block)	40
1.10	Sensor fusion using a Extended Kalman Filter (EKF)	45
1.11	The schematic of artificial neural network (ANN) estimation process.	48
2.1	Bicycle model	73
2.2	Interval estimation with cornering stiffness affected by 5% of its nominal value.	77
2.3	Interval estimation with cornering stiffness affected by 10% of its nominal value.	78
2.4	Interval estimation of the proposed method and \mathcal{H}_∞ based estimator proposed in [103].	79
3.1	Neural network architecture	96
3.2	Vehicle's control input $u(t)$	98
3.3	Estimated vehicle's longitudinal position $x_1(t)$	98
3.4	Estimated vehicle's longitudinal velocity $x_2(t)$	99
3.5	Estimated vehicle's longitudinal acceleration $x_3(t)$	99
3.6	Estimated unknown augmented state $x_4(t) \equiv f(x(t))$	100
3.7	Estimated neural network weights $\hat{W}(t)$	100
3.8	Estimated vehicle's states	101

3.9 Estimated unknown augmented state $x_4(t) \equiv f(x(t))$ and neural network weights $\hat{W}(t)$.	101
3.10 Vehicle's estimated states using observer proposed in [86].	102
3.11 Estimated unknown augmented state using observer proposed in [86].	102
5.1 Vehicle longitudinal model (in red: ego vehicle, in blue : test vehicle)	139
5.2 State estimates using proposed observer methodology in 4.3.4 accounting for speed measurement and the standard high-gain observer using only position measure.	142
5.3 Absolute error of the estimation error and comparaison using observer in 4.3.4 .	143
5.4 Vehicle longitudinal motion tracking scenario (in red: ego vehicle, in blue : test vehicle)	144
5.5 CARLA simulation scenario.	145
5.6 Comparison of radar sensor measurements with ground truth values.	146
5.7 State estimation of the test vehicle using the observer described in 4.3.5, with radar sensor data.	147
5.8 Comparison of state estimates using the proposed observer in 4.3.5 with speed measurement and the standard high-gain observer using only position measurement.	148
5.9 Estimation results with loss of position measurement at $t = 10$ seconds.	150
5.10 Estimation results with loss of position measurement between $t = 2$ and $t = 5$ seconds.	151
5.11 Vehicle state estimation in the straight driving scenario.	156
5.12 Yaw estimation error in the straight driving scenario.	156
5.13 Trajectory estimation in the straight driving scenario.	157
5.14 Vehicle state estimation in the left turn scenario.	157
5.15 Yaw estimation error in the left turn scenario.	158
5.16 Trajectory estimation in the left turn scenario.	158
5.17 Camera capture from the KITTI dataset [135].	159
5.18 State estimation using real data.	160
5.19 Yaw estimation error.	160
5.20 Trajectory estimation.	161
5.21 Velocity estimation on both axes (V_x and V_y).	161
5.22 Simulation of data gaps in GPS signal.	162
5.23 Trajectory estimation.	163

5.24 State estimation (Position).	163
5.25 Yaw angle estimation.	164
5.26 Trajectory estimation.	165
5.27 State estimation (Position).	165
5.28 Yaw angle estimation.	166

Notation and Acronyms

Notation

\mathbb{R}	Set of real numbers
\mathbb{R}^+	Set of real positive numbers
\mathbb{R}^n	Euclidean real space of dimension n
$\mathbb{R}^{n \times m}$	Set of real matrices of dimension $n \times m$
$\ x\ $	Euclidean norm of x , with $x \in \mathbb{R}^n$
$\ A\ $	Induced matrix norm defined as $\sup_{x \in \mathbb{R}^n, x \neq 0} \frac{\ Ax\ }{\ x\ }$
$\ A\ _X^2$	Weighted norm $\ A\ _X^2 = A^T X A$
$A, A > 0$ ($A < 0$)	for square matrix A that this matrix is positive definite (negative definite)
$A \geq 0$	Symmetric positive semi-definite matrix
$\det(A)$	Determinant of the matrix $A \in \mathbb{R}^{n \times n}$
$\lambda_{\min}(A)$	Smallest eigenvalue of the matrix A
$\lambda_{\max}(A)$	Largest eigenvalue of the matrix A
A^T	Transpose of the matrix A
A^{-1}	Inverse of the matrix A
\mathbb{I}_n	An $n \times n$ identity matrix
$0_{n \times m}$	Matrix of dimension $n \times m$ whose entries are all zeros
$\mathcal{H}e\{\mathbb{V}\}$	$\mathbb{V} + \mathbb{V}^\top$
$\text{diag}(a_1, \dots, a_n)$	An $n \times n$ diagonal matrix with a_i as its i -th diagonal element
$\text{col}(a_1, \dots, a_n)$	Column vector with elements (a_1, \dots, a_n)
$e_s(i) = \left(\underbrace{0, \dots, 0}_{s \text{ components}}, \overbrace{1}^{i \text{ th}}, 0, \dots, 0 \right)^T \in \mathbb{R}^s, s \geq 1$	A vector of the canonical basis of \mathbb{R}^s
X^{Y_i}	corresponding to $X^{Y_i} = (y_1, \dots, y_i, x_{i+1}, \dots, x_n)$ such that $X = (x_1, \dots, x_n)^\top$ and $Y = (y_1, \dots, y_n)^\top$ for $i = 1, \dots, n$ with the convention $X^{Y_0} = X$
$\text{SVD}(A)$	denotes singular value decomposition method to decompose the matrix A into three matrices U, Σ , and V^T , such that $A = U \Sigma V^T$

Acronyms

ADAS	Advanced Driver Assistance Systems
DOF	Degrees of Freedom
GPS	Global Positioning System
HGO / SHGO	High-Gain Observer / Standard High-Gain Observer
ISS	Input-to-State-Stability
KF/EKF/UKF	Kalman Filte/ Extended Kalman Filter / Unscented Kalman Filter
LMI	Linear Matrix Inequalities
LKS	Lane Keeping System
LPV	Linear Parameter-Varying
LTI	Linear Time-Invariant

Introduction

Over the past decade, the field of vehicle development has experienced remarkable advancements, driven by industrial enterprises and research and development organizations. These advancements encompass various aspects, including mechanical, electronic, and conceptual design elements that underpin modern vehicles. A vehicle's structure is generally divided into three key components—the vehicle body, suspensions, and tires—each playing a crucial role in vehicle dynamics.

Despite these technological advances, several challenges remain in accurately estimating and tracking vehicle dynamics, which are critical for the effective functioning of modern vehicular systems. This thesis aims to address these challenges by developing innovative observer designs and state estimation algorithms that enhance the robustness and accuracy of vehicle state estimation, particularly in the presence of uncertainties and nonlinearity. The research specifically tackles problematic areas such as the limitations of traditional estimation methods in handling nonlinearities and uncertainties, the incomplete availability of real-time vehicle state information in standard production cars, and the difficulties associated with applying high-gain observers to high-dimensional systems. By addressing these issues, the thesis seeks to contribute to the development of more reliable and effective vehicular control systems.

One of the critical areas of modern vehicle technology is the integration of Advanced Driver Assistance Systems (ADAS), such as ABS, ESP, and TCS, designed to prevent accidents by maintaining vehicle control [1]–[3]. These systems rely heavily on accurate dynamic information, including vehicle speed, steering angles, and acceleration, typically measured by sensors and accessed via the CAN bus. However, as ADAS continue to evolve, certain essential parameters for a comprehensive understanding of vehicle motion are not available in standard production vehicles due to technical and cost constraints [4]–[6]. This gap underscores the need for an in-depth understanding of tire behavior and real-time vehicle states to enhance the performance of active safety systems [7], [8].

State estimation has long been a fundamental aspect of control theory, with applications in diverse fields like robotics and process control. Traditional techniques, such as the Kalman filter, are widely used but often fall short when dealing with systems characterized by significant uncertainties and disturbances [9]. Recognizing this limitation, recent research has explored interval observers, which offer a range within which the system

state is guaranteed to reside [10]. This thesis builds on this concept by introducing a novel Discrete-Time Interval Estimator, directly operating in the discrete-time domain. This approach, inspired by the parity space method and zonotope-based interval analysis, aims to improve the accuracy and robustness of state estimation in vehicle dynamics.

In parallel, the field of control engineering has increasingly embraced data-driven approaches, particularly the use of neural networks for system identification [11], [12]. While neural networks have been extensively applied in system identification, their potential for state estimation in systems with unknown dynamics remains underexplored. To bridge this gap, in this thesis we propose a novel observer design based on machine learning principles, utilizing neural approximators and the Concurrent Learning (CL) technique [13]. This approach enhances the reliability and robustness of state estimation in nonlinear systems, offering a promising alternative to traditional methods.

Furthermore, High-Gain Observers (HGO) have been crucial in achieving high-accuracy state estimation [9]. However, designing HGOs for systems that are not in triangular form or have constraints, such as additional measured outputs, poses theoretical challenges. To overcome these challenges, this thesis introduces convergent observer designs that utilize extra output measurements without directly integrating them into the output equations. This approach broadens the applicability of HGOs to a wider range of system forms, enhances the robustness and accuracy of the estimation process, and facilitates sensor fusion [14].

Finally, accurate tracking of vehicle dynamics is essential for various vehicular technologies, from driver assistance systems to autonomous driving [15], [16]. However, the inherent complexity and nonlinearity of vehicle systems, influenced by external factors such as sensor noise, actuator faults, and environmental disturbances, pose significant challenges. Traditional tracking methods often rely on linear models, which do not adequately capture the nonlinear nature of vehicle motion [17]. This research introduces a high-gain design algorithm for vehicle motion tracking, validated through extensive simulations and real-world data, demonstrating its robustness and effectiveness compared to traditional methods like the Extended Kalman Filter (EKF) [18].

In conclusion, this thesis integrates and extends current research in state estimation, observer design, and vehicle motion tracking, addressing key challenges in the field of vehicle dynamics. By proposing novel methods that leverage both interval analysis and machine learning, the research contributes to the development of more reliable and effective vehicular control systems, ultimately enhancing the safety and performance of modern vehicles. This thesis is organized as follows:

- **Chapter 1** explores Advanced Driver Assistance Systems (ADAS) and the vehicle model used for observer design, discussing how these models help predict vehicle behavior and the role of machine learning in this field.

- **Chapter 2** delves into state estimation techniques, focusing on the development of a novel Discrete-Time Interval Estimator for discrete-time systems and its application in digital control systems.
- **Chapter 3** examines the use of neural networks in control engineering, presenting a novel observer design capable of estimating states and unknown input dynamics using machine learning techniques and Concurrent Learning.
- **Chapter 4** discusses the evolution and application of High-Gain Observers (HGOs), addressing numerical challenges and proposing new convergent observer designs for robust state estimation.
- **Chapter 5** focuses on vehicle dynamics tracking, presenting a high-gain design algorithm for vehicle motion tracking and estimation, validated through both simulations and real-world data.

1

State of the art

Contents

1.1	Introduction	20
1.2	Driver assistance systems	21
1.2.1	Adaptive Cruise Control (ACC)	21
1.2.2	Lateral and steering control	23
1.3	Vehicle modelisation	26
1.3.1	Kinematic model for the vehicle lateral motion	26
1.3.2	Vehicle lateral dynamic model	29
1.3.3	Tire Dynamic Models	32
1.3.4	Vehicle longitudinal dynamic model	34
1.4	Estimation Schemes for Vehicle State Estimation	39
1.4.1	Classical Model-Based Methods for Vehicle State Estimation	40
1.4.2	Data-Driven Based Observers	48
1.4.3	Deep Learning-based Luenberger Observers	49
1.4.4	Machine Learning for Moving Horizon Estimation	51
1.4.5	Neuro-Adaptive Observer	53
1.5	Conclusion	56

1.1 Introduction

In the field of vehicle development, significant progress has been made over the past decade, driven by industrial enterprises and a host of research and development organizations. This progress spans a wide range of elements, including mechanical, electronic, and conceptual design components that form the backbone of a vehicle. The structure of a vehicle is primarily divided into three key components: the vehicle body, suspensions, and the tire. These elements are central to the concept of vehicle dynamics. In recent years, modern automobiles have been equipped with advanced electronic and control systems such as ABS, ESP, and TCS [1]–[3]. These systems are designed to prevent road accidents by averting loss of vehicle control. The introduction of these Advanced Driver Assistance Systems (ADAS) has significantly improved road safety. These safety systems, along with other vehicle stability control systems, require precise dynamics information about the vehicle's motion. This includes parameters like vehicle velocity, steering wheel angle, and acceleration, which can be measured by cost-effective sensors and accessed on the CAN bus. However, with the evolution of ADAS, it has become apparent that certain parameters necessary for a detailed description of the vehicle's motion, which are inputs for these ADAS, are not available in current standard production cars. This is due to technical limitations and cost considerations. It's important to note that the dynamics of ground vehicles are often described in terms of performance, handling, and ride. The term "handling" is often used interchangeably with turning or directional response [10]. The performance of a vehicle is the response to imposed longitudinal forces under acceleration or braking and lateral forces in cornering. Therefore, it is necessary to develop a comprehensive understanding of tire behavior, characterized by the forces and moments generated by the driver's command. The efficacy and potential performance of active safety dynamic control systems in vehicles hinge heavily on real-time knowledge of vehicle states. For example, having precise information about longitudinal and lateral tire-road forces, as well as the vehicle sideslip angle, allows for improved prediction of real-time road conditions and potential vehicle trajectories. This, in turn, leads to enhanced management of vehicle motion. However, measuring some fundamental vehicle states directly in a standard car presents a challenge due to both technical and economic

constraints. The addition of extra vehicle sensors can be prohibitively expensive, and the signals they measure may be lost in complex driving environments [4]–[6]. As a result, these crucial vehicle states and parameter information, such as vehicle velocity, vehicle sideslip angle, tire-road interactive force, and vehicle mass, must be estimated or observed [7], [8]. This is often achieved through the use of advanced sensor fusion techniques and state estimation algorithms, which combine data from multiple sensors to provide a more accurate and reliable estimate of these states.

In this chapter, we'll explore Advanced Driver Assistance Systems (ADAS) and the vehicle model used for observer design. We'll discuss how these models help predict vehicle behavior, a key aspect of ADAS operation.

We'll also examine advancements in observer design, a critical component of control systems. This includes both traditional methods and new approaches using machine learning. By the end of this chapter, you'll have a comprehensive understanding of ADAS, observer design, and the role of machine learning in this field.

1.2 Driver assistance systems

In today's world, a multitude of driver assistance systems are being developed with the aim of simplifying driving, enhancing fuel efficiency, and most importantly, ensuring safety. These advancements are paving the way towards autonomous driving. We will delve into some of these systems that are currently under development.

1.2.1 Adaptive Cruise Control (ACC)

Adaptive Cruise Control (ACC) is an autonomous system that extends the functionality of standard cruise control [19]. It will maintain the speed set by the driver if there are no obstacles. However, if a vehicle is detected ahead, it will adjust its speed to maintain a safe distance, taking into account the speed and acceleration of the preceding vehicle. This is achieved by controlling both the throttle and brakes. The system operates in two modes: speed control and vehicle following. A notable feature that distinguishes ACC from standard cruise control is its ability to maintain a desired spacing between vehicles. Consider a situation depicted in a Figure 1.1 where an Adaptive Cruise Control (ACC) system is in operation. The system aims to maintain a specific distance from the vehicle ahead. Let's denote the location of the i -th vehicle, measured from an inertial reference, as x_i .

The spacing error for the i -th vehicle (the ACC-equipped vehicle under consideration) is defined as $\delta_i = x_i - x_{i-1} - L_{\text{des}}$. Here, L_{des} is the desired spacing and includes the length of the preceding vehicle l_{i-1} .

The desired spacing L_{des} could be chosen as a function of variables such as the vehicle speed \dot{x}_i . The ACC control law is said to provide individual vehicle stability if a certain condition $\dot{x}_{i-1} \rightarrow 0 \Rightarrow \delta_i \rightarrow 0$ is satisfied.

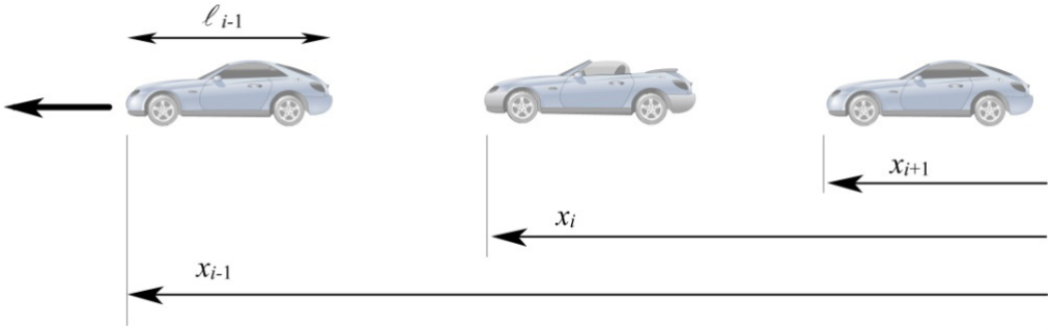


Figure 1.1: Platoon of adaptive cruise control vehicles [7]

The concept of adaptive control presented earlier serves as a basic understanding. However, in practical applications, these systems vary across different manufacturers and depend on how the vehicle obtains the information necessary to operate the system. Consequently, we can identify various types of Adaptive Cruise Control (ACC) systems:

- **Radar-Based Systems :** Radar-based dynamic cruise control and automatic braking systems are designed to detect potential forward collisions. This is a fundamental step towards autonomous vehicles. In such systems, a vehicle adjusts its speed using an intelligent radar-based sensor system and also halts when it detects a likelihood of collision, requiring minimal human intervention. By positioning radar sensors on or around the vehicle's plastic fascias. These sensors scan the vehicle's environment. Working in unison, they generate a detailed image of the vehicle's closeness to other vehicles or potential obstacles. The appearance of these sensors can vary based on the car's design and model [20], [21].
- **Laser-Based Systems :** Laser-based systems, similar to radar-based ones, utilize a type of Lidar sensor to accurately estimate the distance between vehicles. These systems can detect distances more precisely than radar-based systems, with resolution in millimeters compared to radar's meter-level resolution. In addition to distance measurement, laser-based systems can classify detected vehicles and detect weather conditions like fog or rain. However, their performance may be compromised under adverse weather conditions [22]–[24].
- **Stereovision-based ACC systems :** This technology employs small cameras positioned on the back of a vehicle's rearview mirror to identify objects in front of the vehicle. It can accurately detect and classify types of vehicles and uses algorithms, primarily based on machine learning, to estimate the distance to these

vehicles. This method extends beyond adaptive driving and can pave the way to autonomous driving. However, it may occasionally encounter issues with detection or complications due to environmental and weather conditions [23], [25].

- **Multi-sensor :** Adaptive cruise control systems often employ a combination of sensor types to enhance a vehicle's functionality. These multi-sensor systems utilize a variety of sensors to furnish the driver with sophisticated information. The array of sensors may encompass GPS data devices or cameras, which collect data about the vehicle's geographical surroundings and its distance from other vehicles [26].

1.2.2 Lateral and steering control

The objective of lateral control is to ensure the vehicle stays within its lane [7], [27], [28]. Numerous lateral control techniques have been explored for systems such as Lane-Keeping Systems (LKSs) and Lane Change Systems (LXSSs) [29]. Despite these advancements, there are still many challenges to overcome in the realm of autonomous lateral control.

Lane Keeping System (LKS)

A lane-keeping system is designed to automatically manage the steering, ensuring that the vehicle remains within its designated lane and adapts to the lane's curvature [30]. The Lane-Keeping System (LKS) aims to alleviate driver fatigue by enhancing stability on straight highway roads. However, it is crucial for the driver to stay actively involved in steering the vehicle. If the driver disengages, the LKS progressively diminishes its level of assistance. In practical terms, this means that the driver cannot completely disengage and expect the car to drive autonomously.

The primary component of LKS is the forward-facing camera as shown in figure 1.2, typically mounted behind the windshield near the rearview mirror. This camera continuously captures high-resolution images of the road ahead, focusing on lane markings. Advanced image processing software analyzes these images in real-time to identify the lane boundaries. This involves detecting contrasts between the lane lines and the road surface, recognizing road patterns, and interpreting various lane marking styles across different regions and road types.

In addition to cameras, some LKS incorporate radar and lidar sensors. Radar sensors, which use radio waves, can detect the position and speed of objects around the vehicle, providing additional data to ensure accurate lane keeping, especially in conditions where camera visibility is reduced, such as heavy rain or fog. Lidar, which uses laser beams to create precise 3D maps of the environment, enhances the system's

ability to recognize lane markings and other relevant road features, offering a high level of detail and accuracy.

Machine learning and artificial intelligence play pivotal roles in the development and enhancement of LKS. These technologies enable the system to learn from vast amounts of driving data, improving its ability to predict and respond to a variety of driving scenarios. AI algorithms are trained to recognize lane markings, even when they are partially obscured by dirt, shadows, or worn-out paint. They can also adapt to different driving environments, from highways to urban streets, ensuring robust performance across diverse conditions.



Figure 1.2: Lane Keeping System based on a forward-facing camera

Yaw Stability control

Several automotive manufacturers have developed and recently brought to market vehicle stability control systems. These systems prevent vehicles from spinning out and drifting, often referred to as yaw control systems or electronic stability control systems. A schematic representation in Figure 1.3 illustrates the function of a yaw control system. In this figure, the lower curve represents the path that the vehicle would follow in response to a driver's steering input if the road were dry and had a high tire-road friction coefficient (μ). In this scenario, the high friction coefficient provides the lateral force necessary for the vehicle to navigate the curved road.

However, if the friction coefficient were low or the vehicle speed too high, the vehicle would be unable to follow the driver's intended path. Instead, it would travel along a trajectory with a larger radius (or smaller curvature), as depicted by the upper curve in Figure 1.3.

The yaw control system's role is to restore the vehicle's yaw velocity as closely as possible to the driver's expected motion. If the friction coefficient is very small, achieving the nominal yaw rate motion that a driver would achieve on a high friction coefficient

road surface might not be possible. In such a case, the yaw control system would partially succeed by bringing the vehicle's yaw rate closer to the expected nominal yaw rate, as shown by the middle curve in Figure 1.3.

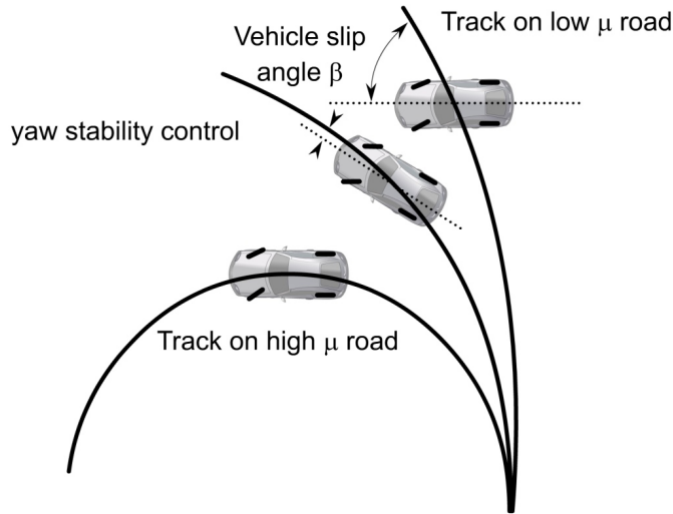


Figure 1.3: Yaw control system [7]

The active yaw stability control system can be implemented through active chassis control in three distinct forms [31], namely:

- **Direct Yaw Moment Control** Also known as differential braking systems that leverage the vehicle's ABS brake system to apply differential braking between the right and left wheels [7], thereby controlling the yaw moment. Differential braking can enhance vehicle stability in critical driving conditions, but it may be less effective during emergency braking on split road surfaces [32], [33]. Additionally, during high-speed steady-state cornering, this control method can reduce the yaw rate and increase the driver's burden. To address these disadvantages, active steering control is proposed as a solution.
- **Active steering control** is an alternative method for enhancing vehicle yaw stability, particularly during steady-state driving conditions where lateral tire forces remain within the linear range. Numerous studies have consistently explored active steering control to boost handling and stability, as documented here. This approach can be implemented in various ways [31], including Active Front Steering (AFS) [34], which is the most prevalent since vehicles typically use the front wheels for steering. Additionally, Active Rear Steering (ARS) [35] is employed, particularly effective in low-speed cornering maneuvers. Each of these systems optimizes vehicle dynamics differently, contributing to overall vehicular control and safety.

- **Active Torque Distribution** Vehicle dynamics control can be significantly enhanced by integrating active chassis control systems such as active steering, active braking, and active suspension or stabilizers [7], [36], [37]. Additionally, systems utilizing active differentials and all-wheel drive technology can independently manage the drive torque distributed to each wheel, providing active control of both traction and yaw moment. This comprehensive approach enhances vehicle yaw stability by effectively controlling yaw rate and sideslip during both emergency maneuvers and steady-state driving conditions.

There are numerous types of controllers used in cars that, when integrated, can make driving more autonomous and easier for the driver. Ongoing research aims to improve these and other controllers to enhance driving safety, as discussed in this section. These controllers are usually designed using vehicle models, which simplify the task for each system by employing simplified models (lateral dynamic, longitudinal, or kinematic) depending on the application. However, these controllers require feedback information that sensors cannot always provide due to technological limitations or cost-effectiveness. Therefore, systems that estimate this information and generate signals using observers and estimators are essential. The next sections will delve into these systems.

1.3 Vehicle modelisation

To examine, analyze, and design controllers and observers for vehicles, vehicle models are essential. There are two main types of models: mathematical models derived from equations and data-based models identified from input and output data sets. This thesis focuses on physics-based modeling, which can be divided into two categories: vehicle kinematic models and vehicle dynamic models. Kinematic models use only geometric and trigonometric equations, while dynamic models are based on Newton's 2nd law, describing the forces and moments acting on the vehicle body and tires.

1.3.1 Kinematic model for the vehicle lateral motion

The vehicle kinematic model can be developed using only geometric relations, meaning we do not account for any interaction forces on the vehicle or the tires. This approach is justified under certain assumptions that will be presented in Remark 1.3.1. In the model depicted in the figure below, we use a bicycle model representation, where the left and right wheels of both the front and rear axles are simplified into a single wheel each, as shown in the figure 1.4.

The steering angles for the front and rear wheels are denoted by δ_f and δ_r , respectively. The model is derived under the assumption that both front and rear wheels can be

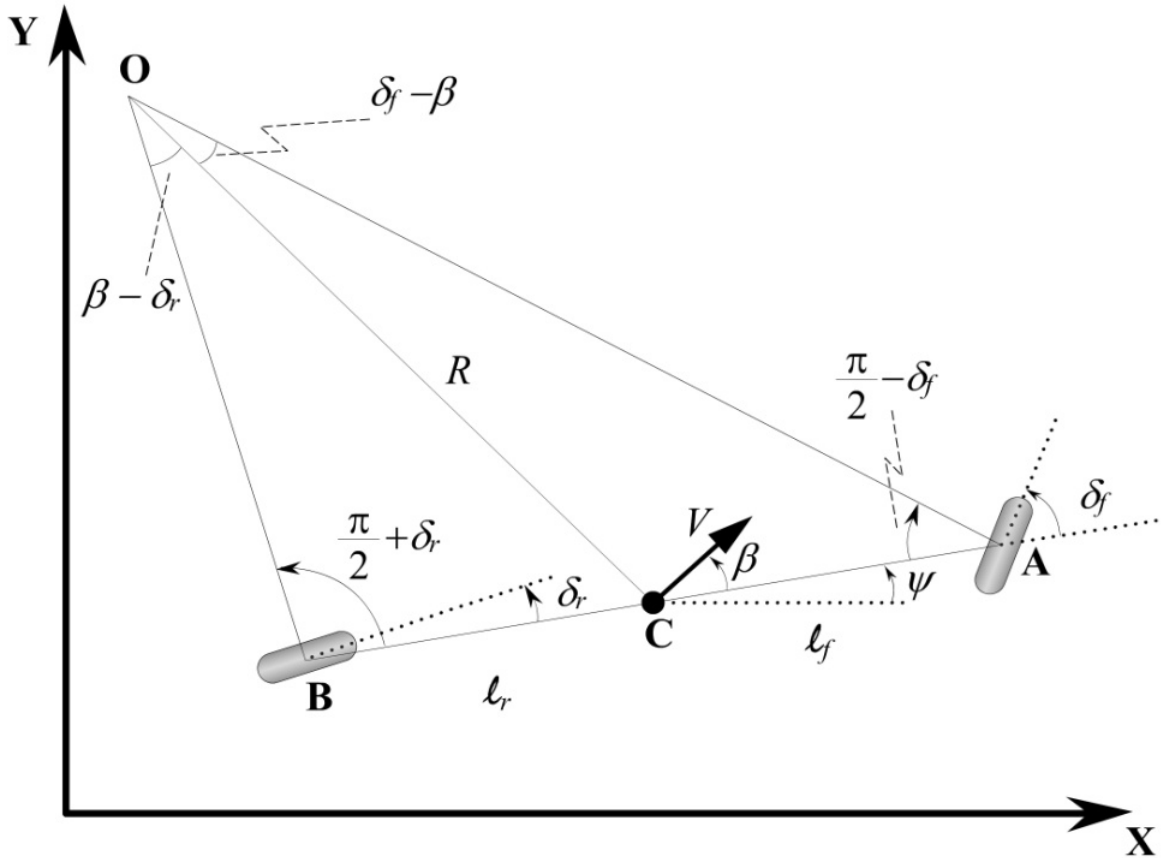


Figure 1.4: Kinematics of lateral vehicle motion [7]

steered. For front-wheel-only steering, the rear steering angle δ_r is set to zero. The center of gravity (c.g.) of the vehicle is located at the middle point. The distances from points front wheel to the center and from the center to rear of the vehicle. are denoted by l_f and l_r , respectively. The wheelbase of the vehicle is represented by L .

The vehicle is assumed to have planar motion, which requires three coordinates to describe: x , y , and ψ . The x and y coordinates represent the inertial position of the vehicle's center of gravity, while ψ describes the vehicle's orientation. The velocity at the c.g. is denoted by v and forms an angle β with the vehicle's longitudinal axis. This angle β is known as the vehicle's slip angle.

Remark 1.3.1. *The validity of this model hinges on the assumption that the side slip angle (β) of each wheel is very small and can be neglected. This assumption holds true at low vehicle speeds, around 30 km/h, making the model suitable for applications in city traffic, for example.*

The radius R of the vehicle's path is defined by the length of the line OC , which connects the center of gravity C to the instantaneous rolling center O . The velocity at the center of gravity C is perpendicular to the line OC . The angle between the velocity at C and the

longitudinal axis of the vehicle is known as the slip angle β . The angle ψ represents the heading angle of the vehicle. The course angle θ for the vehicle is given by $\gamma = \psi + \beta$. To analyze the geometry, the sine rule is applied to triangle OCA [7].

Using trigonometric formulas, we derive the following equation:

For the front

$$\frac{\sin(\delta_f - \beta)}{l_f} = \frac{\sin(\frac{\pi}{2} - \delta_f)}{R} \implies \frac{\cos(\delta_r) \sin(\beta) - \cos(\beta) \sin(\delta_r)}{\cos(\delta_r)} = \frac{l_r}{R} \quad (1.1)$$

And for the rear :

$$\sin(\beta - \delta_r) = \frac{\sin(\frac{\pi}{2} + \delta_r)}{l_r/R} \implies \frac{\cos(\delta_r) \sin(\beta) - \cos(\beta) \sin(\delta_r)}{l_r} = \frac{\cos(\delta_r)}{R} \quad (1.2)$$

After adding both equation(1.1) and (1.2) and doing some manipulation we can get the following :

$$\{\tan(\delta_f) - \tan(\delta_r)\} \cdot \cos(\beta) = \frac{l_f + l_r}{R} \quad (1.3)$$

If we assume that the radius of the vehicle path changes slowly due to low vehicle speed, then the rate of change of the vehicle's orientation (i.e., $\dot{\psi}$) must equal the angular velocity of the vehicle. Given the angular velocity $\frac{V}{R}$ of the vehicle, it follows that

$$\dot{\psi} = \frac{V}{R} \quad (1.4)$$

Using (1.4) and (1.3) we can get :

$$\dot{\psi} = \frac{V \cos(\beta)}{l_f + l_r} (\tan(\delta_f) - \tan(\delta_r)) \quad (1.5)$$

Now we can rewrite the system equation as follow :

$$\dot{X} = V \cos(\psi + \beta) \quad (1.6a)$$

$$\dot{Y} = V \sin(\psi + \beta) \quad (1.6b)$$

$$\dot{\psi} = \frac{V \cos(\beta)}{l_f + l_r} (\tan(\delta_f) - \tan(\delta_r)) \quad (1.6c)$$

The state variables of the kinematic model are X , Y , and ψ , representing the vehicle's position and orientation. The inputs to the model are the steering angles δ_f and δ_r , with V potentially considered as an external variable input.

The slip angle β can be determined by subtracting equation (1.2) multiplied by l_f from equation (1.2) multiplied by l_r .

$$\beta = \tan^{-1} \left(\frac{l_f \tan \delta_r + l_r \delta_f}{l_f + l_r} \right) \quad (1.7)$$

As mentioned earlier, in many vehicles, steering is primarily controlled by the front wheels, denoted as δ . Additionally, when the vehicle is not performing sharp maneuvers—indicating a large radius R compared to the wheelbase L —we can approximate $\beta \approx 0$.

In this case we can write the following system:

$$\dot{X} = V \cos(\psi) \quad (1.8a)$$

$$\dot{Y} = V \sin(\psi) \quad (1.8b)$$

$$\dot{\psi} = \frac{V}{l_f + l_r} (\tan(\delta)) \quad (1.8c)$$

1.3.2 Vehicle lateral dynamic model

At higher vehicle speeds, the assumption that the velocity at each wheel aligns with the wheel direction becomes invalid. In such cases, a dynamic model for lateral vehicle motion must be employed instead of a kinematic model. Here, we continue to use the same bicycle model for the vehicle Figure 1.5, but now we incorporate degrees of freedom for lateral position Y and yaw angle ψ . This dynamic model allows us to accurately represent the forces interacting between the vehicle and its tires.

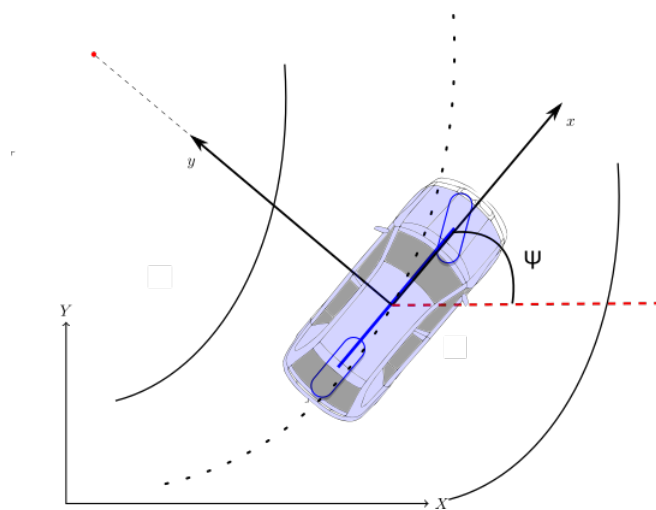


Figure 1.5: Lateral vehicle dynamics

By applying Newton's second law we will have [38] :

$$ma_y = F_{yf} + F_{yr} \quad (1.9)$$

The inertial acceleration a_y is the second derivative of the lateral position, given by $a_y = \frac{d^2y}{dt^2}$. F_{yf} and F_{yr} represent the lateral forces on the front and rear tires, respectively. The vehicle's inertial acceleration consists of two components: the linear acceleration along the y-axis, \ddot{y} , and the centripetal acceleration due to turning, $V_x \dot{\psi}$. Therefore, we have:

$$a_y = \ddot{y} + V_x \dot{\psi} \quad (1.10)$$

By substituting the acceleration from equation (1.10) into equation (1.9), we obtain:

$$m(\ddot{y} + V_x \dot{\psi}) = F_{yf} + F_{yr} \quad (1.11)$$

The moment balance about the axis results in the following equation for the yaw dynamics:

$$I_z \ddot{\psi} = l_f F_{yf} - l_r F_{yr} \quad (1.12)$$

where l_f and l_r are the distances from the center of gravity to the front and rear tires, respectively.

Accurately modeling the tire forces F_{yf} and F_{yr} is quite challenging, leading to various approximations for their analytical expressions. Empirical tests indicate that for sufficiently small slip angles, these forces are proportional to the tire slip angles. This allows for a linear approximation of the forces, enabling us to write the vehicle's lateral model. In the next section, we will explore more precise approximations of these forces. The slip angle of a tire is defined as the angle between the tire's orientation and the direction of the wheel's velocity vector. If we consider that the vehicle is front wheel steered only we can have the following equations:

$$\alpha_f = \delta - \theta_{Vf} \quad \alpha_r = \theta_{Vr} \quad (1.13)$$

where θ_{Vf} and θ_{Vr} denote the angles that the velocity vectors make with the vehicle's longitudinal axis for the front and rear, respectively, and δ represents the front wheel steering angle.

The lateral forces F_{yf} and F_{yr} can be expressed as follows:

$$F_{yf} = 2C_{\alpha f}(\delta - \theta_{Vf}) \quad F_{yr} = 2C_{\alpha r}(-\theta_{Vr}) \quad (1.14)$$

Where $C_{alpha f}$ and $C_{alpha r}$ is the cornering stiffness for front and rear tires, respectively. The angles θ_{Vf} and θ_{Vr} can be expressed as follows:

$$\begin{aligned}\theta_{Vf} &= \frac{\dot{y} + \ell_f \dot{\psi}}{V_x} \\ \theta_{Vr} &= \frac{\dot{y} - \ell_r \dot{\psi}}{V_x}\end{aligned}\quad (1.15)$$

Using the previous equations, so we can rewrite the (1.9) in the state space form as follow :

$$\begin{bmatrix} \dot{y} \\ \ddot{y} \\ \dot{\psi} \\ \ddot{\psi} \end{bmatrix} = \begin{bmatrix} 0 & 0 & 1 & 0 \\ 0 & -\frac{2C_{\alpha f}+2C_{\alpha r}}{mV_x} & 0 & -V_x - \frac{2C_{\alpha f}\ell_f-2C_{\alpha r}\ell_r}{mV_x} \\ 0 & 0 & 0 & 1 \\ 0 & -\frac{2\ell_f C_{\alpha f}-2\ell_r C_{\alpha r}}{I_z V_x} & 0 & -\frac{2\ell_f^2 C_{\alpha f}+2\ell_r^2 C_{\alpha r}}{I_z V_x} \end{bmatrix} \begin{bmatrix} y \\ \dot{y} \\ \psi \\ \dot{\psi} \end{bmatrix} + \begin{Bmatrix} 0 \\ \frac{2C_{\alpha f}}{m} \\ 0 \\ \frac{2\ell_f C_{\alpha f}}{I_z} \end{Bmatrix} \delta \quad (1.16)$$

Lateral Dynamic model in term of yaw rate and slip angle

Assuming small angles, we can rewrite the system equation in (1.16) in terms of the slip angle β and the yaw rate $r \equiv \dot{\psi}$ using the following approximation:

$$\beta = \frac{\dot{y}}{V_x} = \frac{1}{V_x} (\dot{e}_1 - V_x e_2) = \frac{1}{V_x} \dot{e}_1 - e_2 \quad (1.17)$$

And by using the same approximation of small tire slip angles α_f and α_r we can have the tire forces expressed as :

$$F_{yf} = 2C_{\alpha f} \alpha_f \quad F_{yr} = 2C_{\alpha r} \alpha_r \quad (1.18)$$

The state space model can be expressed as follow :

$$\begin{bmatrix} \dot{\beta} \\ \dot{r} \end{bmatrix} = \begin{bmatrix} -\frac{2C_{\alpha f}+2C_{\alpha r}}{mV_x} & -V_x - \frac{2C_{\alpha f}\ell_f-2C_{\alpha r}\ell_r}{mV_x} \\ -\frac{2\ell_f C_{\alpha f}-2\ell_r C_{\alpha r}}{I_z V_x} & -\frac{2\ell_f^2 C_{\alpha f}+2\ell_r^2 C_{\alpha r}}{I_z V_x} \end{bmatrix} \begin{bmatrix} \beta \\ r \end{bmatrix} + \begin{bmatrix} \frac{2C_{\alpha f}}{m} \\ \frac{2\ell_f C_{\alpha f}}{I_z} \end{bmatrix} \delta \quad (1.19)$$

where m is the vehicle mass, V_x is the vehicle's longitudinal velocity, F_{yf} and F_{yr} are the front and rear tire forces, respectively, I_z is the yaw moment of inertia, and ℓ_f and ℓ_r are the distances from the center of gravity (CG) to the front and rear tires,

respectively. Additionally, C_f and C_r represent the cornering stiffness of the front and rear tires, respectively.

1.3.3 Tire Dynamic Models

Linear model :

When tire slip angles and slip ratios are small, the longitudinal and lateral tire forces can be linearly approximated as follows [7], [39], [40]:

$$\begin{aligned} F_{yf} &= C_\alpha \left(\delta - \frac{V_y + \ell_f \dot{\psi}}{V_x} \right) \\ F_{yr} &= C_\alpha \left(-\frac{V_y - \ell_r \dot{\psi}}{V_x} \right) \end{aligned} \quad (1.20)$$

It is important to note that the linear tire model is suitable for normal driving conditions. However, during extreme handling situations where the tire operates in the nonlinear region, it becomes necessary to use widely accepted nonlinear tire models, such as the Pacejka model, Dugoff model, and LuGre model.

LuGre tire model :

When the vehicle is in purely longitudinal motion, the LuGre tire model can be used to represent the tire's longitudinal force in a longitudinal two-wheel model under friction conditions [1], [41]. The LuGre model accounts for transient behaviors of friction and road conditions by incorporating an internal dynamic state of friction between the tire and road interaction, which can be described as follows:

$$F_x = \mu F_z \quad (1.21)$$

$$\mu = \sigma_0 z_f + \sigma_1 \dot{z}_f - \sigma_2 v_r \quad (1.22)$$

With

$$\dot{z}_f = -v_r - \frac{\sigma_0 |v_r|}{f(v_r)} \rho z_f \quad (1.23)$$

$$f(v_r) = \mu_c + (\mu_s - \mu_c) \exp(-\left| \frac{v_r}{v_s} \right|^{\frac{1}{2}}) \quad (1.24)$$

$$v_r = R_e \omega - V_x \quad (1.25)$$

where F_x , F_z represent the longitudinal and vertical tire forces of the wheel, respectively.

Pacejka tire model (magic formula tire model)

The linear tire force model is a good approximations when the slip ratio and slip angle are small, respectively. However, for large slip angles and slip ratios, a more sophisticated model is required. The Magic Formula tire model [42] provides a method to calculate lateral and longitudinal tire forces F_y and F_x , as well as the aligning moment M_z , for a wide range of operating conditions, including large slip angles and slip ratios, as well as combined lateral and longitudinal force generation. In the simpler case where only either lateral or longitudinal force is being generated, the force generated Y can be expressed as a function of the input variable X as follows: The output variable Y can be expressed as a function of the input variable X as follows [7]:

$$Y(X) = y(x) + S_v$$

with

$$y(x) = D \sin [C \arctan \{Bx - E(Bx - \arctan(Bx))\}]$$

and

$$x = X - S_h$$

where Y is the output variable: longitudinal force F_x , lateral force F_y , or aligning moment M_z , S_h horizontal shift S_v vertical shift and tire parameters B , C , D , and E can be determined on the basis of tire vertical force and tire-road friction coefficient [42]–[45].

Dugoff tire model

Dugoff's model [46] calculates forces generated under combined lateral and longitudinal tire interactions. It assumes a uniform vertical pressure distribution on the tire contact patch, which is a simplification compared to the more realistic parabolic pressure distribution used in the Pacejka model [42]. However, Dugoff's model has a significant advantage: it allows for independent values of tire stiffness in both the lateral and longitudinal directions. Longitudinal and lateral tire-road forces can be defined as follows :

$$F_x = -C_\sigma \frac{\sigma_x}{1 - \sigma_x} f(S), \quad (1.26)$$

$$F_y = C_\alpha \frac{\tan(\alpha)}{1 - \sigma_x} f(S), \quad (1.27)$$

where S is given by

$$S = \frac{\mu F_z (1 - \varepsilon_r V_x \sqrt{\sigma_x + \tan^2 \alpha})}{2 \times \sqrt{C_\sigma^2 \sigma_x^2 + C_\alpha^2 \tan^2 \alpha}} (1 - \sigma_x^2)$$

and

$$f(S) = \begin{cases} 1 & \text{if } S > 1 \\ S(2-S) & \text{otherwise} \end{cases}$$

where ε_f and ε_r are the front and rear roll steer coefficients, respectively.

1.3.4 Vehicle longitudinal dynamic model

Developing a vehicle longitudinal dynamic model is essential for understanding and optimizing a vehicle's performance, safety, and efficiency. This model focuses on the forces and motions along the direction of travel, encompassing aspects such as acceleration, braking, and resistance forces. By accurately simulating these dynamics, engineers can predict how a vehicle will respond to various driving conditions and maneuvers. This knowledge is crucial for designing advanced driver assistance systems (ADAS), enhancing fuel efficiency, improving ride comfort, and ensuring regulatory compliance. Additionally, as the automotive industry shifts towards electric and autonomous vehicles, precise longitudinal dynamic modeling becomes even more critical to meet the high standards of control, stability, and energy management required for these advanced technologies.

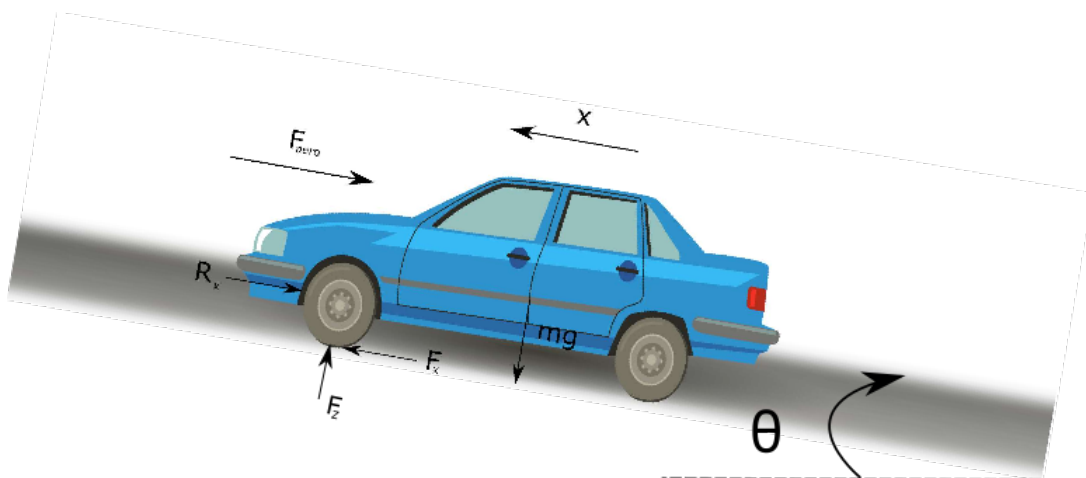


Figure 1.6: Vehicle longitudinal dynamics

Consider a vehicle moving on an inclined road in the longitudinal plane, as shown in Figure 1.6. By applying Newton's second law to account for all external forces

acting on the vehicle's chassis and tires, including gravitational force, aerodynamic drag, longitudinal tire force, and rolling resistance, we derive the following equilibrium equation:

$$m\ddot{x} = F_{xf} + F_{xr} - F_{aero} - R_{xf} - R_{xr} - mg \sin(\theta) \quad (1.28)$$

Where

- F_{xf} is the longitudinal tire force at the front tires
- F_{xr} is the longitudinal tire force at the rear tires
- R_{xf} is the force due to rolling resistance at the front tires
- R_{xr} is the force due to rolling resistance at the rear tires
- m is the mass of the vehicle
- g is the acceleration due to gravity
- θ is the angle of inclination of the road on which the vehicle is traveling

Next we are going to define the forces acting on the vehicle :

Aerodynamic drag force

Aerodynamic drag is the resistive force that opposes a vehicle's motion through the air, caused by the friction and pressure differences around the vehicle's surface as it moves is defined as follow [7]:

$$F_{aero} = \frac{1}{2}\rho C_d A_F (V_x + V_{wind})^2 \quad (1.29)$$

The variables are defined as follows: ρ is the mass density of air, C_d is the aerodynamic drag coefficient, A_F is the frontal area of the vehicle (the projected area of the vehicle in the direction of travel), V_x is the longitudinal vehicle velocity, and V_{wind} is the wind velocity (positive for a headwind and negative for a tailwind). Atmospheric conditions influence air density ρ , which can significantly affect aerodynamic drag. These parameters vary depending on many factors, such as the vehicle's shape, weather conditions, and the vehicle's speed.

Longitudinal tire force

The longitudinal tire forces F_{xf} and F_{xr} are friction forces acting on the tires from the ground. Experimental results show that these forces depend on the slip ratio, the normal load on the tire (which is derived from a portion of the vehicle's weight and influenced by the fore-aft location of the center of gravity), the friction coefficient of the tire-road interface, vehicle longitudinal acceleration, aerodynamic drag forces, and road grade. While these forces are complex, similar to lateral forces, experimental data [42], [46] indicate that under certain conditions—where the friction coefficient is approximately 1

and normal forces are constant—the variation of longitudinal forces can be modeled as a function of the slip ratio as shown in Figure 1.7, defined as follows:

$$F_{xf} = C_{\sigma f} \sigma_{xf} \quad F_{xr} = C_{\sigma r} \sigma_{xr} \quad (1.30)$$

where $C_{\sigma f}$ and $C_{\sigma r}$ are the longitudinal tire stiffness parameters for the front and rear

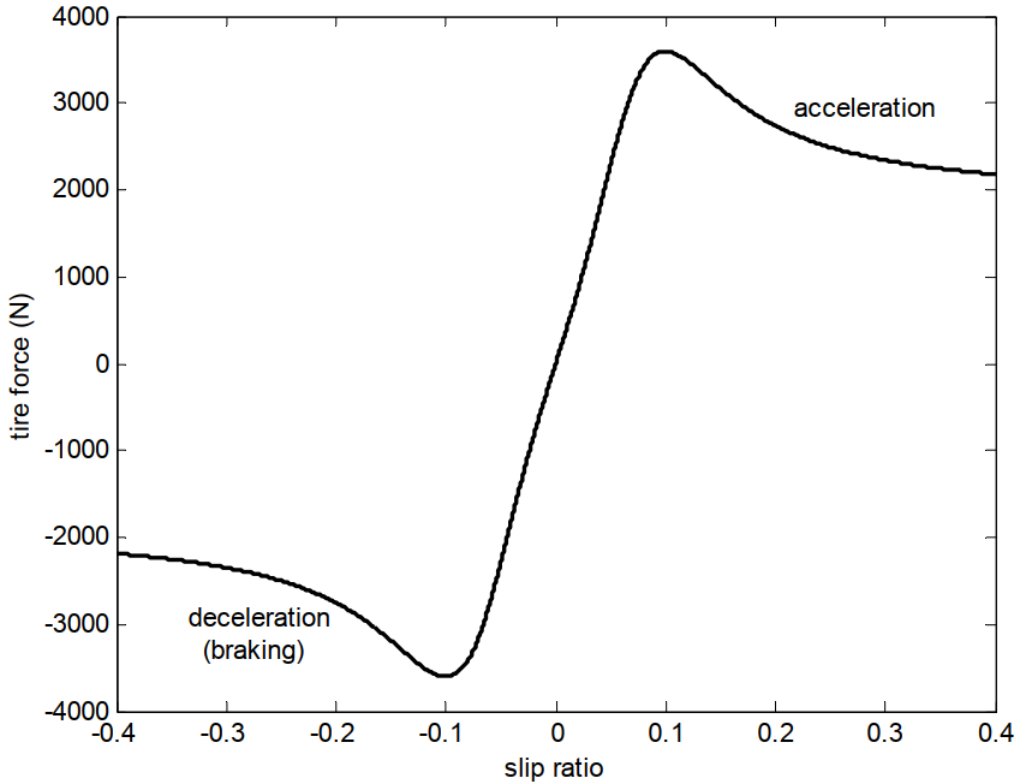


Figure 1.7: Longitudinal tire force as a function of slip ratio [7]

tires, respectively. The slip ratios, σ_{xf} and σ_{xr} , represent the difference between the actual longitudinal velocity at the axle of the wheel, V_x , and the equivalent rotational velocity of the tire, $r_{eff}\omega_w$, as illustrated in Figure 1.8. In other words, the longitudinal slip is $r_{eff}\omega_w - V_x$. The longitudinal slip ratio is defined as follows:

$$\sigma_x = \frac{r_{eff}\omega_w - V_x}{V_x} \quad \text{during braking}$$

$$\sigma_x = \frac{r_{eff}\omega_w - V_x}{r_{eff}\omega_w} \quad \text{during acceleration}$$

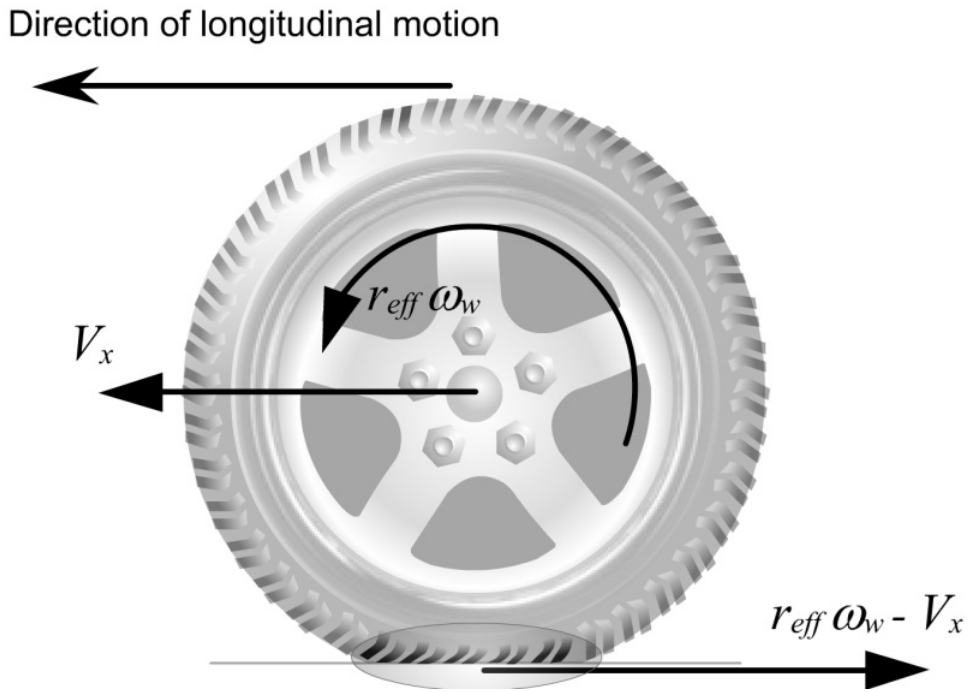


Figure 1.8: Longitudinal force in a driving wheel [47]

Rolling resistance

Rolling resistance refers to the force that opposes the motion of a vehicle's tires as they roll over a surface. It arises from the deformation of the tires and the friction generated between the tires and the road surface. Rolling resistance is influenced by factors such as tire construction, tire pressure, road surface conditions, and vehicle speed. It represents energy losses that must be overcome to maintain the vehicle's motion, affecting fuel efficiency and overall performance. Typically, the rolling resistance is modeled as being roughly proportional to the normal force on each set of tires:

$$R_{xf} + R_{xr} = f(F_{zf} + F_{zr}) \quad (1.31)$$

where the normal forces can be computed from the equation of force balance (1.30) :

$$\begin{aligned} F_{zf} &= \frac{-F_{aero} h_{aero} - m\ddot{x}h - mgh \sin(\theta) + mg\ell_r \cos(\theta)}{\ell_f + \ell_r} \\ F_{zr} &= \frac{F_{aero} h_{aero} + m\ddot{x}h + mgh \sin(\theta) + mg\ell_f \cos(\theta)}{\ell_f + \ell_r} \end{aligned} \quad (1.32)$$

Third-order vehicle longitudinal model for control

The models presented earlier are generally simplified to facilitate their application in control systems, particularly for platoon control and adaptive cruise control. These control strategies rely on accurate and efficient prediction and regulation of vehicle dynamics to maintain safe distances and smooth interactions between vehicles. Simplified models help in achieving real-time computations and decision-making, crucial for dynamic adjustments in traffic conditions. By focusing on essential parameters such as longitudinal forces, slip ratios, and tire characteristics, these simplified models strike a balance between computational efficiency and accuracy, enabling effective implementation in advanced driver assistance systems (ADAS) aimed at enhancing safety and efficiency on the road.

- **Linear Model (Position-Velocity-Acceleration) [48]**

$$\begin{aligned}\dot{p}(t) &= v(t) \\ \dot{v}(t) &= a(t) \\ \dot{a}(t) &= \frac{1}{\tau}c(t) - \frac{1}{\tau}a(t)\end{aligned}\tag{1.33}$$

- **Nonlinear Model (Position-Velocity-Force)[49], [50]**

$$\begin{aligned}\dot{p}(t) &= v(t) \\ \dot{v}(t) &= \frac{1}{m}F(t) - \frac{K_d}{m}v^2(t) - \frac{d_m}{m} \\ \dot{F}(t) &= \frac{1}{\tau}u(t) - \frac{1}{\tau}F(t)\end{aligned}\tag{1.34}$$

- **Nonlinear Model (Position-Velocity-Acceleration) [48], [51]**

$$\begin{aligned}\dot{p}(t) &= v(t) \\ \dot{v}(t) &= a(t) \\ \dot{a}(t) &= \frac{1}{m\tau}u(t) - \frac{2K_d}{m}v(t)a(t) \\ &\quad - \frac{1}{\tau}(a(t) + \frac{K_d}{m}v^2(t) + \frac{d_m}{m})\end{aligned}\tag{1.35}$$

- $p(t)$: Position of mass at time t
- $v(t)$: Velocity of mass at time t
- $a(t)$: Acceleration of mass at time t
- $F(t)$: Force acting on mass at time t
- m : Mass of object
- $u(t)$: Control input for mass i at time t

- τ : Time constant for mass
- K_d : Damping coefficient for mass
- d_m : Constant term in the force equation for mass
- $c(t)$: Control input for acceleration of mass at time t

The previously discussed models are commonly used to represent a platoon system [52]. Derived from Newton's second law of motion and the force balance equation, these models, which become equivalent after certain approximations, encompass both nonlinear and linear approximations. The equation from the nonlinear system in (1.35) can be written in a more compact form, which will be useful for the development of controllers and observers: We can rewrite the system in (3.26) in a compact form as follows:

$$\begin{cases} \dot{\xi} = A\xi + Bf(\xi) + B_u u(t) \\ y = C\xi \end{cases} \quad (1.36)$$

where the state vector is

$$\xi = \begin{bmatrix} \xi_1 \\ \xi_2 \\ \xi_3 \end{bmatrix} = \begin{bmatrix} p(t) \\ v(t) \\ a(t) \end{bmatrix},$$

and

$$A = \begin{bmatrix} 0 & 1 & 0 \\ 0 & 0 & 1 \\ 0 & 0 & 0 \end{bmatrix}, \quad B = \begin{bmatrix} 0 \\ 0 \\ 1 \end{bmatrix}, \quad C = \begin{bmatrix} 1 & 0 & 0 \end{bmatrix},$$

$$B_u = \begin{bmatrix} 0 \\ 0 \\ \frac{1}{m\tau} \end{bmatrix},$$

$$f(\xi) = -\frac{2K_{di}}{m}\xi_2\xi_3 - \frac{1}{\tau} \left(\xi_3 + \frac{K_{di}}{m}\xi_2^2 + \frac{d_m}{m} \right).$$

1.4 Estimation Schemes for Vehicle State Estimation

Effective vehicle control is crucial for enhancing driving operations, reducing driver burden, and ensuring passenger safety, as discussed earlier. Various controllers are available for these purposes, but they typically require complete knowledge of the vehicle and environment to provide feedback. This information is often obtained through sensors, but practical constraints such as cost-effectiveness or technological limitations may prevent the direct measurement of certain physical signals. This is where observers

play a pivotal role in vehicle state estimation by allowing the inference of unmeasurable states from observable outputs as shown in Figure 1.9.

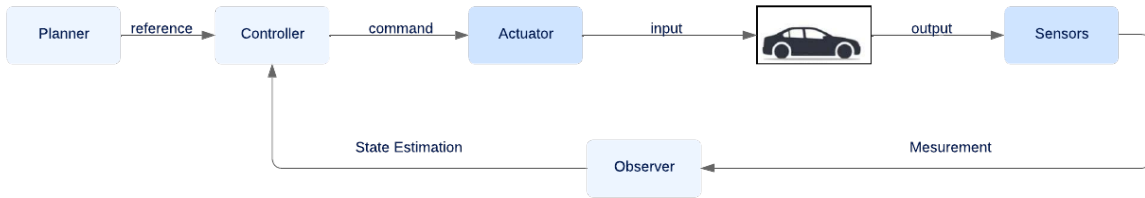


Figure 1.9: The Observation general diagram (light blue is the software blocks and dark blue is a hardware block)

For example, while sensors can directly measure parameters like wheel speeds or yaw rates, they cannot directly measure slip angles or tire forces, which are vital for vehicle dynamics control. Accurate estimation of these states is crucial for implementing advanced control strategies that enhance vehicle safety and performance, especially in diverse road conditions and driving scenarios. The models developed earlier will be instrumental in designing these observers and simulating the behavior of the vehicle. Vehicle system dynamic state estimation is divided into two primary approaches: model-based and data-driven methods. Model-based approaches use mathematical models to describe transient vehicle dynamics, providing higher accuracy in state estimation. This approach remains a focal point in academic research, resulting in the development of various dynamic model-based strategies. Recently, data-driven methods, such as artificial neural network (ANN)-based estimations, have become popular due to advancements in artificial intelligence, demonstrating promising applications in vehicle state estimation. This section will present some of these methods.

1.4.1 Classical Model-Based Methods for Vehicle State Estimation

Model-based observers are fundamental tools in control theory and engineering systems, designed to estimate the unmeasured states of dynamic systems using known system equations and measured outputs. These observers operate under the premise that a mathematical model of the system dynamics is available and accurate. Typically, such observers are developed for systems described by differential equations, where the state variables evolve over time influenced by known inputs and are observed through measurable outputs. The primary objective of a model-based observer is to compute state estimates that closely match the actual system states, enabling real-time monitoring, control, and decision-making processes. These observers play a

crucial role in various applications, from industrial process control to aerospace and robotics, ensuring robust performance and stability by leveraging precise mathematical representations of system dynamics.

One crucial concept in observer design is observability. Traditionally, observability in linear systems has been assessed using tools like the observability matrix. However, the concept of observability for nonlinear systems shifts to local observability, focusing on the system's ability to reconstruct its state from output measurements over a finite time interval. Global considerations, discussed extensively in [53], are outside the scope of this section.

In the context of nonlinear systems, a system is described by the following state-space equations:

$$\begin{aligned}\dot{x}(t) &= f(x(t), u(t)) \\ y(t) &= h(x(t), u(t))\end{aligned}$$

where:

- $x(t)$ is the state vector,
- $u(t)$ is the input vector,
- $y(t)$ is the output vector,
- f is a nonlinear function that describes the system dynamics,
- h is a nonlinear function that describes the output.

In this framework, the system is locally weakly observable from an initial state x_0 if, for any initial state $x(t_0)$ within a neighborhood X_0 of x_0 , there exists a time $t_1 \geq t_0$ such that all trajectories $x(t)$ originating from different states $x_1 \in X_0$ are distinguishable using the input $u(t)$ and output $y(t)$ (meaning that at this time t_1 , the system's responses or outputs are different enough for each initial state so that you can tell them apart). This condition extends to local strong observability if there exists a smaller neighborhood $X_1 \subset X_0$ where $x(t) \in X_1$ holds for $t_0 \leq t \leq t_1$.

The observability of a nonlinear system is often verified through the construction of the observability matrix $W_o(x)$, which involves Lie derivatives of the output function $h(x)$. Starting with the zeroth-order Lie derivative $L_f^0(h) = h$, higher-order Lie derivatives are recursively defined:

$$L_f^k(h) = \frac{\partial}{\partial x} L_f^{k-1}(h) \cdot f \quad \text{for } k \geq 1$$

The observability matrix $W_o(x)$ is formed by stacking these derivatives:

$$W_o(x) = \begin{bmatrix} \frac{\partial h}{\partial x}(x) \\ \frac{\partial L_f(h)}{\partial x}(x) \\ \vdots \\ \frac{\partial L_f^{n-1}(h)}{\partial x}(x) \end{bmatrix}$$

where n is the dimension of the state vector x . The system is locally observable if the rank of $W_o(x)$ equals n .

For multiple output functions $h_1(x), \dots, h_p(x)$, the observability matrix is extended as follows:

$$W_o(x) = \begin{bmatrix} \frac{\partial h_1}{\partial x}(x) & \dots & \frac{\partial h_p}{\partial x}(x) \\ \frac{\partial L_f(h_1)}{\partial x}(x) & \dots & \frac{\partial L_f(h_p)}{\partial x}(x) \\ \vdots & \ddots & \vdots \\ \frac{\partial L_f^{n-1}(h_1)}{\partial x}(x) & \dots & \frac{\partial L_f^{n-1}(h_p)}{\partial x}(x) \end{bmatrix}$$

Different observer designs are tailored to meet specific observability requirements. For systems that exhibit uniform observability, widely used approaches include the extended Luenberger and Kalman observers. In contrast, techniques such as the particle filter and sliding mode observer are specifically designed to address the complexities of nonlinear dynamics, as elaborated in the this section.

Kalman Filter(KF)-Based Estimation

- **General Kalman Filter** Kalman filter (KF)-based estimation methods applied to vehicle dynamics. It begins with a stochastic estimation KF derived from a two degrees-of-freedom (DOF) bicycle model with a linear tire model to estimate vehicle lateral velocity [39]. The integration of GPS and other sensor signals enhances the accuracy of vehicle state estimation [40], [54]. Recognizing limitations in linear models under extreme handling conditions, nonlinear Kalman filters like extended Kalman filter (EKF) and unscented Kalman filter (UKF)have been developed to handle system nonlinearities in vehicle dynamics estimation. The equations of the Kalman filter are given by :

$$\dot{\hat{x}} = A\hat{x} + Bu + L(y - C\hat{x}) \quad (1.37)$$

The feedback matrix L is determined based on the magnitudes of the covariance matrices associated with the process and measurement noise can be calculated solving a matrix Riccati equation.

- **Extended Kalman Filter** The Kalman filter fundamentally requires the system to be linear, which poses a challenge in real-world applications where systems are often nonlinear. This is especially true for complex systems like road vehicles, where nonlinearities are inherent and can be described by equations such as:

$$x_k = f(x_{k-1}, u_{k-1}) + w_{k-1}, \quad y_k = h(x_k) + v_k$$

where $x \in \mathbb{R}^n$ denotes the state vector, $y \in \mathbb{R}^m$ represents the measurement vector, $w_k \sim \mathcal{N}(0, Q_k)$ indicates process noise, and $v_k \sim \mathcal{N}(0, R_k)$ represents measurement noise. Both w and v are zero-mean multivariate Gaussian noises with covariance matrices Q_k and R_k , respectively. The function f is the potentially nonlinear dynamic model function, and h is the potentially nonlinear measurement model function.

Similar to the Kalman filter, the Extended Kalman Filter (EKF) also consists of two main steps. For a first-order EKF, these steps are:

Prediction:

$$\begin{aligned}\hat{x}_{k|k-1} &= f(\hat{x}_{k-1|k-1}, u_{k-1}) \\ P_{k|k-1} &= F_{k-1} P_{k-1|k-1} F_{k-1}^T + Q_{k-1}\end{aligned}$$

Update:

$$\begin{aligned}K_k &= P_{k|k-1} H_k^T (H_k P_{k|k-1} H_k^T + R_k)^{-1} \\ \hat{x}_{k|k} &= \hat{x}_{k|k-1} + K_k (y_k - h(\hat{x}_{k|k-1})) \\ P_{k|k} &= (I - K_k H_k) P_{k|k-1}\end{aligned}$$

Here, f and h represent the nonlinear dynamic and measurement models, $\hat{x}_{k|k-1}$ is the predicted state estimate, $P_{k|k-1}$ is the predicted error covariance, K_k is the Kalman gain, y_k is the measurement, Q_k is the process noise covariance, R_k is the measurement noise covariance, F_k is the state transition matrix(i.e Jacobian of f), and H_k is the measurement Jacobian matrix of h . In vehicle applications, the Extended Kalman Filter (EKF) is utilized to estimate the vehicle slip angle by integrating the single-track model with a simplified Pacejka tire model. Additionally, it is employed to estimate various vehicle parameters [55], [56].

- **Unscented Kalman filter (UKF)-based estimation** Unlike the Extended Kalman Filter (EKF), the Unscented Kalman Filter (UKF) employs a set of sigma points to perform nonlinear transformations directly on the vehicle dynamics systems [57]. This approach approximates the states more accurately by handling nonlinearities effectively. The prediction and update steps of the augmented Unscented Kalman Filter (UKF) in matrix form are as follows:

Prediction:

$$\mathcal{X}_{k-1} = [\hat{x}_{k-1}, \hat{x}_{k-1} \pm \sqrt{P_{k-1} + Q}]$$

$$\hat{\mathcal{X}}_{k|k-1} = f(\mathcal{X}_{k-1}, u_{k-1})$$

$$\hat{x}_{k|k-1} = \sum_i w_i \hat{\mathcal{X}}_{k|k-1}^i$$

$$P_{k|k-1} = \sum_i w_i [\hat{\mathcal{X}}_{k|k-1}^i - \hat{x}_{k|k-1}] [\hat{\mathcal{X}}_{k|k-1}^i - \hat{x}_{k|k-1}]^T + Q$$

Update:

$$\mathcal{Y}_{k|k-1} = h(\hat{\mathcal{X}}_{k|k-1})$$

$$\hat{y}_{k|k-1} = \sum_i w_i \mathcal{Y}_{k|k-1}^i$$

$$P_{yy} = \sum_i w_i [\mathcal{Y}_{k|k-1}^i - \hat{y}_{k|k-1}] [\mathcal{Y}_{k|k-1}^i - \hat{y}_{k|k-1}]^T + R$$

$$P_{xy} = \sum_i w_i [\hat{\mathcal{X}}_{k|k-1}^i - \hat{x}_{k|k-1}] [\mathcal{Y}_{k|k-1}^i - \hat{y}_{k|k-1}]^T$$

$$K_k = P_{xy} P_{yy}^{-1}$$

$$\hat{x}_{k|k} = \hat{x}_{k|k-1} + K_k (y_k - \hat{y}_{k|k-1})$$

$$P_{k|k} = P_{k|k-1} - K_k P_{yy} K_k^T$$

Where \mathcal{X} are the sigma points, w_i are the weights, $\hat{\mathcal{X}}_{k|k-1}$ are the predicted sigma points, $\mathcal{Y}_{k|k-1}$ are the predicted measurement sigma points, $\hat{x}_{k|k-1}$ is the predicted state mean, $P_{k|k-1}$ is the predicted covariance, $\hat{y}_{k|k-1}$ is the predicted measurement mean, P_{yy} is the covariance of the predicted measurement, P_{xy} is the cross-covariance between state and measurement, K_k is the Kalman gain, $\hat{x}_{k|k}$ is the updated state mean, and $P_{k|k}$ is the updated state covariance. The UKF allows for the estimation of the vehicle's nonlinear dynamic model by incorporating complex tire force models such as the Magic Formula and Dugoff model [42], [46]. It can also be applied to a vehicle's six degrees of freedom model and used for identifying tire model parameters, even in the presence of uncertainties and measurement noise [58]–[64].

The Kalman Filters is widely used for sensor fusion in vehicles due to its ability to handle multiple noisy measurements and integrate data from different sensors. It effectively combines measurements of the same variable from various sensors, even when they have different sampling rates as shown in Figure 1.10. It utilizes the vehicle model to estimate the position based on IMU sensor measurements, and then corrects this estimation whenever position data from GNSS or LIDAR

becomes available. This capability is particularly valuable in vehicle applications, where accurate and reliable data integration is crucial for system performance and safety.

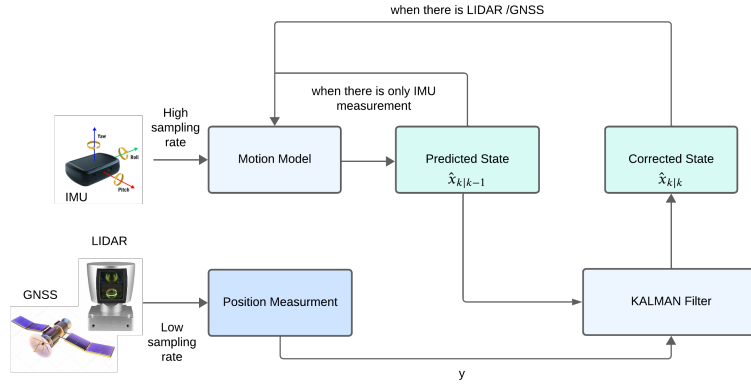


Figure 1.10: Sensor fusion using a Extended Kalman Filter (EKF)

Sliding Mode Observer

Sliding Mode Observers (SMOs) have gained attention for their robustness against uncertainties and disturbances in vehicle state estimation [65]–[71]. Unlike Extended Kalman Filters (EKF) and Unscented Kalman Filters (UKF), which rely on linearizations and Gaussian assumptions, SMOs operate on the principle of sliding mode control, ensuring that the estimation error converges to zero along a predefined sliding surface. In vehicle applications, SMOs have been employed to estimate states such as vehicle velocity, position, and tire forces, leveraging their ability to handle nonlinear dynamics and model uncertainties effectively. Compared to EKF and UKF, which require accurate modeling and assumptions about noise characteristics, SMOs offer advantages in scenarios where the system dynamics are highly nonlinear or when measurements are prone to significant noise and disturbances. However, designing SMOs typically involves tuning parameters related to the sliding surface and gain selection, which can affect convergence speed and robustness. Researchers continue to explore and refine SMO methodologies to enhance their applicability and performance in various vehicle dynamics and control contexts.

The problem of state estimation for a nonlinear system is formulated as follows:

$$\dot{x} = f(x) + B(x)u \quad (1.38)$$

$$y = h(x) \quad (1.39)$$

where $x \in \mathbb{R}^n$ represents the state vector and $y \in \mathbb{R}^m$ is the output vector. In this formulation, $f(x)$ denotes the nonlinear function that describes the system dynamics, $B(x)$ is the control input matrix, and $h(x)$ represents the nonlinear measurement function. For a specific case where $m = 1$ (indicating a scalar output) and $B(x) = 0$ (implying that the system dynamics are not influenced by the control input).

We introduce the following notations: $H(x) = \text{col}(h_1(x), \dots, h_n(x))$, where $h_1(z) = h(z)$ and $h_{i+1}(x)$ is the i -th Lie derivative of the function $h(X)$ along the trajectories of the system [72].

$$h_i(x) = L_f^{i-1} h(x)$$

Let $H(x) = \text{col}(h_1(x) \dots h_n(x))$ and assuming that $\frac{\partial H(x)}{\partial x}$ is invertible (i.e.) :

$$\left| \det \left(\frac{\partial H(x)}{\partial x} \right) \right| \geq \delta > 0$$

To estimate the state variables of System 1.38 using measurements from System 1.39, one can use an observer as described :

$$\dot{\hat{x}} = \left(\frac{\partial H(\hat{x})}{\partial x} \right)^{-1} M(\hat{x}) \text{sign}(V(t) - H(\hat{x})) \quad (1.40)$$

where $V(t) = \text{col}(v_1(t), \dots, v_n(t))$

$$v_1(t) = y(t)$$

and

$$v_{i+1}(t) = (m_i(\hat{x}) + \text{sign}(v_i(t) - h(\hat{x}(t))))_{eq}$$

for $i = 1, \dots, n-1$, and matrix M is an $n \times n$ diagonal matrix with positive elements $m_i(\hat{x})$, $i = 1, \dots, n$:

$$M(\hat{x}) = \text{diag}(m_1(\hat{x}), \dots, m_n(\hat{x}))$$

By choosing M appropriately, the observer in (1.40) converges within any prescribed finite time interval.

Nonlinear Observers

Nonlinear observers are employed to estimate vehicle states due to their ability to accurately model the complex nonlinear dynamics of vehicle systems, especially under

varying and extreme driving conditions. While nonlinear versions of the Kalman Filter, such as the Extended Kalman Filter (EKF) and Unscented Kalman Filter (UKF), offer improved performance over linear approaches by accommodating some degree of nonlinearity, they still have limitations. The EKF relies on linear approximations that can become inaccurate for highly nonlinear systems, and the UKF, although better, can be computationally intensive. Sliding mode observers, though robust to uncertainties and disturbances, can induce chattering and require precise system knowledge, making them difficult to implement in practice.

Experimental tests have shown that the estimation performance of nonlinear observers (NLO) is generally superior to that of the EKF [73]–[75]. Furthermore, nonlinear observers benefit from strong theoretical foundations, particularly regarding input-to-state stability (ISS) theory [74], which ensures robust performance under a wide range of conditions. These advantages make nonlinear observers especially attractive to researchers focusing on vehicle state estimation, control, and safety.

The concept behind nonlinear observers is that they account for a class of nonlinear systems defined as:

$$\dot{x} = f(x, u) \quad (1.41)$$

$$y = Cx \quad (1.42)$$

where $x \in \mathbb{R}^n$ is the state vector, $u \in \mathbb{R}^m$ is the input vector, and $y \in \mathbb{R}^p$ is the output vector. $C \in \mathbb{R}^{p \times n}$ is a matrix of appropriate dimensions. $f(x, u) : \mathbb{R}^n \times \mathbb{R}^m \rightarrow \mathbb{R}^n$ is a vector of differentiable nonlinear functions. Consider the Luenberger observer shown here for the estimated state:

$$\dot{\hat{x}} = f(\hat{x}, u) + L(y - C\hat{x})$$

where L is the observer gain matrix designed to ensure exponential convergence of the estimation error $e = x - \hat{x}$ towards zero.

Observers have been utilized extensively for estimating and tracking vehicle positions [76], highlighting their role in enhancing navigation accuracy and reliability. Moreover, observers have been applied effectively in estimating parameters and states related to vehicle rollover dynamics [77], providing critical insights into vehicle stability and safety. Additionally, observers have been employed for estimating vehicle sideslip angles under uncertain conditions [78], demonstrating their capability to improve handling and control in challenging driving scenarios. In [65], the estimation of road bank was performed using an Unknown Input Observer (UIO) that integrated roll dynamics and employed a dynamic fault thresholds algorithm. Through analysis of the singular values of the observability matrix, tire cornering stiffness was determined based on the estimation

of vehicle sideslip angle using a Nonlinear Observer (NLO) [79]. Concurrently, in [80], [81], a novel Switched Nonlinear Observer (SNLO) was introduced to estimate both vehicle sideslip angle and Tire-Road Friction Coefficient (TRFC) simultaneously. This method utilized simplified Pacejka tire models or rational tire models, applying Lyapunov function techniques for robustness and accuracy.

1.4.2 Data-Driven Based Observers

Data-driven estimation techniques are designed to estimate vehicle states and parameters based on extensive historical and real-time input/output datasets from vehicle dynamics systems. Unlike traditional model-based methods, data-driven approaches do not rely on predefined vehicle models. Instead, they leverage large volumes of data to capture and learn vehicle dynamic characteristics, which helps avoid the limitations and inaccuracies often associated with model-based estimations.

Among the advanced data-driven techniques, artificial neural network (ANN)-based artificial intelligence (AI) stands out as a highly effective method for vehicle state estimation [82]–[85]. ANNs are capable of processing complex patterns and relationships within data, making them suitable for a wide range of estimation tasks. These include estimating energy consumption for ground vehicles, monitoring underwater vehicle dynamics, and controlling hypersonic vehicles and unmanned aerial vehicles. The flexibility and adaptability of ANNs allow them to handle various estimation applications, providing robust and accurate predictions even in the presence of uncertainties and nonlinearities.

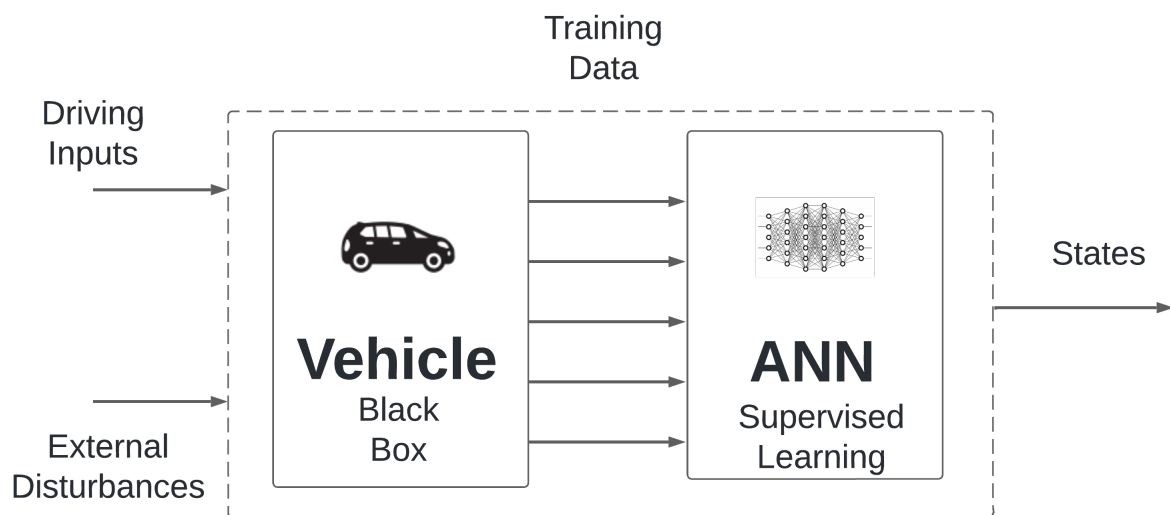


Figure 1.11: The schematic of artificial neural network (ANN) estimation process.

Data-driven observers, which fall under the category of data-driven techniques, significantly improve state estimation by integrating data-driven models. These observers

harness historical data to build precise models that effectively estimate the present state of a vehicle system in real-time. By leveraging artificial neural networks (ANNs), they accommodate uncertainties and unknown dynamics, enhancing the observer's robustness and reliability [86], [87]. This approach can also be seamlessly integrated into the observer design process [88], [89].

The ANN estimation process involves training the network on large datasets to learn the underlying dynamics of the vehicle system as shown in Figure 1.11. Once trained, the network can generalize from the data to make real-time state and parameter estimations. This approach has shown promising results in various applications, highlighting its potential to enhance vehicle control, safety, and performance. Additionally, data-driven observers can be integrated with other AI techniques, such as reinforcement learning and support vector machines, to improve their estimation accuracy and robustness. In this section, we will delve into data-driven observers, highlighting several studies from the literature that integrate classical state observation methods with machine learning and neural networks [86]–[89].

1.4.3 Deep Learning-based Luenberger Observers

This strategy addresses strong nonlinearities in observer design by identifying a mapping that makes nonlinear dynamics approximately linear, allowing the application of standard linear observer designs. The Kazantzis-Kravaris-Luenberger (KKL) observer method immerses nonlinear systems into linear systems with output injection. This work takes a data-driven approach, using deep learning to approximate the required mapping [89].

Problem Statement

The considered nonlinear discrete-time system is described by:

$$\begin{cases} x_{k+1} = F(x_k, u_k) \\ y_k = h(x_k) \end{cases} \quad (1.43)$$

where $x \in \mathbb{R}^{d_x}$ represents the state vector, $u \in \mathbb{R}^{d_u}$ denotes the control input, and $y \in \mathbb{R}^{d_y}$ signifies the output. We define $X_k(x_0, u) = F^k(x_0, u)$ as the state of the system at time k , given the initial condition x_0 and control input u . Let $\mathcal{X}_0 \subset \mathcal{X} \subset \mathbb{R}^{d_x}$ be sets such that for every initial condition $x_0 \in \mathcal{X}_0$ and for all $k \in \mathbb{N} \cup \{0\}$, the state $X_k(x_0)$ remains within \mathcal{X} . The system's equilibrium point is at $(x, u) = (0, 0)$. The following assumptions are made:

Assumption 1.4.1. *The function f is invertible, and f^{-1} and h are continuous.*

Assumption 1.4.2. For all $(x_1, x_2) \in \mathcal{X}^2$ with input u , if $x_1 \neq x_2$, there exists a positive integer i such that $h(F^{-i}(x_1)) \neq h(F^{-i}(x_2))$. This means that for any input u of interest, there exists an open bounded set \mathcal{O} containing \mathcal{X} such that (1.43) is backward \mathcal{O} -distinguishable on \mathcal{X} (i.e if you look at the system's outputs by going backward in time, you should be able to distinguish between any different states in \mathcal{X}).

The objective is to find an injective and continuous map T that transforms the system into a linear Hurwitz form, providing an asymptotically convergent estimate of $T(X(x_0, u))$. Since T is injective, an estimate of $X(x_0, u)$ can be obtained.

KKL Observer

For the system with a null input ($u = 0$):

$$\begin{cases} x_{k+1} = F(x_k, 0) \\ y_k = h(x_k) \end{cases} \quad (1.44)$$

If Assumptions 1.4.1 and 1.4.2 are satisfied, for almost any controllable pair (A, B) of dimension $d_z = d_y(d_x + 1)$ with A Hurwitz, there exists a map $T : \mathcal{X} \rightarrow \mathbb{R}^{d_z}$ that satisfies:

$$T(F(x)) = AT(x) + Bh(x) \quad \forall x \in \mathcal{X} \quad (1.45)$$

and its inverse T^{-1} such that the following system is an observer:

$$\begin{aligned} z_{k+1} &= Az_k + By_k \\ \hat{x}_k &= T^{-1}(z_k) \end{aligned} \quad (1.46)$$

Deep Learning Observer

Given the guaranteed existence of the change of coordinates for a system with a null input under the previous assumptions, deep learning is used to approximate the map T and T^{-1} from data.

Model Architecture

The proposed network is an auto-encoder identifying the mapping T and its inverse T^{-1} :

- The first neural network (see Appendix A.3) (encoder) identifies the latent space $z = T(x)$, respecting the observer dynamic with the loss function:

$$\mathcal{L}_{dyn} = \|T(x_{k+1}) - (AT(x_k) + Bh(x_k))\| \quad (1.47)$$

- The second neural network (decoder) learns T^{-1} to recover the estimation \hat{x} , achieved using the reconstruction loss:

$$\mathcal{L}_{recon} = \|x_k - T^{-1}(T(x_k))\| \quad (1.48)$$

Training

The model is trained by minimizing the loss functions \mathcal{L}_{dyn} and \mathcal{L}_{recon} on a large dataset $D = \{x_k, x_{k+1}\}$, generated from the considered systems. Samples x_k are obtained from a uniform random distribution on \mathcal{X} , while samples x_{k+1} are obtained by applying the system dynamics.

The pair (A, B) is chosen such that A is Hurwitz, with eigenvalues selected to achieve the desired observer response. The matrix B can be chosen to scale the state z , affecting the training process.

1.4.4 Machine Learning for Moving Horizon Estimation

The approach proposed in [88] aims to alleviate the computational burden of the receding horizon observer by training an offline inverse observation function. This function allows for the direct computation of state estimates through simple integration of the system dynamics.

Classical Receding Horizon Observer

Consider the following class of nonlinear systems:

$$\begin{aligned} \dot{x} &= F(x, u), \quad x \in \mathbb{R}^n, \quad x(0) = x_0, \quad u \in \mathbb{R}^m \\ y &= H(x), \quad y \in \mathbb{R}^p \end{aligned} \quad (1.49)$$

where x denotes the state vector, u represents known exogenous inputs, and y denotes measured outputs.

The observability function is defined as $y(t) = \Phi(t, x(t_0))$. The state estimation problem involves using a sequence of output measurements over a time interval to recover the state vector x , assumed to be obtained from physical sensors.

The receding horizon observer estimates states by minimizing a loss function of the output prediction error in a least squares sense over a past receding horizon of length T :

$$\begin{aligned}\{\hat{x}(t-T)\} &= \arg \min_{z \in \mathcal{X}(t-T)} J(t, z, y(.), u(.)) \\ J(t, z, y, u) &= \int_{t-T}^t \|y(\tau) - H(X(\tau, z, u(.)))\|_R^2 d\tau + \|z\|_M^2\end{aligned}\quad (1.50)$$

where the weighting matrix R represents the covariance matrix of the output measurement noise, and M serves as a regularization or uncertainty covariance matrix for z . To avoid solving the optimization problem at each step due to its computational complexity for online applications, neural networks are used to approximate the inverse observability function $\Phi(x, u)^{-1} = \Psi(y, u)$:

$$x(t) = \Psi(y(.), u(.))$$

where $y(.)$ and $u(.)$ are defined over the time interval $[t-T, t]$. If such a function exists, the estimation of $x(t)$ can be obtained for every window of the receding horizon.

Machine Learning Receding Horizon Observer

The challenge lies in approximating the inverse observability function. A one-hidden-layer neural network with N neurons in the hidden layer is employed, with $(n_y + n_u) \times N_T$ input neurons and n output neurons (where N_T is the number of samples in the receding window). The approximation $\Psi(y(.), u(.))$ is given by:

$$\Psi(Z) \approx \sum_{i=1}^N w_i \sigma(\alpha_i^T Z + b_i) + c \quad (1.51)$$

where $Z = (y(t_1), y(t_2), \dots, y(t_{N_T}), u(t_1), u(t_2), \dots, u(t_{N_T}))$ is the vector of sampled inputs and outputs in the interval $[t-T, t]$, $\sigma(.)$ represents the activation function (sigmoid, tanh, etc.), $w_i \in \mathbb{R}^m$, $\alpha_i \in \mathbb{R}^n$ are the weights of the hidden and input layers respectively, and $b_i, c \in \mathbb{R}$ are biases.

The number of neurons N is chosen based on the application, and for large input dimensions, consideration may be given to using convolutional neural networks. Training data consists of M learning samples of initial states $x_k(T)$ and inputs U_k , generated using low-discrepancy sequences to minimize gaps in the training dataset [88], [90]. Given each sample pair $(x_k(T), U_k(T))$, the output sequence can be generated by straightforwardly integrating the system (1.49) over the time interval $[t-T, t]$. The

output sequence is defined as:

$$Y_k(T) = (y_k(t_1), y_k(t_2), \dots, y_k(t_{N_T})) \quad (1.52)$$

A supervised learning technique is employed to optimize the weights of the neural network by addressing the nonlinear regression problem defined by the following loss function:

$$\min_{\theta} \frac{1}{2} \sum_{k=1}^M \|\Psi_{\theta}(Z_k(T)) - x_k(T)\|^2 \quad (1.53)$$

In this context, $Z_k = (Y_k(T), U_k(T))$ for $k = 1, \dots, M$, and θ represents the parameters used to tune the neural network.

Once the network is trained offline, the learned weights can be used for online state observation in each step of the receding horizon.

1.4.5 Neuro-Adaptive Observer

Traditional observer designs for nonlinear systems typically require specific model structures and a priori knowledge of system nonlinearities. Neural networks (NN) have demonstrated significant efficacy in approximating nonlinear functions, leading to the development of adaptive neural network-based observers with online weight adjustment mechanisms.

Problem Statement

Consider a general nonlinear MIMO system:

$$\begin{aligned} \dot{x}(t) &= F(x, u) \\ y(t) &= Cx(t) \end{aligned} \quad (1.54)$$

where $u \in \mathbb{R}^{n_u}$ is the input, $y \in \mathbb{R}^{n_y}$ is the output, $x \in \mathbb{R}^n$ is the state vector, and f is a vector-valued unknown nonlinear function. We assume that the system in (1.54) is observable and that the open-loop system is stable, meaning the states $x(t)$ are bounded in L_{∞} , a common assumption in identification schemes.

Without loss of generality, we can rewrite the system in (1.54) as:

$$\begin{aligned} \dot{x}(t) &= Ax + g(x, u) \\ y(t) &= Cx(t) \end{aligned} \quad (1.55)$$

where A is a Hurwitz matrix, the pair (C, A) is observable, and $g(x, u) = F(x, u) - Ax$. The observer design for this system is:

$$\begin{aligned}\dot{\hat{x}}(t) &= A\hat{x} + \hat{g}(\hat{x}, u) + G(y - C\hat{x}) \\ \hat{y}(t) &= C\hat{x}(t)\end{aligned}\tag{1.56}$$

where \hat{x} is the state of the observer, and the observer gain $G \in \mathbb{R}^{n \times n_y}$ is selected such that $A - GC$ is a Hurwitz matrix, ensuring observability.

Stable Neural Network-Based Observer

Designing a neuro-adaptive observer involves leveraging a neural network to capture nonlinearities while employing a conventional observer for state estimation. A three-layer neural network is capable of approximating nonlinear systems with any level of complexity [87]. For states x confined to a compact set \mathcal{X} , there exist appropriate numbers of hidden layer neurons, weights, and thresholds such that any continuous function defined on \mathcal{X} can be accurately represented.

$$g(x, u) = W\sigma(V\bar{x}) + \varepsilon(x)\tag{1.57}$$

where W and V are the weight matrices of the output and hidden layers, respectively, $\bar{x} = [x \ u]$, $\varepsilon(x)$ is the bounded neural network approximation error, and $\sigma(\cdot)$ is the activation function of the hidden neurons, typically a sigmoidal function.

Thus, g can be approximated by:

$$\hat{g}(\hat{x}, u) = \hat{W}\sigma(\hat{V}\hat{x})\tag{1.58}$$

The proposed observer [87] is then:

$$\begin{aligned}\dot{\hat{x}}(t) &= A\hat{x} + \hat{W}\sigma(\hat{V}\hat{x}) + G(y - C\hat{x}) \\ \hat{y}(t) &= C\hat{x}(t)\end{aligned}\tag{1.59}$$

Defining the estimation error $\tilde{x} = x - \hat{x}$, the error dynamics can be expressed as:

$$\begin{aligned}\dot{\tilde{x}}(t) &= Ax + W\sigma(V\bar{x}) - A\hat{x} - \hat{W}\sigma(\hat{V}\hat{x}) - G(Cx - C\hat{x}) + \varepsilon(x) \\ \tilde{y}(t) &= C\tilde{x}(t)\end{aligned}\tag{1.60}$$

By adding and subtracting $W\sigma(\hat{V}\hat{x})$, we get:

$$\begin{aligned}\dot{\tilde{x}}(t) &= A_c\tilde{x} + \tilde{W}\sigma(\hat{V}\hat{x}) + w(t) \\ \tilde{y}(t) &= C\tilde{x}(t)\end{aligned}\tag{1.61}$$

where $\tilde{W} = W - \hat{W}$, $A_c = A - GC$, and $w(t) = W[\sigma(V\bar{x}) - \sigma(\hat{V}\hat{x})] + \varepsilon(x)$ is a bounded disturbance term, i.e., $\|w(t)\| \leq \bar{w}$ for some positive constant \bar{w} , due to the sigmoidal function and the boundedness of the ideal neural network weights (V, W) .

The weight updating mechanism is based on a modified BP algorithm with an e-modification term for robustness:

$$\begin{aligned}\dot{\hat{W}} &= -\eta_1 (\tilde{y}^T CA_c^{-1})^T (\sigma(\hat{V}\hat{x}))^T - \rho_1 \|\tilde{y}\| \hat{W} \\ \dot{\hat{V}} &= -\eta_2 (\tilde{y}^T CA_c^{-1} \hat{W} (I - \Lambda(\hat{V}\hat{x})))^T \text{sgn}(\hat{x})^T - \rho_2 \|\tilde{y}\| \hat{V}\end{aligned}\tag{1.62}$$

where $\Lambda(\hat{V}\hat{x}) = \text{diag}\{\sigma_i^2(\hat{V}_i\hat{x})\}$ for $i = 1, 2, \dots, m$.

The estimation error, weights errors, and output error \tilde{x} , \tilde{W} , \tilde{V} , \tilde{y} are all bounded in L_∞ . In these equations, $\eta_1, \eta_2 > 0$ are the learning rates, $J = (1/2)(\tilde{y}^T \tilde{y})$ is the objective function, and ρ_1, ρ_2 are small positive numbers.

In (1.62), the first terms are the backpropagation terms and the second terms are e-modification terms that ensure stability and prevent the output error from exploding.

$$\begin{aligned}\dot{\hat{W}} &= -\eta_1 \left(\frac{\partial J}{\partial \hat{W}} \right) - \rho_1 \|\tilde{y}\| \hat{W} \\ \dot{\hat{V}} &= -\eta_2 \left(\frac{\partial J}{\partial \hat{V}} \right) - \rho_2 \|\tilde{y}\| \hat{V}\end{aligned}\tag{1.63}$$

where $\tilde{y} = y(t) - C\hat{x}(t)$.

As the weights W and V are updated online, there are tuning parameters such as the learning rates η_1, η_2 . Larger learning rates lead to faster convergence but may cause overshoots. Damping factors ρ_1 and ρ_2 can improve stability but excessive damping may result in premature convergence to suboptimal weights. The matrix A also affects convergence and accuracy of state estimation.

Form of the Neuro-Adaptive Observer:

The observer design is as follows:

$$\begin{cases} \dot{\hat{x}}(t) = A\hat{x} + \hat{W}\sigma(\hat{V}\hat{x}) + G(y - C\hat{x}) \\ \dot{\hat{W}} = -\eta_1 (\tilde{y}^T CA_c^{-1})^T (\sigma(\hat{V}\hat{x}))^T - \rho_1 \|\tilde{y}\| \hat{W} \\ \dot{\hat{V}} = -\eta_2 (\tilde{y}^T CA_c^{-1} \hat{W} (I - \Lambda(\hat{V}\hat{x})))^T \text{sgn}(\hat{x})^T - \rho_2 \|\tilde{y}\| \hat{V} \end{cases}\tag{1.64}$$

Robust Data-Driven Neuro-Adaptive Observers with Lipschitz Activation Functions

In addressing the same problem, a study [86] proposed using Lipschitz activation functions that are linear-in-parameter and formulated linear matrix inequalities (LMIs) to design neuro-adaptive observers with guaranteed estimation performance.

To estimate the state of the system (1.55), the proposed observer is:

$$\begin{cases} \dot{\hat{x}} = A\hat{x} + \sum_{i=1}^N B_i \hat{W}_i + \hat{W} \bar{\sigma}(\hat{x}, u) + L_0(y - C\hat{x}) & \text{for } i = 1, \dots, n, \\ \dot{\hat{W}}_{ij} = L_k(y - C\hat{x}) & j = 1, \dots, N, \\ & \text{and } k = 1, \dots, nN. \end{cases} \quad (1.65)$$

Here,

$$\bar{\sigma}(\hat{x}, u) = \begin{bmatrix} \sigma_1(H_1\hat{x} + K_1(y - C\hat{x}), u) \\ \vdots \\ \sigma_N(H_N\hat{x} + K_N(y - C\hat{x}), u) \end{bmatrix}$$

The term $\hat{x} \equiv \hat{x}(t)$ represents the estimated state of the system described by (1.55). The matrix $B_i \in \mathbb{R}^{n \times n}$ is a known matrix whose function is detailed in Chapter 3. The vector of estimated weight parameters is denoted by \hat{W} , with the (i, j) th element being \hat{W}_{ij} . The matrices $L_0 \in \mathbb{R}^{n \times n_y}$, $L_k \in \mathbb{R}^{1 \times n_y}$ for $k = 1, \dots, nN$, and $K_i \in \mathbb{R}^{s_i \times n_y}$ for $i = 1, \dots, N$ are observer gain matrices that are determined by solving the observer design LMI.

1.5 Conclusion

In this chapter, we have explored the state of the art in advanced driving assistance systems (ADAS), emphasizing their necessity and the various methodologies employed to achieve effective control. We began by discussing the different types of ADAS, highlighting their critical role in enhancing vehicle safety, improving driving comfort, and reducing the likelihood of accidents.

A key aspect of ADAS is the control mechanisms that govern their operation. These controllers rely heavily on accurate and timely information about the vehicle and its surroundings to function optimally. This necessity underscores the importance of state observers and estimation techniques, which provide the required data for these systems to make informed decisions.

We then presented various vehicle models commonly used in the development of observers. These models are crucial for simulating vehicle dynamics and understanding how different states can be accurately estimated.

Following this, we delved into the different types of state estimation methods, categorizing them into model-based and data-based approaches. We highlighted the strengths and weaknesses of each approach, setting the stage for a discussion on hybrid methodologies that combine the best of both worlds.

Among these hybrid methodologies, we focused on innovative techniques such as neuro-adaptive observers and deep learning-based approaches. Specifically, we examined the Deep KKL observer and the deep learning receding horizon observer, illustrating how these advanced methods leverage both model knowledge and data-driven insights to achieve superior state estimation.

In summary, this chapter has provided a comprehensive overview of the current state of ADAS technology, the vital role of state estimation, and the cutting-edge methodologies being developed to enhance the accuracy and reliability of these systems. These insights lay the groundwork for future advancements in the field, promising even more sophisticated and reliable ADAS solutions.

2

New Discrete Time Interval Observer

Contents

2.1	Introduction	59
2.2	Interval observers for discrete-time LPV systems	60
2.2.1	LPV systems	60
2.2.2	Interval relations	61
2.2.3	Interval Observer for Discrete-LPV systems	61
2.3	Exact finite-time estimation of LPV systems	64
2.3.1	System description	64
2.3.2	Finite time estimation by using two combined observers . . .	65
2.3.3	Design of the estimator parameters	66
2.4	Finite-time interval estimator design	68
2.4.1	Problem formulation	68
2.4.2	Application of developed estimation algorithm to vehicle lateral model	72
2.4.3	Comparative study	76
2.5	Conclusion	79

2.1 Introduction

The field of state estimation has been a cornerstone in control theory and has found extensive applications in various domains, including robotics, navigation, and process control. Traditional state estimation techniques, such as Kalman filters, have been widely used due to their effectiveness in dealing with Gaussian noise and linear systems. However, these methods often fail when dealing with systems characterized by significant uncertainties and disturbances. In recent years, interval observers have emerged as a promising alternative for state estimation in uncertain systems. Unlike point estimators, which provide a single estimate of the state, interval observers provide a range within which the state of the system is guaranteed to reside. This approach takes into account known bounds for the initial condition and uncertain quantities, offering a robust way to handle uncertainties. Despite the advantages of interval observers, their application in discrete-time systems has been relatively limited. Most of the existing methods for interval estimation in discrete-time systems are based on the transformation of continuous-time interval observers. However, these methods often lead to conservative estimates and require the solution of complex optimization problems. In our research, we have developed a novel “Discrete-Time Interval Estimator” that directly operates in the discrete-time domain. This estimator is inspired by the parity space approach, a well-established method in fault detection and isolation. Our approach combines the parity space approach with zonotope-based interval analysis, a mathematical tool that allows efficient computation of interval estimates. The proposed estimator operates by optimizing a parameter matrix to minimize the length of the edges of the outer box of the error zonotope. This approach ensures that the resulting interval estimate is as tight as possible, thereby improving the accuracy of the estimation.

Our work represents a significant advancement in the field of state estimation. By developing a discrete-time interval estimator, we have opened up new possibilities for the application of interval observers in digital control systems. We believe that our work will inspire further research in this area and contribute to the development of more robust and accurate state estimation methods.

The focus of this work is the design of an interval observer for a class of discrete LPV systems that contains measured and unmeasured variable parameters. The finite-time state estimation procedure is used to estimate the exact state without uncertainty, and then algebraically calculated bounds are added to the estimation depending on the parameter variation. Compared to other interval observers, the proposed observer does not rely on conservative assumptions about the system's (e.g., nonnegative Schur stable (resp. Metzler and Hurwitz)). Moreover, no assumptions about the initial state of the observer are assumed, and the added bounds to the nominal estimator are calculated algebraically, giving more accurate results.

2.2 Interval observers for discrete-time LPV systems

The process of designing interval observers for discrete-time LPV systems closely mirrors that of continuous-time LPV systems. This methodology predominantly hinges on leveraging monotone system theory (MST) to establish cooperative interval estimation error dynamics, a task known for its inherent complexity [91], [92].

In response, efforts such as in [93] have introduced an LTI interval observer technique within the L_1/L_2 framework to address LPV systems. However, this approach tends to yield overly conservative solutions. Similarly, [94] proposed an L_∞ performance-based method, but its applicability is limited to LTI processes.

In contrast, a novel approach proposed in [95] centers around designing interval state estimation based on the observability matrix. This method aims to address the aforementioned challenges by utilizing the observability matrix and available input-output measurements to establish guaranteed bounds on the real state of the system. Importantly, this method does not necessitate perfect cooperation within the system and is less restrictive compared to previous techniques.

2.2.1 LPV systems

A Linear Parameter-Varying (LPV) system is a type of control system whose dynamics are linear in the state and input but whose system matrices depend on a set of time-varying parameters, denoted as $\rho(t)$. These parameters can represent varying operating conditions or external influences on the system. The state-space representation of an LPV system can be expressed as follows:

$$\dot{x}(t) = A(\rho)x(t) + w(t) \quad (2.1)$$

with $A(\rho) = \sum_{j=1}^p \rho_j A_j$ and $w(t) \in \mathbb{R}_+^n$ where $x(t) \in \mathbb{R}^n$ and ρ is an exogenous parameter that can be dependent on time as $\sum_{j=1}^p \rho_j(t) = 1, \rho_j(t) \geq 0$ for all $j = 1, 2, \dots, p$.

Definition 2.2.1

A Linear Parameter-Varying (LPV) system is said to be **positive** for any parameter function ρ taking values in the simplex set, if and only if the matrices A_1, A_2, \dots, A_p are Metzler matrices (i.e meaning all their off-diagonal elements are non-negative). This ensures that the state variables do not negatively influence each other).

2.2.2 Interval relations

An interval vector $x \in \mathbb{R}^n$ is defined by $\underline{x} \leq x \leq \bar{x}$, where \underline{x} and \bar{x} are the endpoints, with the inequalities understood elementwise. For two vectors $x_1, x_2 \in \mathbb{R}^n$ or matrices $A_1, A_2 \in \mathbb{R}^{n \times n}$, the relationship $x_1 \leq x_2$ and $A_1 \leq A_2$ is also understood elementwise. For a matrix $A \in \mathbb{R}^{m \times n}$, we define $A^+ = \max\{A, 0\}$, $A^- = \max\{-A, 0\}$, and $A = A^+ - A^-$.

Lemma 2.2.1

Let $x \in \mathbb{R}^n$ be a vector variable, $\underline{x} \leq x \leq \bar{x}$ for some $\underline{x}, \bar{x} \in \mathbb{R}^n$ and $A \in \mathbb{R}^{m \times n}$ be a constant matrix, then

$$A^+ \underline{x} - A^- \bar{x} \leq Ax \leq A^+ \bar{x} - A^- \underline{x}. \quad (2.2)$$

Lemma 2.2.2

Let $\underline{A} \leq A \leq \bar{A}$ for some $\underline{A}, \bar{A}, A \in \mathbb{R}^{n \times n}$ and $\underline{x} \leq x \leq \bar{x}$ for $\underline{x}, \bar{x}, x \in \mathbb{R}^n$, then

$$\underline{A}^+ \underline{x}^+ - \bar{A}^+ \bar{x}^- - \underline{A}^- \bar{x}^+ + \bar{A}^- \underline{x}^- \leq Ax \leq \bar{A}^+ \bar{x}^+ - \underline{A}^+ \bar{x}^- - \bar{A}^- \underline{x}^+ + \underline{A}^- \underline{x}^- . \quad (2.3)$$

2.2.3 Interval Observer for Discrete-LPV systems

System Description

Consider a discrete-time LPV system of the form :

$$\begin{aligned} x_{k+1} &= [A_0 + \Delta A(\rho_k)]x_k + Bu_k + d_k \\ y_k &= Cx_k + v_k \end{aligned} \quad (2.4)$$

Here, $x_k \in \mathbb{R}^n$ is the state, $y_k \in \mathbb{R}^p$ is the output available for measurements, and $u_k \in \mathbb{R}^m$ is the control input. The vector of scheduling parameters is $\rho_k \in \Pi \subset \mathbb{R}^r$, with a known

set Π and $\rho \in \mathcal{L}^{\infty^r}$. The values of the scheduling vector ρ are not directly measurable; only the set of admissible values Π is given. The matrices $A_0 \in \mathbb{R}^{n \times n}$, $B \in \mathbb{R}^{n \times n}$, and $C \in \mathbb{R}^{p \times n}$ are known, and the matrix function $\Delta A : \Pi \rightarrow \mathbb{R}^{n \times n}$ is known. The signals $d \in \mathcal{L}^{\infty^n}$ and $v \in \mathcal{L}_{\infty}^p$ represent the exogenous disturbance and measurement noise, respectively, but their exact current values d_k and v_k are not available.

Assumption 2.2.1. $\underline{d}_k \leq d_k \leq \bar{d}_k$ and $|v_k| \leq V$ for all $t \in \mathbb{Z}_+$ and for some known $d, \bar{d} \in \mathcal{L}_{\infty}^n$ and $V \in \mathbb{R}_+$.

Assumption 2.2.2. $\underline{\Delta A} \leq \Delta A(\rho) \leq \bar{\Delta A}$ for all $\rho \in \Pi$ and some known $\underline{\Delta A}, \bar{\Delta A} \in \mathbb{R}^{n \times n}$.

Observer design

The interval observer equations for system (2.4) are given by:

$$\begin{aligned}\underline{x}_{k+1} &= [A_0 - \underline{LC}] \underline{x}_k + Bu_k + [\underline{\Delta A}^+ \underline{x}_k^+ - \bar{\Delta A}^+ \underline{x}_k^- - \underline{\Delta A}^- \bar{x}_k^+ + \bar{\Delta A}^- \bar{x}_k^-] + \underline{L}y_k - |\underline{L}|VE_p + \underline{d}_k \\ \bar{x}_{k+1} &= [A_0 - \bar{LC}] \bar{x}_k + Bu_k + [\bar{\Delta A} \bar{x}_k^+ - \underline{\Delta A}^+ \bar{x}_k^- - \bar{\Delta A}^- \underline{x}_k^+ + \underline{\Delta A}^- \bar{x}_k^-] + \bar{L}y_k + |\bar{L}|VE_p + \bar{d}_k\end{aligned}\quad (2.5)$$

Here, \underline{x}_t and \bar{x}_t are the lower and upper interval estimates of x_t , respectively. The observer gains, $\underline{L} \in \mathbb{R}^{n \times p}$ and $\bar{L} \in \mathbb{R}^{n \times p}$, need to be designed and E_p denotes the matrix with elements equal to 1 with dimension $p \times 1$. Note that because of the presence of \underline{x}_t^+ , \underline{x}_t^- , \bar{x}_t^+ , and \bar{x}_t^- , the interval observer (2.5) forms a globally Lipschitz nonlinear system.

The conditions that must be imposed on the gains \underline{L} and \bar{L} to ensure interval estimation of x_t and the boundedness of \underline{x}_t and \bar{x}_t are outlined in the following theorem.

Theorem 2.2.1: [92]

Let Assumptions 2.2.2 and Assumptions 2.2.1 be satisfied, Then, the relations

$$\underline{x}_k \leq x_k \leq \bar{x}_k \quad \forall k \in \mathbb{Z}_+ \quad (2.6)$$

are satisfied provided that $\underline{x}_0 \leq x_0 \leq \bar{x}_0$. In addition, if there exist a diagonal matrix $P \in \mathbb{R}^{2n \times 2n}, P > 0$ (i.e. $P > 0$), a matrix $Q \in \mathbb{R}^{2n \times 2n}, Q = Q^T > 0$ and constants $\varepsilon_1 > 0, \varepsilon_2 > 0, \gamma > 0$ such that the following matrix inequality is verified

$$\begin{aligned} \Phi &= \begin{bmatrix} \Psi & G^T P \\ PG & (1 + \varepsilon_2)P - \gamma I_{2n} \end{bmatrix} \preceq 0, \\ \Psi &= (1 + \varepsilon_1)G^T PG - P + Q + \gamma\eta^2 I_{2n}, \end{aligned} \quad (2.7)$$

where $\eta = 2 \left(\left\| \underline{\Delta A}^+ - \bar{\Delta A}^+ \right\|_2 + \left\| \underline{\Delta A}^- \right\|_2 + \left\| \bar{\Delta A}^- \right\|_2 \right)$ and

$$G = \begin{bmatrix} A_0 - \underline{L}C + \underline{\Delta A}^+ & 0 \\ 0 & A_0 - \bar{L}C + \bar{\Delta A}^+ \end{bmatrix},$$

then $\underline{x}, \bar{x} \in \mathcal{L}^n$

Remark 2.2.3. Interval observers are useful for estimating the state of dynamic systems within a bounded range, but they come with some notable limitations [64], [95]–[97], especially in the context of discrete-time Linear Parameter-Varying (LPV) systems. Here are some of the main challenges:

- **Conservatism:** Interval observers can be too conservative, producing larger intervals than necessary. This reduces the precision of the state estimation.
- **Time-Varying Parameters:** In **discrete-time LPV systems**, the parameters change rapidly, making it hard to accurately capture system dynamics within the bounded intervals.
- **Complex Design and Implementation:** The design and implementation of interval observers for these systems require sophisticated mathematical techniques and significant computational resources, making the process complex and computationally demanding.
- **Matrix Transformations:** For discrete-time systems, a Schur stable system must be transformed into a Schur and nonnegative one [98]. This means that sub-observers are designed to simultaneously satisfy positivity and stability conditions for the error dynamics.

- **Cooperativity of Interval Estimation Error Dynamics:** Ensuring that the interval estimation error dynamics are cooperative is a fundamental challenge [64]. This condition is crucial for keeping estimation errors within computed bounds but can be hard to achieve, especially in complex or highly variable systems.

These factors can limit the practicality and real-time applicability of interval observers in certain scenarios, highlighting the need for ongoing research to address these challenges and improve their effectiveness.

2.3 Exact finite-time estimation of LPV systems

2.3.1 System description

We examine the class of Linear Parameter-Varying (LPV) systems characterized by the following set of equations:

$$\begin{aligned} x_{k+1} &= \mathbb{A}(\rho_k)x_k + Bu_k \\ y_k &= Cx_k \end{aligned} \tag{2.8}$$

Here, $\mathbf{x}_k \in \mathbb{R}^n$ represents the state vector, $\mathbf{y}_k \in \mathbb{R}^p$ denotes the output measurement, and $\mathbf{u}_k \in \mathbb{R}^m$ is the control input vector. The parameter $\rho_k \in \Theta \subset \mathbb{R}^r$ is a bounded, time-varying variable. The matrices B and C are constants with appropriate dimensions, while the matrix $\mathbb{A}(\rho_k)$ is affine in ρ_k .

We pose the following assumptions :

Assumption 2.3.1. For any $k \in \mathbb{N}$, the parameter ρ_k is both known and bounded. Additionally, the set Θ remains independent of the specific value chosen for k .

Assumption 2.3.2. The matrix $A(\rho_k)$ can be written in the form:

$$\mathbb{A}(\rho_k) = A_0 + \Delta A(\rho_k),$$

where $\Delta A(\rho_k) \in Co(A_1, \dots, A_{n_p})$, namely

$$\mathbb{A}(\rho_k) = A_0 + \sum_{i=1}^{n_p} \xi^i(\rho_k) A_i \tag{2.9}$$

where for any $k \geq 1$, $\xi^i(\rho) > 0$ and $\sum_{i=1}^{n_p} \xi^i(\rho) = 1$;

Assumption 2.3.3. the pairs (A_i, C) are observable $\forall i = 0, \dots, n_p$.

In this approach [99], the parameters $\xi^i(\rho_k)$, which are functions of ρ_k , are derived by expressing the bounded parameters ρ_k as a convex combination of their constant bounds. This transformation utilizes mathematical principles from convexity and convex sets. A method showing the computation of $\xi^i(\rho_k)$ is provided in (2.37).

2.3.2 Finite time estimation by using two combined observers

In the context of the class of systems described by (2.8), an exact estimation of x_k can be achieved using two combined asymptotic observers, as demonstrated for the continuous-time case in [100], [101]. Before proposing the first observer that provides an exact finite-time estimation of the state x_k , we state the following useful lemma.

Lemma 2.3.1: [99]

Assume that the pairs (A_j, C) are observable for all $j = 0, \dots, n_\rho$. Then, there exist L_i, K_i such that the matrix:

$$\mathbb{E}_m(k) \triangleq \left[\prod_{i=1}^m (\mathbb{A}(\rho_{k-i}) - \mathbb{L}(\rho_{k-i})C) \right]^{-1} - \left[\prod_{i=1}^m (\mathbb{A}(\rho_{k-i}) - \mathbb{K}(\rho_{k-i})C) \right]^{-1}. \quad (2.10)$$

with $\mathbb{A}(\rho_{k-i})$, $\mathbb{L}(\rho_{k-i})$ and $\mathbb{K}(\rho_{k-i})$ defined in (2.9) and (2.17) respectively, exist and is invertible for all $k \geq m$.

Proof. For the proof, please refer to [99]. □

The results are presented in the following theorem.

Theorem 2.3.1: [99]

Assume that the gain matrices L_i and K_i are chosen such that:

- All eigenvalues of $(A_i - L_i C)$ and $(A_i - K_i C)$ are non-zero and lie within the unit circle of the complex plane;
- There exists an integer $m \geq 1$ such that the matrix $\mathbb{E}_m(k)$ exists and is invertible.

Then the combined observers and the estimation of x_k can be written as follow :

$$\zeta_{k+1} = \mathbb{A}(\rho_k) \zeta_k + Bu_k + \mathbb{L}(\rho_k)(y_k - C\zeta_k) \quad (2.11a)$$

$$\eta_{k+1} = \mathbb{A}(\rho_k) \eta_k + Bu_k + \mathbb{K}(\rho_k)(y_k - C\eta_k) \quad (2.11b)$$

$$\begin{aligned} \hat{x}_k &= \mathbb{E}_m^{-1}(k) \left[\left(\prod_{j=1}^m (\mathbb{A}(\rho_{k-j}) - \mathbb{L}(\rho_{k-j})C) \right)^{-1} \zeta_k \right. \\ &\quad \left. - \left(\prod_{j=1}^m (\mathbb{A}(\rho_{k-j}) - \mathbb{K}(\rho_{k-j})C) \right)^{-1} \eta_k \right. \\ &\quad \left. + \eta_{k-m} - \zeta_{k-m} \right] \end{aligned} \quad (2.11c)$$

is an observer for system (2.8), which converges in finite time $m \geq 1$.

2.3.3 Design of the estimator parameters

In this subsection, we provide a complete characterization of the interval estimator by introducing an algorithm to calculate the values of the gains L_i and K_i for $i = 1, \dots, n_\rho$. The design of these gains aims to ensure that the matrix $\mathbb{E}_m(k)$ is invertible for a given $m \geq 1$ and for all $k \geq m$.

The subsequent theorem suggests a design of the gains L_i (and K_i) that guarantees the error $\xi_k - x_k$ (and $\eta_k - x_k$) is asymptotically stable. Since the systems ξ_k and η_k share the same dynamics, setting the gains L_i and K_i too close will lead to a numerical conditioning problem when inverting $E_m(k)$, even if it is invertible. This numerical issue could eventually result in poor estimation. The LMIs proposed in the following theorem consider this numerical conditioning problem.

Theorem 2.3.2: [99]

Assume that there exist symmetric positive definite matrices P_i and square matrices \mathbb{X}_i and \mathbb{Z}_i and positive scalar $\alpha_i < 1$ for $i = 1, \dots, n_p$ such that the following LMI conditions hold:

$$\begin{bmatrix} \mathbb{P}_j - \mathbb{X}_i - \mathbb{X}_i^\top & (\alpha_i)^{-1}(\mathbb{X}_i A_i - \mathbb{Z}_i C) \\ (\alpha_i)^{-1}(\mathbb{X}_i A_i - \mathbb{Z}_i C)^\top & -\mathbb{P}_i \end{bmatrix} < 0 \quad \forall i, j = 0, \dots, n_p. \quad (2.12)$$

Then the estimation error $\xi_k - x_k$ converges asymptotically for $L_i = \mathbb{X}_i^{-1}\mathbb{Z}_i$.

Moreover if the eigenvalues of $A_i - K_i C$ are needed to be greater than the eigenvalues of $A_i - L_i C$ while ensuring the poly-quadratic convergence, the following LMI

$$\begin{bmatrix} \mathbb{P}_j - \mathbb{Y}_i - \mathbb{Y}_i^\top & 2(\mathbb{Y}_i A_i - \mathbb{S}_i C) \\ 2(\mathbb{Y}_i A_i - \mathbb{S}_i C)^\top & -\mathbb{P}_i \end{bmatrix} < 0 \quad (2.13)$$

needs to be solved with respect to the variables \mathbb{Y}_i and \mathbb{S}_i with $K_i = \mathbb{Y}_i^{-1}\mathbb{S}_i$, together with

$$2\beta_i \mathbb{Y}_i - (\mathbb{Y}_i A_i - \mathbb{S}_i C) - (\mathbb{Y}_i A_i - \mathbb{S}_i C)^\top < 0, \quad (2.14)$$

$$-2\beta_i \mathbb{Y}_i + (\mathbb{Y}_i A_i - \mathbb{S}_i C) + (\mathbb{Y}_i A_i - \mathbb{S}_i C)^\top < 0. \quad (2.15)$$

Once the gains L_i and K_i are calculated we check if the matrix $\mathbb{E}_m(k)$ is invertible and well conditioned for $1 \leq m \leq m^*$, where m^* is a fixed integer representing the maximum desired value of m . If there is no $m \leq m^*$ such that $\mathbb{E}_m(k)$ is invertible the scalars α_i, β_i need to be changed and increased and the new gains L_i and K_i to be recomputed. The following algorithm provides a summary of the numerical design procedure.

Remark 2.3.4. *Algorithm 1 is used on a system without any uncertainty to compute the gains \mathbb{L} and \mathbb{K} . It employs sufficient LMI conditions related to poly-quadratic stability, which can sometimes result in a non-invertible matrix $E_m(k)$. To address this, we introduce a second parameter β_i to effectively separate the eigenvalues and utilize QMI regions. This approach reduces the conservatism of the algorithm and increases the likelihood of obtaining an invertible matrix $E_m(k)$. Furthermore, Algorithm 1 is crucial because it ensures the asymptotic stability of the estimation errors $x_i - \hat{x}_i$ and $x_i - \tilde{x}_i$. This is a key reason for its introduction. This property influences the estimation before finite-time convergence (for $k = 1, \dots, m-1$). For example, in high-dimensional systems, the finite-time convergence $m \geq 1$ can be significant. Thus, if the asymptotic convergence of $x_i - \hat{x}_i$ and $x_i - \tilde{x}_i$ is not ensured, the estimation may be inaccurate for $k = 1, \dots, m-1$.*

Algorithm 1 Poly-quadratic stability based algorithm

Step 1. Choose $m^* \geq 1$ and small values $\alpha_i, \beta_i, i = 1, \dots, n_p$, with $\alpha_i < \beta_i$.

Step 2. Solve LMIs (2.12) and compute the gains:

- $L_i = X_i^{-1}Z_i$.

Step 3. Solve jointly LMIs (2.13) and (2.14)

if LMIs (2.13) and (2.14) are feasible **then**

 Compute $K_i = Y_i^{-1}S_i$;

else

 Solve LMIs (2.13) and (2.15) and compute

- $K_i = Y_i^{-1}S_i$.

end if

Step 4. Check invertibility of the matrix $E_l(k)$:

for $l \leftarrow 1$ to m^* and $k \geq 1$ **do**

if $E_l(k)$ is invertible **then**

return $l \leftarrow m$; **break**;

else

 Increase the values of α_i, β_i and go to Step 2 to generate new observer gains L_i and K_i .

end if

end for

2.4 Finite-time interval estimator design

2.4.1 Problem formulation

Designing observers for LPV systems that include both measured and unmeasured time-varying uncertain parameters is generally a challenging task. When it is impossible to estimate the state trajectory with arbitrary accuracy, it becomes particularly useful to estimate an envelope that encompasses all possible state trajectories of the admissible uncertain dynamical system. In process monitoring applications, this estimated interval indicates the worst-case range of the states. In this section, we will present the interval observer design for such a class of LPV systems. We consider the class of LPV systems defined by the following set of equations:

$$\begin{aligned} x_{k+1} &= \mathbb{A}(\rho_k)x_k + B_u u_k + B_v v_k, \\ y_k &= Cx_k, \end{aligned} \tag{2.16}$$

where $x_k \in \mathbb{R}^n$ is the state vector, $y_k \in \mathbb{R}^p$ is the output measurement and $u_k \in \mathbb{R}^m$ is the control input vector, $\rho_k \in \Theta \subset \mathbb{R}^r$ is a bounded measured time-varying parameter and $v_k \in \Xi \subset \mathbb{R}^l$ is a bounded unmeasured time-varying uncertainty.

The technical proofs presented in this section will make use of the cited in previous

section **Assumption 2.3.1**, **Assumption 2.3.2** and **Assumption 2.3.3**. We consider the following LPV observer gains :

$$\mathbb{L}(\rho_k) = L_0 + \sum_{i=1}^{n_\rho} \xi^i(\rho_k) L_i, \quad \mathbb{K}(\rho_k) = K_0 + \sum_{i=1}^{n_\rho} \xi^i(\rho_k) K_i. \quad (2.17)$$

We design the gains $\mathbb{L}(\rho_k)$ and $\mathbb{K}(\rho_k)$ using Algorithm 1.

According to Lemma 2.3.1 , given that the matrix $\mathbb{E}_m(k)$ defined in (2.10) exists and is invertible $\forall k \geq m$ and $m \geq 1$, a direct estimation of the state x_k can be computed as follow, see [99]:

$$\begin{aligned} x_k &= \mathbb{E}_m^{-1}(k) \sum_{j=1}^m \left[\left(\prod_{l=1}^m (\mathbb{A}(\rho_{k-l}) - \mathbb{L}(\rho_{k-l})C) \right)^{-1} \times \left(\prod_{i=1}^{j-1} (\mathbb{A}(\rho_{k-i}) - \mathbb{L}(\rho_{k-i})C) \right) \mathbb{L}(\rho_{k-j}) \right. \\ &\quad \left. - \left(\prod_{l=1}^m (\mathbb{A}(\rho_{k-l}) - \mathbb{K}(\rho_{k-1})C) \right)^{-1} \times \left(\prod_{i=1}^{j-1} (\mathbb{A}(\rho_{k-i}) - \mathbb{K}(\rho_{k-i})C) \right) \mathbb{K}(\rho_{k-j}) \right] y_{k-j} \\ &\quad + \mathbb{E}_m^{-1}(k) \sum_{j=1}^m \left[\left(\prod_{l=1}^m (\mathbb{A}(\rho_{k-l}) - \mathbb{L}(\rho_{k-l})C) \right)^{-1} \times \left(\prod_{i=1}^{j-1} (\mathbb{A}(\rho_{k-i}) - \mathbb{L}(\rho_{k-i})C) \right) \right. \\ &\quad \left. - \left(\prod_{l=1}^m (\mathbb{A}(\rho_{k-l}) - \mathbb{K}(\rho_{k-l})C) \right)^{-1} \times \left(\prod_{i=1}^{j-1} (\mathbb{A}(\rho_{k-i}) - \mathbb{K}(\rho_{k-i})C) \right) \right] B_u u_{k-j} \\ &\quad + \mathbb{E}_m^{-1}(k) \sum_{j=1}^m \left[\left(\prod_{l=1}^m (\mathbb{A}(\rho_{k-l}) - \mathbb{L}(\rho_{k-l})C) \right)^{-1} \times \left(\prod_{i=1}^{j-1} (\mathbb{A}(\rho_{k-i}) - \mathbb{L}(\rho_{k-i})C) \right) \right. \\ &\quad \left. - \left(\prod_{l=1}^m (\mathbb{A}(\rho_{k-l}) - \mathbb{K}(\rho_{k-l})C) \right)^{-1} \times \left(\prod_{i=1}^{j-1} (\mathbb{A}(\rho_{k-i}) - \mathbb{K}(\rho_{k-i})C) \right) \right] B_v v_{k-j}, \end{aligned} \quad (2.18)$$

with the following convention for $j = 1$:

$$\left(\prod_{i=1}^{j-1} (\mathbb{A}(\rho_{k-i}) - \mathbb{L}(\rho_{k-i})C) \right)_{j=1} = \left(\prod_{i=1}^{j-1} (\mathbb{A}(\rho_{k-i}) - \mathbb{K}(\rho_{k-i})C) \right)_{j=1} = \mathbb{I}_n. \quad (2.19)$$

Since the time-varying uncertainty v_k is unmeasurable and unknown, it is not possible to use (2.18) to construct the state x_k directly. This is why an estimation of the state x_k is necessary and can be obtained using two combined asymptotic observers with

state vectors ζ_k and η_k as defined in (2.20).

$$\zeta_{k+1} = \mathbb{A}(\rho_k) \zeta_k + B_u u_k + \mathbb{L}(\rho_k) (y_k - C \zeta_k), \quad (2.20a)$$

$$\eta_{k+1} = \mathbb{A}(\rho_k) \eta_k + B_u u_k + \mathbb{K}(\rho_k) (y_k - C \eta_k), \quad (2.20b)$$

$$\begin{aligned} x_k &= \mathbb{E}_m^{-1}(k) \left[\left(\prod_{j=1}^m (\mathbb{A}(\rho_{k-j}) - \mathbb{L}(\rho_{k-j}) C) \right)^{-1} \zeta_k - \left(\prod_{j=1}^m (\mathbb{A}(\rho_{k-j}) - \mathbb{K}(\rho_{k-j}) C) \right)^{-1} \eta_k \right. \\ &\quad \left. + \eta_{k-m} - \zeta_{k-m} \right] \\ &\quad + \mathbb{E}_m^{-1}(k) \sum_{j=1}^m \left[\left(\prod_{l=1}^m (\mathbb{A}(\rho_{k-l}) - \mathbb{L}(\rho_{k-l}) C) \right)^{-1} \times \left(\prod_{i=1}^{j-1} (\mathbb{A}(\rho_{k-i}) - \mathbb{L}(\rho_{k-i}) C) \right) \right. \\ &\quad \left. - \left(\prod_{l=1}^m (\mathbb{A}(\rho_{k-l}) - \mathbb{K}(\rho_{k-l}) C) \right)^{-1} \times \left(\prod_{i=1}^{j-1} (\mathbb{A}(\rho_{k-i}) - \mathbb{K}(\rho_{k-i}) C) \right) \right] B_v v_{k-j}, \end{aligned} \quad (2.20c)$$

Therefore, we express it in the following form:

$$\begin{aligned} \hat{x}_k &= \mathbb{E}_m^{-1}(k) \left[\left(\prod_{j=1}^m (\mathbb{A}(\rho_{k-j}) - \mathbb{L}(\rho_{k-j}) C) \right)^{-1} \zeta_k \right. \\ &\quad \left. - \left(\prod_{j=1}^m (\mathbb{A}(\rho_{k-j}) - \mathbb{K}(\rho_{k-j}) C) \right)^{-1} + \eta_k + \eta_{k-m} - \zeta_{k-m} \right] \\ &\quad + \sum_{j=1}^m G_j(k) v_{k-j}, \end{aligned} \quad (2.21)$$

with

$$\begin{aligned} G_j(k) &= \mathbb{E}_m^{-1}(k) \left[\left(\prod_{l=1}^m (\mathbb{A}(\rho_{k-l}) - \mathbb{L}(\rho_{k-l}) C) \right)^{-1} \times \left(\prod_{i=1}^{j-1} (\mathbb{A}(\rho_{k-i}) - \mathbb{L}(\rho_{k-i}) C) \right) \right. \\ &\quad \left. - \left(\prod_{l=1}^m (\mathbb{A}(\rho_{k-l}) - \mathbb{K}(\rho_{k-l}) C) \right)^{-1} \times \left(\prod_{i=1}^{j-1} (\mathbb{A}(\rho_{k-i}) - \mathbb{K}(\rho_{k-i}) C) \right) \right] B_v. \end{aligned} \quad (2.22)$$

The precise computation of x_k as shown in equation (2.20c) is not feasible because the variable v_k is not measurable. Therefore, the approach presented next focuses on designing an interval observer that provides both upper and lower bounds for the state

x_k . The estimate \hat{x}_k will represent the mean value between these bounds at each time instant $k \in \mathbb{N}$.

Let us introduce the following notations. For two matrices $A_1, A_2 \in \mathbb{R}^{n \times n}$ or two vectors $x_1, x_2 \in \mathbb{R}^n$, the relations $A_1 \leq A_2$ and $x_1 \leq x_2$ are understood element-wise. Moreover, given a matrix $A \in \mathbb{R}^{n \times n}$, we define $A^+ = \max\{0, A\}$ and $A^- = A^+ - A$. Similarly, for $x \in \mathbb{R}$, where $x^+ = \max\{0, x\}$ and $x^- = x^+ - x$.

Lemma 2.4.1: [102]

Let $x \in \mathbb{R}^n$ be a vector variable, with $\underline{x} \leq x \leq \bar{x}$ for some $\underline{x}, \bar{x} \in \mathbb{R}^n$, and $A \in \mathbb{R}^{n \times n}$ then,

$$A^+ \underline{x} - A^- \bar{x} \leq Ax \leq A^+ \bar{x} - A^- \underline{x}. \quad (2.23)$$

Using Lemma 2.4.1 and the state estimation from (2.21), we can find bounds to the uncertain part ($\sum_{j=1}^m G_j(k) v_{k-j}$) in (2.21) since the system is known in each time instant k and the bounds of the uncertainty are known.

The aim is to calculate an interval of admissible values of the state vector x_k , i.e., $x_k \in [\hat{x}_k^-, \hat{x}_k^+]$. To this end, an interval observer can be designed as follows:

$$\left\{ \begin{array}{l} \hat{x}_k^+ = \mathbb{E}_m^{-1}(k) \left[\left(\prod_{j=1}^m (\mathbb{A}(\rho_{k-j}) - \mathbb{L}(\rho_{k-j}) C) \right)^{-1} \zeta_k - \left(\prod_{j=1}^m (\mathbb{A}(\rho_{k-j}) - \mathbb{K}(\rho_{k-j}) C) \right)^{-1} \eta_k \right. \\ \quad \left. + \eta_{k-m} - \zeta_{k-m} \right] + \bar{\mathbb{G}}(k), \\ \hat{x}_k^- = \mathbb{E}_m^{-1}(k) \left[\left(\prod_{j=1}^m (\mathbb{A}(\rho_{k-j}) - \mathbb{L}(\rho_{k-j}) C) \right)^{-1} \zeta_k - \left(\prod_{j=1}^m (\mathbb{A}(\rho_{k-j}) - \mathbb{K}(\rho_{k-j}) C) \right)^{-1} \eta_k \right. \\ \quad \left. + \eta_{k-m} - \zeta_{k-m} \right] + \underline{\mathbb{G}}(k), \end{array} \right. \quad (2.24)$$

with $\underline{\mathbb{G}}(k) = \sum_j^m \underline{\mathbb{G}}_j(k)$ and $\bar{\mathbb{G}}(k) = \sum_j^m \bar{\mathbb{G}}_j(k)$, where $\underline{\mathbb{G}}_j(k) = G_j^+(k) \underline{v} - G_j^-(k) \bar{v}$ and $\bar{\mathbb{G}}_j(k) = G_j^+(k) \bar{v} - G_j^-(k) \underline{v}$.

Since the bounds of $v_k \in [\underline{v}, \bar{v}]$ are known for all k , based on Lemma 2.4.1 we can get the following bounds:

$$\underbrace{G_j^+(k) \underline{v} - G_j^-(k) \bar{v}}_{\underline{\mathbb{G}}_j(k)} \leq G_j(k) v_k \leq \underbrace{G_j^+(k) \bar{v} - G_j^-(k) \underline{v}}_{\bar{\mathbb{G}}_j(k)}. \quad (2.25)$$

We compute the bounds $\underline{\mathbb{G}}(k)$ and $\overline{\mathbb{G}}(k)$ at each time instant k and we add it to the estimation of the state \hat{x}_k in (2.21). Thus, we will have the original system state bounded as follow :

$$\hat{x}_k^- \leq x_k \leq \hat{x}_k^+ \quad \forall k \geq m$$

Remark 2.4.1. *Our methodology addresses some of the limitations of existing interval observers by employing a novel strategy of connecting two asymptotic observers to estimate the state. This approach allows us to compute bounds algebraically, resulting in smaller estimation intervals. Consequently, the conservative assumptions often used in other studies for designing interval observers for LPV systems are no longer necessary. Additionally, because the intervals are computed algebraically, they are tighter and more precise compared to those produced by traditional LPV interval observers. Furthermore, we have leveraged the existing method of finite-time estimation double observers, enabling us to develop an interval observer that bounds the state in finite time. This significantly enhances the efficiency and practicality of our interval observer in real-time applications.*

2.4.2 Application of developed estimation algorithm to vehicle lateral model

In this part, we demonstrate the efficiency and practicality of the proposed interval observer on the lateral model of the vehicle. The numerical execution is carried out using MATLAB.

Vehicle lateral model

The lateral dynamics of a vehicle can be characterized by a bicycle model, as illustrated in Figure 2.1. This is a two-degree-of-freedom vehicle model with the slip angle and yaw rate as the state variables, according to [7]. The dynamics model is derived from the equations of force balance and moment balance, as follows:

$$\begin{cases} mv_x(\dot{\beta} + r) = F_{yf} + F_{yr}, \\ I_z\dot{r} = l_f F_{yf} - l_r F_{yr}, \end{cases} \quad (2.26)$$

where m , I_z , and l_r , l_f denote the mass of the chassis, the yaw moment and the distances from the rear and the front axle to the center of the gravity, respectively. v_x is the time varying longitudinal velocity, β is the side slip angle of the vehicle and r is the yaw rate. The lateral rear and front forces are described as F_{yr} , F_{yf} , respectively.

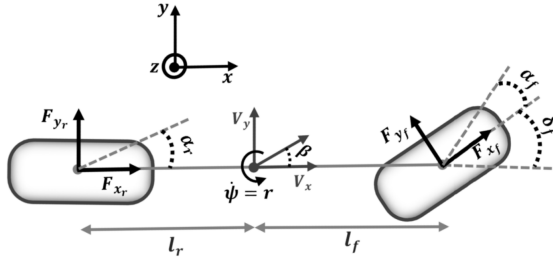


Figure 2.1: Bicycle model

The nonlinear forces F_{yf} and F_{yr} depend on the wheel side slip angle and longitudinal slip. In this work, they are assumed to be linear with respect to the side slip angles of the tires and are given by the following equations:

$$\begin{cases} F_{yf} = c_f \alpha_f, \\ F_{yr} = c_r \alpha_r, \end{cases} \quad (2.27)$$

Here, c_f and c_r represent the cornering stiffness of the front and rear tires, respectively. It is important to highlight that the cornering stiffness parameters c_f, c_r play a significant role in the system as they substantially influence the performance of the vehicle's lateral dynamics. These parameters are presumed to be unknown but bounded, with prior knowledge about their bounds as follows:

$$c_i = c_{Ni} + \Delta c_i, \quad \Delta c_i \in [\underline{\Delta c}_i, \bar{\Delta c}_i], \quad i = f, r \quad (2.28)$$

where c_{Ni} is the nominal value and Δc_i is the uncertain value.

The front and rear side slip angles, namely α_f and α_r respectively, are given as follow:

$$\begin{cases} \alpha_f = \delta_f - \beta - \tan^{-1} \left(\frac{l_f}{v_x} r \cos(\beta) \right), \\ \alpha_r = -\beta + \tan^{-1} \left(\frac{l_r}{v_x} r \cos(\beta) \right), \end{cases} \quad (2.29)$$

where δ_f is the steering angle.

For small slip angles ($\alpha_i \leq 8^\circ$), $i = f, r$, equations (2.29) can be simplified into the following form:

$$\begin{cases} \alpha_f = \delta_f - \beta - \frac{l_f}{v_x} r, \\ \alpha_r = -\beta + \frac{l_r}{v_x} r, \end{cases} \quad (2.30)$$

Taking into account the uncertainty in the cornering stiffness described in (2.28), equation (2.27) becomes:

$$\begin{cases} F_{yf} = (c_{fN} + \Delta c_f) \alpha_f, \\ F_{yr} = (c_{rN} + \Delta c_r) \alpha_r, \end{cases} \quad (2.31)$$

We apply a time discretization to the continuous dynamics in (2.26) using the forward Euler scheme. By combining the resulting discrete model with (2.27) and (2.30), we obtain the following discrete state-space model:

$$\begin{cases} x_{k+1} = A_N(\rho_k)x_k + B_u(\rho_k)u_k + B_v v_k, \\ y_k = Cx_k, \end{cases} \quad (2.32)$$

with

$$A_N(\rho_k) = \mathbb{I}_n + \begin{bmatrix} -\frac{c_{fN} + c_{rN}}{m} \rho_1(k) & \frac{(c_{rN} l_r - c_{fN} l_f)}{m_2} \rho_2(k) - 1 \\ \frac{(c_{rN} l_r - c_{fN} l_f)}{I_z} & -\frac{c_{rN} l_r^2 + c_{fN} l_f^2}{I_z} \rho_1(k) \end{bmatrix} \times T_s, \quad (2.33)$$

and

$$B_u(\rho_k) = \begin{bmatrix} \frac{c_{fN}}{m} \rho_1(k) \\ \frac{c_{fN} l_f}{I_z} \end{bmatrix} \times T_s, \quad (2.34)$$

where the state-space vector $x_k = [\beta_k, r_k]^T \in \mathbb{R}^2$ is composed of the side slip angle and yaw rate. The measurement variable $y_k = r_k \in \mathbb{R}$ is the yaw rate where the output matrix $C = [0 \ 1]$. The input control of the system is the steering angle $u_k = \delta_f \in \mathbb{R}$. T_s is the sampling time. The parameter vector $\rho_k = [\rho_1(k), \rho_2(k)]^T \in \mathbb{R}^2$ is the time-varying measurable scheduling parameter whose components are $\rho_1(k) = \frac{1}{v_x}$ and $\rho_2(k) = \frac{1}{v_x^2}$. It is not the perfect choice since both parameter are dependent but the parameters are handled independent for simplicity.

The uncertainty matrix $B_v = \mathbb{I}_n$ where \mathbb{I}_n is the identity matrix of size n , and the unmeasurable parameter $v_k \in \mathbb{R}$ is $v_k = \Delta A_{\rho_k} x_k + \Delta B_{\rho_k} u_k$, where the matrices $\Delta A_{\rho_k} \in \mathbb{R}^{2 \times 2}$ and $\Delta B_{\rho_k} \in \mathbb{R}^{2 \times 1}$ which are given by the following equations are unknown but bounded.

$$\Delta A_{\rho_k} = \begin{bmatrix} -\frac{\Delta c_f + \Delta c_r}{m} \rho_1(k) & \frac{(\Delta c_r l_r - \Delta c_f l_f)}{m} \rho_2(k) \\ \frac{(\Delta c_r l_r - \Delta c_f l_f)}{I_z} & -\frac{\Delta c_r l_r^2 + \Delta c_f l_f^2}{I_z} \rho_1(k) \end{bmatrix}, \quad (2.35)$$

$$\Delta B_{\rho_k} = \begin{bmatrix} \frac{\Delta c_f}{m} \rho_1(k) \\ \frac{\Delta c_f l_f}{I_z} \end{bmatrix}. \quad (2.36)$$

Since the state-space matrices ΔA_{ρ_k} and ΔB_{ρ_k} depend on Δc_f and Δc_r linearly, then using (2.28) we can conclude about their boundedness with:

$$\underline{\Delta A_{\rho_k}} \leq \Delta A_{\rho_k} \leq \overline{\Delta A_{\rho_k}}, \quad \underline{\Delta B_{\rho_k}} \leq \Delta B_{\rho_k} \leq \overline{\Delta B_{\rho_k}}.$$

Furthermore, the steering angle input u_k is supposed to belong to an admissible set of inputs, i.e., $\underline{u} \leq u_k \leq \bar{u}$. Hence, the vector of uncertainty v_k is bounded.

Simulations results

In order to compute the gains L_i and K_i , we need to express the matrix $A_N(\rho_k)$ defined in (2.33) under the form (2.9) with

$$\begin{aligned} \xi_k^1 &= \left(\frac{\bar{\rho}_1 - \rho_1(k)}{\bar{\rho}_1 - \underline{\rho}_1} \right) \times \left(\frac{\bar{\rho}_2 - \rho_2(k)}{\bar{\rho}_2 - \underline{\rho}_2} \right), \\ \xi_k^2 &= \left(\frac{\bar{\rho}_1 - \rho_1(k)}{\bar{\rho}_1 - \underline{\rho}_1} \right) \times \left(\frac{\rho_2(k) - \underline{\rho}_2}{\bar{\rho}_2 - \underline{\rho}_2} \right), \\ \xi_k^3 &= \left(\frac{\rho_1(k) - \underline{\rho}_1}{\bar{\rho}_1 - \underline{\rho}_1} \right) \times \left(\frac{\bar{\rho}_2 - \rho_2(k)}{\bar{\rho}_2 - \underline{\rho}_2} \right), \\ \xi_k^4 &= \left(\frac{\rho_1(k) - \underline{\rho}_1}{\bar{\rho}_1 - \underline{\rho}_1} \right) \times \left(\frac{\rho_2(k) - \underline{\rho}_2}{\bar{\rho}_2 - \underline{\rho}_2} \right), \end{aligned} \quad (2.37)$$

where $\rho_1(k) = \frac{1}{v_x} \in [1, 6] \times 10^{-2}$ and $\rho_2(k) = \frac{1}{v_x^2} \in [1, 36] \times 10^{-4}$. By solving the LMIs of Theorem 2.3.3, using Yalmip toolbox in MATLAB, we obtain the following solutions:

$$\begin{aligned} L_0 &= \begin{bmatrix} -0.2603 \\ 0.2670 \end{bmatrix}, L_1 = \begin{bmatrix} -0.0271 \\ 0.4457 \end{bmatrix}, L_2 = \begin{bmatrix} -0.0660 \\ -0.0011 \end{bmatrix}, \\ L_3 &= \begin{bmatrix} 0.0642 \\ 0.5662 \end{bmatrix}, L_4 = \begin{bmatrix} -0.1776 \\ 0.2238 \end{bmatrix}, \\ K_0 &= \begin{bmatrix} 0.0124 \\ 0.0856 \end{bmatrix}, K_1 = \begin{bmatrix} 0.0782 \\ -0.0111 \end{bmatrix}, K_2 = \begin{bmatrix} 0.6228 \\ -0.5721 \end{bmatrix}, \\ K_3 &= \begin{bmatrix} 0.0899 \\ -0.0111 \end{bmatrix}, K_4 = \begin{bmatrix} 0.6345 \\ -0.5721 \end{bmatrix}. \end{aligned}$$

We note that these gains guarantee the existence and invertibility of the matrix $\mathbb{E}_m(k)$ in (2.10) $\forall k \geq m$ with $m = 2$.

In our simulations, we assessed the impact of cornering stiffness uncertainties on the proposed state estimator's performance, focusing on fluctuations of 5% and 10% around the nominal value. The initial state variables were specified as $x_0 = [0.1, 0.6]^\top$, $\zeta_0 = [0.015, 0.2]^\top$, and $\eta_0 = [0.02, 0.01]^\top$, with the assumption that $\hat{x}_k = \hat{x}_k^+ = \hat{x}_k^- = [0, 0]^\top$ for all $k < m$.

Figures 2.2 and 2.3 present the simulation results for 5% and 10% uncertainties, respectively. These figures illustrate that the proposed estimator delivers highly accurate results, with the estimated intervals tightly encompassing the true trajectories of the yaw rate r and the side-slip angle β . This indicates that the method effectively captures the vehicle's lateral dynamics.

Furthermore, the results highlight that the method's convergence time is not influenced by the level of uncertainty, demonstrating consistent rapid convergence. This robustness to uncertainty and swift convergence reinforces the reliability and efficiency of the proposed estimator in practical applications.

2.4.3 Comparative study

To highlight the benefits of the proposed estimation approach, we compared our FLPV method with the H_∞ set-membership observer for discrete-time LPV systems as presented in [103]. Both methodologies were implemented in MATLAB, considering a 10% uncertainty around the nominal value of the cornering stiffness variable. The comparison results are depicted in Fig.2.4, clearly demonstrating the superior performance of our proposed method.

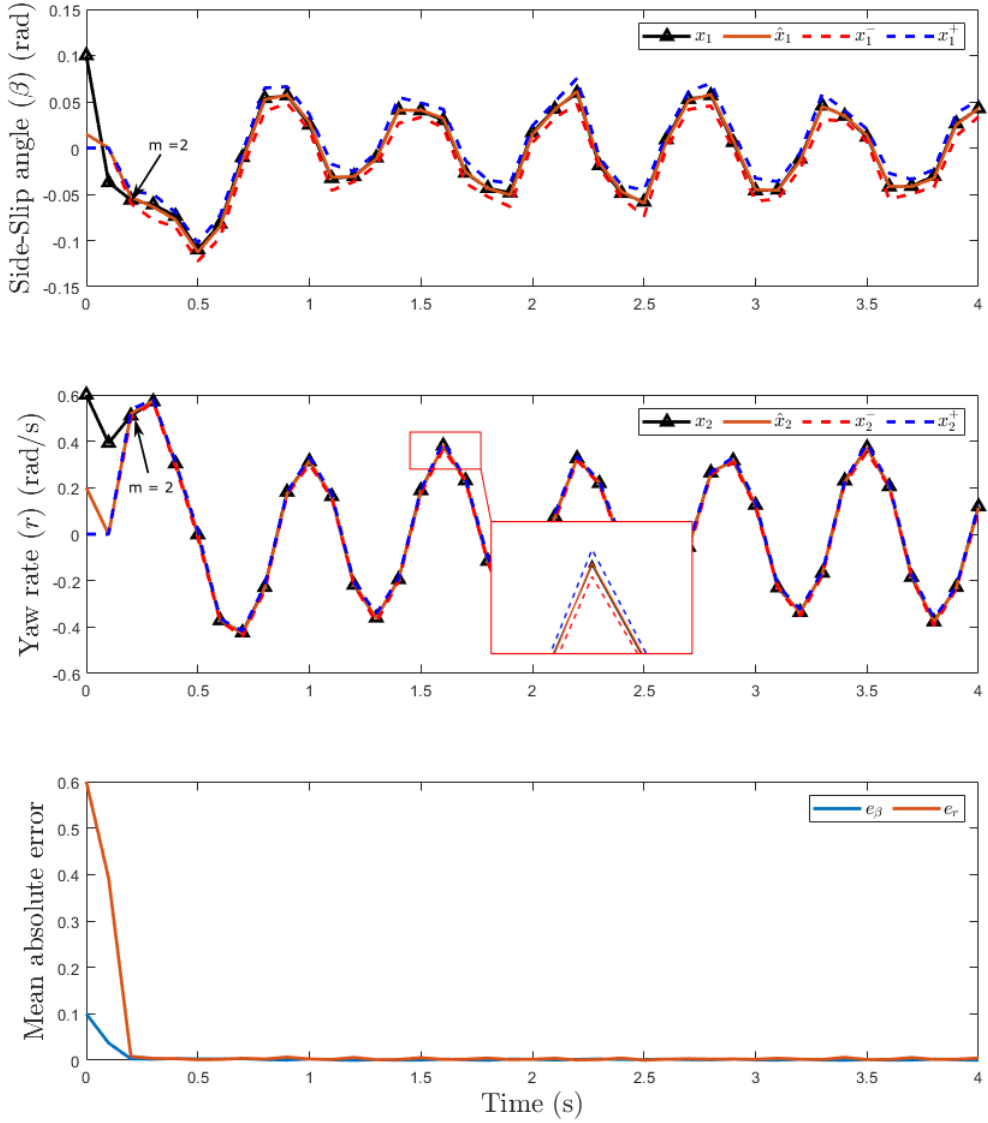


Figure 2.2: Interval estimation with cornering stiffness affected by 5% of its nominal value.

Our FLPV method shows a significantly smaller interval length compared to the H_{∞} set-membership observer, indicating a more precise estimation. Additionally, our method achieves finite-time convergence, whereas the H_{∞} observer converges asymptotically and requires much more time. To evaluate the performance of both estimators, we calculate the mean squared error (MSE) metric for both estimations and present it in Table 2.1. It is important to note that the error is computed using the estimation of the state vector, which is the average value of the interval estimates (i.e., $\hat{x}(k) = \frac{x^+(k)+x^-(k)}{2}$).

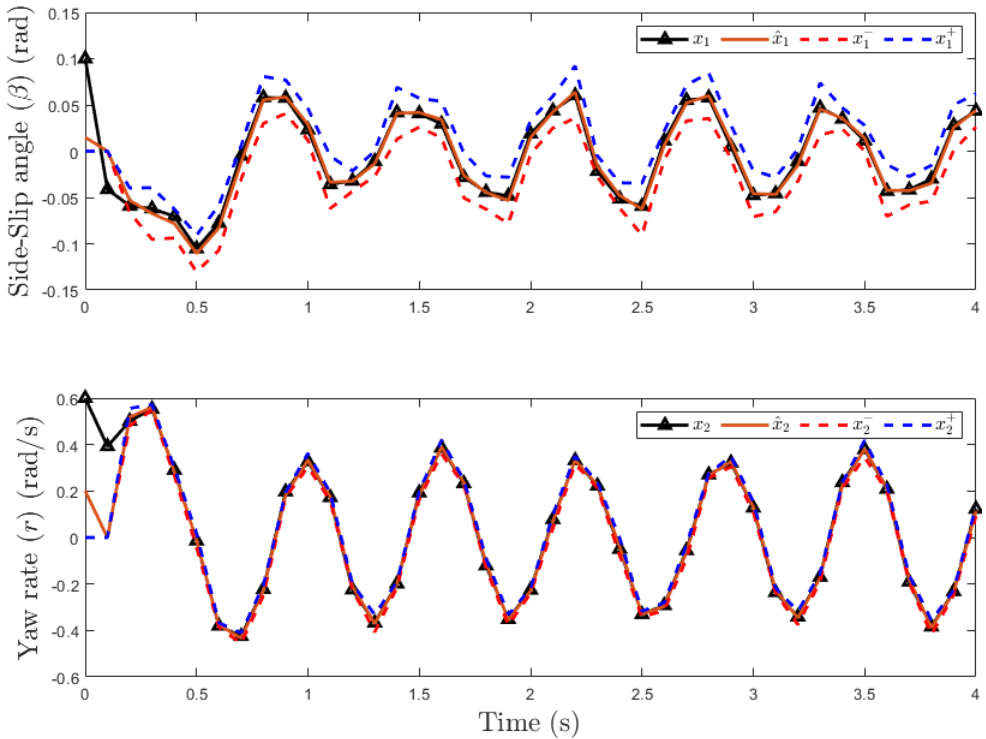


Figure 2.3: Interval estimation with cornering stiffness affected by 10% of its nominal value.

Table 2.1: Comparison between the proposed FLPV and \mathcal{H}_∞ proposed in [103] using MSE

Methods	Error on side-slip angle	Error on yaw rate
FLPV	1.9871×10^{-4}	8.5×10^{-5}
\mathcal{H}_∞	3.9301×10^{-4}	9.1×10^{-3}

Quantitatively, the FLPV method achieved a substantially lower error (1.9871×10^{-4}) compared to the H_∞ observer (3.9301×10^{-4}) in estimating the side-slip angle. Similarly, the FLPV method demonstrated a much lower error (8.5×10^{-5}) compared to the H_∞ observer (9.1×10^{-3}) in estimating the yaw rate. This clearly suggests that the FLPV method is both more accurate and precise in state estimation compared to the H_∞ set-membership observer.

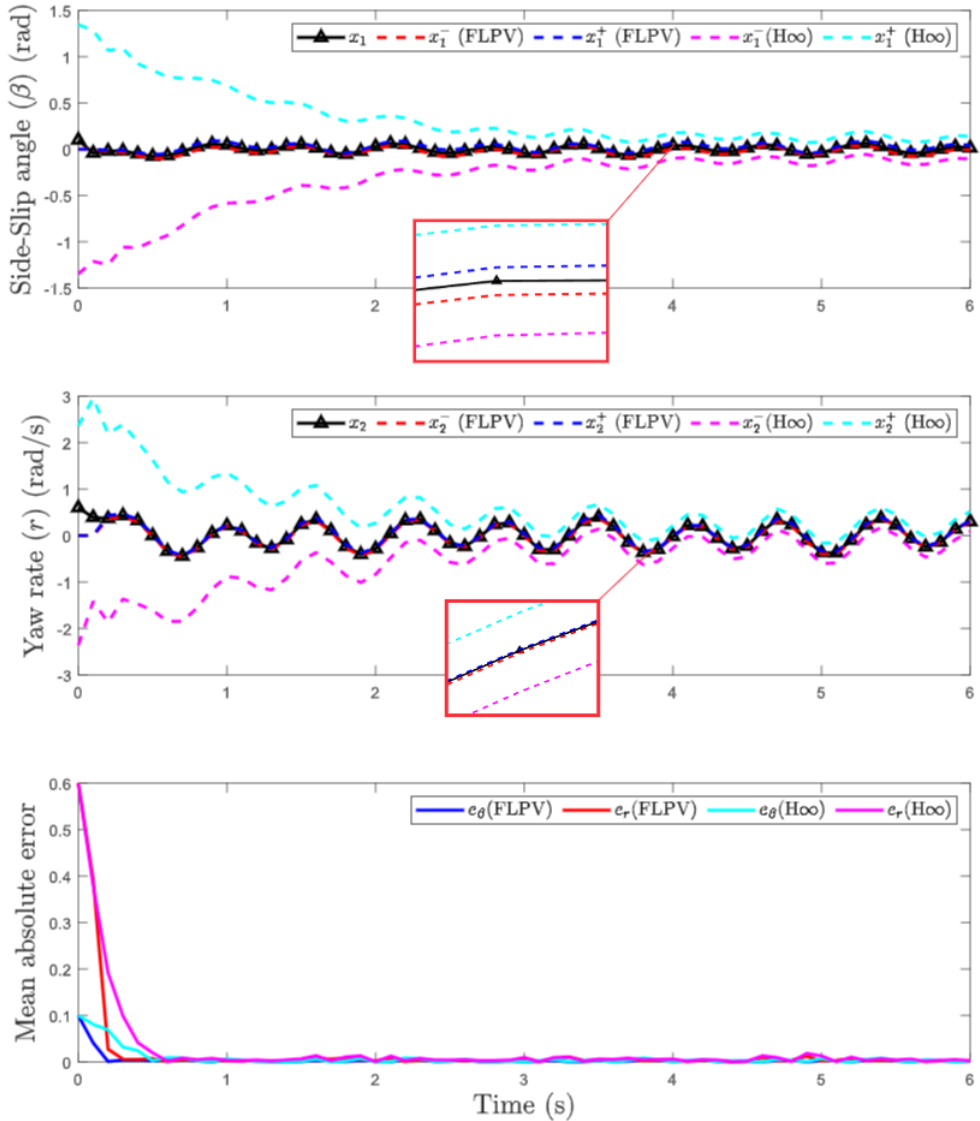


Figure 2.4: Interval estimation of the proposed method and \mathcal{H}_∞ based estimator proposed in [103].

2.5 Conclusion

In this chapter, we have delved into the design of an interval observer for a class of discrete Linear Parameter Varying (LPV) systems. The development of a discrete-time interval estimator has broadened the application scope of interval observers in digital control systems.

The methodology we employed is a unique blend of exact state estimation and interval observers. The goal was to estimate the state of uncertain systems, a task that can be quite challenging due to the inherent variability and unpredictability of these systems. The first step in our approach was to use a finite-time state estimation procedure to

estimate the exact state without uncertainty. This involves using a mathematical model of the system to predict its future states based on its current state and inputs. The exact state estimation provides a precise point estimate of the state at each time step, but it does not account for uncertainty.

To address this, we added interval observers to our methodology. Interval observers provide a range of possible values for the state, accounting for the uncertainty in the system. They do this by adding algebraically calculated bounds to the nominal estimator, which are dependent on the parameter variation. This results in a small interval of estimation, within which the true state is guaranteed to lie.

One of the key innovations of our approach is that we were able to bypass the hard constraints of standard interval observers that rely on nonnegative Schur stability (respectively, Metzler and Hurwitz stability). These are mathematical conditions that ensure the stability of the system, but they can be overly conservative and limit the applicability of the observer.

Furthermore, our methodology does not make any assumptions about the initial state of the observer. This is a significant advantage, as it allows our observer to be applied to a wider range of systems and scenarios.

We proposed a robust interval finite-time estimation algorithm for side-slip angle, employing an uncertain bicycle vehicle LPV model. The velocity was treated as a measurable varying parameter, and a strategy of amalgamating two asymptotic observers was employed to estimate the state with algebraically computed bounds, resulting in a minimal interval of estimation.

In summary, our methodology combines the precision of exact state estimation with the uncertainty handling of interval observers, while avoiding the limitations of traditional approaches. This makes it a powerful tool for state estimation in uncertain systems. We believe that this approach will open up new possibilities for the application of interval observers in digital control systems and inspire further research in this area.

3

Neuro-Adaptive Learning-based Observer for Nonlinear States and Unknown Inputs Estimation

Contents

3.1	Introduction	83
3.2	Neuro-Adaptive Observers	85
3.2.1	Problem Formulation	85
3.2.2	Robust Data-Driven Neuro-Adaptive Observer	85
3.3	Concurrent Learning-Based Adaptive Observation	86
3.3.1	Problem statement	86
3.3.2	Observer Design	87
3.4	Proposed Neuro-Adaptive LMI Based Observer	88
3.5	Application to vehicle longitudinal model	94
3.5.1	Vehicle Longitudinal model	94
3.5.2	Observer design	95
3.5.3	Simulation results	97
3.5.4	Comparison	98

3.6 Conclusion	100
--------------------------	-----

3.1 Introduction

Control engineering has extensively utilized function approximators like neural networks. The primary use of these neural networks is often seen in the identification of dynamical systems using collected measurement data, see in [11], [12]. The application of neural networks for state estimation in systems with unknown dynamics is still largely under-researched. Initial explorations into the realm of neuro-observers, as exemplified in the study referenced as [104], were based on the assumption of model availability. This assumption, while useful in certain contexts, does not fully leverage the potential of neural networks in a data-driven control environment.

The current trend in control engineering is increasingly leaning towards data-driven control. This approach has proven the efficacy of approximators in managing systems without relying on pre-existing models. The power of neural networks lies in their ability to learn and adapt from data, making them ideal for this model-free approach.

The concept of neuro-observers in a model-free setting is not entirely new. It was first explored nearly two decades ago, as documented in the study referenced as [104]. In this pioneering work, the authors proposed an innovative adaptation rule. This rule was designed to facilitate the learning of weights in a linear-in-parameter neural network (LPNN).

The unique aspect of this adaptation rule is that it leads to a uniformly ultimately bounded estimation error dynamics. In simpler terms, this means that the estimation error, while it may vary, will not exceed a certain limit. This is a crucial feature as it ensures the stability and reliability of the system.

The work on neuro-observers and their application in various fields has seen widespread adoption. This includes areas such as robot control, as cited in references [87], [105], [106], rotors [107], and more recently, wind turbines [108]. Despite the broad application of these methodologies, the underlying assumptions and theoretical foundations have seen little evolution.

In most of these methods, the activation functions are generally regarded as radial basis functions. Moreover, the theoretical assurances of learning performance have mostly stayed consistent across these applications [86], [106]. However, they face an issue

where the learning of a known linear function is influenced by numerous factors such as the initial condition of the weights and the duration of training. This can sometimes result in divergence problems or inconsistencies in the estimation.

However, there are exceptions to this trend. For instance, in reference [108], the authors delve into the exploration of input-to-state stability (ISS) observers for the known component of the model. This represents a significant departure from the standard practices in the field. Yet, it's important to note that the performance of the learner in this case is not ISS. Moreover, the weights of the learner require extensive manual tuning, which can be a labor-intensive process.

In this chapter, we present a novel observer design, rooted in machine learning, that is capable of estimating the states and unknown input dynamics of a broad spectrum of nonlinear systems. Our proposed method employs a neural approximator to estimate unknown functions, with the weights of this approximator being updated in real-time. We utilize the Concurrent Learning (CL) technique, as referenced in [13], which allows for the simultaneous consideration of both historical and current data in the adaptation of weights. It's important to note that our proposed observer is designed to handle a more extensive class of nonlinear systems and does not require prior knowledge of the nonlinearity.

Furthermore, the observer we've developed to estimate the unknown states is founded on the principles of Linear Matrix Inequality (LMI). This approach enhances the robustness and reliability of the state estimation process.

By integrating these advanced techniques and methodologies, we aim to push the boundaries of what's possible in the field of control engineering and systems estimation. We believe that our work will contribute significantly to the evolution of neuro-observers and their applications in various domains.

3.2 Neuro-Adaptive Observers

3.2.1 Problem Formulation

We consider nonlinear systems that have the state-space representation

$$\dot{x} = Ax + \varphi(x, u) \quad (3.1a)$$

$$y = Cx + Du. \quad (3.1b)$$

The system's state is represented by $x = x(t) \in \mathbb{R}^n$, the control input is denoted by $u = u(t) \in \mathbb{R}^m$, the measured outputs are signified by $y = y(t) \in \mathbb{R}^p$. The nonlinearity $\varphi(x, u) : \mathbb{R}^n \times \mathbb{R}^m \rightarrow \mathbb{R}^n$, which represents the unmodeled dynamics of the system, is unknown. The matrices A , C , and D are constants with appropriate dimensions, and the pair (A, C) is required to make the system observable.

3.2.2 Robust Data-Driven Neuro-Adaptive Observer

Let suppose that our system in (3.1) verifies the following assumptions :

Assumption 3.2.1. *The state $x \in \mathcal{L}_\infty$ and the measurement noise $v \in \mathcal{L}_\infty$.*

For instance, Assumption 3.2.1 is fulfilled when the system (3.1) is open-loop stable, a common assumption in the identification of dynamical systems. Given that Assumption 3.2.1 implies that x resides in a compact subset of \mathbb{R}^n , one can utilize the neural network approximability results mentioned in [109] to depict the unknown nonlinearity.

$$\varphi(x, i) = \sum_{i=1}^N B_i W_i + W^\top \sigma(a_i(x, u)) + \varepsilon(x, u) \quad (3.2)$$

In this context, $W \in \mathbb{R}^{n \times N}$ denotes a constant yet unknown weight matrix in the output layer of a neural approximator with N neurons. The i th column of W is represented by W_i , and $B_i \in \mathbb{R}^{n \times 1}$ is a known matrix that translates the negative components, without loss of generality, as given by $\sum_{i=1}^N B_i W_i$ [110]. Furthermore, $\sigma(\cdot, \cdot) : \mathbb{R}^n \times \mathbb{R}^m \rightarrow \mathbb{R}^N$ signifies the vector of activation functions, i.e.,

$$\sigma(x, u) = [\sigma_1(H_1 x, u), \dots, \sigma_N(H_N x, u)]^T$$

Assumption 3.2.2. There exist positive scalars p_W , p_e , and p_o such that

$$\|W_\star\|_\infty \leq p_W, \quad \|\varepsilon(\cdot, \cdot)\|_{\mathcal{L}_\infty} \leq p_\varepsilon, \quad \text{and} \quad \|\sigma(\cdot, \cdot)\|_{\mathcal{L}_\infty} \leq p_\sigma.$$

The activation functions are absolutely continuous on \mathbb{R}^n and satisfy

$$-\infty < \check{\sigma}_{ij} < \frac{\partial \sigma_i}{\partial q_j^i}(q_j, u) \leq \hat{\sigma}_{ij} \leq \infty \quad (3.3)$$

for every $q_j \in \mathbb{R}^n$ where the derivative exists, with $q_j = H_j x$ and q_j^i being the i -th component of q_j .

Neuro-adaptive observer

To estimate the state of the system described in equation (3.1), where both the system state and an unknown nonlinear function with uncertain weights need to be simultaneously estimated, a data-driven neuro-adaptive observer is proposed in the form of:

$$\begin{cases} \dot{\hat{x}} = A\hat{x} + \sum_{i=1}^n B_i \tilde{W}_i \sigma(\hat{x}, u) + L_0(y - C\hat{x}), \\ \dot{\tilde{W}}_{ij} = L_k(y - C\hat{x}), \end{cases} \quad (3.4)$$

for $i = 1, \dots, n$, $j = 1, \dots, N$, and $k = 1, \dots, nN$.

$$\sigma(x, u) = \begin{bmatrix} \sigma_1(H_1 x + K_1(y - Cx), u) \\ \vdots \\ \sigma_N(H_N x + K_N(y - Cx), u) \end{bmatrix}, \quad (3.5)$$

Here, $\hat{x}(t)$ is the estimated state of the plant (3.1), \tilde{W} denotes the vector of estimated weight parameters whose (i, j) -th element is \tilde{W}_{ij} , $L_0 \in \mathbb{R}^{n \times p}$, $L_k \in \mathbb{R}^{1 \times p}$ for $k = 1, \dots, nN$, and $K_i \in \mathbb{R}^{s \times n}$ for $i = 1, \dots, N$ are observer gain matrices.

For the design of the observer gain one can refer to [86].

3.3 Concurrent Learning-Based Adaptive Observation

3.3.1 Problem statement

Consider a system in the triangular form as shown in (3.6) :

$$\begin{cases} \dot{x} = Ax + B [W^T \Phi(x) + g(x)u] \\ y = Cx \end{cases} \quad (3.6)$$

where $x = [x_1, \dots, x_n]^T \in \mathbb{R}^n$ is the state, $\Phi(x) : \mathbb{R}^n \rightarrow \mathbb{R}^m$ is the regressor function, $W \in \mathbb{R}^m$ is the unknown constant ideal weight vector, and matrices $A \in \mathbb{R}^{n \times n}$, $B \in \mathbb{R}^{n \times 1}$, and $C \in \mathbb{R}^{1 \times n}$ represent a chain of integrators defined as follow:

$$B = \begin{bmatrix} 0 & \dots & 0 & 1 \end{bmatrix}^T, \quad C = \begin{bmatrix} 1 & 0 & \dots & 0 \end{bmatrix}$$

and

$$(A)_{i,j} = \begin{cases} 1 & \text{if } j = i+1 \\ 0 & \text{if } j \neq i+1 \end{cases}$$

3.3.2 Observer Design

The concept behind the observer design in [13] is to exploit the system's triangular structure and employ an observer similar to a high gain for the system state. This can be accomplished by selecting $\varepsilon < 1$ a small positive constant, also we define the following notations

$$\Gamma_1 = \left[\left(\frac{l_1}{\varepsilon} \right), \left(\frac{l_2}{\varepsilon^2} \right), \dots, \left(\frac{l_n}{\varepsilon^n} \right) \right]^T$$

and

$$\Gamma_2 = \left(\frac{l_{n+1}}{\varepsilon^{n+1}} \right)$$

where ε is a small positive constant less than 1. We choose

$$L = [l_1, l_2, \dots, l_{n+1}]^T \in \mathbb{R}^{n+1}$$

such that the subsequent matrix is Hurwitz:

$$E = \begin{bmatrix} -l_1 & 1 & 0 & \dots & 0 \\ -l_2 & 0 & 1 & \dots & 0 \\ \vdots & \vdots & \vdots & \ddots & \vdots \\ -l_n & 0 & 0 & \dots & 1 \\ -l_{n+1} & 0 & 0 & \dots & 0 \end{bmatrix} \in \mathbb{R}^{(n+1) \times (n+1)}.$$

Let $\rho : \mathbb{R} \rightarrow \mathbb{R}$ be an odd smooth saturation-like function, which is characterized by

$0 < \rho'(v) \leq 1$, $\rho(v) = v$ if $|v| \leq 1$, and $\lim_{v \rightarrow \infty} \rho(v) = 1 + \iota$ with $0 < \iota \ll 1$.

The proposed CL-AEO in [13]

$$\begin{cases} \dot{\hat{x}} = A\hat{x} + \Gamma_1(x_1 - \hat{x}_1) + B[\hat{x}_{n+1} + g(\hat{x})u], \\ \hat{x}_{n+1} = \Gamma_2(x_1 - \hat{x}_1) \\ \bar{x}_i = M_i \rho(\hat{x}_i/M_i), 1 \leq i \leq n+1, \\ \hat{W} = \Gamma_3 \Phi(\bar{x}) (\bar{x}_{n+1} - \hat{W}^T \Phi(\bar{x})) \\ + \sum_{j=1}^p \Gamma_3 \Phi(\bar{x}^j) (\bar{x}_{n+1}^j - \hat{W}^T \Phi(\bar{x}^j)) \end{cases} \quad (3.7)$$

In this context, $\hat{x} = [\hat{x}_1, \dots, \hat{x}_n]^T$, \hat{x}_{n+1} , and \hat{W} are the approximations of x , $x_{n+1} \triangleq W^T \Phi(x)$, and W , respectively. The saturation bounds $M_i \geq \sup_{x \in \mathcal{X}} |x_i|$ are chosen to avoid the peaking phenomenon during the initial phase. The saturated estimate of x is represented as $\bar{x} = [\bar{x}_1, \dots, \bar{x}_n]^T$. Γ_3 is a matrix with positive definite learning rate. The index of a recorded data point is denoted by $j \in \{1, 2, \dots, p\}$ where $p \geq m$. The j th recorded data of \bar{x} and \bar{x}_{n+1} are represented as \bar{x}^j and \bar{x}_{n+1}^j , respectively. More about the recording technique will be presented in the next section.

3.4 Proposed Neuro-Adaptive LMI Based Observer

We consider the class of nonlinear systems in which the nonlinearities affects the system's states not its outputs. This class of systems can be represented by the following state-space representation:

$$\begin{cases} \dot{x} = Ax + Bu + F\varphi(x), \\ y = Cx, \end{cases} \quad (3.8)$$

where $x \equiv x(t) \in \mathbb{R}^n$ represents the state of the system, $y \equiv y(t) \in \mathbb{R}^{n_y}$ represents the measured outputs and $u \equiv u(t) \in \mathbb{R}^{n_u}$ is the input vector. The nonlinearity $\varphi(x) : \mathbb{R}^n \rightarrow \mathbb{R}^1$ represents the nonlinear unmodeled dynamics or parameters of the system and is unknown. The matrices A , B , C , and F are constant with appropriate dimensions. The following assumptions are made on the system and needed in the subsequent analysis of the observer.

Assumption 3.4.1. *The state $x \in \mathcal{L}_\infty$.*

Assumption 3.4.2. *The pair (A, C) is observable.*

Assumption 3.4.1 implies that x lies in a compact subset of \mathbb{R}^n .

A single hidden layer, along with an arbitrary bounded and nonconstant activation

function, can serve as universal approximators [109], and can be utilized to describe and approximate the unknown nonlinearity in the system as follows:

$$\varphi(x) = W^T \sigma(x) + \varepsilon(x), \quad (3.9)$$

where $W \in \mathbb{R}^{N \times 1}$ is a constant but unknown matrix of weights in the output layer of a neural approximator with N neurons. In addition, $\sigma(\cdot) : \mathbb{R}^n \rightarrow \mathbb{R}^N$ denotes the vector of activation functions. Note that the activation function σ is a hyper-parameter to be chosen by the designer, and therefore, its exact parametric form is completely known (although its argument x is to be estimated).

Replacing $\varphi(x)$ in Equation (3.8) with its neural network based representation given in Equation (3.9), we get:

$$\dot{x} = Ax + Bu + F(W^T \sigma(x) + \varepsilon(x)). \quad (3.10)$$

It is worth to note that the unknown nonlinear functions part of $\varphi(x)$ to be estimated is represented as extended state $x_{n+1} \in \mathbb{R}$ and approximated by the neural network decomposition, i.e., $x_{n+1} \triangleq W^T \sigma(x)$. The proposed neuro-adaptive observer to estimate both the states and unknown nonlinear dynamics of model (3.1) is given by the following set of equations :

$$\left\{ \begin{array}{l} \dot{\hat{x}} = A\hat{x} + LC(x - \hat{x}) + Bu + F\hat{x}_{n+1}, \\ \dot{\hat{x}}_{n+1} = KC(x - \hat{x}), \\ \dot{\hat{W}} = \eta \sigma(\hat{x}) \left(\hat{x}_{n+1} - \hat{W}^\top \sigma(\hat{x}) \right) \\ \quad + \sum_{j=1}^p \eta \sigma(\hat{x}^j) \left(\hat{x}_{n+1}^j - \hat{W}^\top \sigma(\hat{x}^j) \right), \end{array} \right. \quad (3.11)$$

where $\hat{x} = [\hat{x}_1 \dots \hat{x}_n]^\top$, \hat{x}_{n+1} , and \hat{W} , are the estimates of x , $x_{n+1} \triangleq W^T \sigma(x)$, and W , respectively. η is positive definite learning rate matrices; $j \in \{1, 2, \dots, p\}$ with $p \geq N$ denotes the index of a recorded data point and \hat{x}^j and \hat{x}_{n+1}^j represent the j -th recorded data of \hat{x} and \hat{x}_{n+1} , respectively.

The fundamental strategy for data recording is to augment the history stack. This is accomplished by appending data matrix to unoccupied slots or, if no such slots are available, by substituting an existing vector. The ultimate aim is to maximize the minimum singular value of Z . The data recording algorithm for the Observer is given in Algorithm 2.

The following theorem contains the convergence analysis results of the proposed observer in (3.11):

Algorithm 2 Data Recording Algorithm for the Observer [13]

Require: $k = 1, Z = \mathbf{0}_{N \times p}, \Lambda = \mathbf{0}_{1 \times p}$

```

if  $k \leq p$  then
     $Z(:, k) = \sigma(\hat{x}); \Lambda(:, k) = \hat{x}_{n+1}$ 
end if
if  $k > p$  then
     $Z_{\text{temp}} = Z$ 
     $S_{\text{old}} = \min PCA(Z^{\top})$ 
    for  $j = 1$  to  $p$  do
         $Z(:, j) = \sigma(\hat{x})$ 
         $S(j) = \min PCA(Z^{\top})$ 
         $Z = Z_{\text{temp}}$ 
    end for
    Find  $S_{\text{new}} = \max_{1 \leq j \leq p} S(j)$  and let  $j'$  denote the corresponding column index
    if  $S_{\text{new}} > S_{\text{old}}$  then
         $Z(:, j') = \sigma(\hat{x}); \Lambda(:, j') = \hat{x}_{n+1}$ 
    end if
end if

```

Theorem 3.4.1

Given the nonlinear system given in (3.8) with assumptions 1-2, the nonlinear neural network approximation given in (3.9), and assume that there exist matrices $P = P^{\top} > 0$, Y of appropriate dimension, a scalar $\lambda > 0$, such that the following conditions are satisfied:

$$\tilde{A}_z^{\top}P + P\tilde{A}_z - Y^{\top}\tilde{C} - \tilde{C}^{\top}Y + \lambda\mathbb{I}_z \leq 0 \quad (3.12)$$

and suppose that the vector signal $\sigma(x(t))$ is excited over a finite time interval $[0, T]$ as defined in Definition 1; then, for any $\gamma > 0$ and $T_0 > 0$, with $\tilde{L} = P^{-1}Y$ and $\eta > 0$ we have:

$$|x_i(t) - \hat{x}_i(t)| \leq \gamma, 1 \leq i \leq n+1, \forall t \geq T_0, \quad (3.13)$$

and

$$\lim_{t \rightarrow \infty} \|W - \hat{W}(t)\| \leq \gamma \quad (3.14)$$

Proof. Since the convergence happens in two time scales for the extended state vector and the weight vector, we will split the convergence proof into two parts. We start first with the convergence of \hat{x} and \hat{x}_{n+1} , then we prove the convergence of the weights \hat{W} . Let us consider the augmented state estimation error $e = [e_1, e_2, \dots, e_{n+1}]^T$ with $e_i = x_i - \hat{x}_i$, $1 \leq i \leq n+1$.

From (3.10) and (3.11), we get the error dynamics as follow :

$$\dot{e} = A_z e + G W^\top \sigma_x(x) [Ax + Bu + FW^\top \sigma(x)], \quad (3.15)$$

where

$$A_z = (\tilde{A}_z - \tilde{L}\tilde{C}) = \begin{bmatrix} A - LC & F \\ -KC & 0 \end{bmatrix}, G = \begin{bmatrix} 0 \\ F^\top \end{bmatrix},$$

and

$$\tilde{A}_z = \begin{bmatrix} A & F \\ 0 & 0 \end{bmatrix}, \tilde{C} = [C \ 0], \tilde{L} = \begin{bmatrix} L \\ K \end{bmatrix}.$$

Given that x is bounded according to Assumption 3.4.1 and the functions σ and $\sigma_x \triangleq \frac{\partial \sigma}{\partial x}$ are continuous, the second term on the right-hand side of equation (3.15) is constrained by a positive constant N_0 . If Assumption 3.4.2 is verified, we assume that P is the solution of the inequality:

$$A_z^\top P + PA_z \leq -\lambda \mathbb{I}. \quad (3.16)$$

We define a Lyapunov function candidate $V_1(e) = e^\top Pe$. It directly follows that:

$$\alpha \|e\|^2 \leq V_1(e) \leq \beta \|e\|^2 \quad (3.17)$$

where $\alpha = \lambda_{min}(P)$ and $\beta = \lambda_{max}(P)$ are the minimal and maximal eigenvalues of the matrix P , respectively.

We have

$$\frac{dV_1(e)}{dt} = \dot{e}^\top Pe + e^\top P\dot{e}, \quad (3.18)$$

Through some simple transformations, and given the errors dynamics (3.15), the derivative of $V_1(e)$ (3.18) satisfies:

$$\frac{dV_1(e)}{dt} \leq e^\top [A_z^\top P + PA_z]e + N_0 Pe_{n+1} + N_0 e_{n+1}^\top P, \quad (3.19)$$

and from (3.16) and (3.17) :

$$\begin{aligned} \frac{dV_1(e)}{dt} &\leq -\lambda \|e\|^2 + 2\beta N_0 \|e\| \\ &\leq -\frac{\lambda}{\beta} V_1(e) + \frac{2\beta N_0}{\sqrt{\alpha}} \sqrt{V_1(e)}. \end{aligned} \quad (3.20)$$

It follows that:

$$\frac{d\sqrt{V_1(e)}}{dt} \leq -\frac{\lambda}{2\beta} \sqrt{V_1(e)} + \frac{\beta N_0}{\sqrt{\alpha}}. \quad (3.21)$$

Given Equations (3.17) and (3.21) we get :

$$\begin{aligned}
\|e\| &\leq \frac{\sqrt{V_1(e)}}{\sqrt{\alpha}} \\
&\leq \left(\frac{\sqrt{V_1(e(0))}}{\sqrt{\alpha}} - \frac{2\beta^2 N_0}{\alpha\lambda} \right) e^{-\frac{2\beta^2 N_0}{\sqrt{\alpha}\lambda}} + \frac{2\beta^2 N_0}{\alpha\lambda} \\
&\leq \sqrt{\frac{\beta}{\alpha}} \|e(0)\| e^{-\frac{2\beta^2 N_0}{\sqrt{\alpha}}\lambda t} + \frac{2\beta^2 N_0}{\alpha\lambda}.
\end{aligned} \tag{3.22}$$

We note that the right-hand side of the inequality (3.22) is on the order of $O(\lambda)$. As $t \rightarrow \infty$, the state enters a ball with a radius of $\frac{2\beta^2 N_0}{\alpha\lambda}$. Therefore, for sufficiently large values of λ , the radius of the ball will be made smaller, and thus we can guarantee the practical convergence of the state estimation as stated in (3.13).

Now, we will examine the convergence of the weights of the neural network approximator. Let us denote $e_W = W - \hat{W}$ with the Lyapunov function $V_2 = \frac{1}{2}e_W^\top \eta^{-1} e_W$. Given that T_0 can be reduced to an arbitrarily small value and the state estimate in the parameter update rule is bounded, e_W is also bounded over the interval $[0, T_0]$. We define a sequence t_1, \dots, t_k where $t_1 \geq T_0$ and each t_k represents a moment in time when the history stack Z is updated. Computing the time derivative of $V_2(e_W)$ over each time interval $[t_k, t_{k+1}]$ yields:

$$\begin{aligned}
\frac{dV_2(e_W)}{dt} &= -e_W^\top \sigma(\hat{x}) \left(\hat{x}_z - \hat{W}^\top \sigma(\hat{x}) \right) \\
&\quad - e_W^\top \sum_{j=1}^p \sigma(\hat{x}^j) \left(\hat{x}_z^j - \hat{W}^\top \sigma(\hat{x}^j) \right) \\
&= -e_W^\top \left[\sigma(x) \sigma^\top(x) + \sum_{j=1}^p \sigma(x^j) \sigma^\top(x^j) \right] e_W \\
&\quad + \delta(e_W),
\end{aligned} \tag{3.23}$$

where

$$\begin{aligned}
\delta(e_W) &= e_W^\top \sigma(x) \left(x_z - \hat{W}^\top \sigma(x) \right) \\
&\quad - e_W^\top \sigma(\hat{x}) \left(\hat{x}_z - \hat{W}^\top \sigma(\hat{x}) \right) \\
&\quad + e_W^\top \sum_{j=1}^p \sigma(x^j) \left(x_z^j - \hat{W}^\top \sigma(x^j) \right) \\
&\quad - e_W^\top \sum_{j=1}^p \sigma(\hat{x}^j) \left(\hat{x}_z^j - \hat{W}^\top \sigma(\hat{x}^j) \right).
\end{aligned}$$

Given the convergence of the state estimate and the locally Lipschitz property of the activation function σ , we can establish that $\delta(e_W) \leq l_1 \|e_W\|^2 + l_2 \|e_W\|$ for some positive constants l_1 and l_2 . Coupled with the fact that $t\sigma(x)\sigma^\top(x) \geq 0, \forall \sigma(x)$, we can deduce

that

$$\frac{dV_2(e_W)}{dt} \leq -e_W^\top \Sigma e_W + l_1 \|e_W\|^2 + l_2 \|e_W\|, \quad (3.24)$$

where $\Sigma = \sum_{j=1}^p \sigma(x^j) \sigma^\top(x^j) \geq 0$. It's important to note that (3.24) ensures that e_W is bounded over each finite time interval $[t_k, t_{k+1}]$ if $t_{k+1} \leq T$. Remember that $\sigma(x)$ is exciting over the time interval $[0, T]$, and Algorithm 2 ensures that the history stack Z includes at least m linearly independent elements for all $t \geq T$ (i.e., $\text{rank}(Z) = m$). Hence, for $t \geq T$, we have $\Sigma = \sum_{j=1}^p \sigma(x^j) \sigma^\top(x^j) \geq 0$ so we can have :

$$\frac{dV_2(e_W)}{dt} \leq -(\lambda_{\min}(\Sigma) - l_1) \|e_W\|^2 + l_2 \|e_W\|. \quad (3.25)$$

Given that $\lambda_{\min}(\Sigma)$ increases monotonically, $V_2(e_W)$ is a common Lyapunov function. As a result, equation (3.25) confirms the practical convergence of e_W as defined in equation (3.14). This concludes the proof of Theorem 1. \square

Remark 3.4.3 (Data Recording Algorithm 2). *In the proposed Neuro-Adaptive LMI-based observer (3.11), the collected data comprises the vectors $\sigma(\hat{x}^j)$ and the corresponding information \hat{x}_{n+1}^j . Let $Z = [\sigma(\hat{x}^1), \dots, \sigma(\hat{x}^p)]$ denote the history stack and $\Lambda = [\hat{x}_{n+1}^1, \dots, \hat{x}_{n+1}^p]$. Following the approach in [13], the fundamental concept for data recording is to update the history stack by adding data points to vacant slots or replacing an existing point if no empty slot is available, with the aim of maximizing the minimum singular value of Z . It's crucial to note that other methods, such as Principal Component Analysis (PCA), were tested in addition to Singular Value Decomposition (SVD). However, after comparing the data enhancement and computational time, we found that the compromise is better when using SVD.*

Remark 3.4.4. *In the proposed observer, we introduce a notable improvement over the approach presented in [13] and detailed in equation (3.7). While their observer is limited to handling a specific triangular form of the nonlinear system, our method accommodates a more general nonlinear system structure. In their approach, it is assumed that the functional form of $f(x)$ is known, and they focus solely on estimating the parameters. In contrast, our observer is designed to handle situations where the function itself is unknown. We employ a neural approximator to estimate both the function and its weights.*

Furthermore, the neuro-adaptive observer proposed in [86] and outlined in equation (3.4) typically requires a good initial estimate of the neural network weights W to ensure convergence. Without such initial estimates, the weights may fail to converge even after the states have converged, leading to a discrepancy where states converge quickly while weights do not. We address this challenge by implementing a two-time scale

convergence strategy and utilizing recorded data to ensure that the weights converge effectively even after the states have stabilized.

Remark 3.4.5. The observer learns from the augmented state, assuming that the state converges more rapidly than the weights. Additionally, the stored data ensures that the error in the weights remains bounded.

3.5 Application to vehicle longitudinal model

The suggested technique is utilized for estimating the motion of vehicles in situations where the vehicle's longitudinal dynamics have unknown nonlinearities and system parameters. This method is especially useful in adaptive cruise control systems, where it is vital to monitor the movement of another vehicle, even if its dynamic behavior is not known.

3.5.1 Vehicle Longitudinal model

The vehicle is treated as a point mass. By invoking Newton's second law, we can derive a system of equations. This approach provides a rigorous and precise understanding of the vehicle's dynamics [51]:

$$\begin{cases} \dot{p}(t) = v(t), \\ \dot{v}(t) = a(t), \\ \dot{a}(t) = \frac{1}{m\tau}u(t) - \frac{2K_{di}}{m}v(t)a(t) \\ \quad - \frac{1}{\tau} \left(a(t) + \frac{K_{di}}{m}v^2(t) + \frac{d_m}{m} \right), \end{cases} \quad (3.26)$$

where

- p is the longitudinal position of the vehicle.
- v is the longitudinal velocity of the vehicle.
- a is the longitudinal acceleration of the vehicle.
- u is the vehicle control input representing the desired driving/braking force.
- m is the mass of the vehicle.
- τ is the engine's time lag.
- d_m is the mechanical drag.
- K_d is the aerodynamic drag coefficient.

We can restructure the system into the following compact state-space representation:

$$\begin{cases} \dot{x} = Ax + Bf(x) + B_u u(t), \\ y = Cx, \end{cases} \quad (3.27)$$

where the state vector is

$$x = \begin{bmatrix} x_1 \\ x_2 \\ x_3 \end{bmatrix} = \begin{bmatrix} p(t) \\ v(t) \\ a(t) \end{bmatrix},$$

and

$$A = \begin{bmatrix} 0 & 1 & 0 \\ 0 & 0 & 1 \\ 0 & 0 & 0 \end{bmatrix}, \quad B = \begin{bmatrix} 0 \\ 0 \\ 1 \end{bmatrix}, \quad C = \begin{bmatrix} 1 & 0 & 0 \end{bmatrix},$$

$$B_u = \begin{bmatrix} 0 \\ 0 \\ \frac{1}{m\tau} \end{bmatrix}, \quad f(x) = -\frac{2K_{di}}{m}x_2x_3 - \frac{1}{\tau} \left(x_3 + \frac{K_{di}}{m}x_2^2 + \frac{d_m}{m} \right).$$

3.5.2 Observer design

The Observer's design process involves solving the Linear Matrix Inequality (LMI) that results in the gains L and K , as indicated in the referenced theorem. This is accomplished by extending the system for the longitudinal dynamic model that includes the unknown nonlinear function $f(x)$. The unknown component is approximated using a neural network in the following manner:

$$f(x) = W^\top \sigma(x) + \varepsilon(x, u). \quad (3.28)$$

The actual system is simulated using the model as per equation (3.27), and the observer is implemented as described in equation (3.11). The computation of the observer gains L and K necessitates the solution of the (LMI) presented in equation (3.12), with

$$\lambda = 10^5$$

. This is accomplished using the SDPT3 solver in MATLAB. We impose a constraint that

$$P \leq \text{diag}(10^{-2}, 10^{-3}, 10^{-4}, 10^{-5})$$

to individually regulate the convergence rate of each state. This is necessary to ensure the augmented state converges prior to the system states. The resulting calculated gains are as follows:

$$L = 10^6 \times \begin{bmatrix} 0.0364 \\ 0.5032 \\ 5.6725 \end{bmatrix}, \quad K = 10^7 \times 3.1690.$$

For the neural network component of the observer, we utilized three nodes with a fixed input gain set to the identity matrix. We selected the Sigmoid function for this purpose, which is defined as follows:

$$\sigma(x) = \frac{1}{1 + e^{-x}}. \quad (3.29)$$

The neural network model architecture is given in the following: In the dynamic equation

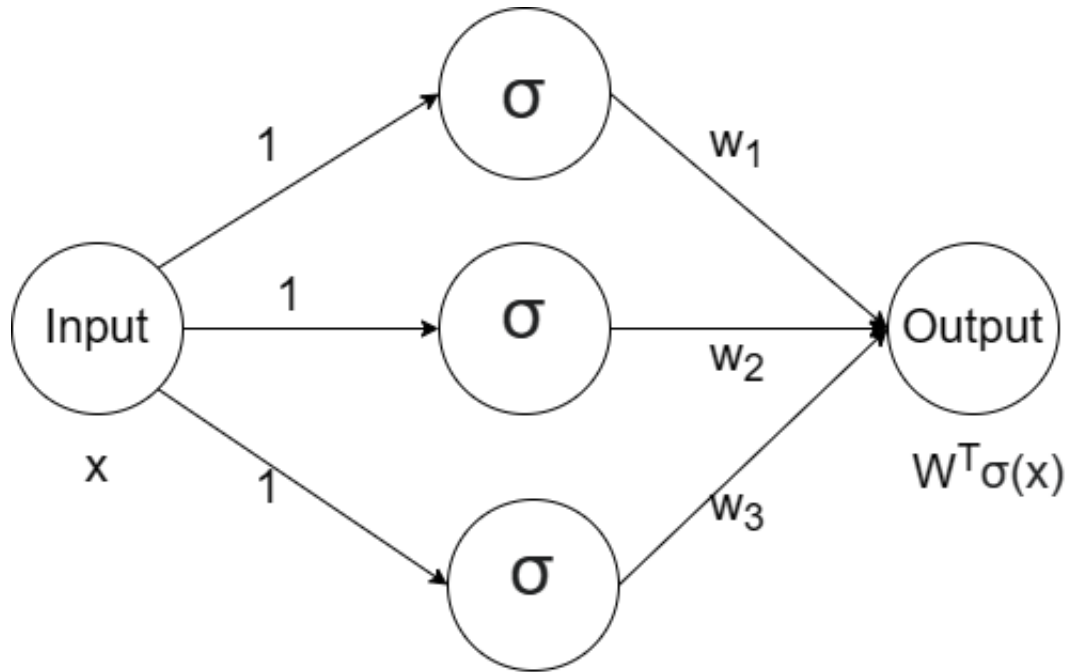


Figure 3.1: Neural network architecture

for updating the weights, we selected the learning rate values as $\eta_1 = 10^3$ and $\eta_2 = 10$. Additionally, for algorithm 2 that retains the previous value of the augmented state and the nonlinear function, we set the parameter $p = 10$.

3.5.3 Simulation results

In the simulation, we employed the following parameters for the vehicle: mass (m) is 1850kg , time constant (τ) is 0.5s , drag coefficient (K_d) is $0.3\text{Ns}^2/\text{m}^2$, and drag force (d_m) is 100N , and the input function is as follows:

$$u(t) = \begin{cases} 0.1 \times t & \text{if } 0s < t < 10s \\ 1 & \text{if } 10s \leq t < 20s \\ \frac{5}{3} - \frac{t}{30} & \text{if } 20s \leq t < 30s \\ \frac{t}{40} & \text{if } 30s \leq t < 40s \\ 1 & \text{if } 40s \leq t < 50s \\ \frac{11}{6} - \frac{t}{60} & \text{if } 50s \leq t < 60s \end{cases} \quad (3.30)$$

In this case, we make the assumption that the control input is measurable and known, as shown in Figure 3.2. The observer that has been proposed exhibits superior performance in estimating the states of the vehicle, as demonstrated in Figures 3.3-3.5. The position, speed, and acceleration of the vehicle are estimated with exceptional accuracy, with the steady-state estimation error $|x - \hat{x}|$ remaining below 10^{-6} . A zoomed-in view reveals a rapid convergence rate, with the state converging in under 0.1 seconds. Additionally, it is noteworthy that the neural approximator's weights are initialized randomly, yet the results consistently exhibit similar performance. Furthermore, Figure 3.6 presents the estimated nonlinear function of the forces. We notice that both the augmented state and the neural approximator converge, This allows us to derive an approximate analytical equation for these unknown forces :

$$F = \hat{W}\sigma(x) + \varepsilon(x, u) \quad (3.31)$$

Figure 3.7 illustrates the adaptation of the weights based on the driving scenario.

It's important to mention that we've carried out comprehensive numerical simulations to evaluate the efficacy of the proposed observer in estimating the vehicle's states and unknown nonlinear dynamics using more assertive input signals. Specifically, we have tested a sinusoidal input that results in a quick switch between acceleration and braking. To showcase the robustness in various driving scenarios, we will employ a more assertive input in the upcoming simulation example. We have selected an input of the form:

$$u(t) = M\sin(t) \quad \text{where } M > 0$$

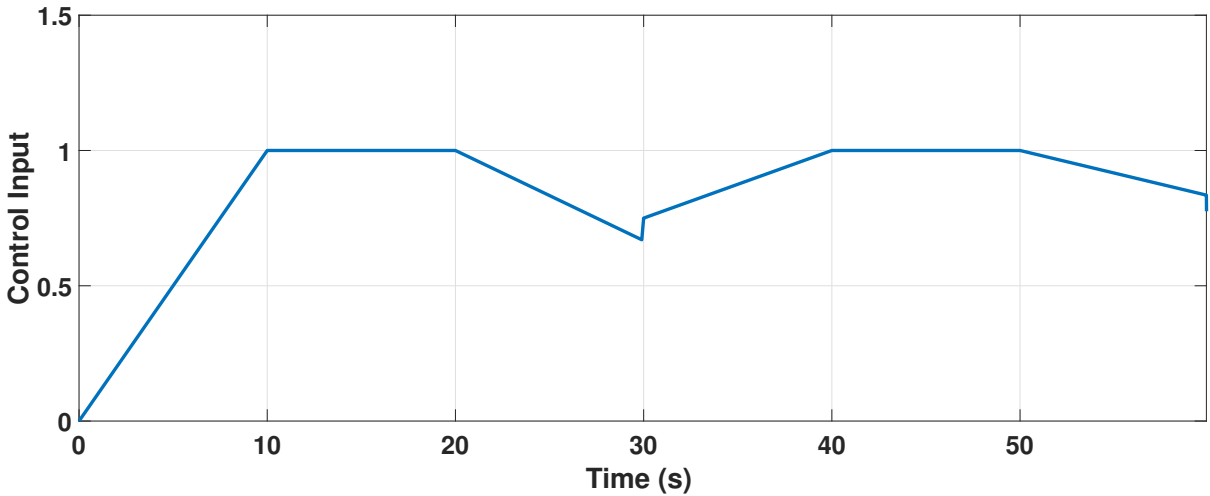


Figure 3.2: Vehicle's control input $u(t)$.

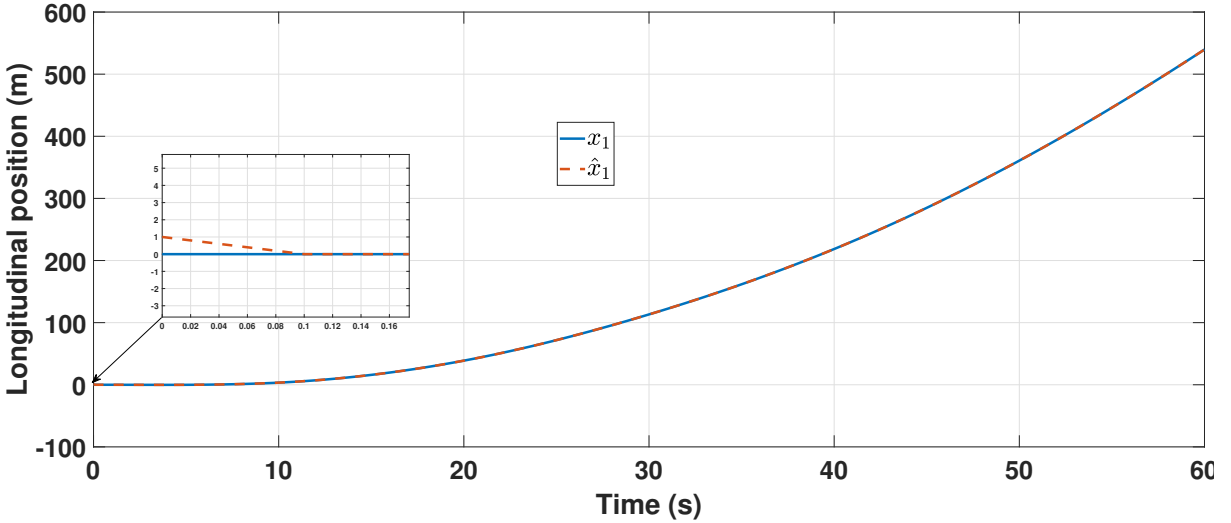


Figure 3.3: Estimated vehicle's longitudinal position $x_1(t)$.

which indicates that the input rapidly alternates between acceleration and braking. As illustrated in figure 3.8, the precision of the state estimation is noteworthy, showcasing strong performance even in more demanding driving scenarios. In figure 3.9, the estimation of the nonlinear function is adequately accurate. Moreover, the adaptive weights display changes corresponding to different driving scenarios.

3.5.4 Comparison

To highlight the advantages of our proposed estimation method, we carried out a comparison with a similar neuro-adaptive observer technique developed in [86]. To make the comparison fair, we kept the same number of neurons and used the same

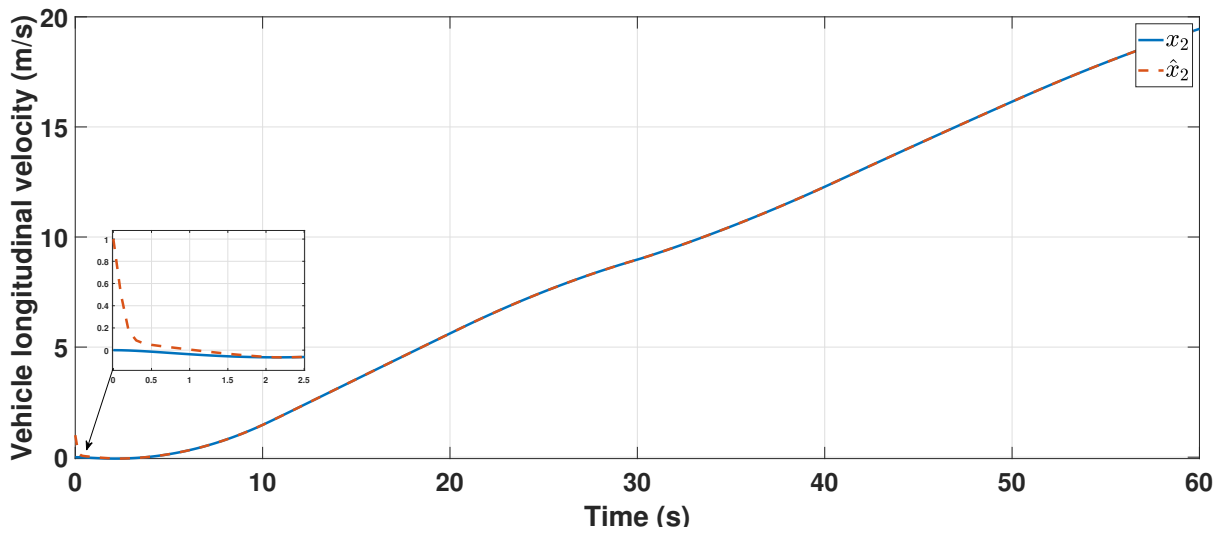


Figure 3.4: Estimated vehicle's longitudinal velocity $x_2(t)$.

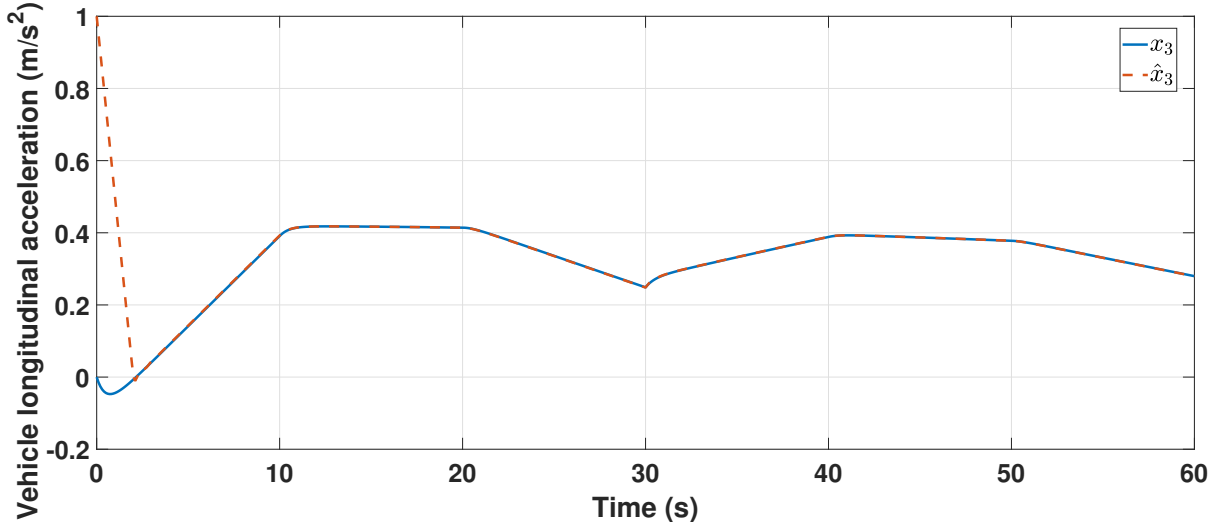


Figure 3.5: Estimated vehicle's longitudinal acceleration $x_3(t)$.

activation functions, as these were the most logical choices. The simulation results for the states and unknown function are depicted in Figures 3.10-3.11. While the estimation method proposed in [86] accurately captures the dynamics of the vehicle's position and velocity similar to our proposed observer, it significantly falls short in precisely estimating the vehicle's acceleration and the unknown nonlinear function, where the estimates oscillate and do not converge to the actual dynamics. Notably, in comparison to [86], [106], our method ensures that the weights of the neural network continue to update even after the states have converged, thanks to the proposed learning and update paradigms. It can handle a broader range of activation functions, as it operates without any specific assumptions or constraints on them and does not necessitate complex fine-tuning of its parameters or initial conditions for the weights.

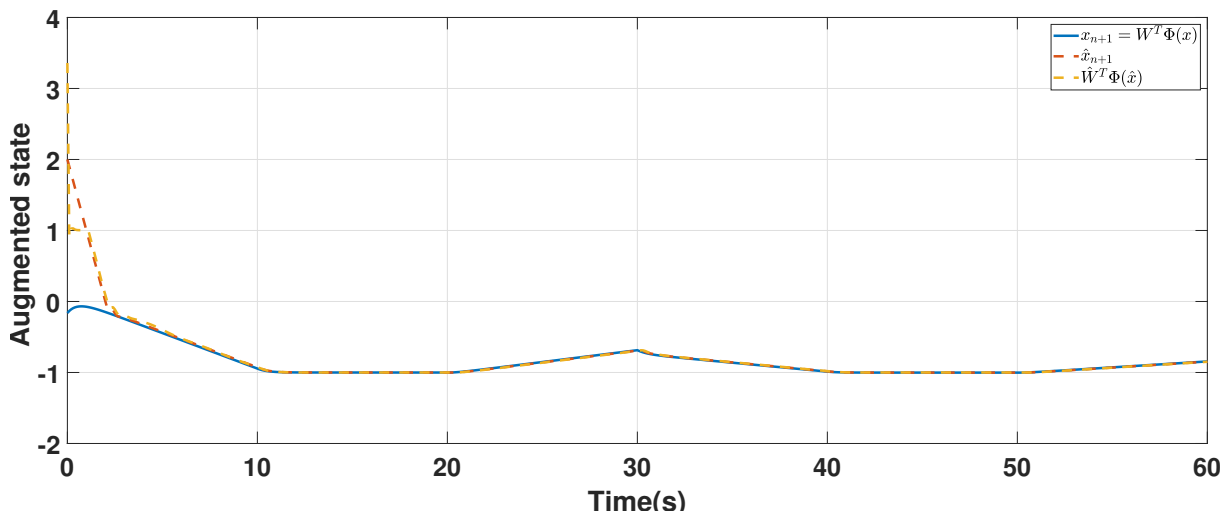


Figure 3.6: Estimated unknown augmented state $x_4(t) \equiv f(x(t))$.

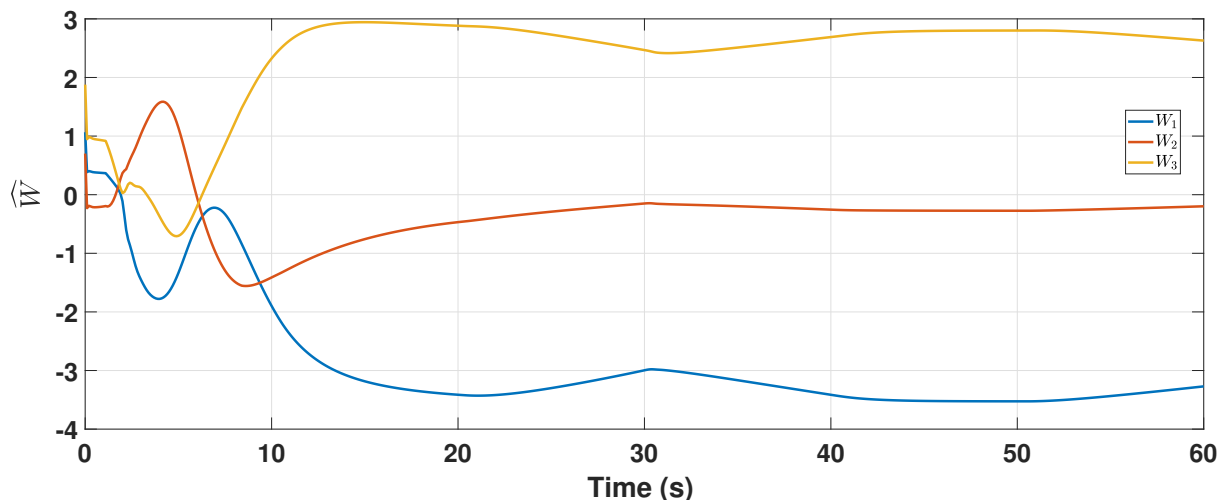


Figure 3.7: Estimated neural network weights $\hat{W}(t)$.

3.6 Conclusion

In this chapter, we began by discussing the concept of neuro-adaptive observers, which integrate neural networks to adaptively estimate states and unknown dynamics in systems. We reviewed an existing method of neuro-adaptive observers applied to vehicle state estimation, highlighting its strengths and limitations. Subsequently, we explored a method that employs concurrent learning observers, which enhance estimation accuracy by utilizing recorded data. Building on these insights, we proposed a novel approach that combines the strengths of both methods to address their respective drawbacks. Our proposed method is designed to be robust against unmodeled dynamics in vehicle models by jointly estimating the states and the unknown dynamics. The observer is formulated using Linear Matrix Inequalities (LMIs) and employs a concurrent learning

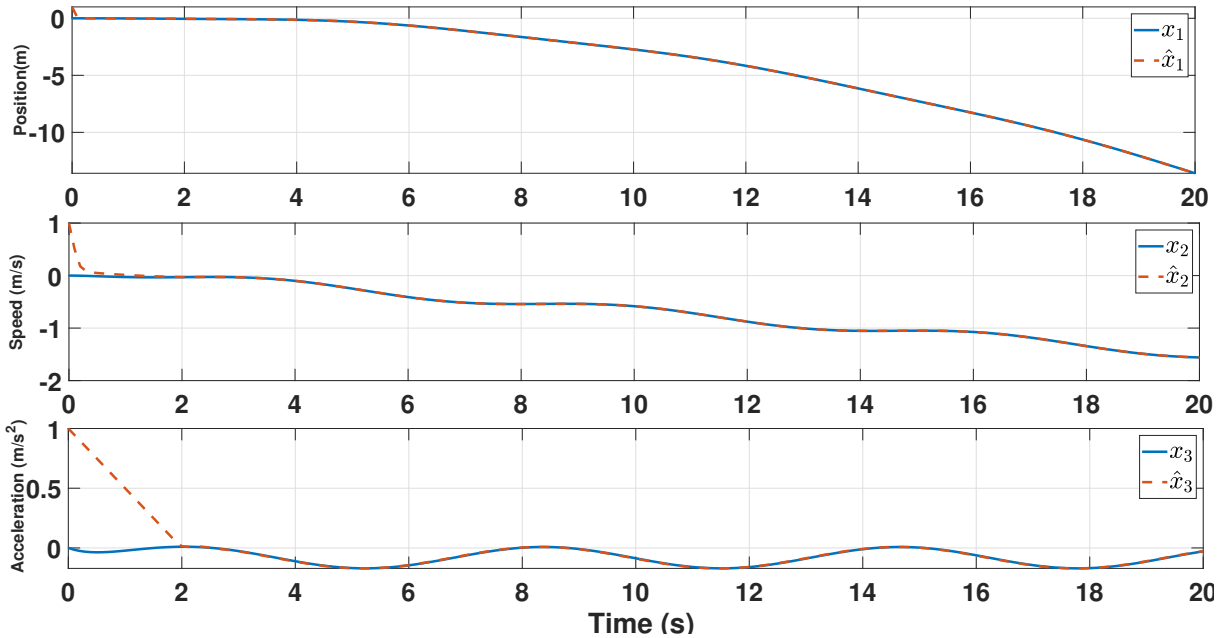


Figure 3.8: Estimated vehicle's states

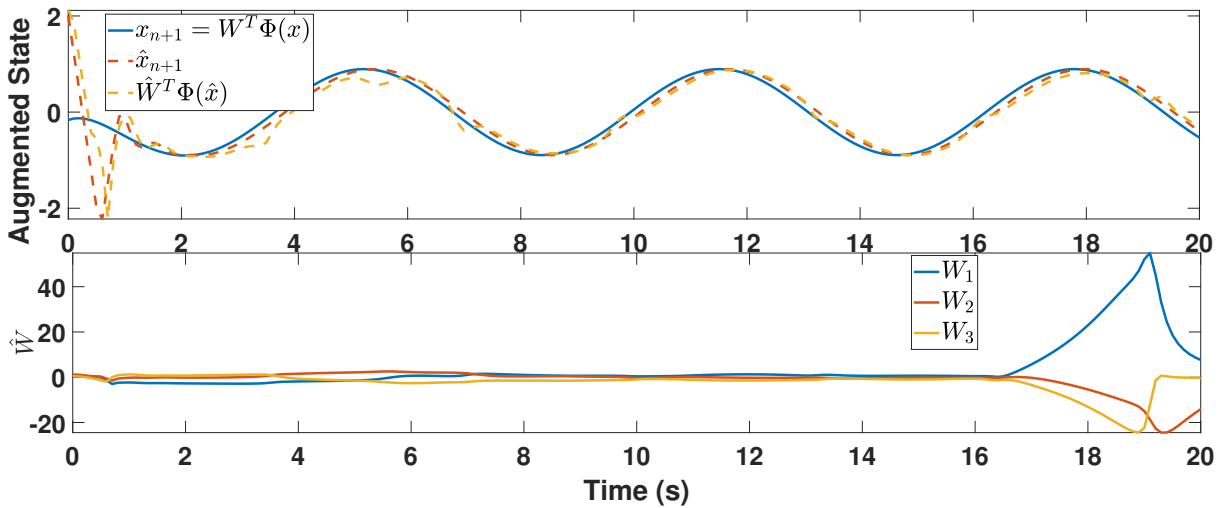


Figure 3.9: Estimated unknown augmented state $x_4(t) \equiv f(x(t))$ and neural network weights $\hat{W}(t)$.

technique to iteratively update the weights of the neural approximator. This dual-update mechanism ensures that both the state estimates and the neural network weights converge effectively.

The observer's gains are carefully designed by solving the derived LMI, ensuring the convergence of the states. Once the states converge, the learning weights of the neural approximator are also proven to be practically convergent. This dual convergence mechanism enhances the reliability and accuracy of the observer, making it a powerful tool for vehicle state estimation in the presence of unmodeled dynamics.

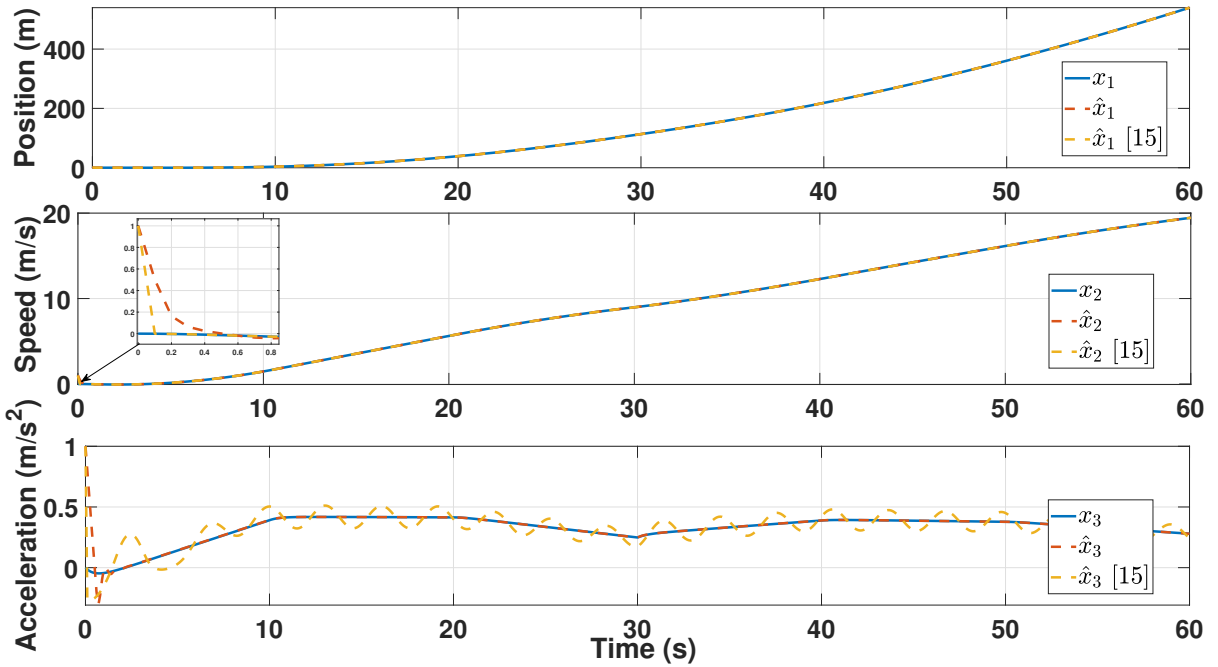


Figure 3.10: Vehicle's estimated states using observer proposed in [86].

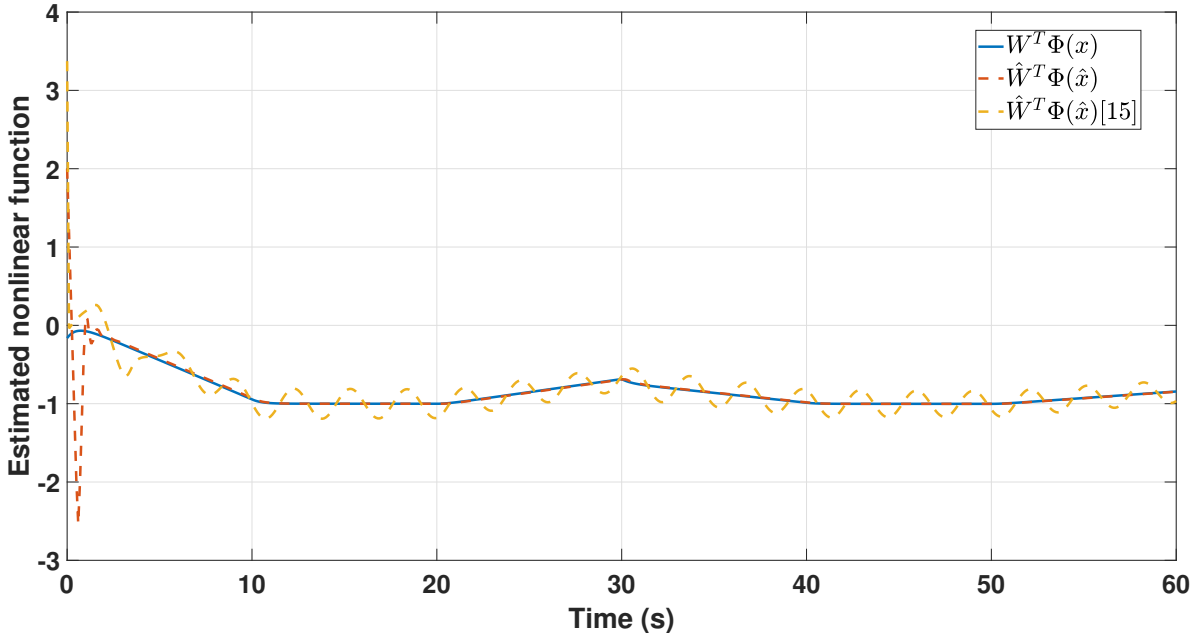


Figure 3.11: Estimated unknown augmented state using observer proposed in [86].

We then conducted simulations on the vehicle longitudinal model to demonstrate the performance of our method. The results were compared with an existing method of neuro-adaptive observers. Our method showed superior performance, particularly in terms of fewer design and simulation constraints. Unlike other methods, our approach does not impose hard constraints on the activation function and does not require a

specific initialization strategy for the weights. We proved that our observer converges in two time scales: first, the states converge, followed by the weights, which continue to update even after the states have converged due to the data recording algorithm. In summary, our proposed observer offers a more flexible and robust solution for vehicle state estimation, effectively addressing unmodeled dynamics while simplifying design and implementation requirements.

4

Generalize High-Gain Observer with Multi Output

Contents

4.1	Introduction	106
4.2	Overview of High-Gain Observer	107
4.2.1	Observability canonical forms	108
4.2.2	High-Gain observer design	111
4.2.3	Limitations of High-Gain observers	113
4.3	New Multi-Output High-Gain observer Design	115
4.3.1	Preliminary tool	115
4.3.2	Callback on the standard High-Gain observer	115
4.3.3	Problem formulation and objectives	118
4.3.4	New Observer Design Methodologies	118
4.3.5	Generalized High-Gain with ISS bounds	123
4.4	Output-based dynamic extension High-Gain observer	128
4.4.1	System transformation and observer structure	128
4.4.2	Generalized High-Gain observer-based design	130
4.4.3	Simplification of the design conditions	133

4.1 Introduction

The concept of the High-Gain observer (HGO) originated in the mid-20th century as a critical tool in control theory, designed to estimate the states of a dynamic system with high accuracy. Early contributions can be traced back to the foundational work on linear state observers by Kalman in the 1960s [9], which laid the groundwork for subsequent developments in nonlinear observer design. The High-Gain observer, specifically, emerged as an effective method for dealing with systems where rapid convergence of the state estimates is crucial. This approach was further refined in the 1980s and 1990s with the introduction of robust and adaptive techniques to handle uncertainties and nonlinearities in practical applications [14], [111], [112]. Over the years, HGOs have been successfully applied in various fields [113], from aerospace engineering to robotics, proving their versatility and robustness in both theoretical and practical contexts. The continuous evolution of HGOs has led to more sophisticated versions, addressing limitations of earlier designs and expanding their applicability in modern control systems [114].

While the effectiveness of High-Gain observers has been well documented in various studies [53], their application to high-dimensional systems presents significant numerical challenges. Specifically, in the design of a standard High-Gain observer, the observer gain is determined by powers of the tuning parameter (θ), which in turn is related to the state dimension (n) [115]. This results in difficulties during numerical implementation when dealing with high state dimensions or when a large High-Gain parameter is required for rapid estimation . Furthermore, High-Gain observers exhibit a high sensitivity to measurement noise, rendering state estimates impractical, particularly in higher-dimensional systems that involve nonlinearities and large Lipschitz constants [116].

Earlier research on High-Gain observers includes the development of the extended High-Gain observer (EHGO) integrated with the extended Kalman filter (EKF) for state estimation [117]. To manage system disturbances, various gain adaptation methods have been proposed [118], [119]. High gains are essential to address nonlinearities in error dynamics, which are often modeled as Lipschitz functions . Recent advancements

have aimed to limit the observer gain's power to enhance performance against measurement noise [14]; however, challenges such as numerical implementation difficulties and peaking phenomena remain. New approaches, such as cascading reduced-order High-Gain observers [120], have been introduced to tackle these issues. Despite these efforts, sensitivity improvements over standard High-Gain observers have been limited. This chapter focuses on analyzing and addressing the implementation issues in both noise-free and noisy scenarios, striving to balance fast state reconstruction, minimize steady-state estimation error. For nonlinear systems in triangular form, stable High-Gain observers are guaranteed if the nonlinear functions are Lipschitz continuous [111], [121]. Consequently, High-Gain observers always have a feasible solution, unlike the more general class of LMI-based observers. Despite their advantages, converting nonlinear systems to the triangular form is challenging. Among the existing LMI-based methods, the LPV/LMI approach [122] is the least conservative. It converts the estimation error dynamics into a polytopic system and uses the convexity principle to solve a finite number of LMI conditions without relying on large upper bounds to manage system nonlinearity. Therefore, this work employs the LPV/LMI method alongside the standard High-Gain observer technique, demonstrating that LMIs can enhance state observer performance. The primary motivation of this work is to propose convergent observer designs that leverage any available additional output measurements without incorporating them into the output equations, which could alter or violate the theoretical properties of the nonlinear system, such as observability, detectability, or the companion form required by standard High-Gain methods. The first observer proposed in this work accounts for measurement noise and introduces a new set of LMI conditions governed by a tuning parameter. An explicit condition for this parameter is derived to ensure the solvability of the LMI while guaranteeing an Input-to-State Stability (ISS) bound on the estimation error, making the observer more robust and versatile in handling real-world scenarios with inevitable measurement noise.

The second proposed method combines the system output with the additional measurement to define a new system form that is in triangular form, ensuring the feasibility of the LMI and providing a systematic design method for an exponential ISS observer.

4.2 Overview of High-Gain Observer

This section aims to present an overview of the sufficient conditions required for the existence of observability canonical forms in nonlinear systems. These forms are a specific instance of feedback forms. When these conditions are satisfied, the nonlinear system can be transformed into a system for which observer design techniques are

well-known. For clarity, we focus on single-input single-output (SISO) nonlinear systems. Extending these results to multi-input multi-output (MIMO) systems is not straightforward.

4.2.1 Observability canonical forms

Observability Canonical Form is essential for control systems as it ensures that every distinct initial state can be inferred from the system's output, given the right input. These inputs are universal, applying across different system states. In linear systems, this form simplifies the state-space model, making it easier to design state observers for accurate state estimation. However, in nonlinear systems, not every input achieves this level of discernibility. Instead, certain inputs may only affect specific states. For such systems, uniform observability is crucial, ensuring that state observability remains consistent over time, regardless of initial conditions. The Observability Canonical Form helps in structuring these systems to meet the criteria for uniform observability.

In the context of observation, an extension of stationary linear systems involves considering linear systems with output injection:

$$\begin{aligned}\dot{x} &= Ax + f(u(t), y(t)) \\ y &= Cx\end{aligned}\tag{4.1}$$

where $x \in \mathbb{R}^n$, $u \in \mathbb{R}^m$, and $y \in \mathbb{R}^p$. Here, the state $x = (x_1, \dots, x_n)^T$ evolves within a compact subset I_x of \mathbb{R}^n , and $y = (y_1, \dots, y_p)^T$ is measured from C, I_x , involving a compact subset I_u of the input space \mathbb{R}^m . The observability of (C, A) implies that system (4.1) is observable regardless of the input.

For system (4.1), the input can be extended using the Luenberger observer:

$$\dot{\hat{x}} = A\hat{x} + f(u, y) + L(y - C\hat{x})\tag{4.2}$$

where L is a constant matrix that ensures system stability (i.e $(A - LC)$ is Hurwitz). Given this advantageous observability property and the intrinsic nature of observability (independent of system coordinates), the challenge of transforming a nonlinear system into the form (4.1), through a coordinate change has been explored in [111].

Autonomous system case uniform observability

For more simple case let's consider an autonomous system with single output as follow [111]:

$$\begin{cases} \dot{x} = f(x) \\ y = h(x) \end{cases} \quad (4.3)$$

in which $x \in \mathbb{R}^n$ and $y \in \mathbb{R}$ the necessary conditions in order to transform the system in (4.3) to the canonical form as follow :

$$\begin{cases} \dot{x} = Ax + Bf(x) \\ y = Cx \end{cases} \quad (4.4)$$

where,

$$A = \begin{pmatrix} 0 & 1 & 0 & \cdots & 0 \\ 0 & 0 & 1 & \cdots & 0 \\ \vdots & \vdots & \vdots & \ddots & \vdots \\ 0 & 0 & 0 & \cdots & 1 \\ 0 & 0 & 0 & \cdots & 0 \end{pmatrix}, \quad C = [1 \ 0 \ \cdots \ 0] \quad \text{and} \quad B = \begin{bmatrix} 0 \\ 0 \\ \vdots \\ 1 \end{bmatrix}$$

We assume that (4.3) is observable on $\Omega \subset \mathbb{R}^n$, i.e., the output $y(t)$ on any finite time interval $[t_0, t_1]$, where $t_1 > t_0$, completely determines the initial state $x(t_0)$, at least for trajectories $x(t)$ such that $x(t) \in \Omega$ for all t . The observability of (4.3) is equivalent to the requirement that the set of functions, known as the "observation space" of (4.3),

$$\{h, L_f h, L_f^2 h, \dots, L_f^i h, \dots\}$$

where $i \geq 0$, separates points on Ω , i.e., for all $x_p, x_q \in \Omega$, there exists an i such that $L_f^i h(x_p) \neq L_f^i h(x_q)$. Here, L denotes the Lie derivative operator. This is due to the formula:

$$y(t) = \sum_{k=0}^{+\infty} \frac{L_f^k h(x_0) t^k}{k!}.$$

If the system (4.3) is observable then there exist a map :

$$F : \mathbb{R}^n \rightarrow \mathbb{R}^n \quad x \mapsto \begin{pmatrix} h(x) \\ L_f h(x) \\ \vdots \\ L_f^{n-1} h(x) \end{pmatrix}$$

If the map F is a diffeomorphism from Ω onto $F(\Omega)$, the system in (4.3) can be transformed and represented as the system in (4.4).

Assumption 4.2.1. *The function f can be extended from Ω to the entire \mathbb{R}^n by a C^∞ function that is globally Lipschitz on \mathbb{R}^n with respect to any norm.*

Definition 4.2.1

If the system (4.3) can be written in the form (4.4) and assumption 4.2.1 holds, we say that the system (4.3) is *uniformly observable* on Ω .

Uniform observability means that the initial state can be reconstructed based on the data formed by the output and its first $(n - 1)$ derivatives.

Non-Autonomous system case uniform observability

For nonlinear systems with inputs, designing an observer is challenging because the input can render the system unobservable. Therefore, we focus on systems that remain observable for universal inputs.

Consider the following single-output affine control nonlinear system:

$$\begin{cases} \dot{\hat{x}} = f(x) + g(x)u, \\ y = h(x). \end{cases} \quad (4.5)$$

If we assume the following:

Assumption 4.2.2. *The drift part of the system (4.5):*

$$\begin{cases} \dot{x} = f(x) \\ y = h(x) \end{cases}$$

is uniformly observable in the sense of definition 4.2.1

Assumption 4.2.3. *The system (4.5) is observable for every input $u \in L^\infty([0, T], \mathbb{R}^m)$, where $T > 0$ is fixed, indicating that u is a universal input. Specifically, for any initial states x_0 and x_1 , the corresponding outputs $y(x_0, u, t)$ and $y(x_1, u, t)$ are not identically equal on*

$[0, T(x_0, x_1, u)]$, where $T(x_0, x_1, u) \leq T$ is the maximum time for which the trajectories $x(t)$ and $x_1(t)$ are well-defined for every $t \in [0, T(x_0, x_1, u)]$.

Definition 4.2.2

If Assumption 4.2.2 and Assumption 4.2.3 hold for the system (4.5), then we can conclude that the system is uniformly observable for any input.

A simpler characterization of these systems is provided in the following theorem:

Theorem 4.2.1

The system (4.5) is uniformly observable for any input if and only if there exists a diffeomorphism $f : \mathbb{R}^n \rightarrow \mathbb{R}^n$ that transforms the system (4.5) into the canonical form:

$$\dot{z} = Az + Bf(z) + G(z)u,$$

$$y = Cz,$$

where $z = f(x)$ and $f(z)$ captures the transformed nonlinear dynamics with,

$$A = \begin{pmatrix} 0 & 1 & 0 & \cdots & 0 \\ 0 & 0 & 1 & \cdots & 0 \\ \vdots & \vdots & \vdots & \ddots & \vdots \\ 0 & 0 & 0 & \cdots & 1 \\ 0 & 0 & 0 & \cdots & 0 \end{pmatrix}, \quad B = \begin{bmatrix} 0 \\ \vdots \\ 1 \end{bmatrix}, \quad C = \begin{bmatrix} 1 & 0 & \cdots & 0 \end{bmatrix} \text{ and } G(z) = \begin{pmatrix} g_1(z_1) \\ g_2(z_1, z_2) \\ \vdots \\ g_n(z_1, \dots, z_n) \end{pmatrix}.$$

For proof, the reader can refer to [111].

4.2.2 High-Gain observer design

Consider a nonlinear system that can be written in the canonical form:

$$\begin{aligned} \dot{z} &= Az + Bf(z) + G(z)u, \\ y &= Cz, \end{aligned} \tag{4.6}$$

where $x \in \mathbb{R}^n$ is the state vector, $u \in \mathbb{R}^m$ is the input vector, and $y \in \mathbb{R}$ is the output vector. Here, A , B , and C are constant matrices of appropriate dimensions, with

$$A = \begin{pmatrix} 0 & 1 & 0 & \cdots & 0 \\ 0 & 0 & 1 & \cdots & 0 \\ \vdots & \vdots & \vdots & \ddots & \vdots \\ 0 & 0 & 0 & \cdots & 1 \\ 0 & 0 & 0 & \cdots & 0 \end{pmatrix}, \quad B = \begin{bmatrix} 0 \\ \vdots \\ 1 \end{bmatrix}, \quad C = \begin{bmatrix} 1 & 0 & \cdots & 0 \end{bmatrix} \text{ and } G(z) = \begin{pmatrix} g_1(z_1) \\ g_2(z_1, z_2) \\ \vdots \\ g_n(z_1, \dots, z_n) \end{pmatrix}.$$

Assumption 4.2.4. *The nonlinear function $f(z)$ is assumed to be globally Lipschitz continuous with respect to z . This means there exists a constant $\gamma > 0$ such that for all $z_1, z_2 \in \mathbb{R}^n$ and for all $u \in \mathbb{R}^m$:*

$$\|f(z_1) - f(z_2)\| \leq \gamma \|z_1 - z_2\|.$$

The High-Gain observer for the system is designed as:

$$\begin{aligned} \dot{\hat{x}} &= A\hat{x} + Bf(\hat{x}) + G(\hat{x})u + T(\theta)L(y - \hat{y}), \\ \hat{y} &= C\hat{x}, \end{aligned}$$

where $\hat{x} \in \mathbb{R}^n$ is the estimated state vector, $\hat{y} \in \mathbb{R}$ is the estimated output vector, and $T(\theta)$ is a diagonal matrix given by:

$$T(\theta) = \text{diag}(\theta, \theta^2, \dots, \theta^n),$$

where θ is large positive parameter.

The gain L is design such that $A - LC$ is a Hurwitz matrix.

Then we get the following the theorem:

Theorem 4.2.2

If Assumption 4.2.4 holds, then for sufficiently large θ , the High-Gain observer guarantees that the estimation error $e = x - \hat{x}$ converges to zero exponentially. Specifically, there exist constants $\alpha > 0$ and $\beta > 0$ such that:

$$\|e(t)\| \leq \alpha e^{-\beta t} \|e(0)\|,$$

where $x(t)$ is the unknown trajectory we are trying to estimate.

Remark 4.2.5. *The High-Gain observer is straightforward to tune. It essentially consists of a replica of the system dynamics coupled with a correction term. This correction term is independent of the specific system but depends solely on the dimension of the state vector and the desired convergence rate, which is controlled by the parameter θ .*

4.2.3 Limitations of High-Gain observers

High-Gain observers are effective tools for state estimation in nonlinear systems. However, they have certain limitations and challenges that must be addressed to ensure their effectiveness and practical application.

1. Implementation Issues

- **Computational Load:** As the dimension of the state vector increases, the gain matrix $T(\theta)$ becomes larger, leading to increased computational demands. This can strain the computational resources of real-time systems, requiring efficient algorithms and potentially specialized hardware.
- **Gain Tuning:** Selecting appropriate gain parameters θ is critical. The values of these parameters must be large enough to ensure rapid convergence but not so large as to cause instability or excessive noise amplification. Finding a balance requires experience and trial-and-error, often guided by simulations and empirical adjustments.
- **Algorithmic Complexity:** The algorithms used to implement High-Gain observers must handle the potentially high-frequency oscillations and transient effects induced by large gains. This can complicate both the design and implementation processes, necessitating robust numerical methods and stability analysis.

2. Peaking Phenomenon

the peaking phenomenon refers to the rapid and often significant increase in the observer's transient response due to excessively large gain values. This phenomenon has several implications:

- **Transient Response:** With very high gains, the transient response of the observer can become excessively large. This manifests as a spike or "peak" in the estimation error, which can overshoot and oscillate before converging to the true state. This behavior is undesirable as it can cause instability or degrade system performance.
- **Impact on Stability:** The peaking phenomenon can potentially lead to instability if the observer is not properly tuned. Large transient responses can interact with the system dynamics in unpredictable ways, leading to sustained oscillations or even divergence in extreme cases.

3. Sensitivity to Measurement Noise

High-Gain observers are particularly sensitive to measurement noise due to their amplification of small deviations:

- **Noise Amplification:** The large values of the gain matrix $T(\theta)$ result in a strong sensitivity to noise in the measurements. Even small amounts of noise can be amplified, leading to significant inaccuracies in the estimated state. This can severely impact the performance of the observer, particularly in noisy environments.
- **Impact on Estimation:** The amplified noise can cause the estimated states to deviate significantly from their true values, reducing the accuracy and reliability of the state estimates. This is especially problematic in applications where precise state information is crucial.

4. **System Form Requirements** High-Gain observers are designed based on the assumption that the system is in a specific canonical form. This implies:

- **Canonical Form Requirement:** The system must be expressed in a canonical form suitable for applying the High-Gain observer design. If the system is not in this form, applying a High-Gain observer directly may not be feasible or effective.
- **Lack of Additional Measurements or Constraints:** The design of the High-Gain observer does not accommodate additional measurements or constraints beyond those provided by the system's canonical form. This means that if extra measurements or constraints are available, they cannot be used to enhance observer performance. The observer's effectiveness is strictly limited to the information provided by the canonical form and cannot leverage additional system insights or modifications.

Efforts have been made to address the limitations of High-Gain observers. For instance, the peaking phenomenon has been investigated in the works [115], [116], [123], where various strategies are discussed. The literature provides several solutions, such as rescaling techniques outlined in [115], projections discussed in [124], and time-varying gains [125], [126]. Recent publications have introduced advanced methods, including nested saturation techniques as described in [127] and the combination of High-Gain observers with LPV LMI observers, as explored in [121]. To address noise sensitivity, several strategies can be employed, including filtering techniques, robust estimation methods, and noise reduction algorithms [121], [128]–[130]. Additionally, tuning the gain parameters to a level that balances performance with noise robustness is essential for example having large value for θ in transient and then decrease it during the steady state [113].

In the following section, we will present a novel High-Gain observer design that addresses some of the previously mentioned limitations, particularly for multi-output systems.

4.3 New Multi-Output High-Gain observer Design

In this section, we present a novel generalized High-Gain observer tailored for multi-output systems. This observer is specifically designed to accommodate additional measurements that diverge from the conventional triangular form. The design integrates general observer conditions, combining Linear Matrix Inequality (LMI) criteria with a threshold constraint on the High-Gain parameter.

4.3.1 Preliminary tool

Lemma 4.3.1: [122]

Consider a function $\Psi : \mathbb{R}^n \rightarrow \mathbb{R}^p$. Then, the two following items are equivalent:

- Ψ is γ_Ψ -Lipschitz with respect to its argument, i.e.:

$$\|\Psi(X) - \Psi(Y)\| \leq \gamma_\Psi \|X - Y\|, \quad \forall X, Y \in \mathbb{R}^n. \quad (4.7)$$

- for all $i = 1, \dots, p$, $j = 1, \dots, n$, there exist functions

$$\psi_{ij} : \mathbb{R}^n \times \mathbb{R}^n \rightarrow \mathbb{R}$$

and constants $\underline{\gamma}_{\psi_{ij}}$ and $\bar{\gamma}_{\psi_{ij}}$, so that $\forall X, Y \in \mathbb{R}^n$,

$$\Psi(X) - \Psi(Y) = \sum_{i=1}^{i=n} \sum_{j=1}^{j=n} \psi_{ij} \mathcal{H}_{ij}^{p,n}(X - Y), \quad (4.8)$$

and

$$-\gamma_\Psi \leq \underline{\gamma}_{\psi_{ij}} \leq \psi_{ij} \leq \bar{\gamma}_{\psi_{ij}} \leq \gamma_\Psi, \quad (4.9)$$

where

$$\psi_{ij} \triangleq \psi_{ij}(X^{Y_{j-1}}, X^{Y_j}) \text{ and } \mathcal{H}_{ij}^{p,n} = \mathbf{e}_p(i) \mathbf{e}_n^\top(j).$$

4.3.2 Callback on the standard High-Gain observer

This part is dedicated to revisiting the standard High-Gain observer methodology, which will be employed in subsequent sections of this work. We focus on a specific class of triangular systems characterized by the presence of a nonlinear term in the final

component of the system:

$$\left\{ \begin{array}{l} \dot{x} = \begin{bmatrix} \dot{x}_1 \\ \dot{x}_2 \\ \vdots \\ \vdots \\ \dot{x}_{n-1} \\ \dot{x}_n \end{bmatrix} = \begin{bmatrix} x_2 \\ x_3 \\ \vdots \\ \vdots \\ x_n \\ f(x) \end{bmatrix}, \\ y = x_1. \end{array} \right. \quad (4.10)$$

where $x \in \mathbb{R}^n$ is the state vector, $y \in \mathbb{R}$ is the measured output, and the function $f : \mathbb{R}^n \rightarrow \mathbb{R}$ satisfies the Lipschitz condition in the following form:

$$|f(x_1 + \Delta_1, \dots, x_n + \Delta_n) - f(x_1, \dots, x_n)| \leq \gamma_f \sum_{j=1}^n |\Delta_j|. \quad (4.11)$$

For the sake of brevity, we express system (4.10) in the following form:

$$\left\{ \begin{array}{l} \dot{x} = Ax + Bf(x), \\ y = Cx, \end{array} \right. \quad (4.12)$$

where

$$B = \begin{bmatrix} 0 & \dots & 0 & 1 \end{bmatrix}^\top, \quad C = \begin{bmatrix} 1 & 0 & \dots & 0 \end{bmatrix}, \quad (4.13)$$

and the state matrix A is defined as

$$(A)_{i,j} = \begin{cases} 1 & \text{if } j = i+1, \\ 0 & \text{if } j \neq i+1. \end{cases} \quad (4.14)$$

In accordance with the standard High-Gain observer methodology, we consider the following state observer:

$$\dot{\hat{x}} = A\hat{x} + Bf(\hat{x}) + L(y - C\hat{x}), \quad (4.15)$$

where the gain matrix L is defined as

$$L \triangleq T(\theta)K, \quad \theta > 1, \quad (4.16)$$

with

$$T(\theta) \triangleq \text{diag}(\theta, \dots, \theta^n) \text{ and } K \in \mathbb{R}^{n \times p}.$$

This formulation allows for the systematic tuning of the observer gain through the parameter θ , thereby facilitating the design of observers with desired convergence properties. The transformed estimation error forms the basis of the High-Gain methodology and is defined as follows:

$$\hat{e} := T^{-1}(\theta)\tilde{e}, \quad (4.17)$$

where $T^{-1}(\theta)$ denotes the inverse of $T(\theta)$.

In the context of the standard High-Gain method, the dynamics of the transformed error \hat{e} are described by:

$$\dot{\hat{e}} = \theta(A - KC)\hat{e} + \frac{1}{\theta^n}B\Delta f, \quad (4.18)$$

where

$$\Delta f := f(x) - f(x - T(\theta)\hat{e}).$$

Using the Lipschitz condition (4.11) and the fact that $\theta \geq 1$, it can be demonstrated that there exists a positive constant k_f , independent of θ , such that

$$\|T^{-1}(\theta)B\Delta f\| \leq k_f\|\hat{e}\|. \quad (4.19)$$

We now recall the following theorem, which is standard in the High-Gain observer methodology.

Theorem 4.3.1: [131]

Consider that there exist matrices $P > 0$, $\lambda > 0$, Y , and a scalar $\theta \geq 1$ such that the following conditions are satisfied:

$$A^\top P + PA - C^\top Y - Y^\top C + \lambda I < 0, \quad (4.20)$$

$$\theta > \theta_0 = \frac{2k_f\lambda_{\max}(P)}{\lambda}, \quad (4.21)$$

where $k_f \geq \gamma_f$ is a constant independent of θ .

Then, for $K = P^{-1}Y^\top$, the observer (4.15) converges exponentially.

Proof. For a detailed proof, refer to [131]. The proof employs the Lyapunov function $\vartheta(\hat{e}) = \hat{e}^\top P\hat{e}$, where \square

4.3.3 Problem formulation and objectives

Standard High-Gain observers are limited in their ability to handle additional outputs or system constraints. Although the High-Gain approach guarantees convergence, it is susceptible to internal or external disturbances, especially in systems with measurement noise.

To address these limitations, we propose a more generalized design of High-Gain observer that can leverage extra measurements or constraints of the system. This approach is also applicable when the system is not in triangular form, which precludes the use of standard High-Gain observers. By utilizing additional system information, this new methodology enhances observer accuracy. This will be achieved by incorporating the extra constraints into the observer design and establishing the conditions under which the High-Gain observer is applicable. Let consider the system as follow :

$$\begin{cases} \dot{x} = Ax + Bf(x) \\ y = Cx \\ z = h(x) \end{cases} \quad (4.22)$$

with $f, h : \mathbb{R}^n \rightarrow \mathbb{R}$ satisfy the Lipschitz property formulated under the form shown in (4.11).

Similarly to f in (4.19), we can show that there exists a positive constant k_h , independent of θ , such that:

$$\|T^{-1}(\theta)\Delta h\| \leq k_h \|\hat{e}\|. \quad (4.23)$$

Consider the following Luenberger observer as follows:

$$\dot{\hat{x}} = A\hat{x} + Bf(\hat{x}) + L(y - C\hat{x}) + M(z - h(\hat{x})) \quad (4.24)$$

where

The dynamics of the estimation error $\tilde{e} = x - \hat{x}$ is given by

$$\dot{\tilde{e}} = (A - LC)\tilde{e} + B[f(x) - f(\hat{x})] - M[h(x) - h(\hat{x})] \quad (4.25)$$

4.3.4 New Observer Design Methodologies

This section focuses on theoretical observer design methodologies for triangular systems with additional output measurements. The first approach is a direct extension of the High-

Gain method. In contrast, the second approach, which serves as an alternative, utilizes LMI-based techniques to address some of the limitations inherent in the first method.

First Method

This section addresses the conditions required to incorporate additional output measurements into the observer design. The core idea is to solve the same LMI as in the standard High-Gain method, but with an additional constraint on the gain parameter θ , as outlined in the following theorem:

Theorem 4.3.2

Consider that there exist symmetric positive definite matrices $P > 0$ and Y of appropriate dimensions, as well as the scalars $\lambda > 0$, $\theta > 0$, and $\alpha \in (0, 1)$, such that the following conditions are satisfied:

$$A^\top P + PA - C^\top Y - Y^\top C + \lambda I < 0 \quad (4.26)$$

$$\theta > \max \left(1, \frac{2k_f \lambda_{\max}(P)}{\alpha \lambda} \right) \quad (4.27a)$$

$$\theta < \left(\frac{(1-\alpha)\lambda}{2k_h \|M\| \lambda_{\max}(P)} \right)^{\frac{1}{n-2}} \quad (4.27b)$$

Then the state observer (4.24) with $K = P^{-1}Y^\top$ converges exponentially. Here, $\lambda_{\max}(P)$ denotes the maximum eigenvalue of P , and $\|M\|$ represents the norm of the observer gain M corresponding to the additional outputs $z(t)$.

Proof. Using the condition (4.23) and the fact that $\theta \geq 1$, we have

$$\begin{aligned} \|T^{-1}(\theta)M(h(x) - h(\hat{x}))\| &\leq \frac{1}{\theta} \|M\| \|\Delta h\| \\ &\leq \frac{1}{\theta} \|M\| k_h \|T(\theta)\hat{e}\| \\ &\leq \frac{1}{\theta} \|M\| k_h \theta^n \|\hat{e}\| \\ &\leq \theta^{n-1} k_h \|M\| \|\hat{e}\|, \end{aligned} \quad (4.28)$$

where $\hat{e} = T^{-1}\tilde{e}$ is the transformed error, with its dynamics defined as follows:

$$\dot{\hat{e}} = \theta (A - KC) \hat{e} - \frac{1}{\theta^n} B \Delta f + T^{-1} M \Delta h \quad (4.29)$$

Thus, differentiating the Lyapunov function $V(\hat{e}) \triangleq \hat{e}^\top P \hat{e}$ along the trajectories of $\dot{\hat{e}}$, we obtain

$$\begin{aligned} \dot{V}(\hat{e}) &= \theta \hat{e}^\top \left[P(A - KC) + (A - KC)^\top P \right] \hat{e} \\ &\quad + 2\hat{e}^\top PT^{-1}(\theta)B\Delta f - 2\hat{e}^\top PT^{-1}(\theta)M\Delta h \\ &\leq \theta \hat{e}^\top (A - KC)\hat{e} + k_f \|P\| \|\hat{e}\|^2 \\ &\quad + \theta^{n-1} k_h \|P\| \|M\| \|\hat{e}\|^2 \\ &\leq (-\theta\lambda + 2k_f \lambda_{\max}(P) + 2\theta^{n-1} k_h \|M\| \lambda_{\max}(P)) \|\hat{e}\|^2, \end{aligned} \quad (4.30)$$

where we used (4.19), (4.20), and

$$\hat{e}^\top PT^{-1}(\theta)B\Delta f \leq k_f \lambda_{\max}(P) \hat{e}^\top \hat{e},$$

$$\hat{e}^\top PT^{-1}(\theta)M\Delta h \leq \theta^{n-1} k_h \lambda_{\max}(P) \|M\| \|\hat{e}\|^2.$$

To ensure exponential convergence of the estimation error, the following inequality must hold:

$$\theta > \frac{2k_f \lambda_{\max}(P)}{\lambda} + \frac{2\theta^{n-1} k_h \|M\| \lambda_{\max}(P)}{\lambda}. \quad (4.31)$$

Given $\alpha \in (0, 1)$, we can write

$$\theta = \alpha\theta + (1 - \alpha)\theta.$$

Therefore, using equations (4.27a) and (4.27b), we obtain:

$$\begin{aligned} \alpha\theta &> \frac{2k_f \lambda_{\max}(P)}{\lambda}, \\ (1 - \alpha)\theta &> \frac{2\theta^{n-1} k_h \|M\| \lambda_{\max}(P)}{\lambda}, \end{aligned}$$

which leads to (4.31).

Working in the Archimedean space [53], there exists $\delta_\theta > 0$, depending on θ , such that

$$\dot{V}(\hat{e}) \leq -\delta_\theta \|\hat{e}\|^2 \leq -\frac{\delta_\theta}{\lambda_{\min}(P)} V(\hat{e}),$$

implying that the estimation error \hat{e} satisfies

$$\|\hat{e}(t)\| \leq \sqrt{\frac{\lambda_{\max}(P)}{\lambda_{\min}(P)}} \|\hat{e}_0\| e^{-\frac{\delta_\theta}{2\lambda_{\min}(P)} t}. \quad (4.32)$$

Thus, from (4.32) and (4.17), the estimation error $\tilde{e}(t)$ converges exponentially to zero. This concludes the proof. \square

Note that the conditions (4.26), (4.27a), and (4.27b) are always satisfiable. In particular, (4.26) always admits a solution due to the observability of the pair (A, C) . Therefore, θ can be chosen to satisfy (4.27a). The matrix M must be selected to satisfy (4.27b), or equivalently:

$$\|M\| \leq \frac{(1-\alpha)\lambda}{2k_h\lambda_{\max}(P)\theta^{n-2}}, \quad (4.33)$$

where α is chosen to balance the bounds in (4.27a) and (4.33).

While this method provides a valid observer design, the constraint (4.33) may lead to a very small matrix M , rendering the additional output measurements $z(t)$ relatively ineffective. To address this limitation, we propose an alternative method in the following section that employs LMI techniques and convexity principles.

Second Method

We propose an alternative design methodology to address the limitation imposed by constraint (4.33). This approach leverages the LPV/LMI technique to manage the nonlinear output function $h(\cdot)$, as detailed in [122]. Thus, by applying Lemma 4.3.1 to the nonlinear function $h(\cdot)$, we can identify functions

$$\psi_j : \mathbb{R}^n \times \mathbb{R}^n \rightarrow \mathbb{R}, \quad (4.34)$$

such that:

$$h(x) - h(\hat{x}) = \Delta h = \sum_{j=1}^n \psi_j e_n^T(j)$$

along with constants $\underline{\gamma}_j \leq 0$ and $\bar{\gamma}_j \geq 0$ such that $\underline{\gamma}_j \leq \psi_j \leq \bar{\gamma}_j$. Consequently, the error dynamics in (4.25), for $M \neq 0$, can be reformulated as follows:

$$\dot{\tilde{e}} = \theta (A - KC - \bar{M}\Sigma(\theta, \Psi)) \tilde{e} + B[f(x) - f(\hat{x})], \quad (4.35)$$

where

$$\Sigma(\theta, \Psi) \triangleq \sum_{j=1}^n \theta^{j-1} \psi_j e_n^T(j), \quad (4.36)$$

$$\bar{M} = T^{-1}(\theta)M, \quad \Psi = [\psi_1 \ \dots \ \psi_n]^\top. \quad (4.37)$$

Given that the functions ψ_j for $j = 1, \dots, n$ are bounded, the vector Ψ belongs to a bounded convex set \mathcal{S}^Ψ , where the set of vertices is given by

$$\mathcal{V}_\Psi \triangleq \left\{ v \in \mathbb{R}^n : v_j \in \{\underline{\gamma}_j, \bar{\gamma}_j\} \right\}. \quad (4.38)$$

In light of this, and using the LPV/LMI approach along with convexity principles, we present the following theorem:

Theorem 4.3.3

Suppose there exist matrices $P = P^\top > 0$, Y , and Z of suitable dimensions, along with scalars $\lambda > 0$ and $\sigma > 0$, such that the following conditions are met:

$$A^\top P + PA - C^\top Y - Y^\top C - \Sigma^\top(\sigma, w)Z - Z^\top \Sigma(\sigma, w) + \lambda I < 0 \quad \forall w \in \mathcal{V}_\Psi, \quad (4.39)$$

$$\frac{2k_f \lambda_{\max}(P)}{\lambda} < \theta \leq \sigma. \quad (4.40)$$

Then, the estimation error \tilde{e} is exponentially stable with

$$K = P^{-1}Y^\top \quad \text{and} \quad M = P^{-1}Z^\top.$$

Proof. We use the quadratic Lyapunov function

$$V(\hat{e}) \triangleq \hat{e}^\top P \hat{e},$$

By defining the variable changes $Y^\top = PK$ and $Z^\top = PM$, the derivative along the trajectories of (4.35) satisfies:

$$\begin{aligned} \dot{V}(\hat{e}) &= \theta \hat{e}^\top [A^\top P + PA - C^\top Y - Y^\top C] \hat{e} \\ &\quad - \hat{e}^\top [\Sigma^\top(\theta, \Psi)Z + Z^\top \Sigma(\theta, \Psi)] \hat{e} \\ &\quad + 2\hat{e}^\top PT^{-1}(\theta)B\Delta f \end{aligned} \quad (4.41)$$

and then by using (4.19), we obtain:

$$\begin{aligned}\dot{V}(\hat{e}) &\leq \theta \hat{e}^\top \left[A^\top P + PA - C^\top Y - Y^\top C \right] \hat{e} \\ &\quad - \hat{e}^\top \left[\Sigma^\top(\theta, \Psi) Z + Z^\top \Sigma(\theta, \Psi) \right] \hat{e} \\ &\quad + 2k_f \lambda_{\max}(P) \|\hat{e}\|^2.\end{aligned}\tag{4.42}$$

Given that

$$\Sigma(\theta, \Psi) = \Sigma(\sigma, \Psi^{\theta, \sigma}),$$

where $\Psi_j^{\theta, \sigma} \triangleq \left(\frac{\theta}{\sigma}\right)^{j-1} \psi_j$, the feasibility of (4.57) holds for $\Psi^{\theta, \sigma}$ for all $\theta \leq \sigma$, because $\Psi^{\theta, \sigma} \in \mathcal{S}^\Psi$ for any $\theta \leq \sigma$ (i.e., $\frac{\theta}{\sigma} \leq 1$), and $\Psi \in \mathcal{S}^\Psi$. Hence,

$$\dot{V}(\hat{e}) \leq (-\theta \lambda + 2k_f \lambda_{\max}(P)) \|\hat{e}\|^2.\tag{4.43}$$

This implies exponential convergence of the estimation error if $\theta > \frac{2k_f \lambda_{\max}(P)}{\lambda}$. This completes the proof. \square

Remark 4.3.1. *This second design method addresses the limitations of the first method, specifically avoiding excessively small values for the matrix M . By incorporating additional constraints into the LMI (4.57) and the constraint (4.40), one can better control the matrix M . For example, imposing upper bounds on P and lower bounds on Z can enhance the control over M . A detailed numerical design procedure can be developed to optimize solutions for (4.57) and (4.40) by adding linear constraints and employing a gridding method for scalar parameters.*

4.3.5 Generalized High-Gain with ISS bounds

In this section, we develop a design methodology for High-Gain observers capable of accommodating multiple outputs, thereby generalizing the conventional High-Gain observer approach. We propose a novel condition on the parameter θ that is linked to the solvability of the associated Linear Matrix Inequality (LMI). This condition ensures not only exponential stability but also provides an input-to-state stability (ISS) bound for the estimation error. We will now analyze the following system:

$$\begin{cases} \dot{x} = Ax + Bf(x) \\ y = Cx + w \\ z = h(x) \end{cases}\tag{4.44}$$

where $x \in \mathbb{R}^n$ is the state vector, $y \in \mathbb{R}$ is the measured output, z is the additional measured output, and $w \in \mathcal{L}_\infty$ is the measurement noise.

Let us consider the following generalized High-Gain observer structure:

$$\dot{\hat{x}} = A\hat{x} + Bf(\hat{x}) + L(y - C\hat{x}) + \mathcal{M}(z - h(\hat{x})). \quad (4.45)$$

where L and M are two observer gains related to the measured outputs y and z respectively. As we exploit the High-Gain methodology, the gain L is expressed under the form

$$L \triangleq T(\theta)K, \quad M \triangleq T(\theta)\mathcal{N}_\theta, \quad \theta > 1, \quad (4.46)$$

The dynamics of the estimation error \tilde{e} is given as follows:

$$\dot{\tilde{e}} = (A - LC)\tilde{e} + B[f(x) - f(\hat{x})] - M[h(x) - h(\hat{x})] - Lw. \quad (4.47)$$

Furthermore, before tackling the stability analysis, we introduce the transformed error

$$\varepsilon(t) \triangleq T^{-1}(\theta)\tilde{e}(t). \quad (4.48)$$

Let us express the dynamic of the transformed estimation error, $\varepsilon(t)$, as follows:

$$\dot{\varepsilon} = \theta(A - KC)\varepsilon + \frac{1}{\theta^n}B\Delta f - \mathcal{N}_\theta\Delta h - Kw. \quad (4.49)$$

By applying Lemma 4.3.1 on the Lipschitz function h , there exist functions $\psi_j : \mathbb{R}^n \times \mathbb{R}^n \rightarrow \mathbb{R}$ and constants $\underline{\gamma}_j \leq 0$ and $\bar{\gamma}_j \geq 0$, with $\underline{\gamma}_j \leq \psi_j \leq \bar{\gamma}_j$, such that

$$\Delta h = \left(\sum_{j=1}^n \theta^j \psi_j e_n^\top(j) \right) \varepsilon. \quad (4.50)$$

Consequently, the dynamic equation of the transformed estimation error, ε , is expressed as follows:

$$\dot{\varepsilon} = \theta \left(A - \mathcal{N}_\theta \left(\sum_{j=1}^n \theta^{j-1} \psi_j e_n^\top(j) \right) - KC \right) \varepsilon + \frac{1}{\theta^n}B\Delta f - Kw. \quad (4.51)$$

The occurrence of powers of θ in the High-Gain observer design complicates the formulation of practical conditions for selecting an adequately large θ while ensuring an input-to-state stability (ISS) bound on the estimation error. To address this challenge, we first define:

$$\mathcal{N}_\theta = \frac{1}{\theta^n} \mathcal{N},$$

where $\mathcal{N} \in \mathbb{R}^{n \times 1}$ is a constant vector. By introducing the notation:

$$\mathcal{A}(\Psi^\theta) \triangleq - \sum_{j=1}^n \psi_j^\theta \mathbf{e}_n^\top(j), \quad (4.52)$$

where

$$\Psi^\theta \triangleq \begin{bmatrix} \psi_1^\theta & \dots & \psi_n^\theta \end{bmatrix}^\top, \quad \psi_j^\theta \triangleq \theta^{j-n-1} \psi_j,$$

the error dynamics described by equation (4.51) can be simplified to:

$$\dot{\varepsilon} = \theta \left(A + \mathcal{N} \mathcal{A}(\Psi^\theta) - KC \right) \varepsilon + \frac{1}{\theta^n} B \Delta f - Kw. \quad (4.53)$$

Given that the functions ψ_j for $j = 1, \dots, n$ are bounded, the vector $\Psi \triangleq [\psi_1 \ \dots \ \psi_n]^\top$ belongs to a bounded convex set \mathcal{S} , where the set of vertices is:

$$\mathcal{V} \triangleq \left\{ v \in \mathbb{R}^n \mid v_j \in \{\underline{\gamma}_j, \bar{\gamma}_j\} \right\}. \quad (4.54)$$

Consequently, the vector Ψ^θ belongs to a bounded convex set \mathcal{S}^θ , with the set of vertices given by:

$$\mathcal{V}^\theta \triangleq \left\{ v \in \mathbb{R}^n \mid v_j \in \{\underline{\gamma}_j \theta^{j-n-1}, \bar{\gamma}_j \theta^{j-n-1}\} \right\}. \quad (4.55)$$

The following inclusion is significant for the subsequent discussion:

$$\forall \theta \geq 1, \sigma \geq 1, \text{ if } \theta \geq \sigma, \text{ then } \mathcal{S}^\theta \subseteq \mathcal{S}^\sigma. \quad (4.56)$$

We now summarize the design methodology in the following theorem.

Theorem 4.3.4

Assume that there exist matrices $\mathcal{P} = \mathcal{P}^\top > 0$, \mathcal{X} , \mathcal{Y} , and \mathcal{Z} , of appropriate dimensions, and two scalars $\lambda > 0$ and $\sigma \geq 1$, such that the following conditions are satisfied:

$$\begin{bmatrix} \mathcal{H}e\left\{\mathcal{P}A - \mathcal{Y}^\top C + \mathcal{Z}^\top \mathcal{A}(\xi)\right\} + \lambda \mathbb{I}_n & \mathcal{Y}^\top \\ \mathcal{Y} & -\mathcal{X} \end{bmatrix} < 0, \quad \forall \xi \in \mathcal{V}^\sigma, \quad (4.57)$$

$$\theta > \max\left(\sigma, \frac{2k_f \lambda_{\max}(\mathcal{P})}{\lambda}\right), \quad (4.58)$$

where

$$\mathcal{H}e\left\{\mathbb{V}\right\} \triangleq \mathbb{V} + \mathbb{V}^\top$$

for any given matrix \mathbb{V} . Then, with $K = \mathcal{P}^{-1} \mathcal{Y}^\top$ and $\mathcal{N} = \mathcal{P}^{-1} \mathcal{Z}^\top$, the estimation error \tilde{e} satisfies the following exponential ISS bound:

$$\begin{aligned} \|\tilde{e}(t)\| &\leq \theta^{n-1} \sqrt{\frac{\lambda_{\max}(\mathcal{P})}{\lambda_{\min}(\mathcal{P})}} \|\tilde{e}_0\| e^{-\frac{\kappa}{2}t} \\ &\quad + \frac{\theta^{n-\frac{1}{2}}}{\sqrt{\kappa}} \sqrt{\frac{\lambda_{\max}(\mathcal{X})}{\lambda_{\min}(\mathcal{P})}} \sup_{s \in [0,t]} \|w(s)\|, \end{aligned} \quad (4.59)$$

where

$$\kappa \triangleq \frac{\theta \lambda - 2k_f \lambda_{\max}(\mathcal{P})}{\lambda_{\max}(\mathcal{P})}. \quad (4.60)$$

Proof. We use the quadratic Lyapunov function

$$\vartheta(\varepsilon) \triangleq \varepsilon^\top \mathcal{P} \varepsilon.$$

Introducing the substitutions $\mathcal{P}K = \mathcal{Y}^\top$ and $\mathcal{P}\mathcal{N} = \mathcal{Z}^\top$, and expanding the derivative of $\vartheta(\varepsilon)$ along the trajectories of (4.53), we obtain:

$$\begin{aligned}\dot{\vartheta}(\varepsilon) &\leq \theta \varepsilon^\top \mathcal{H} e \left\{ \mathcal{P} A - \mathcal{Y}^\top C + \mathcal{Z}^\top \mathcal{A}(\Psi^\theta) \right\} \varepsilon \\ &\quad + 2k_f \lambda_{\max}(\mathcal{P}) \|\varepsilon\|^2 - 2\varepsilon^\top \mathcal{P} K w.\end{aligned}\tag{4.61}$$

Applying Young's inequality [132] (see Appendix A.1.5), we get:

$$\begin{aligned}\dot{\vartheta}(\varepsilon) &\leq \theta \varepsilon^\top \left[\mathcal{H} e \left\{ \mathcal{P} A - \mathcal{Y}^\top C + \mathcal{Z}^\top \mathcal{A}(\xi) \right\} \right. \\ &\quad \left. + \mathcal{Y}^\top \mathcal{X}^{-1} \mathcal{Y} \right] \varepsilon + 2k_f \lambda_{\max}(\mathcal{P}) \|\varepsilon\|^2 \\ &\quad + \frac{\lambda_{\max}(\mathcal{X})}{\theta} \|w\|^2.\end{aligned}\tag{4.62}$$

From Schur's Lemma, LMI (4.57) is equivalent to:

$$\mathcal{H} e \left\{ \mathcal{P} A - \mathcal{Y}^\top C + \mathcal{Z}^\top \mathcal{A}(\Psi^\theta) \right\} + \mathcal{Y}^\top \mathcal{X}^{-1} \mathcal{Y} \leq \lambda \mathbb{I}_n,\tag{4.63}$$

which, combined with the inclusion (4.56), ensures that for any $\theta \geq \sigma$, the inequality:

$$\mathcal{H} e \left\{ \mathcal{P} A - \mathcal{Y}^\top C + \mathcal{Z}^\top \mathcal{A}(\Psi^\theta) \right\} + \mathcal{Y}^\top \mathcal{X}^{-1} \mathcal{Y} \leq \lambda \mathbb{I}_n,\tag{4.64}$$

remains valid. Consequently, using (4.64), (4.58), and

$$\lambda_{\min}(\mathcal{P}) \|\varepsilon\|^2 \leq \vartheta(\varepsilon) \leq \lambda_{\max}(\mathcal{P}) \|\varepsilon\|^2,$$

we obtain:

$$\dot{\vartheta}(\varepsilon) \leq -\kappa \vartheta(\varepsilon) + \frac{\lambda_{\max}(\mathcal{X})}{\theta} \|w\|^2.\tag{4.65}$$

Applying the comparison theorem [53], we get:

$$\begin{aligned}\|\varepsilon(t)\| &\leq \sqrt{\frac{\lambda_{\max}(\mathcal{P})}{\lambda_{\min}(\mathcal{P})}} \|\varepsilon_0\| e^{-\frac{\kappa}{2}t} \\ &\quad + \frac{1}{\sqrt{\theta} \sqrt{\kappa}} \sqrt{\frac{\lambda_{\max}(\mathcal{X})}{\lambda_{\min}(\mathcal{P})}} \sup_{s \in [0,t]} \|w(s)\|.\end{aligned}\tag{4.66}$$

Finally, using the inequality:

$$\theta \|\varepsilon(t)\| \leq \|\tilde{e}(t)\| \leq \theta^n \|\varepsilon(t)\|, \quad \forall t \geq 0,$$

the ISS bound (4.59) follows. This concludes the proof. □

4.4 Output-based dynamic extension High-Gain observer

In this section, we introduce an innovative observer design method leveraging the standard High-Gain (SHGO) methodology. The core concept involves applying SHGO to a modified nonlinear form of a triangular nonlinear system, incorporating additional outputs that do not conform to the companion structure. The theoretical contributions of this approach are threefold:

1. It addresses the challenge of designing a High-Gain observer for systems with nonlinear outputs.
2. It allows the integration of additional measured outputs into the observer structure, potentially enhancing estimation performance.
3. It extends the applicability of SHGO to nonlinear systems that include non-triangular nonlinear components.

We consider the same system as in (4.44). As highlighted in the previous section, the SHGO methodology cannot be directly applied to the model (4.44) while also utilizing the extra output z . Therefore, we need to adapt the observer strategy. The first key idea of this work involves transforming the system (4.44). Subsequently, an observer is designed for the transformed system, providing an estimation \hat{x} of the original state x .

4.4.1 System transformation and observer structure

This section elaborates on the central concepts of the proposed theoretical framework. To effectively utilize both outputs y and z , we introduce a new output measurement, y_{new} , which is a combination of y and z . The definition of this new output is given by:

$$\begin{cases} \dot{\mu}(t) = \alpha y(t) + \beta^{n-1} z(t), \\ \mu(0) = \mu_0, \\ y_{\text{new}} = \mu(t), \end{cases} \quad (4.67)$$

where μ_0 is a known initial value of μ . The constants α and β are non-negative and will be determined through specific design conditions introduced in the following section.

Next, we define the following matrices and functions:

$$\xi \triangleq \begin{bmatrix} \mu \\ x \end{bmatrix}, \quad y_\xi \triangleq C_\xi \xi = y_{\text{new}}, \quad C_\xi \triangleq \begin{bmatrix} C & 0 \end{bmatrix}, \quad (4.68)$$

$$A_\xi \triangleq \begin{bmatrix} [0 & \alpha] & 0_{1 \times (n-1)} \\ 0_{n \times 1} & A \end{bmatrix}, \quad B_w \triangleq C_\xi^\top, \quad (4.69)$$

$$B_f \triangleq \begin{bmatrix} 0 \\ B \end{bmatrix}, \quad B_\xi \triangleq \begin{bmatrix} 0 \\ B_u \end{bmatrix}, \quad B_h \triangleq C_\xi^\top, \quad (4.70)$$

$$f_\xi(\xi) \triangleq f(x), \quad (4.71)$$

$$h_\xi(\xi) \triangleq h(x), \quad (4.72)$$

Using these definitions, we transform system (4.44) into the following form:

$$\begin{cases} \dot{\xi} = A_\xi \xi + \alpha B_w w + B_f f_\xi(\xi) + \beta^{n-1} B_h h_\xi(\xi) + B_\xi u(t), \\ y_\xi = C_\xi \xi, \\ x = \begin{bmatrix} 0 & \mathbb{I}_n \end{bmatrix} \xi. \end{cases} \quad (4.73)$$

We propose the following state observer, designed to estimate the state \hat{x} of x :

$$\begin{cases} \dot{\hat{\xi}} = A_\xi \hat{\xi} + B_f f_\xi(\hat{\xi}) + \beta^{n-1} B_h h_\xi(\hat{\xi}) + B_\xi u(t) + T(\theta)K(y_\xi - C_\xi \hat{\xi}), \\ \hat{x} = \begin{bmatrix} 0 & \mathbb{I}_n \end{bmatrix} \hat{\xi}, \end{cases} \quad (4.74)$$

where

$$T(\theta) \triangleq \text{diag}(\theta, \dots, \theta^{n+1}), \quad \theta \geq 1.$$

The objective is to determine the non-negative constants α and β , the parameter $\theta \geq 1$, and the matrix $K \in \mathbb{R}^{n+1 \times 1}$ such that the estimation error $\tilde{\xi} \triangleq \xi - \hat{\xi}$ converges exponentially to zero. To achieve this, we extend the SHGO method to this class of systems (4.73), excluding the triangular term $h_\xi(\xi)$. By introducing the transformed estimation error $\varepsilon \triangleq T^{-1}(\theta)\tilde{\xi}$, we derive the following error dynamics:

$$\dot{\varepsilon} = \theta (A_\xi - KC_\xi) \varepsilon + \frac{\alpha}{\theta} B_w w + \frac{1}{\theta^{n+1}} B_f \Delta f_\xi(\xi, \hat{\xi}) + \frac{\beta^{n-1}}{\theta} B_h \Delta h_\xi(\xi, \hat{\xi}), \quad (4.75)$$

where

$$\Delta f_\xi(\xi, \hat{\xi}) \triangleq f_\xi(\xi) - f_\xi(\hat{\xi}) = f_\xi(\hat{\xi} + T(\theta)\varepsilon) - f_\xi(\hat{\xi}), \quad (4.76a)$$

$$\Delta h_\xi(\xi, \hat{\xi}) \triangleq h_\xi(\xi) - h_\xi(\hat{\xi}) = h_\xi(\hat{\xi} + T(\theta)\varepsilon) - h_\xi(\hat{\xi}). \quad (4.76b)$$

First, consider the nonlinear term $\Delta f_\xi(\xi, \hat{\xi})$. According to (4.76a) and considering the structure and Lipschitz property of f , since $\theta \geq 1$, there exists a constant $k_f \geq 0$, independent of θ , such that the following inequality holds:

$$\left\| \frac{1}{\theta^{n+1}} B_f \Delta f_\xi(\xi, \hat{\xi}) \right\| \leq k_f \|\varepsilon\|. \quad (4.77)$$

As for the term $\Delta h_\xi(\xi, \hat{\xi})$, it requires a different handling method compared to $\Delta f_\xi(\xi, \hat{\xi})$. This difference arises because this term appears in the first component of the error system and depends on the second component of the error vector, namely ε_2 . Due to this structure, it is not possible to find a constant $k_h \geq 0$, independent of θ , such that

$$\left\| \frac{1}{\theta} B_h \Delta h_\xi(\xi, \hat{\xi}) \right\| \leq k_h \|\varepsilon\|. \quad (4.78)$$

We can only guarantee the existence of a function $k_h(\theta) \geq 0$ to ensure a similar inequality to (4.78). Indeed, since $\theta \geq 1$, we have $\theta^j \leq \theta^{n+1}$ for all $j = 1, \dots, n+1$. Hence, considering that the term $\Delta h_\xi(\xi, \hat{\xi})$ is in the first component of the system (4.75), we can show that there exists $k_h \geq 0$, independent of θ , such that

$$\left\| \frac{\beta^{n-1}}{\theta} B_h \Delta h_\xi(\xi, \hat{\xi}) \right\| \leq \underbrace{\beta^{n-1} \theta^n k_h}_{k_h(\theta)} \|\varepsilon\|. \quad (4.79)$$

4.4.2 Generalized High-Gain observer-based design

Consider the Lyapunov function $\vartheta(\varepsilon) = \varepsilon^\top \mathcal{P} \varepsilon$. Using the results from (4.77) and (4.79), the derivative of $\vartheta(\varepsilon)$ along the trajectories of (4.75) satisfies the following inequality:

$$\begin{aligned} \dot{\vartheta}(\varepsilon) &\leq \theta \varepsilon^\top \left[A_\xi^\top \mathcal{P} + \mathcal{P} A_\xi - C_\xi^\top \mathcal{Z} - \mathcal{Z}^\top C_\xi \right] \varepsilon \\ &\quad + 2\varepsilon^\top \mathcal{P} T(\theta) B_f \Delta f_\xi \\ &\quad + 2\varepsilon^\top \mathcal{P} T(\theta) B_h \Delta h_\xi \\ &\quad + 2\frac{\alpha}{\theta} \varepsilon^\top \mathcal{P} B_w w. \end{aligned} \quad (4.80)$$

then by using (4.77) and (4.79), we get:

$$\begin{aligned}\dot{\vartheta}(\varepsilon) &\leq \theta \varepsilon^\top \left[A_\xi^\top \mathcal{P} + \mathcal{P} A_\xi - C_\xi^\top \mathcal{Z} - \mathcal{Z}^\top C_\xi \right] \varepsilon \\ &\quad + 2k_f \lambda_{\max}(\mathcal{P}) \|\varepsilon\|^2 \\ &\quad + 2\beta^{n-1} k_h \lambda_{\max}(\mathcal{P}) \theta^n \|\varepsilon\|^2 \\ &\quad + 2 \frac{\alpha}{\theta} \varepsilon^\top \mathcal{P} B_w w.\end{aligned}\tag{4.81}$$

Applying Young's inequality [132], for any symmetric positive definite matrix \mathcal{S} , we have:

$$2 \frac{\alpha}{\theta} \varepsilon^\top \mathcal{P} B_w w \leq \theta \varepsilon^\top (\mathcal{P} B_w) \mathcal{S}^{-1} (\mathcal{P} B_w)^\top \varepsilon + \frac{\alpha^2}{\theta^3} \lambda_{\max}(\mathcal{S}) \|w\|^2.\tag{4.82}$$

Hence, we obtain the following inequality:

$$\begin{aligned}\dot{\vartheta}(\varepsilon) &\leq \theta \varepsilon^\top \left[A_\xi^\top \mathcal{P} + \mathcal{P} A_\xi - C_\xi^\top \mathcal{Z} - \mathcal{Z}^\top C_\xi \right] \varepsilon \\ &\quad + \theta \varepsilon^\top (\mathcal{P} B_w) \mathcal{S}^{-1} (\mathcal{P} B_w)^\top \varepsilon \\ &\quad + 2\lambda_{\max}(\mathcal{P}) [k_f + \beta^{n-1} k_h \theta^n] \|\varepsilon\|^2 \\ &\quad + \frac{\alpha^2}{\theta^3} \lambda_{\max}(\mathcal{S}) \|w\|^2.\end{aligned}\tag{4.83}$$

We are now prepared to state the main theorem, which provides the synthesis conditions ensuring an exponential ISS (Input-to-State Stability) bound on the estimation error.

Theorem 4.4.1

Let $\mathcal{P} = \mathcal{P}^\top > 0$, $\mathcal{S} = \mathcal{S}^\top > 0$, and \mathcal{L} be matrices of appropriate dimensions, with $\theta > 0$ and $0 \leq \sigma \leq 1$ as scalars, such that the following conditions hold:

$$\begin{bmatrix} A_\xi^\top \mathcal{P} + \mathcal{P} A_\xi - C_\xi^\top \mathcal{L} - \mathcal{L}^\top C_\xi + \lambda \mathbb{I}_n & \mathcal{P} B_w \\ (\mathcal{P} B_w)^\top & -\mathcal{S} \end{bmatrix} < 0, \quad (4.84)$$

$$\theta > \max \left(1, \frac{2k_f \lambda_{\max}(\mathcal{P})}{\lambda \sigma} \right), \quad (4.85)$$

$$\theta \leq \frac{1}{\beta} \left(\frac{(1-\sigma)\lambda}{2k_h \lambda_{\max}(\mathcal{P})} \right)^{\frac{1}{n-1}}. \quad (4.86)$$

Then, with $K = \mathcal{P}^{-1} \mathcal{L}^\top$, the estimation error $\tilde{\xi}$ satisfies the following exponential ISS inequality:

$$\|\tilde{\xi}(t)\| \leq \theta^n \sqrt{\frac{\lambda_{\max}(\mathcal{P})}{\lambda_{\min}(\mathcal{P})}} \|\tilde{\xi}(0)\| \exp\left(-\frac{\kappa}{2}t\right) + \frac{\alpha \theta^{n-\frac{1}{2}}}{\sqrt{\kappa}} \sqrt{\frac{\lambda_{\max}(\mathcal{S})}{\lambda_{\min}(\mathcal{P})}} \sup_{s \in [0,t]} \|w(s)\|, \quad (4.87)$$

where

Moreover, for $\hat{\mu}(0) = \mu(0)$, the ISS bound on the state \tilde{x} is given by:

$$\|x(t) - \hat{x}(t)\| \leq \theta^n \sqrt{\frac{\lambda_{\max}(\mathcal{P})}{\lambda_{\min}(\mathcal{P})}} \|x_0 - \hat{x}_0\| \exp\left(-\frac{\kappa}{2}t\right) + \frac{\alpha \theta^{n-\frac{1}{2}}}{\sqrt{\kappa}} \sqrt{\frac{\lambda_{\max}(\mathcal{S})}{\lambda_{\min}(\mathcal{P})}} \sup_{s \in [0,t]} \|w(s)\|. \quad (4.88)$$

Proof. From the Schur lemma and inequality (4.83), condition (4.84) implies:

$$\begin{aligned} \dot{\vartheta}(\varepsilon) &\leq -(\theta\lambda - 2\lambda_{\max}(\mathcal{P})[k_f + \beta^{n-1}k_h\theta^n])\|\varepsilon\|^2 \\ &\quad + \frac{\alpha^2}{\theta^3}\lambda_{\max}(\mathcal{S})\|w\|^2 \\ &\leq -\kappa\vartheta(\varepsilon) + \frac{\alpha^2}{\theta^3}\lambda_{\max}(\mathcal{S})\|w\|^2, \end{aligned} \quad (4.89)$$

where κ is defined in (4.60).

On the other hand, since $\theta = \sigma\theta + (1-\sigma)\theta$ for $0 \leq \sigma \leq 1$, the conditions (4.85)–(4.86)

ensure that $\kappa > 0$. By applying the comparison theorem [53], we obtain:

$$\begin{aligned}\|\varepsilon(t)\| &\leq \sqrt{\frac{\lambda_{\max}(\mathcal{P})}{\lambda_{\min}(\mathcal{P})}} \|\varepsilon(0)\| \exp\left(-\frac{\kappa}{2}t\right) \\ &+ \frac{\alpha}{\sqrt{\theta^3} \sqrt{\kappa}} \sqrt{\frac{\lambda_{\max}(\mathcal{S})}{\lambda_{\min}(\mathcal{P})}} \sup_{s \in [0,t]} \|w(s)\|,\end{aligned}\quad (4.90)$$

which leads to the result in (4.87) by noting that:

$$\theta \|\varepsilon(t)\| \leq \|\tilde{\xi}(t)\| \leq \theta^{n+1} \|\varepsilon(t)\|, \quad \forall t \geq 0.$$

Moreover, if $\hat{\mu}(0) = \mu(0)$, which is straightforward since $\mu(0) = \mu_0$ in (4.67) is known, then the relation (4.88) follows directly. \square

Remark 4.4.1. First, note that the LMI condition (4.84) is always feasible. Furthermore, there always exists a tuning parameter θ such that the conditions (4.85)–(4.86) are satisfied. Specifically, for any θ satisfying (4.85), there exists a sufficiently small $\beta \geq 0$ such that (4.86) holds. Consequently, the design procedure outlined in Theorem 4.4.2 is systematic and ensures that an exponential ISS observer for the system (4.44) can always be designed.

4.4.3 Simplification of the design conditions

While implementing the constraints (4.85)–(4.86) is not overly complex, there is an opportunity to simplify them further by consolidating them into a single condition on the tuning parameter θ . The goal is to establish a unique condition on θ that is applicable to any β . This can be achieved by parameterizing β as follows:

$$\beta = \frac{\varpi^{\frac{1}{n-1}}}{\theta^{1+\frac{1}{n-1}}}, \quad (4.91)$$

where $\varpi \geq 0$ is a new tuning parameter.

First Simplification

Substituting β from (4.91) into (4.86), we obtain:

$$\theta \geq \frac{2k_h \varpi \lambda_{\max}(\mathcal{P})}{(1-\sigma)\lambda}. \quad (4.92)$$

By combining this with (4.85), we derive a unique sufficient condition on θ :

$$\theta > \max \left(1, \frac{2k_f \lambda_{\max}(\mathcal{P})}{\lambda \sigma}, \frac{2k_h \varpi \lambda_{\max}(\mathcal{P})}{(1-\sigma)\lambda} \right). \quad (4.93)$$

In this approach, the design procedure involves solving the LMI condition (4.84) and choosing θ to be sufficiently large, in accordance with (4.93), for any $\varpi \geq 0$. If we consider an observer without the additional measurement z , we obtain a condition similar to that of a standard High-Gain observer. Specifically, for $\varpi = 0$, condition (4.93) simplifies to:

$$\theta > \max \left(1, \frac{2k_f \lambda_{\max}(\mathcal{P})}{\lambda \sigma} \right). \quad (4.94)$$

Second simplification

We now return to the inequality (4.89) before introducing the parameter σ . By substituting β from (4.91) into (4.89), we obtain:

$$\begin{aligned} \dot{\vartheta}(\varepsilon) &\leq -(\theta\lambda - 2\lambda_{\max}(\mathcal{P})[k_f + k_h\varpi])\|\varepsilon\|^2 \\ &\quad + \frac{\alpha^2}{\theta^3}\lambda_{\max}(\mathcal{S})\|w\|^2 \\ &\leq -\kappa_\varpi\vartheta(\varepsilon) + \frac{\alpha^2}{\theta^3}\lambda_{\max}(\mathcal{S})\|w\|^2, \end{aligned} \quad (4.95)$$

where

$$\kappa_\varpi \triangleq \frac{\theta\lambda - 2\lambda_{\max}(\mathcal{P})[k_f + k_h\varpi]}{\lambda_{\max}(\mathcal{P})}. \quad (4.96)$$

Thus, in this case, it is not necessary to introduce the parameter σ . The constraints (4.85)–(4.86) are simplified to the following unique condition on θ :

$$\theta > \max \left(1, \frac{2\lambda_{\max}(\mathcal{P})[k_f + k_h\varpi]}{\lambda} \right), \quad (4.97)$$

which ensures the exponential ISS bound (4.88) with κ_ϖ instead of κ . When the extra measurement z is not included, i.e., $\varpi = 0$, the constraint (4.97) reduces to the standard High-Gain observer condition.

4.5 Conclusion

In this chapter, we have delved into the intricacies of High-Gain observer theory and its application. We began with a thorough presentation of the High-Gain observer, outlining its fundamental principles and underlying theory. However, we also highlighted the inherent limitations of the High-Gain observer, particularly when applied to systems where extra measurements cannot be utilized effectively.

Recognizing these limitations, we introduced a novel methodology designed to integrate additional measurements or constraints into the system. This new approach enables the incorporation of supplementary data that the traditional High-Gain observer framework could not accommodate. We provided rigorous proofs of the convergence of this enhanced observer, demonstrating its effectiveness through an Input-to-State Stability (ISS) bound. Our proofs employed a combination of High-Gain and LPV/LMI observer methodologies.

Furthermore, we extended our discussion to address more complex system forms and nonlinear outputs. By augmenting the system states with an extended output, we showcased a more general strategy to manage various system configurations. This approach not only broadens the applicability of our observer design but also enhances its robustness to measurement noise, ensuring reliable performance in practical scenarios. Overall, this chapter has established a comprehensive framework for the design and implementation of High-Gain observers, addressing both traditional challenges and new opportunities for incorporating additional measurements. Our contributions provide a solid foundation for future research and practical applications, advancing the state of the art in observer design for complex systems.

5

Vehicle Applications and Simulations

Contents

5.1	Introduction	137
5.2	Vehicle Longitudinal Tracking	138
5.2.1	Vehicle dynamic longitudinal model	139
5.2.2	MATLAB simulation results	140
5.2.3	CARLA-based simulation scenarios and estimation results . .	144
5.2.4	Comparison with the Standard High-Gain Observer	147
5.3	Vehicle Motion Estimation	152
5.3.1	Vehicle kinematic model	152
5.3.2	Triangular Transformation	152
5.3.3	Observer Design for the Vehicle Model	154
5.3.4	Simulation Results	155
5.3.5	Experimental Results	158
5.4	Conclusion	166

5.1 Introduction

The precise and robust tracking of vehicle dynamics plays a pivotal role in various vehicular technologies, from driver assistance systems to autonomous driving [15], [16]. Achieving accurate and reliable vehicle tracking, however, presents numerous challenges that require sophisticated solutions. Vehicle systems are inherently complex and nonlinear, with dynamics influenced by external factors such as sensor noise, actuator faults, and environmental disturbances. These uncertainties can significantly disrupt tracking accuracy, making it difficult to predict and reconstruct the true state of the vehicle. While sensors provide valuable measurements [15], they inherently offer incomplete information about the vehicle's state. Sensor limitations, such as noise, delays, and bandwidth constraints, further exacerbate the challenge of obtaining a precise picture of the vehicle's behavior.

Traditional tracking methods often rely on linear models, despite the inherently nonlinear nature of vehicle motion. Previous approaches have attempted to address this complexity through piecewise linearization, introducing separate models for specific maneuvers [17]. These methods typically employed Interacting Multiple Model (IMM) filters [18], [133], such as IMM Kalman Filters, for state estimation. However, linearization-based methods suffer from several limitations:

- **Lack of Stability Proofs:** These methods often lack formal guarantees of stability, raising concerns about their performance under real-world driving conditions.
- **Limited Maneuver Coverage:** The chosen linear models might not encompass the full spectrum of possible vehicle maneuvers, potentially leading to inaccurate tracking during more complex movements.
- **Computational Demands:** Implementing IMM filters can be computationally expensive, requiring real-time evaluation of probabilities associated with each individual model, which can strain resources on embedded systems.

Therefore, it is crucial to explore alternative approaches that can effectively handle the inherent nonlinearities of vehicle motion without sacrificing stability, maneuverability, or computational efficiency.

Our approach begins with the tracking of longitudinal motion of other vehicles. Initially, Matlab simulations were employed to validate our algorithm's developed in Chapter 4

effectiveness in a controlled environment. Following this, the scenario was replicated in the CARLA simulator, which provided a more dynamic and realistic testing ground. The consistent performance in both environments demonstrated the robustness of our high-gain design algorithm.

Furthermore, we extended the application of our algorithm to estimate vehicle motion using a kinematic model. This phase involved Matlab testing, which was subsequently validated using the KITTI dataset, a comprehensive collection of real-world driving data. These steps were critical in assessing the algorithm's practical viability and accuracy. In some scenarios, we compared our algorithm to the Extended Kalman Filter (EKF) and demonstrated that our algorithms (Chapter 4) can perform better, especially in cases of data loss.

This chapter builds upon previous discussions of the high-gain observer and vehicle models, integrating these foundational elements into applied scenarios. By the end of this chapter, readers will have a comprehensive understanding of how high-gain design can be effectively utilized for vehicle motion tracking and estimation, backed by both simulation and real-world data.

5.2 Vehicle Longitudinal Tracking

Longitudinal tracking of vehicle motion is a critical component in the development of advanced driver assistance systems (ADAS) and autonomous driving technologies. It involves monitoring and controlling the vehicle's speed and distance relative to other vehicles on the same path. This process ensures safe and efficient driving by maintaining a set speed or adjusting it to keep a safe following distance from the preceding vehicle. Accurate longitudinal tracking is essential for tasks such as adaptive cruise control, collision avoidance, and automated highway driving. The complexity of this task arises from the need to account for various dynamic factors, including changes in speed, acceleration, and potential disturbances from the surrounding environment. Implementing a robust and reliable tracking system requires sophisticated algorithms capable of handling these challenges while ensuring real-time performance and stability. In this section, we explore the application of high-gain design for longitudinal tracking, starting with Matlab simulations to validate our approach before moving to more dynamic scenarios in the CARLA simulator.

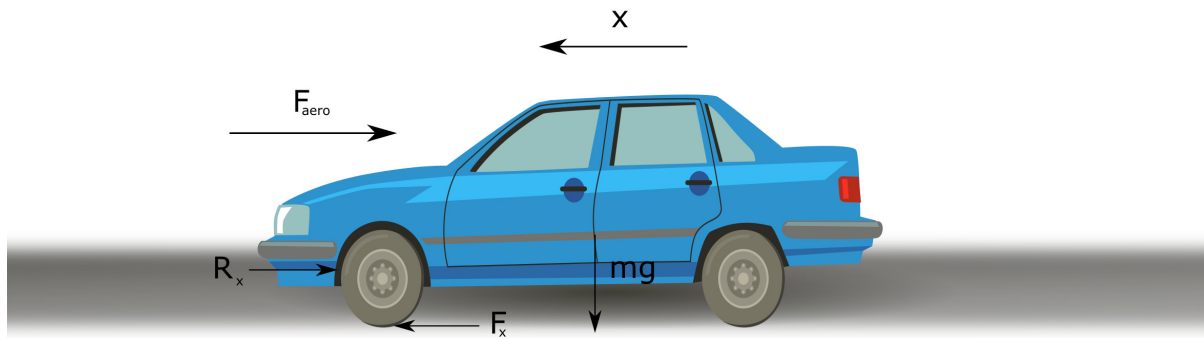


Figure 5.1: Vehicle longitudinal model (in red: ego vehicle, in blue : test vehicle)

5.2.1 Vehicle dynamic longitudinal model

The longitudinal model in Figure 5.1 considers the vehicle (blue) as a mass point and employs Newton's second law to establish the system of equations [51], [52]. This model is written in the relative reference of the ego vehicle (red). Since all the states of the ego vehicle are known, the dynamical model is given as follows (see (1.35) in Chapter 1):

$$\begin{cases} \dot{p}(t) = v(t), \\ \dot{v}(t) = a(t), \\ \dot{a}(t) = -\frac{2K_d}{m}v(t)a(t) \\ \quad - \frac{1}{\tau} \left(a(t) + \frac{K_d}{m}v^2(t) + \frac{d_m}{m} \right), \end{cases} \quad (5.1)$$

where

- p , v , a is the longitudinal position, velocity and acceleration of the blue vehicle, respectively.
- m is the mass of the blue vehicle.
- τ is the engine's time lag.
- d_m is the mechanical drag.
- K_d is the aerodynamic drag coefficient.

We can rewrite the system in (5.1) in a compact form as follows:

$$\begin{cases} \dot{\xi} = A\xi + Bf(\xi) + B_u u(t) \\ y = C\xi \end{cases} \quad (5.2)$$

where the state vector is

$$\xi = \begin{bmatrix} \xi_1 & \xi_2 & \xi_3 \end{bmatrix}^T = \begin{bmatrix} p(t) & v(t) & a(t) \end{bmatrix}^T,$$

and

$$A = \begin{bmatrix} 0 & 1 & 0 \\ 0 & 0 & 1 \\ 0 & 0 & 0 \end{bmatrix}, \quad B = \begin{bmatrix} 0 \\ 0 \\ 1 \end{bmatrix}, \quad C = \begin{bmatrix} 1 & 0 & 0 \end{bmatrix},$$

$$f(\xi) = -\frac{2K_d}{m}\xi_2\xi_3 - \frac{1}{\tau} \left(\xi_3 + \frac{K_{di}}{m}\xi_2^2 + \frac{d_m}{m} \right).$$

In addition to the position measurement, an additional vehicle's speed measurement is used to test the performance of the proposed observer design in 4.3.4 and 4.3.4. Thus, the extra measurement z can be written as:

$$z = D\xi, \text{ with } D = \begin{bmatrix} 0 & 1 & 0 \end{bmatrix}. \quad (5.3)$$

5.2.2 MATLAB simulation results

In this subsection, we will simulate the observer design presented in Section 4.3 and compare it to the standard high-gain observer to illustrate the design procedure and evaluate performance.

The proposed methodology is implemented in MATLAB and applied to the vehicle longitudinal model given in (5.2) with the additional velocity measure (5.3). The vehicle's parameters are taken as: $m = 1850$ kg; $\tau = 0.5$ s, $K_d = 0.3$ N $\frac{s^2}{m^2}$ and $d_m = 100$ N. The Lipschitz constants of the functions $f(\cdot)$ and $h(\cdot)$ are $k_f = 1.9964$ and $k_h = 1$, respectively.

- a) First, we compute the gains using the standard high-gain observer method for the system (5.2). Following Theorem 4.3.2, we take $\lambda = 1$ without loss of generality. By using the YALMIP toolbox in MATLAB, we obtain the following observer parameters:

$$Y = [2.3626, 6.5068, -1.5796],$$

$$\theta = 39.3974,$$

$$P = \begin{bmatrix} 6.5068 & -1.5796 & -2.3284 \\ -1.5796 & 3.0199 & -1.5796 \\ -2.3284 & -1.5796 & 6.5068 \end{bmatrix},$$

as solutions to (4.20). Then, we get

$$K = [1.7255, 3.7263, 1.2793]^T.$$

- b) To address the problem arising from the small value of M in the first method as discussed in Remark 4.3.1, we add more restrictions to the LMI (4.39) by taking

the constrain $Z > 10^4$ to ensure that the M matrix has an effect on the observer design in the second methodology 4.3.4. In this case, we obtain:

$$\begin{aligned}\theta &= 30.3704, \quad ||M|| = 1.5338, \\ Y &= [104.6494, 350.2155, -29.3206]^T, \\ Z &= [2.9269, 1.6601, 2.0146]^T, \\ P &= \begin{bmatrix} 294.6169 & -85.2035 & -111.2819 \\ -85.2035 & 105.2495 & -49.4222 \\ -111.2819 & -49.4222 & 211.9653 \end{bmatrix}.\end{aligned}$$

The observer gain is then given as follows:

$$K = [4.7563, 9.3042, 4.5281]^T.$$

Figure 5.2 shows the estimates of the three states of the longitudinal model, namely position, speed, and acceleration dynamics, using the proposed observer design using Theorem 4.3.4, and Figure 5.3 represents the estimation absolute error. Regarding the position state, we notice that the proposed observer and the standard high-gain observer behave almost the same, which is expected given that the measurement of the vehicle position is considered in all types of observers. However, regarding the vehicle velocity and, more importantly, the vehicle acceleration dynamics, the proposed observer techniques that use the additional speed information perform better than the standard high-gain observer that does not account for it.

Table 5.1: Mean absolute value of the error

Methods	Error on position	Error on velocity	Error on acceleration
High Gain	4.9760×10^{-4}	6.2370×10^{-4}	0.4642
Method 1 (Th. 4.3.4)	4.9754×10^{-4}	5.6257×10^{-4}	0.2961
Method 2 (Th. 4.3.4)	4.9751×10^{-4}	5.0743×10^{-4}	0.0185

Table 5.1 presents the mean absolute value of the error for three different methods: the standard high-gain observer, Method 1, and Method 2. The errors are evaluated across three states: position, velocity, and acceleration. The standard high-gain observer shows a position error of 4.9760×10^{-4} , a velocity error of 6.2370×10^{-4} , and a significantly higher acceleration error of 0.4642. Method 1 improves on the velocity and acceleration errors, reducing them to 5.6257×10^{-4} and 0.2961 respectively, while maintaining a

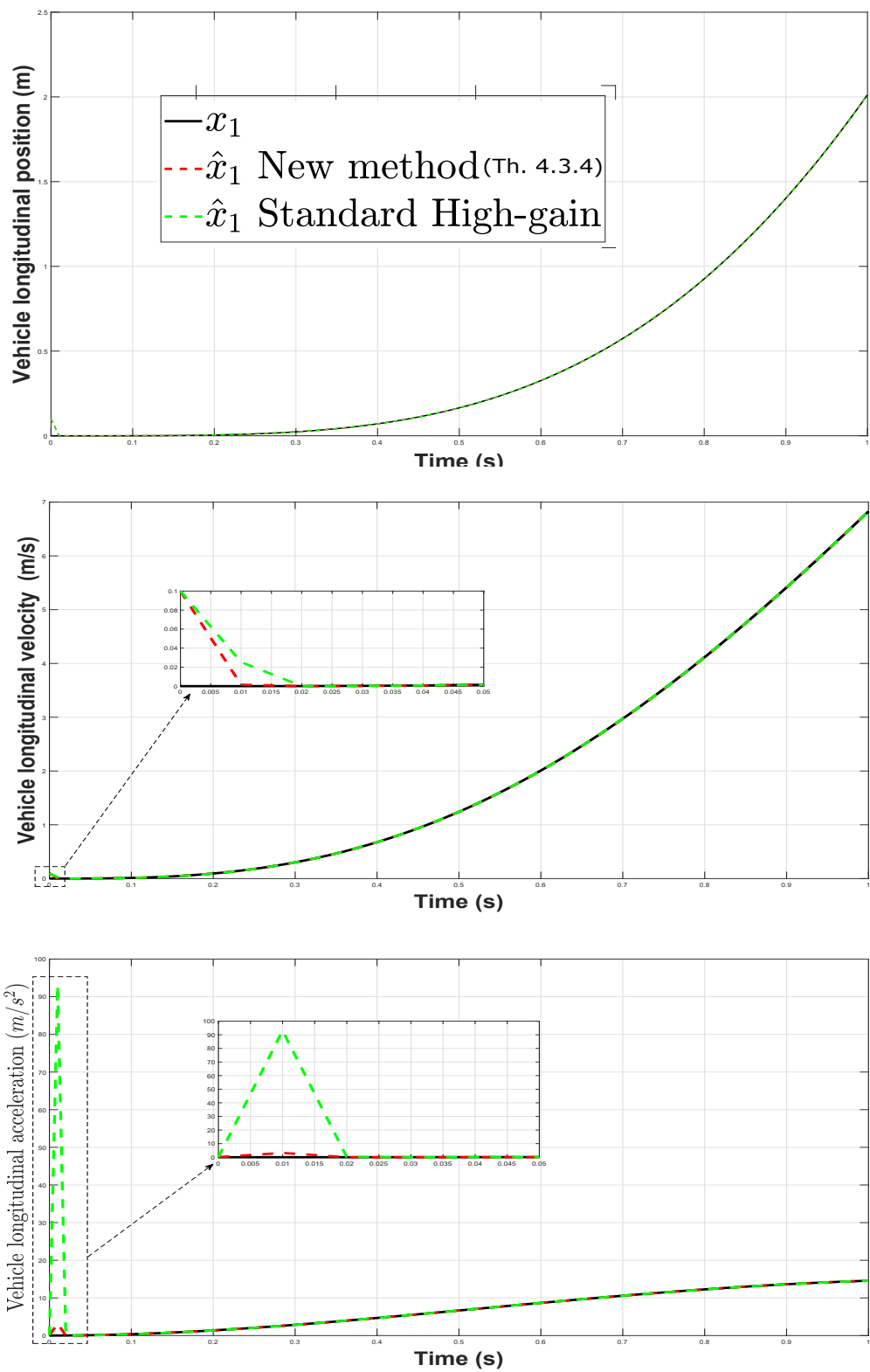


Figure 5.2: State estimates using proposed observer methodology in 4.3.4 accounting for speed measurement and the standard high-gain observer using only position measure.

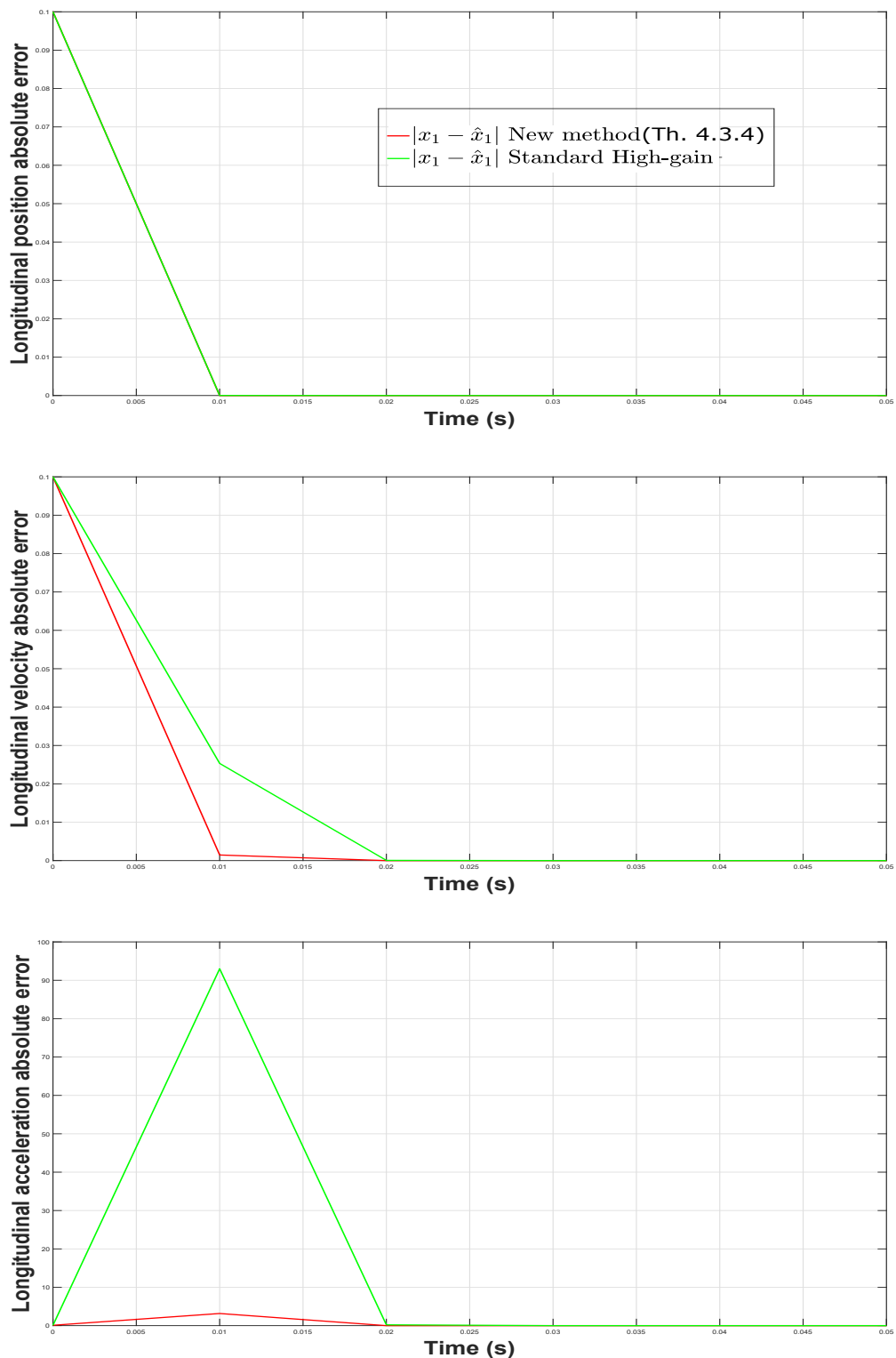


Figure 5.3: Absolute error of the estimation error and comparaison using observer in 4.3.4

similar position error of 4.9754×10^{-4} . Method 2 shows the best performance, achieving the lowest errors across all three states: a position error of 4.9751×10^{-4} , a velocity error of 5.0743×10^{-4} , and a notably lower acceleration error of 0.0185. This comparison highlights the effectiveness of Method 2 in improving the accuracy of vehicle state estimation, particularly in terms of acceleration.

5.2.3 CARLA-based simulation scenarios and estimation results

We demonstrate the advantages of the proposed method in the context of vehicle motion estimation using a nonlinear longitudinal dynamic model that incorporates both speed and position measurements. This application serves as an ideal test case for our estimation method because it provides both distance and velocity data from the radar sensor as shown in Figure 5.4. This enables our method to leverage the additional velocity measurement to enhance the accuracy of the state estimation algorithm, in contrast to the high-gain observer, which relies solely on distance measurement. Moreover, estimating the state of a moving vehicle presents a complex challenge that our method is designed to address. The use of a radar sensor, a common component in autonomous vehicles, further underscores the practical applicability of our method to real-world scenarios.

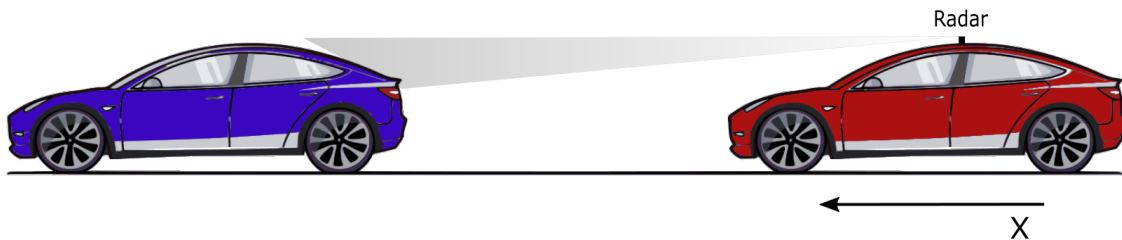


Figure 5.4: Vehicle longitudinal motion tracking scenario (in red: ego vehicle, in blue : test vehicle)

We conducted simulations within the CARLA simulation environment to evaluate the performance of the proposed observer. CARLA is an open-source simulator for autonomous driving that offers a realistic testing ground for various state estimation algorithms. The simulation scenario, depicted in Figure 5.5, involves two vehicles: the ego vehicle and the test vehicle. The ego vehicle, which is equipped with a radar sensor, follows the test vehicle. This radar sensor measures the distance between the two vehicles as well as the velocity of the test vehicle [134]. The radar data is processed to extract measurements only from the points where the radar beam interacts with the test vehicle. These measurements are then utilized by the proposed observer to estimate the unmeasured states of the test vehicle, specifically its acceleration. Additionally, the observer is employed to enhance the accuracy of measurements from both the

radar and accelerometer sensors. The accelerometer sensor, mounted on the ego vehicle, measures its acceleration. This is crucial because the proposed observer uses a relative model to estimate the state of the test vehicle relative to the ego vehicle's motion. Accurate estimation of the test vehicle's state requires accounting for the ego vehicle's acceleration.



Figure 5.5: CARLA simulation scenario.

Figure 5.6 compares the measurements of distance and velocity from the radar sensor to the ground truth values. The discrepancies between the measured values and the ground truth are due to the following factors:

- **Distance:** The radar sensor measures the distance between the center of the ego vehicle and the rear of the test vehicle. To align with the actual value, the measured distance can be adjusted by adding the length of the test vehicle.
- **Velocity:** The velocity measurement of the test vehicle is affected by the speed of the ego vehicle. Since the ego vehicle's speed is known, it can be added to the measured velocity to obtain the true velocity of the test vehicle.

The vehicle parameters used in the simulation are: $m = 1845 \text{ kg}$; $\tau = 0.7 \text{ s}$, $K_d = 0.5 \text{ N} \frac{\text{s}^2}{\text{m}^2}$, and $d_m = 100 \text{ N}$. We applied the algorithm and solved the LMI in Theorem 4.3.5 with $\lambda = 1$ using the YALMIP toolbox in MATLAB. The resulting observer parameters are:

$$\theta = 30.3704, \quad \|\mathcal{M}\| = 7.4225.$$

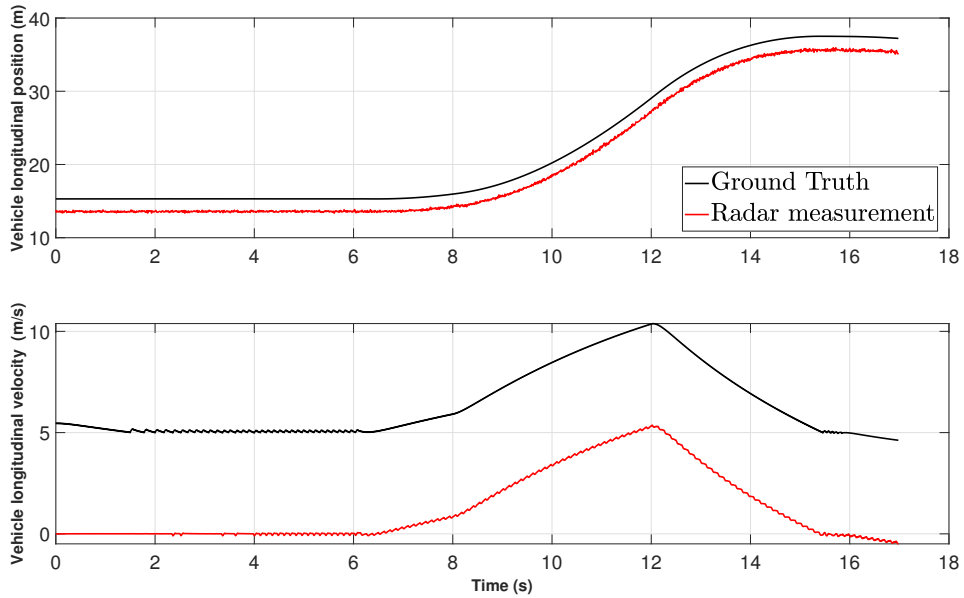


Figure 5.6: Comparison of radar sensor measurements with ground truth values.

$$\mathcal{Y} = [104.6494 \quad 350.2155 \quad -29.3206]^T,$$

$$\mathcal{Z} = [2.9269 \quad 1.6601 \quad 2.0146]^T.$$

and

$$P = \begin{bmatrix} 294.6169 & -85.2035 & -111.2819 \\ -85.2035 & 105.2495 & -49.4222 \\ -111.2819 & -49.4222 & 211.9653 \end{bmatrix}.$$

The observer gain \mathcal{N} is then given as follows:

$$\mathcal{N} = [4.7563 \quad 9.3042 \quad 4.5281]^T.$$

Figure 5.7 illustrates the estimation results obtained with the proposed algorithm, using measurements from the CARLA environment for the test vehicle's three states: position, velocity, and acceleration. Figure 5.7 demonstrates that the proposed algorithm effectively tracks the true state of the test vehicle with high accuracy. The estimation error between the predicted and actual states diminishes over time, reflecting the algorithm's convergence. The results indicate that the proposed method shows promise in estimating the state of a moving vehicle, even in the presence of sensor noise. Additionally, the acceleration estimates provided by the proposed algorithm closely follow the ground truth and exhibit smoother behavior compared to the noisy accelerometer data, which is characterized by high-frequency oscillations and requires additional filtering.

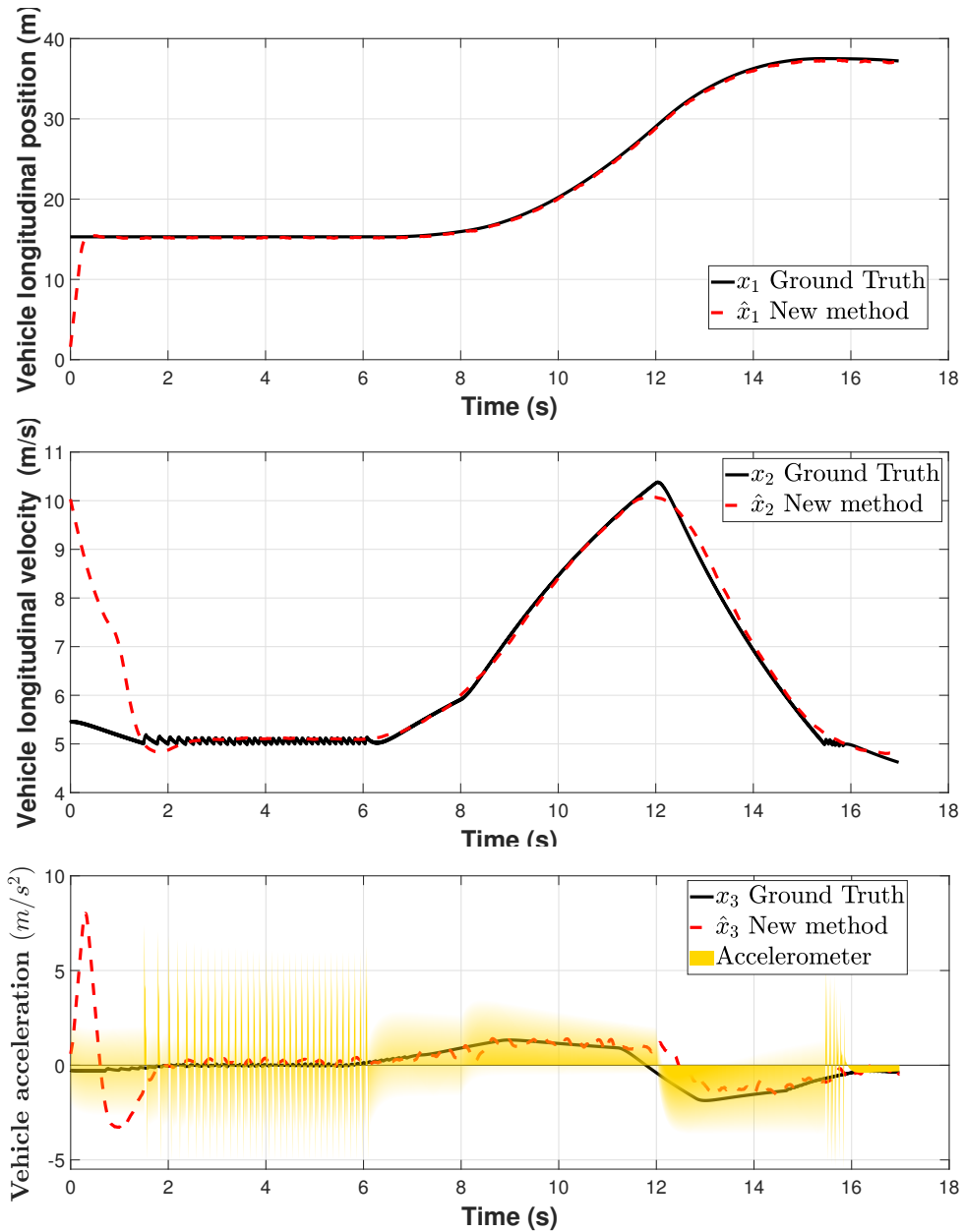


Figure 5.7: State estimation of the test vehicle using the observer described in 4.3.5, with radar sensor data.

5.2.4 Comparison with the Standard High-Gain Observer

To evaluate the effectiveness of our proposed methodology, we compare it with the standard high-gain observer. For this comparison, the high-gain observer is implemented using state-of-the-art techniques with only distance measurements in the same vehicle driving scenario.

Figure 5.8 highlights the comparative performance of the proposed algorithm and the standard high-gain observer in terms of convergence speed, accuracy, and noise rejec-

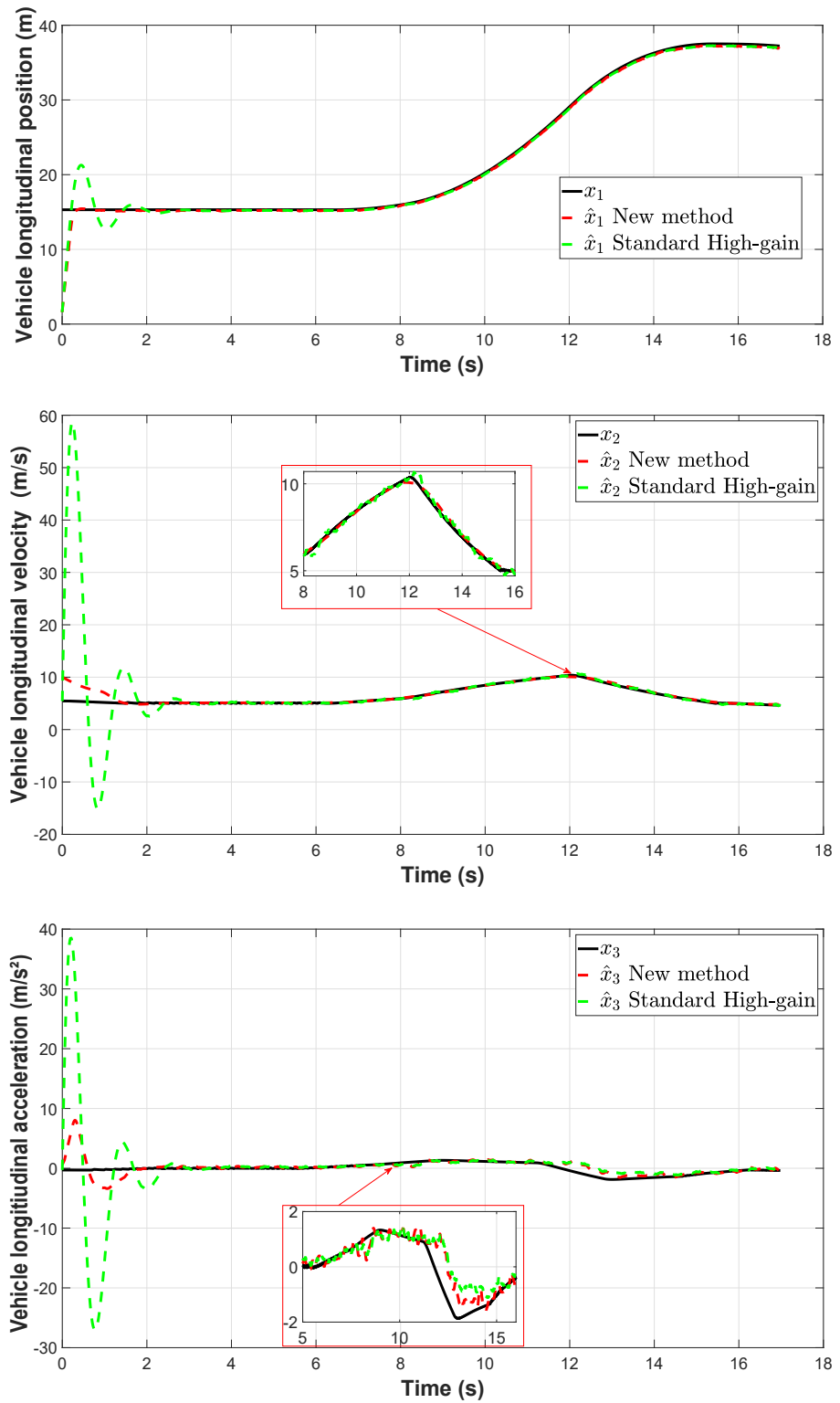


Figure 5.8: Comparison of state estimates using the proposed observer in 4.3.5 with speed measurement and the standard high-gain observer using only position measurement.

tion:

- **Convergence Speed:** The proposed algorithm converges to the true state significantly faster than the standard high-gain observer. This enhanced convergence is attributed to the algorithm's robustness to noise, allowing it to reach accurate estimates more quickly.
- **Accuracy:** The standard high-gain observer may experience a peaking phenomenon, where the state estimate oscillates with high amplitude before settling. In contrast, the proposed algorithm exhibits smoother and more accurate state estimates, being less prone to such oscillations.
- **Noise Rejection:** The proposed algorithm is more effective at minimizing noise in state estimates compared to the standard high-gain observer. This improvement is particularly evident in vehicle speed estimation, where the additional velocity measurement enhances performance. Extensive simulations reveal that the standard high-gain observer struggles with higher noise levels, resulting in less accurate estimates.

Figures 5.9 and 5.10 illustrate the performance of the proposed algorithm and the standard high-gain observer under conditions where the position measurement is lost. Specifically, Figure 5.9 shows the scenario at $t = 10$ seconds, while Figure 5.10 depicts the scenario between $t = 2$ seconds and $t = 5$ seconds, where only speed measurements are available.

The results indicate that the proposed algorithm maintains accurate performance despite the loss of position measurement, while the standard high-gain observer shows divergence. This robustness is attributed to the proposed algorithm's utilization of the additional velocity measurement, which enhances its performance in the absence of position data. Conversely, the standard high-gain observer relies solely on position measurements and does not accommodate velocity information, leading to decreased performance under these conditions.

These observations demonstrate that the proposed algorithm is more resilient to sensor failures compared to the standard high-gain observer. However, it is important to note that if the velocity measurement is lost, both algorithms perform equally well by relying solely on the available position measurement.

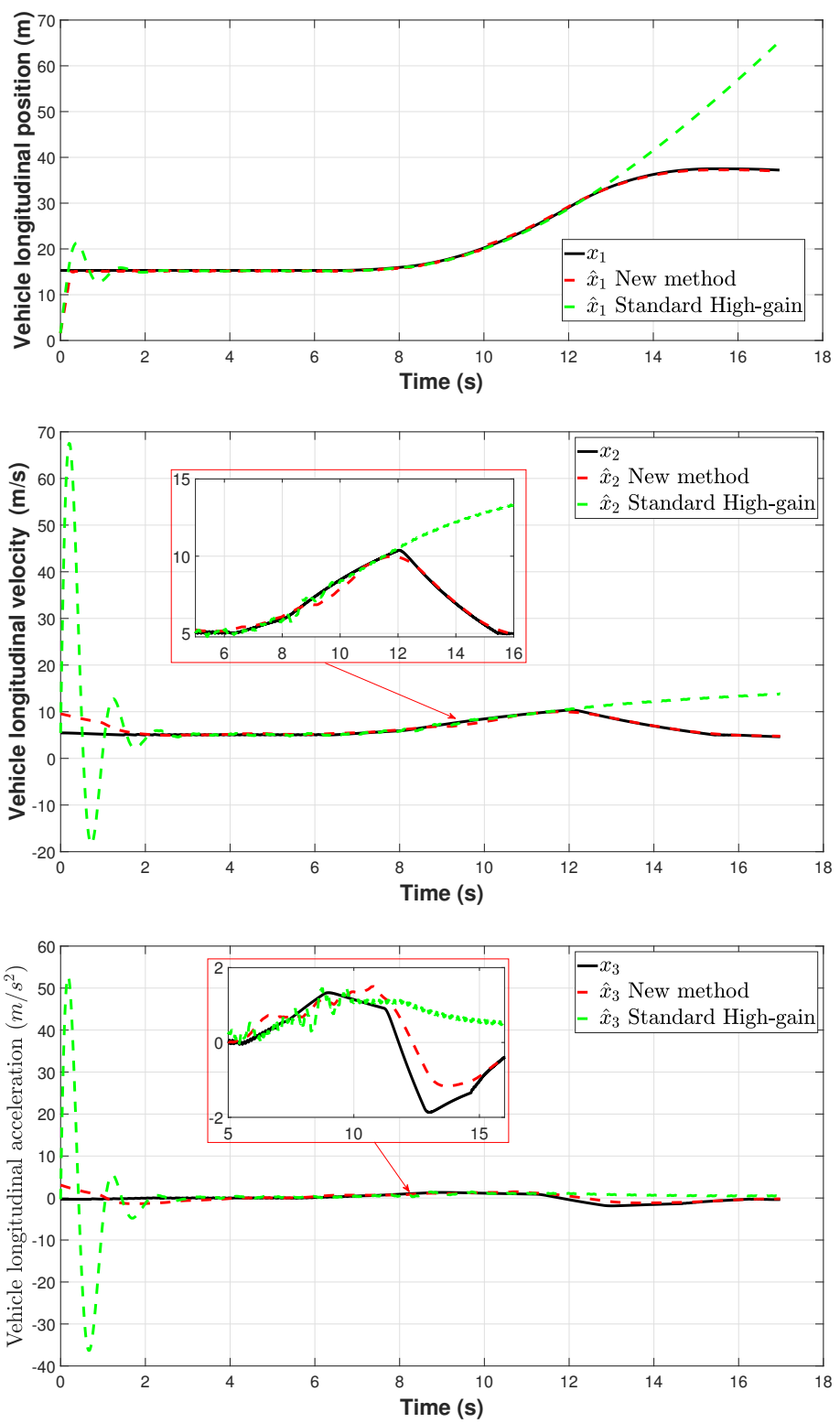


Figure 5.9: Estimation results with loss of position measurement at $t = 10$ seconds.

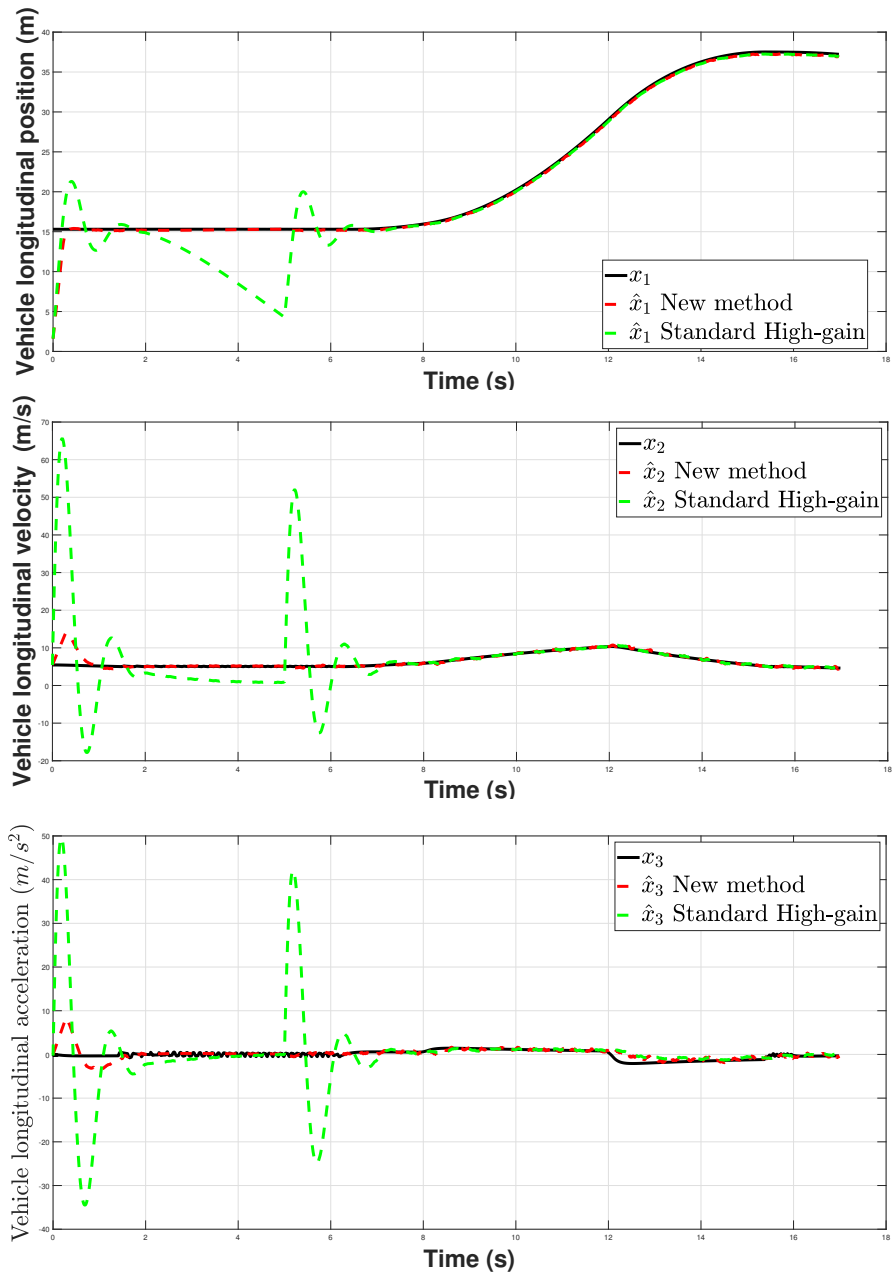


Figure 5.10: Estimation results with loss of position measurement between $t = 2$ and $t = 5$ seconds.

5.3 Vehicle Motion Estimation

5.3.1 Vehicle kinematic model

This subsection explores the triangular transformation of the vehicle model depicted in Figure 1.4 [7]. The model equations are given by:

$$\begin{bmatrix} \dot{X} \\ \dot{Y} \\ \dot{\psi} \\ \dot{\delta}_f \end{bmatrix} = \begin{bmatrix} v\cos(\psi + \beta) \\ v\sin(\psi + \beta) \\ \frac{v}{l_f + l_r} \cos \beta \tan(\delta_f) \\ 0 \end{bmatrix}, \quad (5.4)$$

where:

- X is the relative longitudinal position of the vehicle.
- Y is the relative lateral position of the vehicle.
- ψ is the yaw angle of the vehicle.
- δ_f is the steering angle of the front wheel.
- v is the vehicle's speed.
- β is the vehicle slip angle.
- l_f and l_r are the distances from the vehicle's center of gravity to the front and rear tires, respectively.

To simplify, as noted in Remark 1.3.1, if we assume that the vehicle is not performing sharp maneuvers and the turning radius R is much larger than the vehicle length L , we can approximate the derivative of the steering angle as zero and assume that the vehicle slip angle β is negligible.

The location of the vehicle is measured, and thus the output equation is given by:

$$y = \begin{bmatrix} X \\ Y \end{bmatrix} + \omega, \quad (5.5)$$

where $\omega \in \mathbb{R}^{2 \times 1}$ represents the measurement noise.

5.3.2 Triangular Transformation

The kinematic model described by (5.4) poses challenges for observer design because traditional LMI-based observers are not applicable due to non-monotonic outputs, leading to infeasibility of existing LMI conditions. To address this, we apply a nonlinear transformation to the model, allowing us to utilize a high-gain observer while preserving the system's constraints.

Consider the following nonlinear transformation applied to the vehicle model (5.4):

$$\begin{cases} z_1 = y_1 = X, \\ z_2 = \dot{z}_1 = \dot{X} = v \cos(\psi), \\ z_3 = \dot{z}_2 = \ddot{X} = -v \sin(\psi) \dot{\psi} = -\gamma \times v \sin(\psi) = -\gamma \times z_5, \\ z_4 = y_2 = Y, \\ z_5 = \dot{z}_4 = \dot{Y} = v \sin(\psi), \\ z_6 = \dot{z}_5 = \ddot{Y} = v \cos(\psi) \dot{\psi} = \gamma \times v \cos(\psi) = \gamma \times z_2, \end{cases} \quad (5.6)$$

where

$$\gamma = \frac{v}{l_f + l_r} \tan(\delta_f).$$

After some mathematical development, we have:

$$\gamma = \frac{1}{v^2} (-z_5 z_3 + z_2 z_6) = \frac{1}{z_2^2 + z_5^2} (-z_5 z_3 + z_2 z_6). \quad (5.7)$$

From this, we derive:

$$\dot{z}_3 = -\gamma^2 z_2, \quad (5.8)$$

$$\dot{z}_6 = \gamma^2 z_5. \quad (5.9)$$

The transformed system is then expressed as:

$$\begin{cases} \dot{z}_1 = z_2, \\ \dot{z}_2 = z_3, \\ \dot{z}_3 = -\gamma^2 z_2, \\ \dot{z}_4 = z_5, \\ \dot{z}_5 = z_6, \\ \dot{z}_6 = \gamma^2 z_5. \end{cases} \quad (5.10)$$

For compact representation, we write the system as:

$$\begin{cases} \dot{z} = Az + Bf(z), \\ y = Cz + \omega, \end{cases} \quad (5.11)$$

where

$$A = \begin{bmatrix} A_1 & \\ & A_1 \end{bmatrix}, \text{ with } A_1 = \begin{bmatrix} 0 & 1 & 0 \\ 0 & 0 & 1 \\ 0 & 0 & 0 \end{bmatrix},$$

$$C = \text{Diag}(C_1, C_1), \text{ with } C_1 = [1, 0, 0],$$

$$B = \text{Diag}(B_1, B_1), \text{ with } B_1 = [0, 0, 1]^\top,$$

and

$$f(z) = \begin{bmatrix} f_1(z) \\ f_2(z) \end{bmatrix} = \begin{bmatrix} -z_5 \times \gamma \\ z_2 \times \gamma \end{bmatrix}.$$

Since the transformed model does not include the yaw angle as a state, it can be computed using:

$$\psi(t) = \tan^{-1} \left(\frac{z_5(t)}{z_2(t)} \right). \quad (5.12)$$

Additional geometric constraints from the original system can be incorporated into the transformed system:

$$\dot{X}^2 + \dot{Y}^2 = v^2 \Rightarrow z_2^2 + z_5^2 = v^2, \quad (5.13)$$

$$\dot{X}\ddot{X} + \dot{Y}\ddot{Y} = 0 \Rightarrow z_2 z_3 + z_5 z_6 = 0. \quad (5.14)$$

Introducing these constraints as extra outputs, we have:

$$h(z) = \begin{bmatrix} \sqrt{z_2^2 + z_5^2} \\ z_2 z_3 + z_5 z_6 \end{bmatrix}.$$

5.3.3 Observer Design for the Vehicle Model

The design of our high-gain observer begins with the transformation of the vehicle model into triangular form, a crucial step for enabling the subsequent observer design. After this transformation, we solve the Linear Matrix Inequality (LMI) as outlined in Theorem 4.3.5, which provides the observer gains K and \mathcal{N} .

Simultaneously, we compute the Lipschitz constants, which are essential for determining the permissible values of the parameter θ . The real system is then simulated using the model described in (5.4), while the observer operates with the transformed system. Notably, speed measurements are included as an additional output for the observer. This comprehensive design approach ensures the high-gain observer's

effectiveness in accurately estimating the vehicle's trajectory, considering various factors and system dynamics.

The observer gains K and \mathcal{N} are determined by solving the LMI (see Appendix A.1) in equation (4.57) with $\lambda = 10^7$, using the SDPT3 solver in MATLAB. We imposed a constraint of $Z > 10^4$ to ensure that the eigenvalue of the gain \mathcal{N} is sufficiently large to make the added measurement influential in the observer. The resulting gains are:

$$K = \begin{bmatrix} 392.8 & 680.9 & 392.7 & 0 & 0 & 0 \\ 0 & 0 & 0 & 392.8 & 680.9 & 392.7 \end{bmatrix}^\top,$$

$$\mathcal{N} = \begin{bmatrix} 4.72 & 8.14 & 4.71 & 4.72 & 8.14 & 4.71 \\ 9.72 & 1.14 & 0.71 & 9.72 & 1.14 & 0.71 \end{bmatrix}^\top.$$

To determine the parameter k_f , which is influenced by the Lipschitz constant of the nonlinear function f defined in (5.7), we compute the Jacobian matrix and bound the states (it is explained in Appendix A.2). Given that $x_i \in [a_i, b_i]$ for $i = 1, \dots, n$, the Jacobian matrix $J(x)$ is expressed as:

$$J(x) = \left[\frac{\partial f}{\partial x_1}, \dots, \frac{\partial f}{\partial x_n} \right] = \begin{bmatrix} \frac{\partial f_1}{\partial x_1} & \dots & \frac{\partial f_1}{\partial x_n} \\ \frac{\partial f_2}{\partial x_1} & \dots & \frac{\partial f_2}{\partial x_n} \end{bmatrix}$$

We define k_f as:

$$k_f = \sup_{x \in [a, b]} \|J(x)\|$$

In this case, we find $k_f = 0.1005$. This value allows us to calculate $\theta_0 = 1.36$ using (4.58) and set $\theta = 5.2$ with $\sigma = 5$.

5.3.4 Simulation Results

We simulate two different scenarios, each at a constant speed. In the first scenario, the vehicle travels in a straight line, while in the second scenario, it makes a left turn. Measurement noise with a Gaussian distribution of $\sigma = 10^{-2}$ is added to the position data in both scenarios.

Scenario: Driving Straight with Measurement Noise

In this scenario as shown in Figures 5.13, the vehicle moves along a straight path with a constant speed of $v = 5$ m/s on the X axis. To mimic real-world conditions and evaluate the robustness of our observer model, we introduce noise into the position

measurements. This noise simulates potential inaccuracies in actual position tracking systems due to sensor errors or environmental factors.

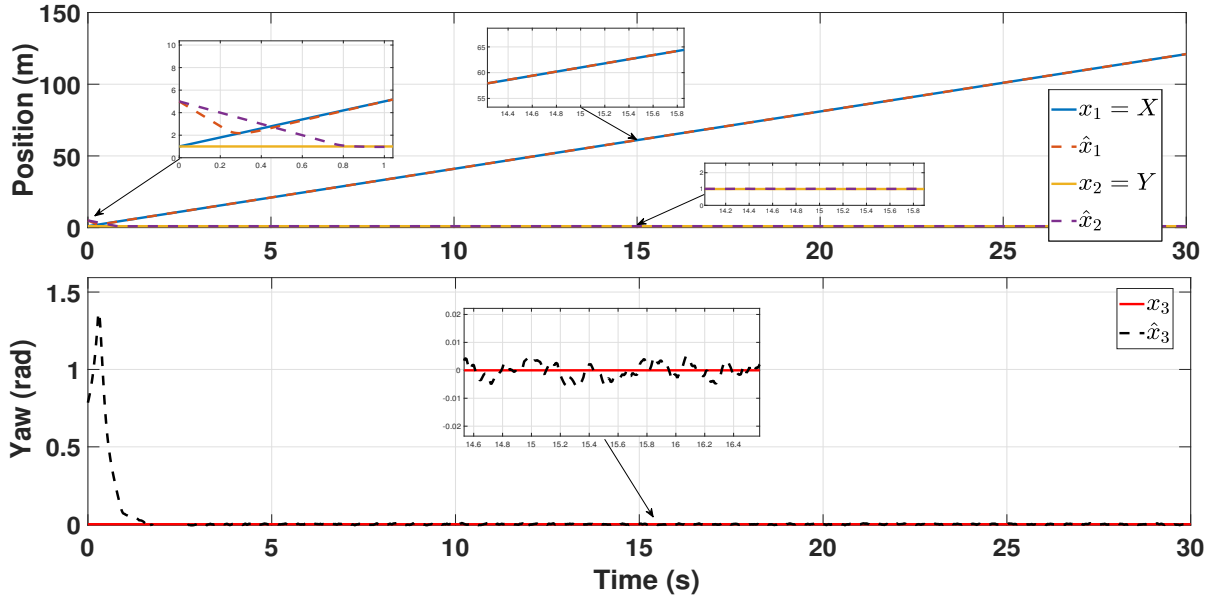


Figure 5.11: Vehicle state estimation in the straight driving scenario.

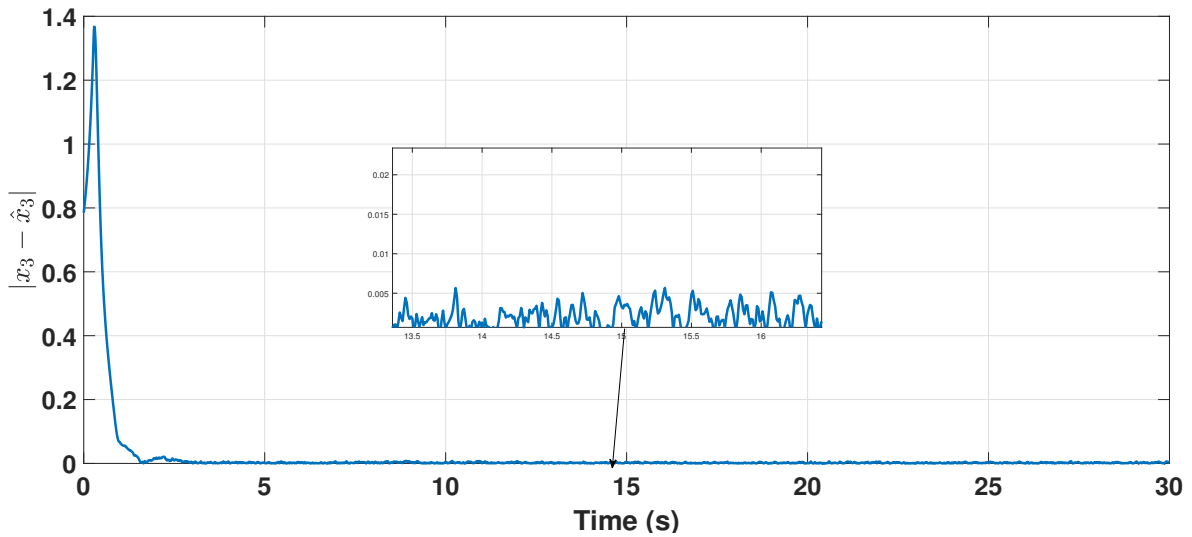


Figure 5.12: Yaw estimation error in the straight driving scenario.

Scenario: Turning Left

In this scenario, we examine a vehicle executing a left turn. The steering angle is gradually varied to maintain the assumptions of our model, while the vehicle maintains a constant speed. This scenario allows us to study the system's response to changes

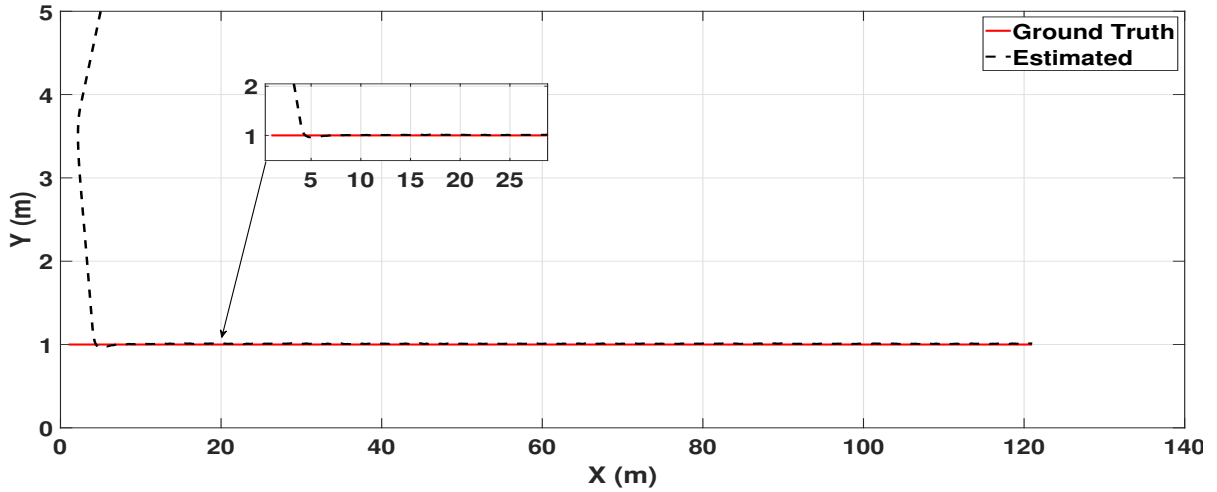


Figure 5.13: Trajectory estimation in the straight driving scenario.

in steering input, providing insights into the performance and stability of our observer model under different driving conditions.

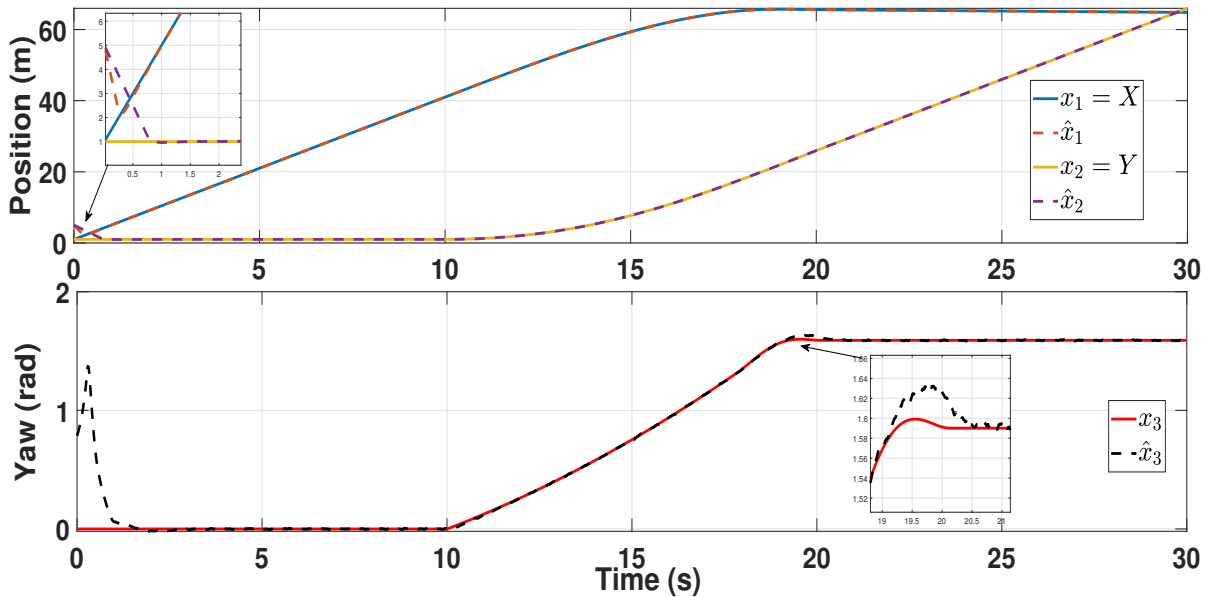


Figure 5.14: Vehicle state estimation in the left turn scenario.

Figures 5.12 and 5.15 illustrate that the observer accurately estimates the yaw angle and converges to the true values in both scenarios. The oscillation and peaking phenomena commonly associated with high-gain observers are minimized, validating the effectiveness of our proposed method. Figures 5.12 and 5.15 demonstrate the yaw angle estimation error and the quick convergence of the observer, while Figures 5.13

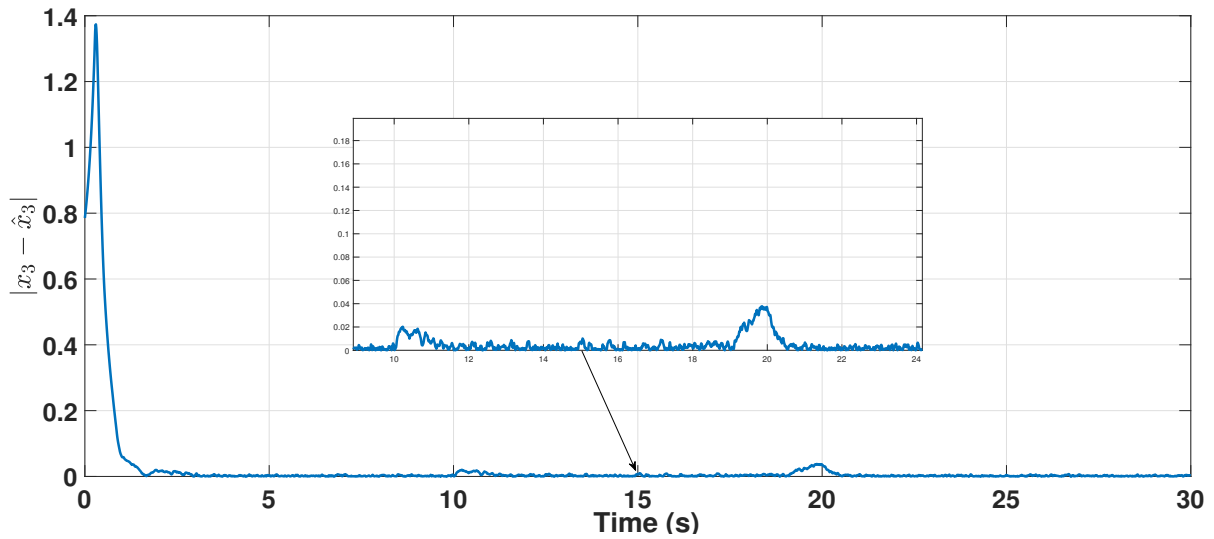


Figure 5.15: Yaw estimation error in the left turn scenario.

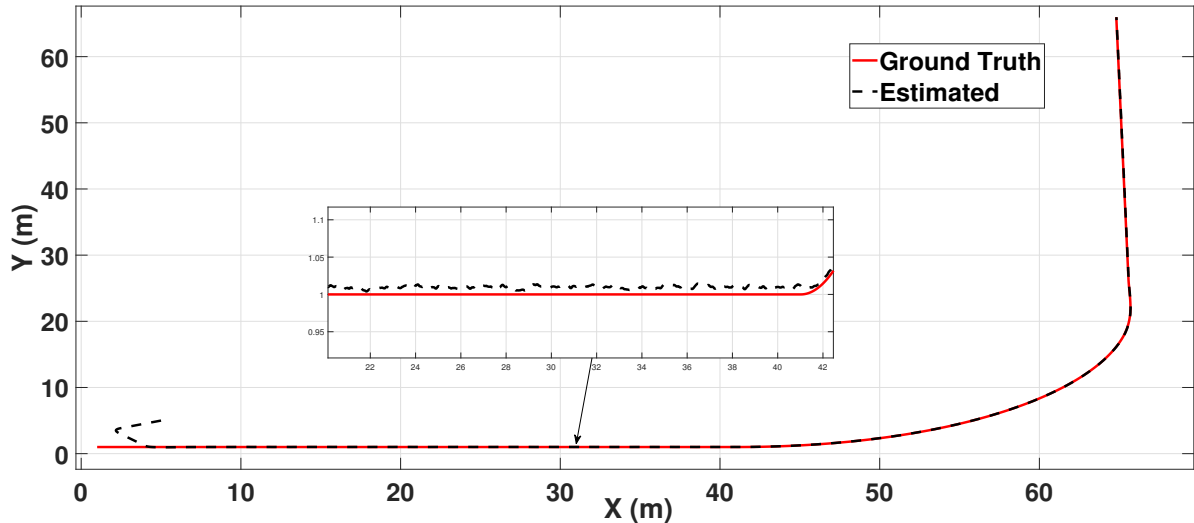


Figure 5.16: Trajectory estimation in the left turn scenario.

and 5.16 show that the position estimation effectively filters out measurement noise and accurately estimates the vehicle's state.

5.3.5 Experimental Results

KITTI Dataset

In addition to simulations, we evaluated the effectiveness of our observer design using the KITTI dataset [135]. This dataset contains data from a vehicle equipped with a 6-axis, 100 Hz GPS/IMU (OXTS RT3003) featuring L1/L2 RTK and a resolution of

$0.02 \text{ m} / 0.1^\circ$. The dataset provides highly accurate position measurements (up to 1 cm) as ground truth, which is crucial for validating our estimated states.

The KITTI dataset includes data synchronized at a rate of 10 Hz, encompassing geographic coordinates (longitude and latitude), global orientation, and velocities. We focused on localizing the ego vehicle using the same kinematic nonlinear model applied in our simulations. We anticipated that incorporating additional outputs would significantly enhance performance compared to traditional high-gain observers.



Figure 5.17: Camera capture from the KITTI dataset [135].

After processing the raw GPS data, we extracted the vehicle's position and velocity and used the filtered Inertial Measurement Unit (IMU) measurement of the yaw angle as the ground truth for validation.

The experimental scenario involved the vehicle traveling along a dynamic path: starting with variable speed on a straight line, followed by a left turn, and then continuing on a curved right path, eventually stopping at a red light. Although the scenario lasted 45 seconds, our focus was on a 35-second interval when the vehicle was in motion. To handle potential short GPS data gaps, we employed interpolation. We also explored the observer's performance under data or signal loss conditions.

The experimental results confirm the effectiveness of our proposed observer. Figures 5.18 and 5.19 show that the observer accurately estimates the vehicle's yaw angle with rapid convergence. Figure 5.20 demonstrates precise position estimation from GPS data, while Figure 5.21 indicates accurate velocity estimation. Despite varying velocity and steering angles, the observer's performance remains robust.

We also simulated data with communication gaps of 10%, 40%, and 80% by randomly omitting position information from the measurement vector Y . Only velocity information was used to estimate the vehicle trajectory.

Figure 5.22 shows that vehicle trajectory estimation remains accurate with 10% and 40% data loss. The estimation error increases with 80% data loss but remains acceptable given the lack of position information and the use of a simplified vehicle model. These results highlight the robustness of our observer.

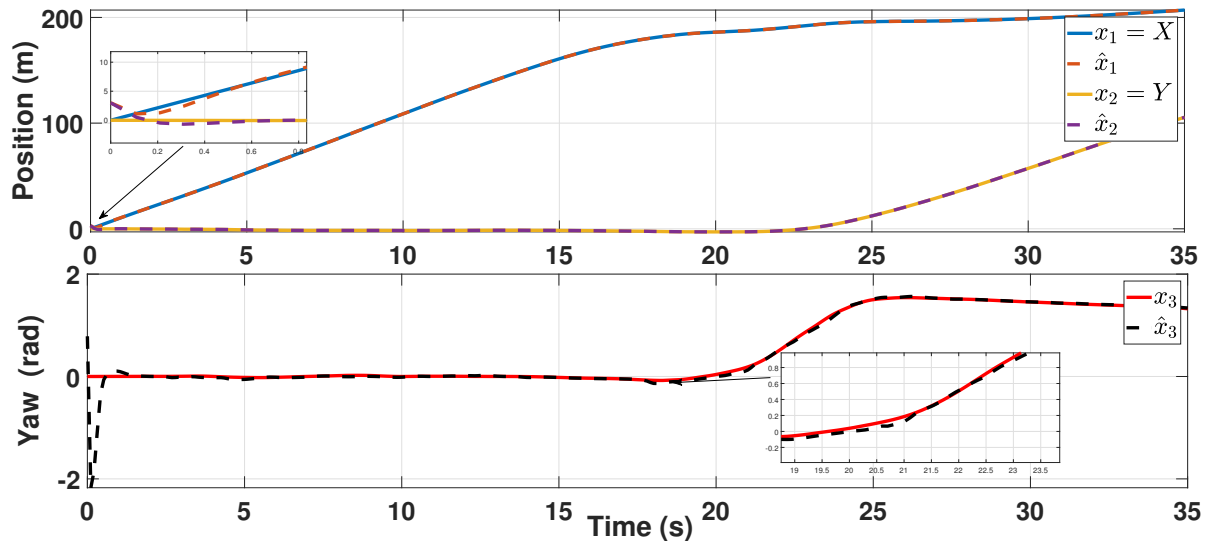


Figure 5.18: State estimation using real data.

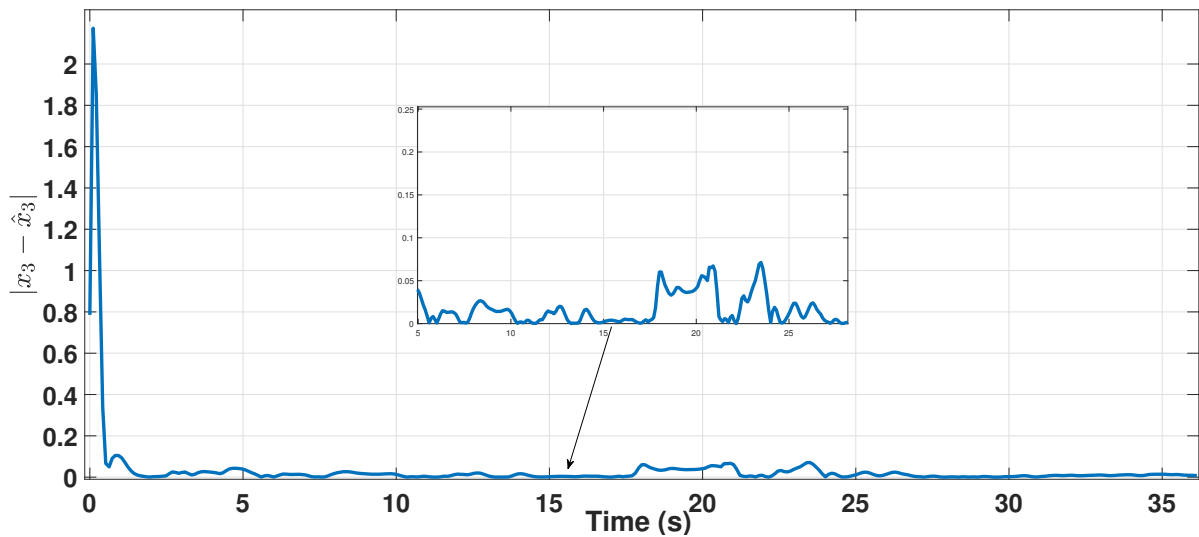


Figure 5.19: Yaw estimation error.

Comparison with Extended Kalman Filter (EKF)

To compare the high-gain observer with a traditional estimation filter, we evaluated its performance against the Extended Kalman Filter (EKF) under a specific scenario, as depicted in Figure 5.23. The EKF was based on model (5.4), incorporating acceleration into the state vector. This comparison emphasizes the advantages of the high-gain observer. We used only velocity v as an additional measurement for updating the gains, and relied solely on GPS measurements (Position and Velocity) for consistency. Both observers were initialized with the same initial conditions, distinct from the first estimation.

In our test scenario with a 40% data gap:

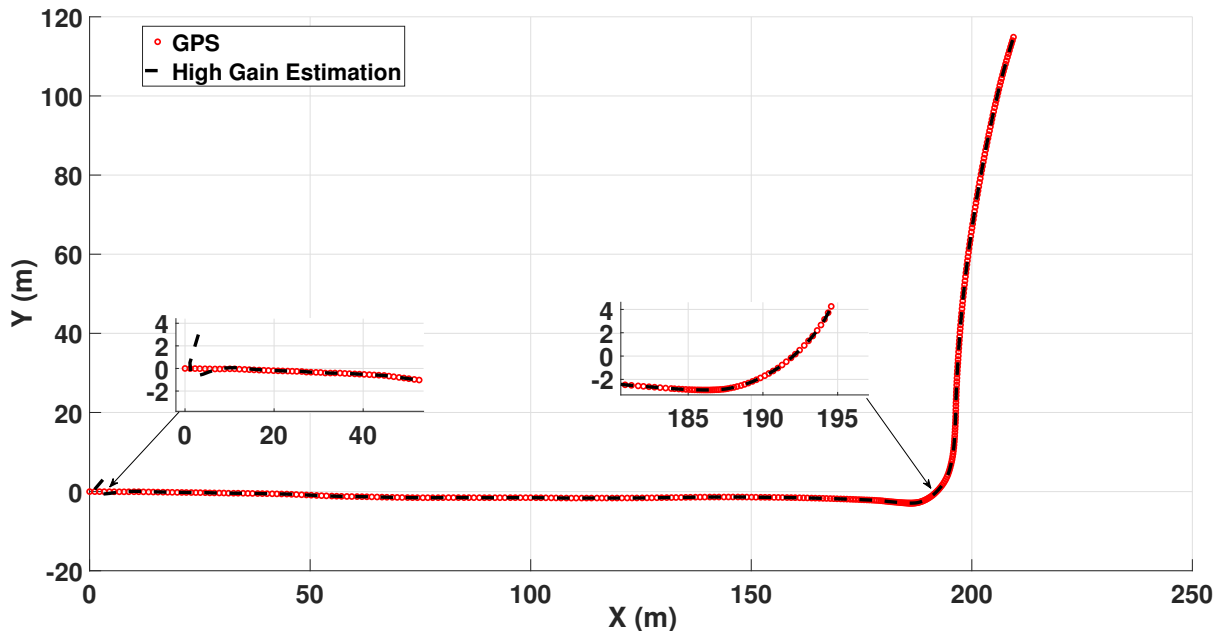


Figure 5.20: Trajectory estimation.

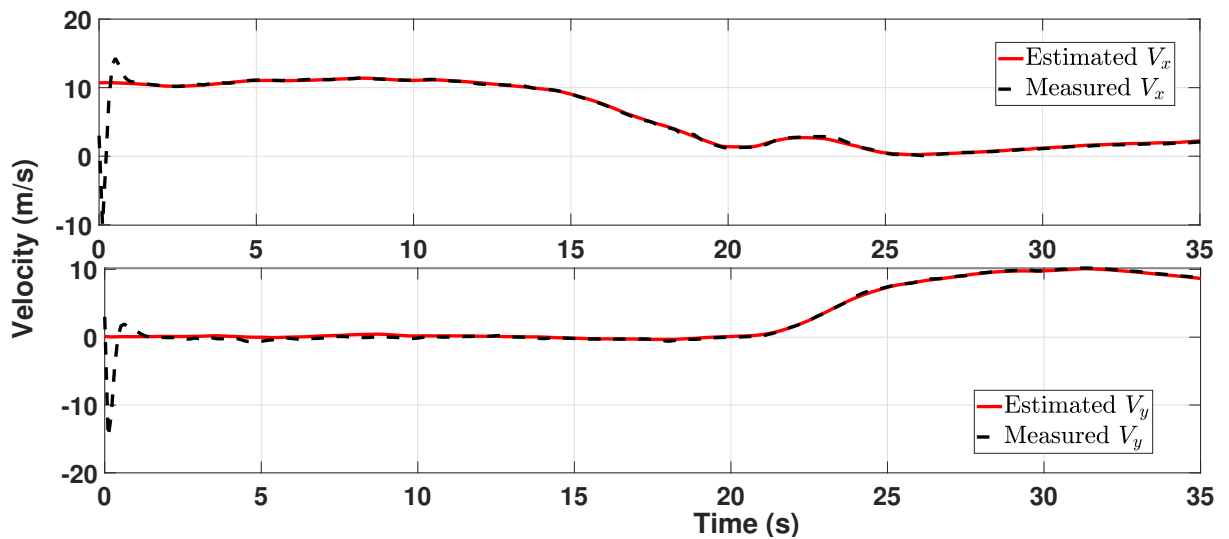
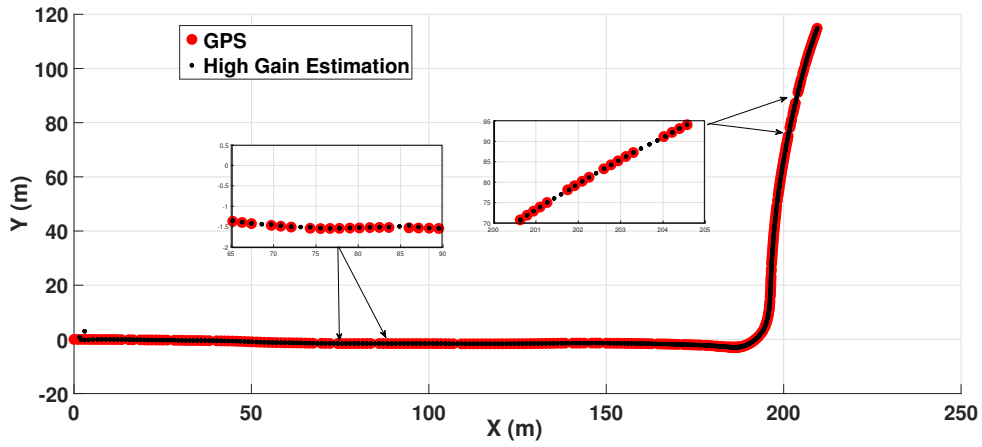
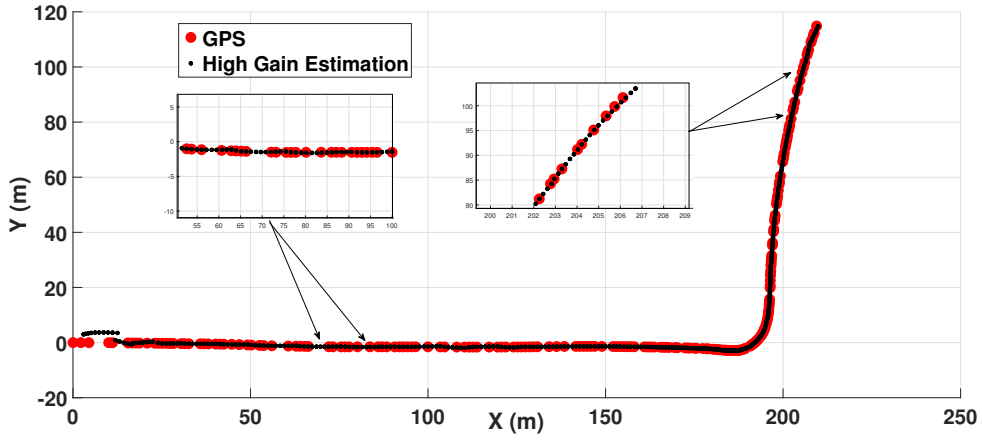


Figure 5.21: Velocity estimation on both axes (V_x and V_y).

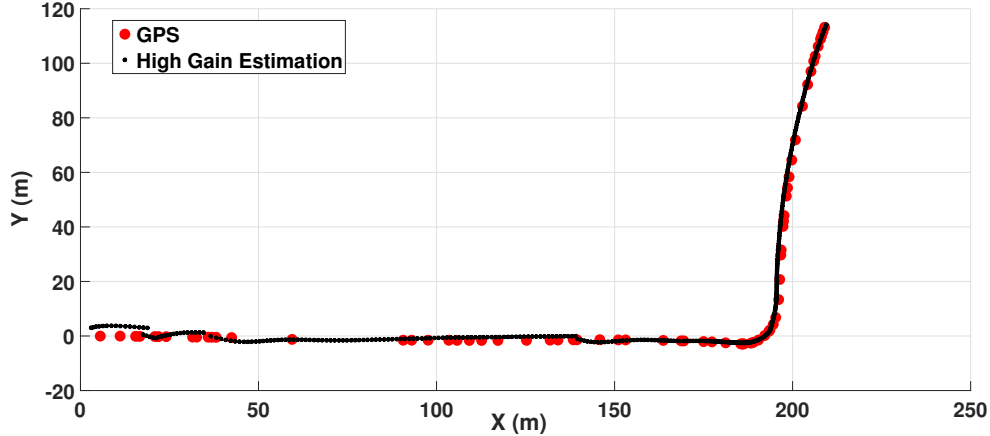
The high-gain observer demonstrates faster convergence than the EKF in the presence of a 40% data gap, as shown in Figures 5.24 and 5.23. Although the EKF occasionally provides more precise yaw angle estimates (Figure 5.25), it generally lags behind the high-gain observer in position correction and estimation.



(a) 10% Missing Data.



(b) 40% Missing Data.



(c) 80% Missing Data.

Figure 5.22: Simulation of data gaps in GPS signal.

Sensor Fusion with Extended Kalman Filter (EKF)

In vehicle tracking, sensor fusion is common, often using an Extended Kalman Filter (EKF) [136]–[138]. To integrate multiple measurements, we introduce an additional

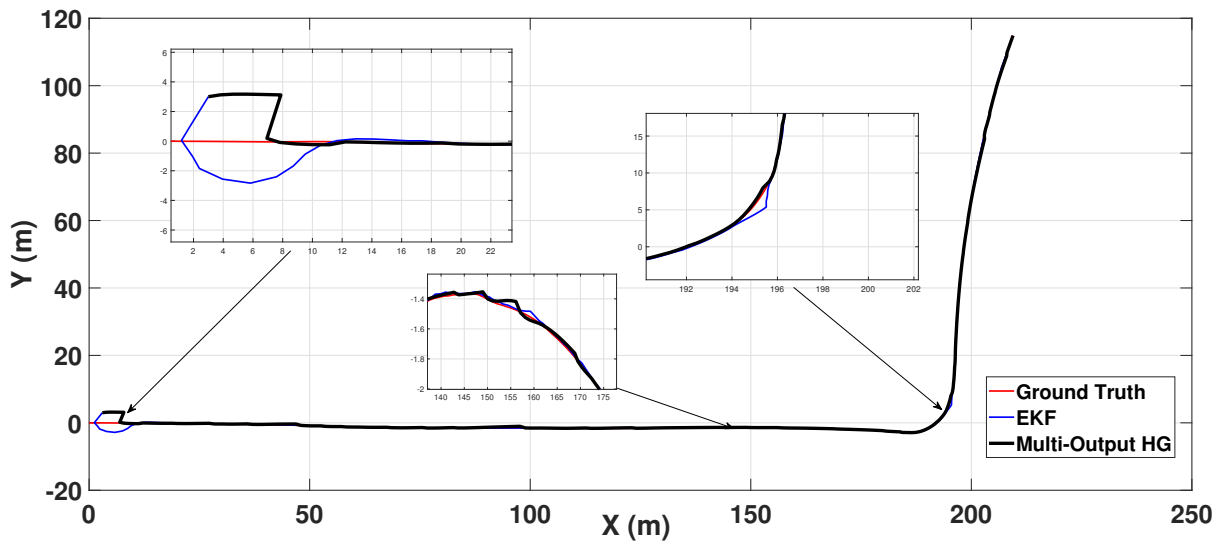


Figure 5.23: Trajectory estimation.

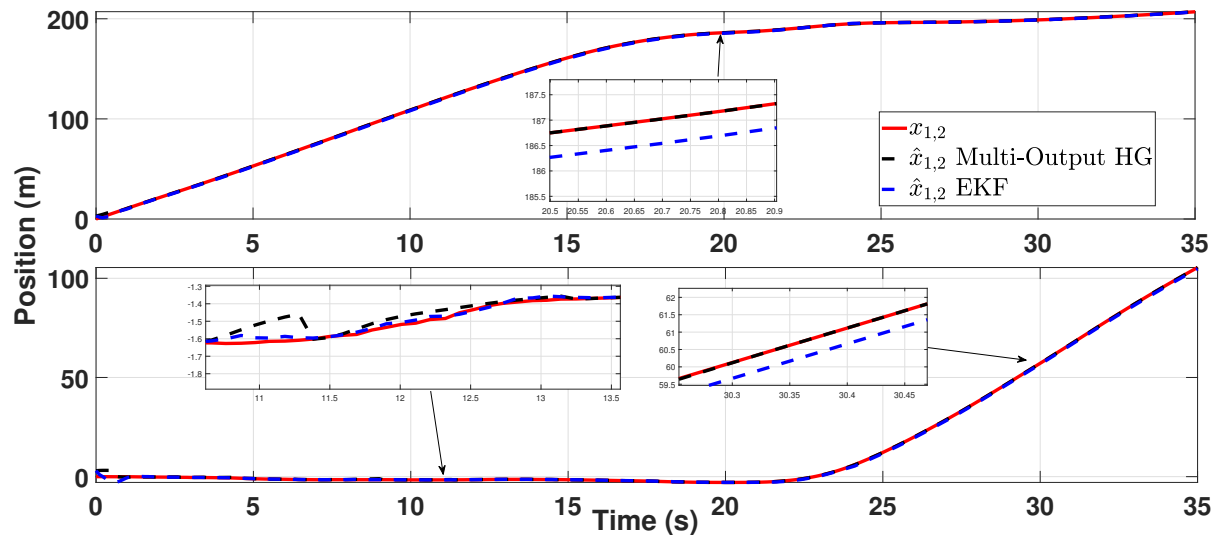


Figure 5.24: State estimation (Position).

output or measurement, denoted as h_3 , using an Inertial Measurement Unit (IMU) to measure the yaw rate. This additional measurement is expressed as:

$$h_3(z) = \dot{\psi}(t) = \gamma = \frac{(-z_5 z_3 + z_2 z_6)}{z_2^2 + z_5^2}. \quad (5.15)$$

Thus, the measurement vector becomes:

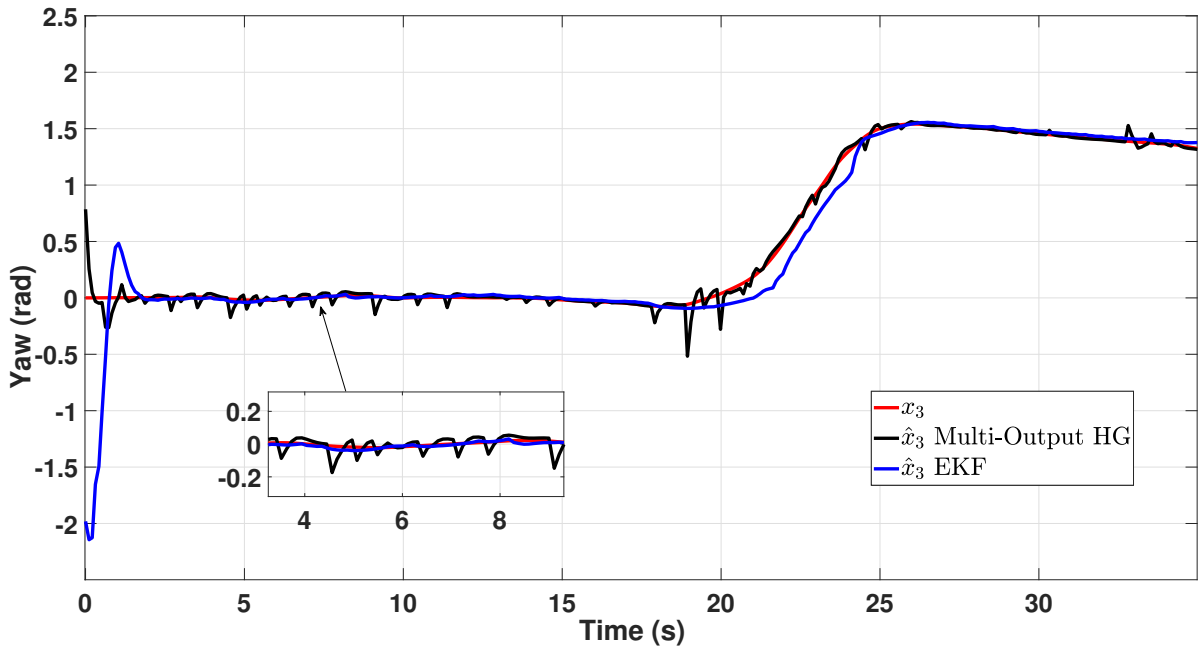


Figure 5.25: Yaw angle estimation.

$$h(z) = \begin{bmatrix} h_1(z) \\ h_2(z) \\ h_3(z) \end{bmatrix} = \begin{bmatrix} \sqrt{z_2^2 + z_5^2} \\ z_2 z_3 + z_5 z_6 \\ \frac{(-z_5 z_3 + z_2 z_6)}{z_2^2 + z_5^2} \end{bmatrix}. \quad (5.16)$$

We compared the EKF with our observer using simulated GPS position measurements with Gaussian noise (standard deviation $\sigma = 1.5$ m). This noise reflects typical uncertainties in conventional GPS without RTK correction, though velocity measurements are more precise, with an uncertainty of about ± 0.05 m/s.

Applying the theory from 3.4, we adjusted the observer gains with greater emphasis on the extra output in LMI (4.57), resulting in:

$$K = \begin{bmatrix} 0.2247 & 0.4704 & 0.1832 & 0 & 0 & 0 \end{bmatrix}^\top,$$

$$\mathcal{N} = \begin{bmatrix} 0.4858 & 0.7402 & 0.4603 & 0.4858 & 0.7402 & 0.4603 \\ 0.8858 & 0.3402 & 0.1603 & 0.8858 & 0.3402 & 0.1603 \\ 0.4858 & 0.7402 & 0.4603 & 0.4858 & 0.7402 & 0.4603 \end{bmatrix}^\top,$$

with $\theta = 3$.

Introducing measurement noise into the vehicle position led to adjustments in gains and the parameter θ . While this improved the influence of measured speed and yaw

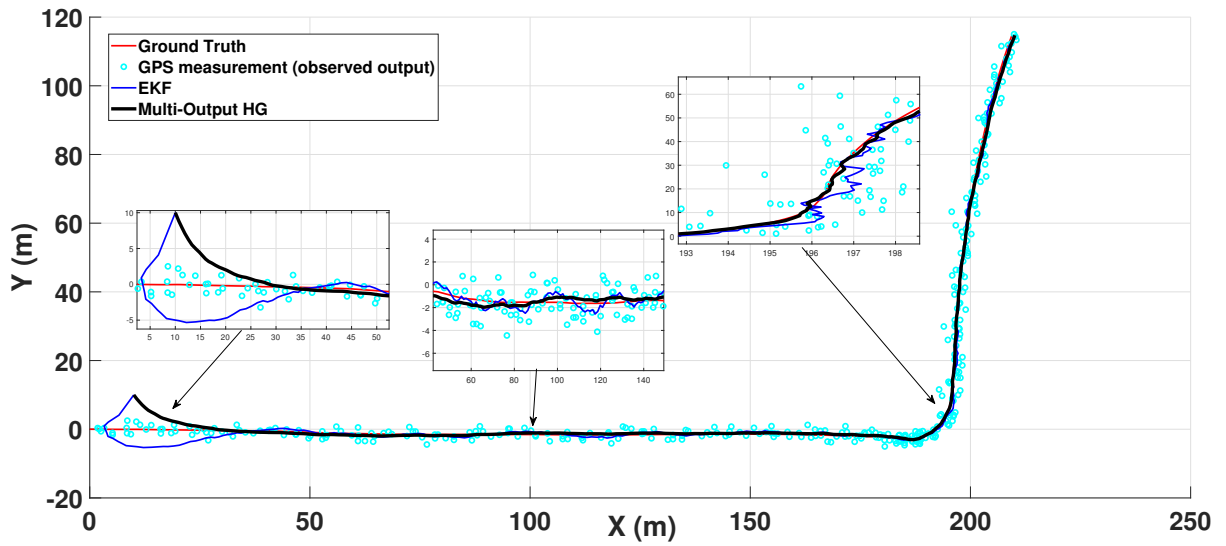


Figure 5.26: Trajectory estimation.

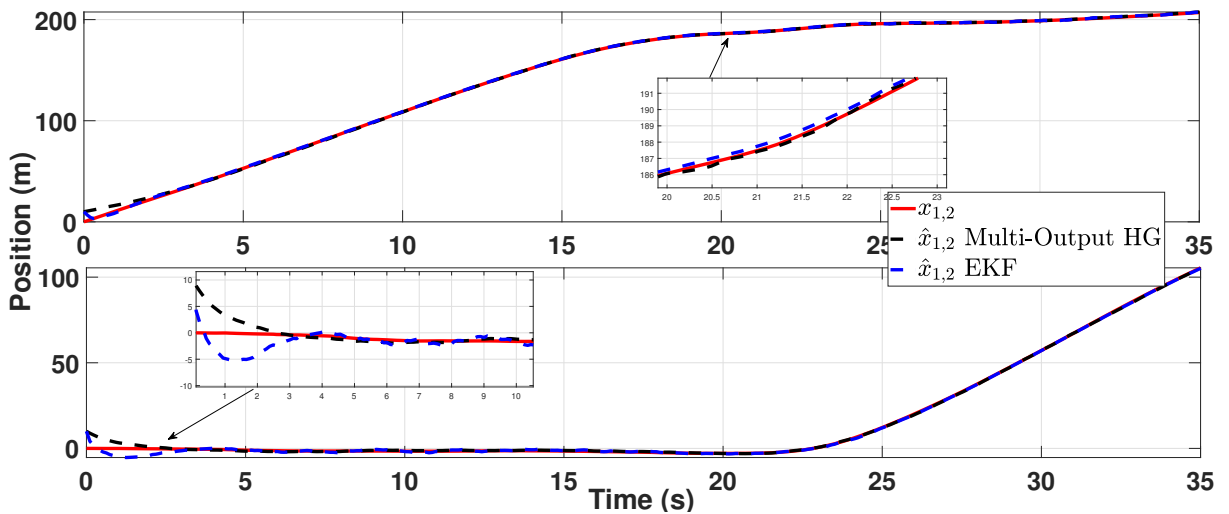


Figure 5.27: State estimation (Position).

rate, it resulted in a slight decrease in convergence rate and increased oscillation in yaw angle estimation. Despite this, the high-gain observer remains superior in position correction and estimation (Figures 5.26 and 5.27), although the EKF performs better in yaw angle estimation under significant rate changes.

By employing the triangular model, our method can be extended to estimate additional states such as longitudinal and lateral accelerations and velocities.

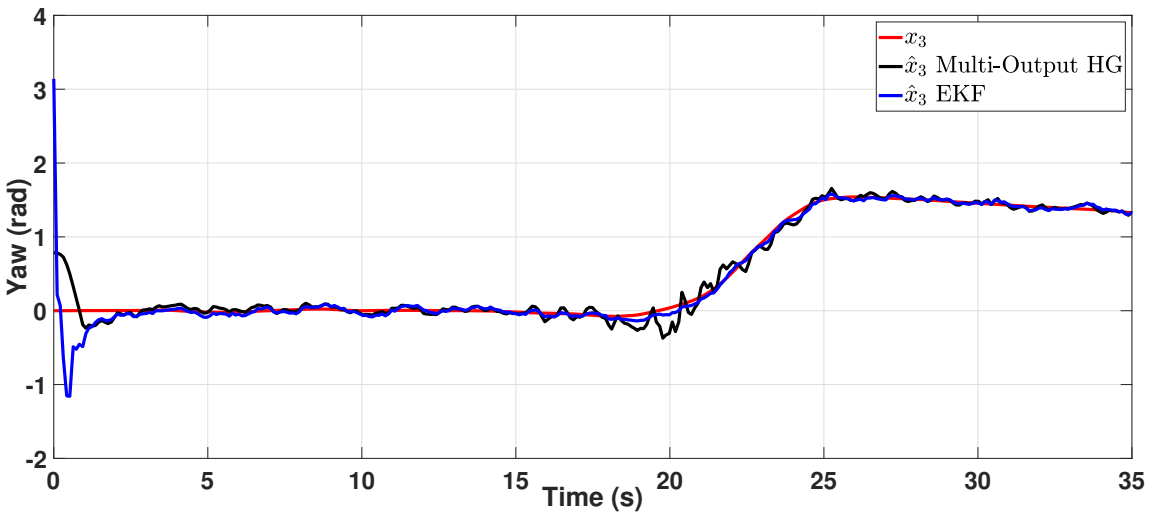


Figure 5.28: Yaw angle estimation.

5.4 Conclusion

In this chapter, we presented a comprehensive evaluation of our proposed high-gain observer using both simulations and real-world data from the KITTI dataset. The results underscore the robustness and accuracy of our observer in vehicle localization tasks, even in the presence of significant data gaps and noise.

Through our experiments with the KITTI dataset, we demonstrated that the high-gain observer effectively estimates vehicle states, including position, velocity, and yaw angle, with high precision. The observer's performance was particularly notable in scenarios involving varying speeds and complex trajectories, maintaining accuracy and convergence speed even with up to 40% data loss. The results showed that our observer outperformed the traditional Extended Kalman Filter (EKF) in terms of convergence rate and overall estimation accuracy, especially in position estimation. However, despite ensuring the stability of the observer, the proposed methodology still struggles with measurement noise, resulting in a noisy estimation.

Additionally, we explored the benefits of incorporating additional outputs such as yaw rate measurements, highlighting the observer's adaptability and enhanced performance in sensor fusion applications. The observer's gains were adjusted to prioritize the additional measurements, further improving state estimation under noisy conditions. Overall, our findings validate the effectiveness and resilience of the proposed high-gain observer, suggesting its potential for real-world applications in autonomous vehicle navigation and other dynamic systems requiring precise state estimation.

Conclusion and perspectives

This thesis has made significant strides in the field of vehicle state estimation and advanced driving assistance systems (ADAS) by exploring and validating various innovative observer methodologies. Across five chapters, we have systematically developed and assessed advanced techniques to enhance the accuracy, robustness, and applicability of state estimation in dynamic systems, particularly for autonomous vehicles.

We began with a comprehensive overview of ADAS technology, emphasizing their critical role in vehicle safety and driving comfort. The necessity for accurate state information in these systems led us to explore various state estimation techniques, including model-based and data-based approaches. Our focus on hybrid methodologies, such as neuro-adaptive and deep learning-based observers, highlighted their potential in achieving superior state estimation accuracy and reliability.

The development of a discrete-time interval observer for uncertain Linear Parameter Varying (LPV) systems broadened the application scope of interval observers in digital control. By combining exact state estimation with interval observers, our method effectively handled system uncertainties without restrictive stability constraints, demonstrating robust and precise interval estimation.

We then introduced a neuro-adaptive observer integrating neural networks for adaptive state and unknown dynamics estimation. Our novel method, which employed concurrent learning observers and Linear Matrix Inequalities (LMIs), proved particularly robust against unmodeled dynamics. Simulations showed that our approach offered superior performance and flexibility compared to existing methods, making it a powerful tool for vehicle state estimation.

High-Gain observer theory was further explored, addressing its limitations by incorporating additional measurements and constraints. By blending High-Gain and LPV/LMI methodologies and proving convergence through Input-to-State Stability (ISS) bounds, we extended the observer's applicability to more complex systems and nonlinear outputs. This enhanced observer design demonstrated increased robustness to measurement noise, ensuring reliable performance in practical scenarios.

Finally, we validated our high-gain observer through simulations and real-world data from the KITTI dataset. The observer exhibited robustness and accuracy in vehicle localization tasks, even with significant data gaps and noise. It outperformed traditional methods like the Extended Kalman Filter (EKF) in terms of convergence rate and estimation accuracy, particularly in position estimation. Despite some challenges with

measurement noise, the observer's adaptability and enhanced performance in sensor fusion applications were evident.

Our work opens up new research opportunities for further contributions to these topics, some of these are cited below :

- One potential avenue for future work on the finite-time LPV interval observer is to generalize it for nonlinear systems. This could involve finding a transformation to rewrite a nonlinear system directly in LPV form. Additionally, we are exploring the use of neural networks to achieve this transformation.
- For the neuro-adaptive observer, we are exploring its application to the vehicle lateral dynamic model, where the nonlinear functions are highly complex, difficult to model, and vary depending on the driving scenarios. Additionally, we are applying it to the system to verify its applicability in real-time conditions.
- For the High-Gain observer methodology we presented, challenges remain, particularly regarding measurement noise. We are working on implementing the methodology with filters and techniques to reduce noise effects. For the application part, the idea is to test it on a real vehicle, potentially extending this approach to more complex scenarios and integrating additional sensor data to further enhance the observer's performance and reliability.

A

Appendix

A.1 Linear Matrix Inequalities (LMIs)

A.1.1 Definition of Linear Matrix Inequalities (LMIs)

A Linear Matrix Inequality (LMI) is a constraint of the form:

$$F(x) \leq 0$$

where $F(x)$ is an affine matrix function of the vector $x = [x_1, x_2, \dots, x_n]^T$. Specifically, $F(x)$ can be expressed as:

$$F(x) = F_0 + x_1 F_1 + x_2 F_2 + \dots + x_n F_n$$

where F_0, F_1, \dots, F_n are given symmetric matrices of appropriate dimensions, and ≤ 0 denotes that the matrix $F(x)$ is negative semidefinite.

A.1.2 Convexity of LMIs

An LMI defines a convex set. This property arises from the fact that the set of symmetric matrices that are negative semidefinite is a convex set. More formally, if $F(x) \leq 0$ and $F(y) \leq 0$, then for any $\lambda \in [0, 1]$:

$$F(\lambda x + (1 - \lambda)y) = \lambda F(x) + (1 - \lambda)F(y) \leq 0$$

This shows that the feasible set defined by the LMI $F(x) \leq 0$ is convex.

Lemma A.1.1: Convexity of the Feasible Set Defined by an LMI

If $F(x) = F_0 + \sum_{i=1}^n x_i F_i$ is an affine matrix function and $\mathcal{F} = \{x \in \mathbb{R}^n \mid F(x) \leq 0\}$, then \mathcal{F} is a convex set.

Proof. Let $x, y \in \mathcal{F}$ and $\lambda \in [0, 1]$. Then:

$$F(x) \leq 0 \quad \text{and} \quad F(y) \leq 0$$

Consider $z = \lambda x + (1 - \lambda)y$. Then:

$$F(z) = F(\lambda x + (1 - \lambda)y) = \lambda F(x) + (1 - \lambda)F(y)$$

Since $\lambda \geq 0$ and $1 - \lambda \geq 0$, and using the properties of matrix inequality:

$$\lambda F(x) \leq 0 \quad \text{and} \quad (1 - \lambda)F(y) \leq 0$$

Therefore:

$$\lambda F(x) + (1 - \lambda)F(y) \leq 0$$

Hence, $F(z) \leq 0$, and thus $z \in \mathcal{F}$. This proves that \mathcal{F} is convex. \square

A.1.3 Congruence Transformation

Congruence transformation is a transformation of the form:

$$A \mapsto P^T A P$$

where P is an invertible matrix. If A is symmetric, the congruence transformation preserves the definiteness of A . Specifically, A is positive semidefinite (resp. definite) if and only if $P^T A P$ is positive semidefinite (resp. definite).

Lemma A.1.2: Preservation of Semidefiniteness Under Congruence Transformation

Let $A \in \mathbb{R}^{n \times n}$ be a symmetric matrix and $P \in \mathbb{R}^{n \times n}$ be an invertible matrix. Then $A \geq 0$ if and only if $P^T A P \geq 0$.

Proof. Assume $A \geq 0$. For any $x \in \mathbb{R}^n$:

$$x^T (P^T A P) x = (Px)^T A (Px)$$

Let $y = Px$. Since P is invertible, y can be any vector in \mathbb{R}^n :

$$(Px)^T A (Px) = y^T A y \geq 0$$

Thus, $P^T A P \geq 0$. Conversely, assume $P^T A P \geq 0$. For any $y \in \mathbb{R}^n$:

$$y^T A y = (P^{-1}y)^T (P^T A P) (P^{-1}y) \geq 0$$

Thus, $A \geq 0$. \square

A.1.4 Schur Complement

Given a symmetric matrix M partitioned as:

$$M = \begin{pmatrix} A & B \\ B^T & C \end{pmatrix}$$

where A and C are symmetric matrices, the Schur complement of the block A in M is defined as:

$$S = C - B^T A^{-1} B$$

If A is positive definite, the matrix M is positive semidefinite if and only if S is positive semidefinite.

Lemma A.1.3: Schur Complement

Let $M = \begin{pmatrix} A & B \\ B^T & C \end{pmatrix}$ be a symmetric matrix, where A is nonsingular. Then $M \geq 0$ if and only if $A \geq 0$ and $S = C - B^T A^{-1} B \geq 0$.

Proof. 1. *Sufficiency:* Assume $A \geq 0$ and $S = C - B^T A^{-1} B \geq 0$. Let $z = \begin{pmatrix} u \\ v \end{pmatrix}$ for $u, v \in \mathbb{R}^n$. Then:

$$\begin{aligned} z^T M z &= \begin{pmatrix} u \\ v \end{pmatrix}^T \begin{pmatrix} A & B \\ B^T & C \end{pmatrix} \begin{pmatrix} u \\ v \end{pmatrix} = u^T A u + 2u^T B v + v^T C v \\ &= u^T A u + 2u^T B v + v^T (C - B^T A^{-1} B) v + v^T B^T A^{-1} B v \\ &= u^T A u + v^T S v + (u + A^{-1} B v)^T A (u + A^{-1} B v) - v^T B^T A^{-1} B v \end{aligned}$$

Since $A \geq 0$ and $S \geq 0$, each term is non-negative, thus $M \geq 0$.

2. *Necessity:* Assume $M \geq 0$. For any $u \in \mathbb{R}^n$, choose $z = \begin{pmatrix} u \\ 0 \end{pmatrix}$:

$$z^T M z = u^T A u \geq 0$$

Thus, $A \geq 0$. For any $v \in \mathbb{R}^n$, choose $z = \begin{pmatrix} -A^{-1}Bv \\ v \end{pmatrix}$:

$$\begin{aligned} z^T M z &= \begin{pmatrix} -A^{-1}Bv \\ v \end{pmatrix}^T \begin{pmatrix} A & B \\ B^T & C \end{pmatrix} \begin{pmatrix} -A^{-1}Bv \\ v \end{pmatrix} \\ &= (-A^{-1}Bv)^T A (-A^{-1}Bv) + 2(-A^{-1}Bv)^T B v + v^T C v \\ &= v^T B^T A^{-1} B v - 2v^T B^T A^{-1} B v + v^T C v \\ &= v^T (C - B^T A^{-1} B) v \geq 0 \end{aligned}$$

Thus, $S = C - B^T A^{-1} B \geq 0$. \square

\square

A.1.5 Young Inequality

For any non-negative numbers a and b , and for positive numbers p and q such that $\frac{1}{p} + \frac{1}{q} = 1$, the inequality given by Young's inequality is:

$$ab \leq \frac{a^p}{p} + \frac{b^q}{q}$$

This inequality indicates that the product ab can be bounded by a combination of a and b raised to specific powers. Young's inequality plays a crucial role in simplifying and solving Linear Matrix Inequalities (LMIs) by transforming nonlinear terms into linear ones. It is particularly useful in the design of observers for control systems. Young's inequality can be expressed as follows:

$$\mathbf{X}^\top \mathbf{Y} + \mathbf{Y}^\top \mathbf{X} \leq \mathbf{X}^\top \mathbf{Z}^{-1} \mathbf{X} + \mathbf{Y}^\top \mathbf{Z} \mathbf{Y} \quad (\text{A.1})$$

for any two vectors $\mathbf{X}, \mathbf{Y} \in \mathbb{R}^n$ and a positive definite matrix $\mathbf{Z} \in \mathbb{R}^{n \times n}$, where $\mathbf{Z} = \mathbf{Z}^\top > 0$. In [132], a variant of Young's inequality is proposed, which is given by:

$$\mathbf{X}^\top \mathbf{Y} + \mathbf{Y}^\top \mathbf{X} \leq \frac{1}{2} (\mathbf{X} + \mathbf{Z} \mathbf{Y})^\top \mathbf{Z}^{-1} (\mathbf{X} + \mathbf{Z} \mathbf{Y}) \quad (\text{A.2})$$

This can be expressed as:

$$\mathbf{X}^\top \mathbf{Y} + \mathbf{Y}^\top \mathbf{X} \leq \frac{1}{2} (\mathbf{X} + \mathbf{Z} \mathbf{Y})^\top \mathbf{Z}^{-1} (\mathbf{X} + \mathbf{Z} \mathbf{Y}) \leq \mathbf{X}^\top \mathbf{Z}^{-1} \mathbf{X} + \mathbf{Y}^\top \mathbf{Z} \mathbf{Y}$$

Both (A.1) and (A.2) are employed in observer design approaches, especially those based on LMIs.

A.1.6 Feasibility of LMIs

The feasibility problem for LMIs involves finding a vector x such that $F(x) \leq 0$. This is a convex feasibility problem since the set of solutions is convex. The feasibility problem can be solved using various numerical algorithms such as interior-point methods.

A.1.7 Optimization with LMIs

Optimization problems with LMI constraints can be formulated as:

$$\begin{aligned} & \text{minimize} && c^T x \\ & \text{subject to} && F(x) \leq 0 \end{aligned}$$

where c is a given vector. This is a convex optimization problem and can be efficiently solved using semidefinite programming (SDP) techniques.

A.1.8 Solving LMIs

- **Algorithms:** Interior-point methods and semidefinite programming (SDP) are commonly used algorithms for solving LMI problems.
- **Software:** Tools like MATLAB's LMI toolbox and YALMIP facilitate the solution of LMI problems.

A.2 Lipschitz Constant Computation for Nonlinear Functions

A.2.1 Definition of Lipschitz Continuity

A function $f : \mathbb{R}^n \rightarrow \mathbb{R}^m$ is called Lipschitz continuous if there exists a constant $L \geq 0$ such that for all $x, y \in \mathbb{R}^n$:

$$\|f(x) - f(y)\| \leq L\|x - y\|$$

The smallest such constant L is called the Lipschitz constant of f .

A.2.2 Computing the Lipschitz Constant for Differentiable Functions

For a differentiable function $f : \mathbb{R}^n \rightarrow \mathbb{R}^m$, an upper bound for the Lipschitz constant can be given by the supremum of the norm of its Jacobian matrix J_f :

$$L = \sup_{x \in \mathbb{R}^n} \|J_f(x)\|$$

where $J_f(x)$ is the matrix of first-order partial derivatives of f .

Example: Consider $f(x) = \begin{pmatrix} \sin(x_1) \\ \cos(x_2) \end{pmatrix}$. The Jacobian is:

$$J_f(x) = \begin{pmatrix} \cos(x_1) & 0 \\ 0 & -\sin(x_2) \end{pmatrix}$$

Thus,

$$\|J_f(x)\| = \max\{|\cos(x_1)|, |\sin(x_2)|\} \leq 1$$

So, the Lipschitz constant for f is $L = 1$.

A.2.3 Numerical Computation of Lipschitz Constants

For nonlinear vector-valued functions, the Lipschitz constant can be computed numerically using the following methods:

Gradient Norm Approach: Evaluate the norm of the Jacobian $J_f(x)$ at multiple points within the domain and take the supremum:

$$L \approx \max_{x \in \mathcal{D}} \|J_f(x)\|$$

where \mathcal{D} is a discretized version of the domain.

Example: Consider the function $f(x) = \begin{pmatrix} e^{x_1} \\ \sin(x_2) \end{pmatrix}$. The Jacobian is:

$$J_f(x) = \begin{pmatrix} e^{x_1} & 0 \\ 0 & \cos(x_2) \end{pmatrix}$$

To find the Lipschitz constant over a bounded domain $x_1 \in [a, b]$ and $x_2 \in [c, d]$, evaluate:

$$\|J_f(x)\| = \max\{|e^{x_1}|, |\cos(x_2)|\}$$

Since e^{x_1} is monotonically increasing, $\|e^{x_1}\|$ is maximized at $x_1 = b$ and $|\cos(x_2)| \leq 1$, we get:

$$L = \max\{e^b, 1\}$$

Algorithm:

1. Discretize the domain $[a, b] \times [c, d]$ into a grid.
2. Compute $J_f(x)$ at each grid point.
3. Evaluate the norm $\|J_f(x)\|$ at each grid point.
4. Take the maximum value as the Lipschitz constant L .

Example: Assume $a = 0$, $b = 1$, $c = 0$, and $d = 1$. Compute $J_f(x)$ over this grid and find the maximum norm.

A.2.4 Lipschitz Constant for Composite Nonlinear Functions

For a composite function $g \circ f$, where $f : \mathbb{R}^n \rightarrow \mathbb{R}^m$ and $g : \mathbb{R}^m \rightarrow \mathbb{R}^p$, the Lipschitz constant can be bounded by the product of the Lipschitz constants of f and g :

$$L_{g \circ f} \leq L_g L_f$$

Example: Let $f(x) = \begin{pmatrix} \sin(x_1) \\ x_2^2 \end{pmatrix}$ and $g(y) = y_1 + e^{y_2}$. The Jacobians are:

$$J_f(x) = \begin{pmatrix} \cos(x_1) & 0 \\ 0 & 2x_2 \end{pmatrix}, \quad J_g(y) = \begin{pmatrix} 1 & e^{y_2} \end{pmatrix}$$

The norms are:

$$L_f = \max_{x_1 \in [a,b], x_2 \in [c,d]} \max\{|\cos(x_1)|, 2|x_2|\} = \max\{1, 2d\}$$

$$L_g = \max_{y_2 \in [f_2(c), f_2(d)]} \sqrt{1 + e^{2y_2}}$$

Thus, the composite Lipschitz constant is:

$$L_{g \circ f} \leq \max\{1, 2d\} \max_{y_2 \in [c^2, d^2]} \sqrt{1 + e^{2y_2}}$$

A.3 Basic Artificial Neural Networks (ANNs)

A.3.1 Overview

Artificial Neural Networks (ANNs) are computational models inspired by biological neural networks. They consist of nodes (neurons) arranged in layers, where each node performs computations and passes results to other nodes. The learning process involves adjusting the parameters (weights and biases) to minimize the error in predictions.

A.3.2 Structure of an ANN

Neurons

Each neuron computes a weighted sum of its inputs and applies an activation function. The output of a neuron is given by:

$$a_j = f \left(\sum_i w_{ij} x_i + b_j \right) \tag{A.3}$$

where:

- x_i are the input values,
- w_{ij} are the weights connecting the i -th input to the j -th neuron,
- b_j is the bias of the j -th neuron,

- f is the activation function,
- a_j is the output of the j -th neuron.

Layers

- **Input Layer:** Directly receives the input features. There are no weights or activation functions here.
- **Hidden Layers:** Perform intermediate computations. Each neuron's output in a hidden layer is computed as:

$$a_j = f \left(\sum_i w_{ij} x_i + b_j \right) \quad (\text{A.4})$$

- **Output Layer:** Produces the final output. For a classification problem with C classes, the output layer often uses the softmax function to convert raw scores into probabilities:

$$\hat{y}_j = \frac{e^{z_j}}{\sum_k e^{z_k}} \quad (\text{A.5})$$

where z_j is the raw score (logit) for class j , and \hat{y}_j is the predicted probability for class j .

Weights and Biases

- **Weights:** w_{ij} are parameters that are learned during training. They are adjusted to minimize the loss function.
- **Biases:** b_j are additional parameters added to the weighted sum to allow the model to better fit the data.

A.3.3 Activation Functions

Activation functions introduce non-linearity to the model. They are applied to the weighted sum of inputs:

Sigmoid Function

$$\sigma(x) = \frac{1}{1 + e^{-x}} \quad (\text{A.6})$$

- **Range:** $(0, 1)$
- **Derivative:**

$$\sigma'(x) = \sigma(x) \cdot (1 - \sigma(x)) \quad (\text{A.7})$$

ReLU (Rectified Linear Unit)

$$\text{ReLU}(x) = \max(0, x) \quad (\text{A.8})$$

- **Range:** $[0, \infty)$
- **Derivative:**

$$\text{ReLU}'(x) = \begin{cases} 1 & \text{if } x > 0 \\ 0 & \text{if } x \leq 0 \end{cases} \quad (\text{A.9})$$

Tanh (Hyperbolic Tangent)

$$\tanh(x) = \frac{e^x - e^{-x}}{e^x + e^{-x}} \quad (\text{A.10})$$

- **Range:** $(-1, 1)$
- **Derivative:**

$$\tanh'(x) = 1 - \tanh^2(x) \quad (\text{A.11})$$

Softmax Function

$$\text{softmax}(z_j) = \frac{e^{z_j}}{\sum_k e^{z_k}} \quad (\text{A.12})$$

Converts raw scores into probabilities for multi-class classification.

A.3.4 Training an ANN

Training involves optimizing the weights and biases to minimize the error between predicted and actual values. This process involves:

Forward Propagation

Compute the output of each neuron by passing inputs through the network, applying weights, biases, and activation functions.

Loss Function

Quantifies the error between predictions and actual values. Common loss functions include:

- **Mean Squared Error (MSE):**

$$\text{MSE} = \frac{1}{N} \sum_{i=1}^N (y_i - \hat{y}_i)^2 \quad (\text{A.13})$$

where N is the number of samples, y_i is the actual value, and \hat{y}_i is the predicted value.

- **Mean Absolute Error (MAE):**

$$\text{MAE} = \frac{1}{N} \sum_{i=1}^N |y_i - \hat{y}_i| \quad (\text{A.14})$$

- **Binary Cross-Entropy Loss:**

$$\text{Binary Cross-Entropy} = -\frac{1}{N} \sum_{i=1}^N [y_i \log(\hat{y}_i) + (1 - y_i) \log(1 - \hat{y}_i)] \quad (\text{A.15})$$

where y_i is the actual binary label (0 or 1), and \hat{y}_i is the predicted probability.

- **Categorical Cross-Entropy Loss:**

$$\text{Categorical Cross-Entropy} = -\frac{1}{N} \sum_{i=1}^N \sum_{j=1}^C y_{i,j} \log(\hat{y}_{i,j}) \quad (\text{A.16})$$

where C is the number of classes, $y_{i,j}$ is 1 if the i -th sample belongs to class j and 0 otherwise, and $\hat{y}_{i,j}$ is the predicted probability for class j .

- **Huber Loss:**

$$\text{Huber Loss} = \begin{cases} \frac{1}{2}(y_i - \hat{y}_i)^2 & \text{for } |y_i - \hat{y}_i| \leq \delta \\ \delta|y_i - \hat{y}_i| - \frac{1}{2}\delta^2 & \text{otherwise} \end{cases} \quad (\text{A.17})$$

where δ is a threshold parameter. It combines MSE and MAE to be less sensitive to outliers.

Backpropagation

Compute gradients of the loss function with respect to each weight using the chain rule. Update weights and biases using optimization algorithms.

Optimization Algorithms

- **Stochastic Gradient Descent (SGD):**

$$w_{ij} = w_{ij} - \eta \frac{\partial \text{Loss}}{\partial w_{ij}} \quad (\text{A.18})$$

where η is the learning rate.

- **Adam (Adaptive Moment Estimation):**

$$m_t = \beta_1 m_{t-1} + (1 - \beta_1) \frac{\partial \text{Loss}}{\partial w} \quad (\text{A.19})$$

$$v_t = \beta_2 v_{t-1} + (1 - \beta_2) \left(\frac{\partial \text{Loss}}{\partial w} \right)^2 \quad (\text{A.20})$$

$$\hat{m}_t = \frac{m_t}{1 - \beta_1^t} \quad (\text{A.21})$$

$$\hat{v}_t = \frac{v_t}{1 - \beta_2^t} \quad (\text{A.22})$$

$$w = w - \eta \frac{\hat{m}_t}{\sqrt{\hat{v}_t} + \epsilon} \quad (\text{A.23})$$

where m_t and v_t are estimates of the first and second moments of the gradients, β_1 and β_2 are decay rates, and ϵ is a small constant to prevent division by zero.

A.3.5 Examples

- **Single-Layer Perceptron:** A basic neural network with no hidden layers. It applies a linear transformation followed by an activation function.

$$\hat{y} = f \left(\sum_i w_i x_i + b \right) \quad (\text{A.24})$$

- **Multi-Layer Perceptron (MLP):** A neural network with one or more hidden layers, allowing it to learn complex patterns. Each layer computes its output as follows:

$$a_j^{(l)} = f \left(\sum_i w_{ij}^{(l)} a_i^{(l-1)} + b_j^{(l)} \right) \quad (\text{A.25})$$

where l denotes the layer index, and $a_i^{(l-1)}$ are the activations from the previous layer.

B

Bibliography

Contents

References	184
List of publications	195

References

- [1] S. L. Perić, D. S. Antić, M. B. Milovanović, D. B. Mití, M. T. Milojkoví, and S. S. Nikolí, “Quasi-sliding mode control with orthogonal endocrine neural network-based estimator applied in anti-lock braking system,” *IEEE/ASME Transactions on Mechatronics*, vol. 21, 2 2016.
- [2] A. Dadashnialehi, A. Bab-Hadiashar, Z. Cao, and A. Kapoor, “Intelligent sensorless abs for in-wheel electric vehicles,” *IEEE Transactions on Industrial Electronics*, vol. 61, 4 2014.
- [3] T. Tanaka and K. Isoda, “Traction control system,” *Nihon Kikai Gakkai Ronbunshu, C Hen/Transactions of the Japan Society of Mechanical Engineers, Part C*, vol. 57, 534 1991.
- [4] S. Melzi and E. Sabbioni, “On the vehicle sideslip angle estimation through neural networks: Numerical and experimental results,” *Mechanical Systems and Signal Processing*, vol. 25, 6 2011.
- [5] H. Lee, “Reliability indexed sensor fusion and its application to vehicle velocity estimation,” *Journal of Dynamic Systems, Measurement and Control, Transactions of the ASME*, vol. 128, 2 2006.
- [6] D. Piyabongkarn, R. Rajamani, J. A. Grogg, and J. Y. Lew, “Development and experimental evaluation of a slip angle estimator for vehicle stability control,” *IEEE Transactions on Control Systems Technology*, vol. 17, 1 2009.
- [7] R. Rajamani, “Lateral vehicle dynamics,” in (Mechanical Engineering Series), Mechanical Engineering Series. Springer US, 2012.
- [8] M. Guiggiani, *The Science of Vehicle Dynamics*. Springer Dordrecht, 2023.
- [9] R. E. Kalman, “A new approach to linear filtering and prediction problems,” *Journal of Fluids Engineering, Transactions of the ASME*, vol. 82, 1 1960.
- [10] T. D. Gillespie, *Fundamentals of Vehicle Dynamics - Revised Edition*. SAE International, 2021.

- [11] K. S. Narendra and K. Parthasarathy, “Identification and control of dynamical systems using neural networks,” *IEEE Transactions on Neural Networks*, vol. 1, 1 1990.
- [12] P. A. Ioannou and M. A. Christodoulou, “High-order neural network structures for identification of dynamical systems,” *IEEE Transactions on Neural Networks*, vol. 6, 2 1995.
- [13] M. Ran and L. Xie, “Adaptive observation-based efficient reinforcement learning for uncertain systems,” *IEEE Transactions on Neural Networks and Learning Systems*, vol. 33, 10 2022.
- [14] A. Astolfi and L. Marconi, *Analysis and design of nonlinear control systems: In honor of Alberto Isidori*. Springer Berlin, Heidelberg, 2008.
- [15] Y. Wang and R. Sun, “A novel gps fault detection and exclusion algorithm aided by imu and vo data for vehicle integrated navigation in urban environments,” vol. 48, 2023.
- [16] S. Kumar, J. Paefgen, E. Wilhelm, and S. E. Sarma, “Integrating on-board diagnostics speed data with sparse gps measurements for vehicle trajectory estimation,” 2013.
- [17] Y. B. Shalom, X. R. Li, and T. Kirubarajan, *Estimation with Applications to Tracking and Navigation*. John Wiley and Sons, 2002.
- [18] G. Park, “Vehicle sideslip angle estimation based on interacting multiple model kalman filter using low-cost sensor fusion,” *IEEE Transactions on Vehicular Technology*, vol. 71, 6 2022.
- [19] I. Verpraet, “The history of adaptive cruise control,” *ADAS and Autonomous Vehicle International*, 2018.
- [20] J. D. Woll, “Radar based adaptive cruise control for truck applications,” 1997.
- [21] Z. Zhao and C. Wei, “An analysis of the brake performance of radar-based adaptive cruise control during ramp merging on simulation software,” 2022.
- [22] G. R. Widmann, M. K. Daniels, L. Hamilton, *et al.*, “Comparison of lidar-based and radar-based adaptive cruise control systems,” 2000.
- [23] S. Kang, I. Yoo, M. Shin, and S. Seo, “Accurate inter-vehicle distance measurement based on monocular camera and line laser,” *IEICE Electronics Express*, vol. 11, 9 2014.
- [24] A. K. Yadav and J. Szpytko, “Safety problems in vehicles with adaptive cruise control system,” *Journal of Konbin*, vol. 42, 1 2017.
- [25] B. Wang, Y. Han, D. Tian, and T. Guan, *Sensor-based environmental perception technology for intelligent vehicles*, 2021.

- [26] “Adaptive cruise control system with traffic jam tracking function based on multi-sensors and the driving behavior of skilled drivers,” *Advances in Mechanical Engineering*, vol. 10, 9 2018.
- [27] J. Navarro, F. Mars, and M. S. Young, *Lateral control assistance in car driving: Classification, review and future prospects*, 2011.
- [28] W. Cho, J. Choi, C. Kim, S. Choi, and K. Yi, “Unified chassis control for the improvement of agility, maneuverability, and lateral stability,” *IEEE Transactions on Vehicular Technology*, vol. 61, 3 2012.
- [29] J. E. Naranjo, C. González, R. García, and T. D. Pedro, “Lane-change fuzzy control in autonomous vehicles for the overtaking maneuver,” *IEEE Transactions on Intelligent Transportation Systems*, vol. 9, 3 2008.
- [30] R. Rajamani, H. S. Tan, B. K. Law, and W. B. Zhang, “Demonstration of integrated longitudinal and lateral control for the operation of automated vehicles in platoons,” *IEEE Transactions on Control Systems Technology*, vol. 8, 4 2000.
- [31] M. K. Aripin, Y. M. Sam, K. A. Danapalasingam, K. Peng, N. Hamzah, and M. F. Ismail, *A review of active yaw control system for vehicle handling and stability enhancement*, 2014.
- [32] H. Zhou and Z. Liu, “Vehicle yaw stability-control system design based on sliding mode and backstepping control approach,” *IEEE Transactions on Vehicular Technology*, vol. 59, 7 2010.
- [33] B. Lacroix, Z. Liu, and P. Seers, “A comparison of two control methods for vehicle stability control by direct yaw moment,” vol. 120, 2012.
- [34] P. Falcone, F. Borrelli, J. Asgari, H. E. Tseng, and D. Hrovat, “Predictive active steering control for autonomous vehicle systems,” *IEEE Transactions on Control Systems Technology*, vol. 15, 3 2007.
- [35] C. Zhang, P. Gao, J. Wang, M. Dang, X. Yang, and Y. Feng, “Research on active rear-wheel steering control method with sliding mode control optimized by model predictive,” *IEEE Access*, vol. 11, 2023.
- [36] F. Yu, D. F. Li, and D. A. Crolla, “Integrated vehicle dynamics control-state-of-the art review,” 2008.
- [37] S. B. Lu, Y. N. Li, S. B. Choi, L. Zheng, and M. S. Seong, “Integrated control on mr vehicle suspension system associated with braking and steering control,” *Vehicle System Dynamics*, vol. 49, 1-2 2011.
- [38] J. Guldner, H. S. Tan, and S. Patwardhan, “Analysis of automatic steering control for highway vehicles with look-down lateral reference systems,” *Vehicle System Dynamics*, vol. 26, 4 1996.

- [39] P. J. Venhovens and K. Naab, "Vehicle dynamics estimation using kalman filters," *Vehicle System Dynamics*, vol. 32, 2 1999.
- [40] K. Nam, S. Oh, H. Fujimoto, and Y. Hori, "Estimation of sideslip and roll angles of electric vehicles using lateral tire force sensors through rls and kalman filter approaches," *IEEE Transactions on Industrial Electronics*, vol. 60, 3 2013.
- [41] C. Poussot-Vassal, O. Sename, L. Dugard, and S. M. Savaresi, "Vehicle dynamic stability improvements through gain-scheduled steering and braking control," *Vehicle System Dynamics*, vol. 49, 10 2011.
- [42] H. B. Pacejka and E. Bakker, "The magic formula tyre model," *Vehicle System Dynamics*, vol. 21, sup1 1992.
- [43] J. Kim, "Identification of lateral tyre force dynamics using an extended kalman filter from experimental road test data," *Control Engineering Practice*, vol. 17, 3 2009.
- [44] J. Kim, "Effect of vehicle model on the estimation of lateral vehicle dynamics," *International Journal of Automotive Technology*, vol. 11, 3 2010.
- [45] X. Li, X. Song, and C. Chan, "Reliable vehicle sideslip angle fusion estimation using low-cost sensors," *Measurement: Journal of the International Measurement Confederation*, vol. 51, 1 2014.
- [46] H. Dugoff, P. S. Fancher, and L. Segel, "An analysis of tire traction properties and their influence on vehicle dynamic performance," 1970.
- [47] R. Rajamani, *Vehicle Dynamics and Control* (Mechanical Engineering Series). Springer US, 2011. [Online]. Available: <https://books.google.fr/books?id=cZJFDox4KuUC>.
- [48] S. E. Li, Y. Zheng, K. Li, *et al.*, "Dynamical modeling and distributed control of connected and automated vehicles: Challenges and opportunities," *IEEE Intelligent Transportation Systems Magazine*, vol. 9, 3 2017.
- [49] G. Guo and W. Yue, "Autonomous platoon control allowing range-limited sensors," *IEEE Transactions on Vehicular Technology*, vol. 61, 7 2012.
- [50] Y. Liu, C. Pan, H. Gao, and G. Guo, "Cooperative spacing control for interconnected vehicle systems with input delays," *IEEE Transactions on Vehicular Technology*, vol. 66, 12 2017.
- [51] S. Seshagiri and H. K. Khalil, "Longitudinal adaptive control of a platoon of vehicles," vol. 5, 1999.
- [52] Y. Zhu, J. Wu, and H. Su, "V2v-based cooperative control of uncertain, disturbed and constrained nonlinear cavs platoon," *IEEE Transactions on Intelligent Transportation Systems*, vol. 23, 3 2022.

- [53] H. K. Khalil, *Nonlinear Systems, Third Edition*. Prentice Hall, 2002.
- [54] R. Anderson and D. M. Bevly, “Using gps with a model-based estimator to estimate critical vehicle states,” *Vehicle System Dynamics*, vol. 48, 12 2010.
- [55] M. Gadola, D. Chindamo, M. Romano, and F. Padula, “Development and validation of a kalman filter-based model for vehicle slip angle estimation,” *Vehicle System Dynamics*, vol. 52, 1 2014.
- [56] K. Nam, H. Fujimoto, and Y. Hori, “Lateral stability control of in-wheel-motor-driven electric vehicles based on sideslip angle estimation using lateral tire force sensors,” *IEEE Transactions on Vehicular Technology*, vol. 61, 5 2012.
- [57] J. K. Uhlmann and S. J. Julier, “A new extension of the kalman filter to nonlinear systems,” *Signal processing, sensor fusion, and target recognition VI*, vol. 3068, 1997.
- [58] M. Doumiati, A. Victorino, A. Charara, and D. Lechner, “Estimation of vehicle lateral tire-road forces: A comparison between extended and unscented kalman filtering,” 2014.
- [59] S. Antonov, A. Fehn, and A. Kugi, “Unscented kalman filter for vehicle state estimation,” *Vehicle System Dynamics*, vol. 49, 9 2011.
- [60] Q. Cheng, A. Correa-Victorino, and A. Charara, “A new nonlinear observer of sideslip angle with unknown vehicle parameter using the dual unscented kalman filter,” 2012.
- [61] M. Doumiati, A. C. Victorino, A. Charara, and D. Lechner, “Onboard real-time estimation of vehicle lateral tire-road forces and sideslip angle,” *IEEE/ASME Transactions on Mechatronics*, vol. 16, 4 2011.
- [62] S. Strano and M. Terzo, “Constrained nonlinear filter for vehicle sideslip angle estimation with no a priori knowledge of tyre characteristics,” *Control Engineering Practice*, vol. 71, 2018.
- [63] Z. Wang, Y. Qin, L. Gu, and M. Dong, “Vehicle system state estimation based on adaptive unscented kalman filtering combing with road classification,” *IEEE Access*, vol. 5, 2017.
- [64] Z. Wang, C. C. Lim, and Y. Shen, “Interval observer design for uncertain discrete-time linear systems,” *Systems and Control Letters*, vol. 116, 2018.
- [65] E. Hashemi, S. Khosravani, A. Khajepour, A. Kasaiezadeh, S. K. Chen, and B. Litkouhi, “Longitudinal vehicle state estimation using nonlinear and parameter-varying observers,” *Mechatronics*, vol. 43, 2017.
- [66] J. Zhao, J. Zhang, and B. Zhu, “Coordinative traction control of vehicles based on identification of the tyre-road friction coefficient,” *Proceedings of the Institution*

of Mechanical Engineers, Part D: Journal of Automobile Engineering, vol. 230, 12 2016.

- [67] J. C. Cadiou, A. E. Hadri, and F. Chikhi, “Non-linear tyre forces estimation based on vehicle dynamics observation in a finite time,” *Proceedings of the I MECH E Part D Journal of Automobile Engineering*, vol. 218, 12 2004.
- [68] D. J. Lee and Y. S. Park, “Sliding-mode-based parameter identification with application to tire pressure and tire-road friction,” *International Journal of Automotive Technology*, vol. 12, 4 2011.
- [69] Z. B. Song, Y. H. Zweiri, L. D. Seneviratne, and K. Althoefer, “Non-linear observer for slip estimation of tracked vehicles,” *Proceedings of the Institution of Mechanical Engineers, Part D: Journal of Automobile Engineering*, vol. 222, 4 2008.
- [70] B. Subudhi and S. S. Ge, “Sliding-mode-observer-based adaptive slip ratio control for electric and hybrid vehicles,” *IEEE Transactions on Intelligent Transportation Systems*, vol. 13, 4 2012.
- [71] N. Patel, C. Edwards, and S. K. Spurgeon, “Optimal braking and estimation of tyre friction in automotive vehicles using sliding modes,” *International Journal of Systems Science*, vol. 38, 11 2007.
- [72] S. Drakunov and V. Utkin, “Sliding mode observers. tutorial,” vol. 4, 1995.
- [73] X. Gao, Z. Yu, J. Neubeck, and J. Wiedemann, “Sideslip angle estimation based on input-output linearisation with tire-road friction adaptation,” *Vehicle System Dynamics*, vol. 48, 2 2010.
- [74] H. Guo, H. Chen, D. Cao, and W. Jin, “Design of a reduced-order non-linear observer for vehicle velocities estimation,” *IET Control Theory and Applications*, vol. 7, 17 2013.
- [75] L. H. Zhao, Z. Y. Liu, and H. Chen, “Design of a nonlinear observer for vehicle velocity estimation and experiments,” *IEEE Transactions on Control Systems Technology*, vol. 19, 3 2011.
- [76] W. Jeon, A. Zemouche, and R. Rajamani, “Tracking of vehicle motion on highways and urban roads using a nonlinear observer,” *IEEE/ASME Transactions on Mechatronics*, vol. 24, 2 2019.
- [77] R. Rajamani, D. Piyabongkarn, V. Tsourapas, and J. Y. Lew, “Parameter and state estimation in vehicle roll dynamics,” *IEEE Transactions on Intelligent Transportation Systems*, vol. 12, 4 2011.

- [78] J. Stephan, A. Charara, and D. Meizel, “Virtual sensor: Application to vehicle sideslip angle and transversal forces,” *IEEE Transactions on Industrial Electronics*, vol. 51, 2 2004.
- [79] J. Stéphant and A. Charara, “Observability matrix and parameter identification: Application to vehicle tire cornering stiffness,” vol. 2005, 2005.
- [80] F. Sun, X. Huang, J. Rudolph, and K. Lolenko, “Vehicle state estimation for anti-lock control with nonlinear observer,” *Control Engineering Practice*, vol. 43, 2015.
- [81] S. Solmaz and S. Ç. Başlamoğlu, “Simultaneous estimation of road friction and sideslip angle based on switched multiple non-linear observers,” *IET Control Theory and Applications*, vol. 6, 14 2012.
- [82] L. Vargas-Melendez, B. L. Boada, M. J. L. Boada, A. Gauchia, and V. Diaz, “Sensor fusion based on an integrated neural network and probability density function (pdf) dual kalman filter for on-line estimation of vehicle parameters and states,” *Sensors (Switzerland)*, vol. 17, 5 2017.
- [83] M. Nguyen-h and C. Zhou, “Improving gps ins integration through neural networks,” *Simulation*, vol. 2, 2 2010.
- [84] M. Gwak, K. Jo, and M. Sunwoo, “Neural-network multiple models filter (nmm)-based position estimation system for autonomous vehicles,” *International Journal of Automotive Technology*, vol. 14, 2 2013.
- [85] W. Wei, B. Shaoyi, Z. Lanchun, Z. Kai, W. Yongzhi, and H. Weixing, “Vehicle sideslip angle estimation based on general regression neural network,” *Mathematical Problems in Engineering*, vol. 2016, 2016.
- [86] A. Chakrabarty, A. Zemouche, R. Rajamani, and M. Benosman, “Robust data-driven neuro-adaptive observers with lipschitz activation functions,” vol. 2019-December, 2019.
- [87] F. Abdollahi, H. A. Talebi, and R. V. Patel, “A stable neural network-based observer with application to flexible-joint manipulators,” *IEEE Transactions on Neural Networks*, vol. 17, 1 2006.
- [88] D. Georges, “Machine learning for receding horizon observer design: Application to traffic density estimation,” vol. 53, 2020.
- [89] J. Peralez and M. Nadri, “Deep learning-based luenberger observer design for discrete-time nonlinear systems,” vol. 2021-December, 2021.
- [90] H. Niederreiter, “Low-discrepancy and low-dispersion sequences,” *Journal of Number Theory*, vol. 30, 1 1988.

- [91] Y. Wang, D. M. Bevly, and R. Rajamani, “Interval observer design for lpv systems with parametric uncertainty,” *Automatica*, vol. 60, 2015.
- [92] D. Efimov, T. Raïssi, W. Perruquetti, and A. Zolghadri, “Estimation and control of discrete-time lpv systems using interval observers,” 2013.
- [93] S. Chebotarev, D. Efimov, T. Raïssi, and A. Zolghadri, “Interval observers for continuous-time lpv systems with $\mathcal{L}_1/\mathcal{L}_2$ performance,” *Automatica*, vol. 58, 2015.
- [94] C. Briat and M. Khammash, “Interval peak-to-peak observers for continuous- and discrete-time systems with persistent inputs and delays,” *Automatica*, vol. 74, 2016.
- [95] A. Khan, X. Bai, B. Zhang, and P. Yan, “Interval state estimator design for linear parameter varying (lpv) systems,” *IEEE Transactions on Circuits and Systems II: Express Briefs*, vol. 68, 8 2021.
- [96] D. Efimov, W. Perruquetti, T. Raïssi, and A. Zolghadri, “Interval observers for time-varying discrete-time systems,” *IEEE Transactions on Automatic Control*, vol. 58, 12 2013.
- [97] T. N. Dinh, G. Marouani, T. Raïssi, Z. Wang, and H. Messaoud, “Optimal interval observers for discrete-time linear switched systems,” *International Journal of Control*, vol. 93, 11 2020.
- [98] R. E. H. Thabet, T. Raïssi, C. Combastel, D. Efimov, and A. Zolghadri, “An effective method to interval observer design for time-varying systems,” *Automatica*, vol. 50, 10 2014.
- [99] K. Chaib-Draa, A. Zemouche, F. Bedouhene, *et al.*, “Finite-time estimation algorithms for lpv discrete-time systems with application to output feedback stabilization,” *Automatica*, vol. 125, 2021.
- [100] R. Engel and G. Kreisselmeier, “A continuous-time observer which converges in finite time,” *IEEE Transactions on Automatic Control*, vol. 47, 7 2002.
- [101] F. Mazenc, E. Fridman, and W. Djema, “Estimation of solutions of observable nonlinear systems with disturbances,” *Systems and Control Letters*, vol. 79, 2015.
- [102] D. Efimov, L. Fridman, T. Raïssi, A. Zolghadri, and R. Seydou, “Interval estimation for lpv systems applying high order sliding mode techniques,” vol. 48, 2012.
- [103] J. J. Martinez, N. Loukkas, and N. Meslem, “H-infinity set-membership observer design for discrete-time lpv systems,” *International Journal of Control*, vol. 93, 10 2020.

- [104] Y. H. Kim, F. L. Lewis, and C. T. Abdallah, "A dynamic recurrent neural-network-based adaptive observer for a class of nonlinear systems," *Automatica*, vol. 33, 8 1997.
- [105] X. Liu, C. Yang, Z. Chen, M. Wang, and C. Y. Su, "Neuro-adaptive observer based control of flexible joint robot," *Neurocomputing*, vol. 275, 2018.
- [106] W. Jeon, A. Chakrabarty, A. Zemouche, and R. Rajamani, "Simultaneous state estimation and tire model learning for autonomous vehicle applications," *IEEE/ASME Transactions on Mechatronics*, vol. 26, 4 2021.
- [107] B. Pratap and S. Purwar, "Neural network observer for twin rotor mimo system: An lmi based approach," 2010.
- [108] R. Rahimilarki, Z. Gao, A. Zhang, and R. Binns, "Robust neural network fault estimation approach for nonlinear dynamic systems with applications to wind turbine systems," *IEEE Transactions on Industrial Informatics*, vol. 15, 12 2019.
- [109] K. Hornik, "Approximation capabilities of multilayer feedforward networks," *Neural Networks*, vol. 4, 2 1991.
- [110] A. Zemouche and M. Boutayeb, "A unified h-infinity adaptive observer synthesis method for a class of systems with both lipschitz and monotone nonlinearities," *Systems and Control Letters*, vol. 58, 4 2009.
- [111] J. P. Gauthier, H. Hammouri, and S. Othman, "A simple observer for nonlinear systems applications to bioreactors," *IEEE Transactions on Automatic Control*, vol. 37, 6 1992.
- [112] T. Liu, Z. P. Jiang, and D. J. Hill, *Nonlinear control of dynamic networks*. CRC Press, 2014.
- [113] H. K. Khalil and L. Praly, "High-gain observers in nonlinear feedback control," *International Journal of Robust and Nonlinear Control*, vol. 24, 6 2014.
- [114] D. Astolfi and L. Marconi, "A high-gain nonlinear observer with limited gain power," *IEEE Transactions on Automatic Control*, vol. 60, 11 2015.
- [115] F. Esfandiari and H. K. Khalil, "Output feedback stabilization of fully linearizable systems," *International Journal of Control*, vol. 56, 5 1992.
- [116] T. Mita, "On zeros and responses of linear regulators and linear observers," *IEEE Transactions on Automatic Control*, vol. 22, 3 1977.
- [117] A. M. Boker and H. K. Khalil, "Nonlinear observers comprising high-gain observers and extended kalman filters," *Automatica*, vol. 49, 12 2013.
- [118] Z. Jiang, Y. He, and J. Han, "High gain disturbance observer and its application in robust control attenuation," 2013.

- [119] G. Besançon, "High-gain observation with disturbance attenuation and application to robust fault detection," *Automatica*, vol. 39, 6 2003.
- [120] P. Krishnamurthy, F. Khorrami, and R. S. Chandra, "Global high-gain-based observer and backstepping controller for generalized output-feedback canonical form," *IEEE Transactions on Automatic Control*, vol. 48, 12 2003.
- [121] A. Zemouche, F. Zhang, F. Mazenc, and R. Rajamani, "High-gain nonlinear observer with lower tuning parameter," *IEEE Transactions on Automatic Control*, vol. 64, 8 2019.
- [122] A. Zemouche and M. Boutayeb, "On lmi conditions to design observers for lipschitz nonlinear systems," *Automatica*, vol. 49, 2 2013.
- [123] A. Teel and L. Praly, "Global stabilizability and observability imply semi-global stabilizability by output feedback," *Systems and Control Letters*, vol. 22, 5 1994.
- [124] M. Maggiore and K. M. Passino, "A separation principle for a class of non-ucco systems," *IEEE Transactions on Automatic Control*, vol. 48, 7 2003.
- [125] E. H. E. Yaagoubi, A. E. Assoudi, and H. Hammouri, "High gain observer: Attenuation of the peak phenomena," vol. 5, 2004.
- [126] M. Shakarami, K. Esfandiari, A. A. Suratgar, and H. A. Talebi, "Peaking attenuation of high-gain observers using adaptive techniques: State estimation and feedback control," *IEEE Transactions on Automatic Control*, vol. 65, 10 2020.
- [127] A. R. Teel, "Further variants of the astolfi/marconi high-gain observer," vol. 2016-July, 2016.
- [128] R. G. Sanfelice and L. Praly, "On the performance of high-gain observers with gain adaptation under measurement noise," vol. 47, 2011.
- [129] N. Boizot, E. Busvelle, and J. P. Gauthier, "An adaptive high-gain observer for nonlinear systems," *Automatica*, vol. 46, 9 2010.
- [130] J. H. Ahrens and H. K. Khalil, "High-gain observers in the presence of measurement noise: A switched-gain approach," *Automatica*, vol. 45, 4 2009.
- [131] J. P. Gauthier and I. A. Kupka, "Observability and observers for nonlinear systems," *SIAM Journal on Control and Optimization*, vol. 32, 4 1994.
- [132] A. Zemouche, R. Rajamani, G. Phanomchoeng, B. Boulkroune, H. Rafaralahy, and M. Zasadzinski, "Circle criterion-based H_∞ observer design for lipschitz and monotonic nonlinear systems – enhanced lmi conditions and constructive discussions," *Automatica*, vol. 85, 2017.
- [133] G. Park, "Interacting multiple model kalman filtering for optimal vehicle state estimation," 2022.

- [134] *Carla Simulation Scenario*, https://github.com/hichem-bessa/Vehicle_Longitudinal_Dynamic_Estimation_Using_Radar_only/blob/main/videoSc.mp4.
- [135] A. Geiger, P. Lenz, C. Stiller, and R. Urtasun, “Vision meets robotics: The kitti dataset,” *International Journal of Robotics Research*, vol. 32, 11 2013.
- [136] H. J. von der Hardt, D. Wolf, and R. Husson, “Dead reckoning localization system of the wheeled mobile robot romane,” 1996.
- [137] I. Ullah, S. Qian, Z. Deng, and J. H. Lee, “Extended kalman filter-based localization algorithm by edge computing in wireless sensor networks,” *Digital Communications and Networks*, vol. 7, 2 2021.
- [138] J. J. Leonard and H. F. Durrant-Whyte, “Mobile robot localization by tracking geometric beacons,” *IEEE Transactions on Robotics and Automation*, vol. 7, 3 1991.

List of publications

International Conferences

H. Bessafa, C. Delattre, Z. Belkhatir, R. Khemmar, and A. Zemouche, “A new discrete-time interval estimator for vehicle side-slip angle estimation,” *IFAC-PapersOnLine*, vol. 55, 35 2022.

H. Bessafa, C. Delattre, Z. Belkhatir, A. Zemouche, and R. Rajamani, “Nonlinear observer design methods based on high-gain methodology and lmis with application to vehicle tracking,” *Proceedings of the American Control Conference*, vol. 2023-May, 2023.

H. Bessafa, C. Delattre, Z. Belkhatir, A. Zemouche, and R. Rajamani, “High-gain like observer design for nonlinear systems applied to vehicle motion estimation,” *22nd IFAC World Congress: Yokohama, Japan*, vol. 56, 2 2023.

H. Bessafa, C. Delattre, Z. Belkhatir, A. Zemouche, and R. Rajamani, “Radar sensor-based longitudinal motion estimation by using a generalized high-gain observer,” *Proceedings of the American Control Conference*, vol. 2024-July, 2024.

Algorithmes d'Estimation Avancés pour les Applications des Véhicules Connectés et Autonomes

Résumé :

Cette thèse est dédiée au développement d'algorithmes d'estimation avancés spécifiquement conçus pour les applications des véhicules autonomes. Initialement, nous fournissons un aperçu complet des différents contrôleurs de véhicules et des systèmes avancés d'assistance à la conduite, préparant le terrain pour une discussion approfondie sur les modèles de dynamique et de cinématique des véhicules. Nous explorons ensuite les observateurs classiques (basés sur des modèles) et ceux basés sur l'apprentissage automatique (pilotés par les données), en examinant leur littérature et leurs applications dans les contextes des véhicules et de la robotique. Notre recherche introduit plusieurs méthodologies novatrices : d'abord, une approche d'estimation sur un intervalle de temps fini pour les systèmes à paramètres variables linéaires (LPV) discrets, appliquée à la dynamique latérale du véhicule pour estimer le dérapage malgré les incertitudes de la rigidité en courbe. Ensuite, nous proposons un observateur neuro-adaptatif qui combine les réseaux neuronaux avec l'apprentissage concurrent pour estimer les forces inconnues dans le modèle longitudinal du véhicule. En outre, nous présentons un observateur généralisé à grand gain, incorporant des conditions de matrice linéairement inégalitaire (LMI) et une contrainte de seuil sur le paramètre de grand gain, conçu pour gérer des mesures et des contraintes supplémentaires. Cet observateur garantit des bornes de stabilité entrée-état (ISS) sur le bruit de mesure et s'adapte aux systèmes non canoniques via une transformation de sortie et une conception de système augmenté. Enfin, nous validons nos méthodes par des simulations étendues en utilisant le simulateur CARLA et l'estimation de trajectoire avec le jeu de données KITTI, démontrant une performance supérieure en termes de précision, de vitesse de convergence et de robustesse dans divers scénarios de véhicules. Les résultats illustrent des améliorations significatives par rapport aux méthodes traditionnelles, soulignant le potentiel pratique de nos techniques d'estimation avancées pour améliorer les performances des véhicules autonomes.

Mots clés : Véhicules autonomes; Estimation d'état du véhicule; Conception d'observateurs; Estimation sur un intervalle de temps fini; Observateur neuro-adaptatif; Observateur à grand gain

Advanced Estimation Algorithms for Connected and Autonomous Vehicle Applications

Abstract:

This thesis is dedicated to the development of advanced estimation algorithms specifically designed for autonomous vehicle applications. Initially, we provide a comprehensive overview of various vehicle controllers and advanced driving assistance systems, setting the stage for an in-depth discussion of vehicle dynamics and kinematics models. We then explore both classical (model-based) and machine learning-based (data-driven) observers, examining their literature and applications within vehicular and robotics contexts. Our research introduces several novel methodologies: first, a finite time interval estimation approach for discrete Linear Parameter Varying (LPV) systems, applied to the vehicle's lateral dynamics to estimate side slip despite uncertainties in cornering stiffness. Next, we propose a neuro-adaptive observer that combines neural networks with concurrent learning to estimate unknown forces in the vehicle's longitudinal model. Furthermore, we present a generalized high-gain observer, incorporating Linear Matrix Inequality (LMI) conditions and a threshold constraint on the high-gain parameter, designed to handle additional measurements and constraints. This observer ensures Input-to-State Stability (ISS) bounds on measurement noise and adapts to non-canonical systems via output transformation and augmented system design. Finally, we validate our methods through extensive simulations using the CARLA simulator and trajectory estimation with the KITTI dataset, demonstrating superior performance in terms of accuracy, convergence speed, and robustness in various vehicular scenarios. The outcomes illustrate significant improvements over traditional methods, highlighting the practical potential of our advanced estimation techniques in enhancing autonomous vehicle performance.

Keywords: Autonomous Vehicles; Vehicle State Estimation; Observer Design; Finite Time Interval Estimation; Neuro-Adaptive Observer; High-Gain Observer

Résumé étendu

Chapitre 1

Ce chapitre explore les avancées récentes dans le développement des véhicules, en mettant l'accent sur les systèmes de conduite assistée avancés (ADAS) et les modèles de véhicule utilisés pour la conception d'observateurs. Il souligne les défis liés à la collecte précise des données dynamiques du véhicule, nécessaires pour améliorer la sécurité et la performance des systèmes de contrôle dynamique. Les sections les plus importantes discutées sont la conception des systèmes de contrôle de la stabilité latérale et de la direction, ainsi que les différentes technologies utilisées pour les systèmes de régulation de la vitesse adaptative. L'accent est mis sur la nécessité d'estimer ou d'observer des états critiques du véhicule en raison des limitations techniques et économiques des capteurs standard. les section principes du Chapitre 1 sont les suivantes:

Systèmes d'Assistance au Conducteur et Contrôle des Véhicules

Dans le monde actuel, une multitude de systèmes d'assistance au conducteur sont développés dans le but de simplifier la conduite, d'améliorer l'efficacité énergétique et surtout, d'assurer la sécurité. Ces avancées ouvrent la voie à la conduite autonome. Nous examinerons certains de ces systèmes actuellement en cours de développement.

- **Contrôle de Croisière Adaptatif (ACC)** Le Contrôle de Croisière Adaptatif (ACC) est un système autonome qui étend la fonctionnalité du régulateur de vitesse classique [19]. Il maintient la vitesse fixée par le conducteur en l'absence d'obstacles, mais ajuste sa vitesse pour maintenir une distance sécurisée si un véhicule est détecté devant, en tenant compte de la vitesse et de l'accélération du véhicule précédent. Le système fonctionne en contrôlant à la fois l'accélérateur et les freins, et se distingue par sa capacité à maintenir un espacement souhaité entre les véhicules. Il opère en deux modes : contrôle de vitesse et suivi de véhicule.

Les systèmes de régulation de vitesse adaptatifs peuvent être basés sur plusieurs technologies :

- **Systèmes à Radar** : Utilisent des capteurs radar pour détecter les collisions potentielles et ajuster la vitesse en conséquence. Ces systèmes, en scannant

l'environnement autour du véhicule, fournissent une image détaillée de la proximité des autres véhicules ou obstacles [20], [21].

- **Systèmes à Laser** : Utilisent des capteurs Lidar pour mesurer les distances avec une précision millimétrique et détecter les conditions météorologiques. Leur performance peut cependant être réduite par des conditions météorologiques défavorables [22]–[24].
 - **Systèmes basés sur la Stéréovision** : Utilisent des caméras pour identifier les objets devant le véhicule et estimer les distances à l'aide d'algorithmes d'apprentissage automatique, mais peuvent rencontrer des difficultés liées aux conditions environnementales [23], [25].
 - **Systèmes Multi-capteurs** : Combinent plusieurs types de capteurs (GPS, caméras, etc.) pour fournir des informations sophistiquées sur l'environnement et la distance aux autres véhicules [26].
- **Contrôle Latéral et de Direction** Le contrôle latéral vise à garantir que le véhicule reste dans sa voie [7], [27], [28]. Les systèmes de maintien de voie (LKS) et de changement de voie (LXS) ont été largement explorés, bien que des défis subsistent pour le contrôle latéral autonome.
 - **Système de Maintien de Voie (LKS)** Conçu pour gérer automatiquement la direction et maintenir le véhicule dans sa voie, tout en s'adaptant à la courbure de celle-ci [30]. Ce système utilise généralement une caméra avant pour capturer des images haute résolution des marquages de voie, et des capteurs radar ou lidar pour améliorer la détection en cas de visibilité réduite.
 - **Contrôle de Stabilité de Yaw** Des systèmes de contrôle de la stabilité du véhicule ont été développés pour prévenir le dérapage et les dérives [7]. Ces systèmes utilisent différentes approches, telles que le contrôle de couple de yaw direct, le contrôle de direction actif et la distribution de couple actif, pour améliorer la stabilité du véhicule en conditions critiques.
De nombreux types de contrôleurs sont utilisés dans les véhicules pour rendre la conduite plus autonome et facile. La recherche continue d'améliorer ces contrôleurs et d'autres pour renforcer la sécurité de conduite. Ces contrôleurs sont souvent conçus à l'aide de modèles de véhicule simplifiés (dynamiques latérales, longitudinales ou cinématiques). Cependant, les informations nécessaires à ces systèmes ne sont pas toujours fournies par les capteurs en raison de limitations technologiques ou de coûts. Par conséquent, les systèmes qui estimate ces informations à l'aide d'observateurs et d'estimateurs sont essentiels. Les prochaines sections approfondiront ces systèmes.

Modélisation des véhicules

La modélisation des véhicules est cruciale pour l'analyse, la conception des contrôleurs et des observateurs. Il existe deux principaux types de modèles : les modèles mathématiques

basés sur des équations et les modèles basés sur des données. Cette thèse se concentre sur la modélisation physique, qui se divise en deux catégories : les modèles cinématiques et les modèles dynamiques. Les modèles cinématiques utilisent des équations géométriques et trigonométriques, tandis que les modèles dynamiques reposent sur la deuxième loi de Newton, décrivant les forces et moments agissant sur le véhicule et ses pneus.

- **Modèle cinématique du mouvement latéral du véhicule:**

Le modèle cinématique du véhicule est développé en utilisant uniquement des relations géométriques, sans prendre en compte les forces d'interaction sur le véhicule ou les pneus. Ce modèle simplifié, représenté par le modèle de bicyclette, est valide sous certaines hypothèses, comme une faible vitesse du véhicule. Il utilise les angles de braquage des roues avant et arrière pour déterminer le mouvement latéral. Les équations résultantes décrivent la relation entre les angles de braquage, la vitesse du véhicule et le rayon de courbure.

- **Modèle dynamique latéral du véhicule :**

À des vitesses plus élevées, le modèle cinématique n'est plus valable, et un modèle dynamique devient nécessaire. Ce modèle dynamique intègre les forces latérales sur les pneus et les moments de lacet, en utilisant les équations de Newton pour les forces et les moments agissant sur le véhicule. Les forces latérales sur les pneus peuvent être approximées par des modèles linéaires ou non linéaires, comme le modèle de Pacejka, selon les conditions de conduite.

- **Modèle dynamique longitudinal du véhicule :**

Le modèle dynamique longitudinal est essentiel pour comprendre les performances et la sécurité du véhicule en termes d'accélération, de freinage et de résistance. Il prend en compte les forces externes comme la traînée aérodynamique, les forces de frottement longitudinales et la résistance au roulement. Le modèle considère également l'inclinaison de la route et les forces agissant sur les pneus pour prédire la réponse du véhicule à diverses conditions de conduite.

En résumé, ces modèles permettent une analyse approfondie du comportement dynamique des véhicules et sont essentiels pour concevoir des systèmes de contrôle avancés et optimiser la performance des véhicules.

Schémas d'estimation pour l'estimation de l'état du véhicule

- **Observateurs Basés sur les Modèles**

Les observateurs basés sur les modèles utilisent des modèles mathématiques connus pour estimer les états non mesurés des systèmes dynamiques. Ils sont essentiels pour les systèmes décrits par des équations différentielles, où les variables d'état évoluent au fil du temps en fonction des entrées connues et des sorties mesurables. L'objectif principal est d'obtenir des estimations d'état proches des états réels pour permettre une surveillance, un contrôle et une prise de décision en temps réel.

Observabilité :

- **Observabilité Traditionnelle** : Évaluée à l'aide de la matrice d'observabilité pour les systèmes linéaires.
- **Observabilité Locale pour les Systèmes Non Linéaires** : Vérifiée à l'aide de la matrice d'observabilité basée sur les dérivées de Lie pour les systèmes non linéaires. Cette approche se concentre sur la capacité à reconstruire l'état à partir des mesures de sortie sur un intervalle de temps limité.

Filtres de Kalman Basés sur l'Estimation Les filtres de Kalman sont largement utilisés pour l'estimation d'état en raison de leur capacité à traiter les mesures bruyantes et à fusionner les données provenant de différents capteurs. Ils se déclinent en plusieurs variantes :

- **Filtre de Kalman Général** : Appliqué à des modèles linéaires pour estimer des paramètres comme la vitesse latérale d'un véhicule. L'intégration des signaux GPS et d'autres capteurs améliore l'exactitude de l'estimation.
- **Filtre de Kalman Étendu (EKF)** : Conçu pour gérer les systèmes non linéaires en utilisant des approximations linéaires autour de l'état estimé. Il est couramment utilisé pour estimer des paramètres tels que l'angle de dérapage du véhicule.
- **Filtre de Kalman Non Linéaire Unscented (UKF)** : Utilise des points sigma pour traiter directement les transformations non linéaires dans les systèmes dynamiques. Il est plus précis que l'EKF pour des systèmes fortement non linéaires et est appliqué pour des modèles complexes comme les modèles de forces de pneus.

Observateurs en Mode Glissant (SMO) Les observateurs en mode glissant sont utilisés pour leur robustesse face aux incertitudes et perturbations dans les systèmes non linéaires. Contrairement aux filtres de Kalman, ils ne reposent pas sur des hypothèses de linéarisation ou de distribution gaussienne, mais plutôt sur le principe du contrôle en mode glissant pour faire converger l'erreur d'estimation vers zéro.

Principes : Les SMOs assurent que l'erreur d'estimation converge rapidement en suivant une surface glissante prédéfinie, ce qui les rend particulièrement adaptés aux systèmes non linéaires et aux perturbations.

Observateurs Non Linéaires (NLO) Les observateurs non linéaires sont utilisés pour modéliser les dynamiques complexes des systèmes non linéaires de véhicules. Ils sont particulièrement utiles pour les conditions de conduite extrêmes et offrent une meilleure performance que les variantes linéaires des filtres de Kalman.

Formulation : Modélisent les systèmes non linéaires et estiment les états en utilisant des approches qui prennent en compte les non-linéarités inhérentes des modèles de dynamique du véhicule.

- **Observateurs Basés sur les Données**

Les techniques d'estimation basées sur les données utilisent des ensembles de données historiques et en temps réel pour estimer les états et les paramètres des véhicules sans se baser sur des modèles prédéfinis. Parmi ces techniques, les réseaux de neurones artificiels (ANN) se distinguent pour leur capacité à traiter des modèles complexes et fournir des estimations robustes même en présence d'incertitudes et de non-linéarités [82]–[85]. Les observateurs basés sur les données améliorent l'estimation des états en intégrant des modèles construits à partir de données historiques, augmentant ainsi la précision et la fiabilité des estimations [86], [87].

Observateur de Luenberger basé sur l'apprentissage profond Les observateurs basés sur l'apprentissage profond, comme les observateurs de Luenberger, adressent les non-linéarités en approximant des cartes qui transforment les dynamiques non linéaires en formes linéaires [89]. La méthode KKL, par exemple, utilise l'apprentissage profond pour trouver cette transformation [89].

Observateur neuro-adaptatif Les observateurs neuro-adaptatifs utilisent des réseaux de neurones pour estimer les non-linéarités des systèmes MIMO, avec des mécanismes d'ajustement des poids en ligne pour améliorer les performances [87]. Une approche robuste utilise des fonctions d'activation Lipschitz et des inégalités matricielles pour garantir les performances d'estimation [86].

Apprentissage Automatique pour l'Estimation du Horizon Mobile L'approche proposée par [88] réduit la charge computationnelle de l'observateur à horizon mobile en formant une fonction d'observation inverse. Cette fonction permet de calculer directement les estimations d'état en intégrant les dynamiques du système de manière simple. Une méthode d'apprentissage automatique approximant cette fonction inverse est utilisée pour améliorer l'efficacité et la précision des estimations [88].

Conclusion

Ce chapitre explore les systèmes avancés d'assistance à la conduite (ADAS), leur importance pour la sécurité, le confort et la réduction des accidents. Nous avons discuté des différents types d'ADAS et des mécanismes de contrôle qui nécessitent des informations précises et opportunes sur le véhicule et son environnement, soulignant l'importance des observateurs d'état et des techniques d'estimation.

Nous avons présenté divers modèles de véhicules pour la simulation et l'estimation des états, puis examiné les méthodes d'estimation d'état basées sur des modèles et des données. Nous avons mis en avant les méthodologies hybrides, telles que les observateurs neuro-adaptatifs et les approches basées sur l'apprentissage profond, comme le Deep KKL et les observateurs à horizon glissant.

En résumé, le chapitre offre un aperçu des technologies ADAS, du rôle crucial de l'estimation d'état et des méthodes innovantes pour améliorer leur précision et fiabilité.

Chapitre 2

Le domaine de l'estimation d'état est fondamental en théorie du contrôle, avec des applications variées telles que la robotique, la navigation et le contrôle de processus. Les techniques traditionnelles comme les filtres de Kalman sont efficaces pour les systèmes linéaires et le bruit gaussien, mais montrent leurs limites face aux incertitudes et aux perturbations importantes. Les observateurs d'intervalle, qui fournissent une plage dans laquelle l'état du système est garanti de se situer, offrent une solution robuste pour ces systèmes incertains. Cependant, leur utilisation en temps discret est encore limitée, avec des méthodes souvent basées sur des transformations de systèmes en temps continu, entraînant des estimations conservatrices et des problèmes d'optimisation complexes.

Notre recherche propose un « Estimateur d'Intervalle en Temps Discret », directement opérationnel dans le domaine discret. Inspiré par l'approche espace de parité, notre méthode utilise une analyse d'intervalle basée sur les zonotopes pour optimiser les estimations. Ce nouvel estimateur améliore la précision des estimations en minimisant la longueur des arêtes de la boîte externe du zonotope d'erreur, ouvrant ainsi des perspectives pour des systèmes de contrôle numériques plus robustes et précis.

Les principales sections de ce chapitre sont présentées comme suit :

Observateurs d'intervalle pour les systèmes LPV en temps discret

Méthodologie de conception La conception des observateurs d'intervalle pour les systèmes LPV en temps discret suit une approche similaire à celle des systèmes LPV en temps continu, utilisant principalement la théorie des systèmes monotones pour établir les dynamiques d'erreur d'estimation en intervalle, une tâche complexe.

Des méthodes comme celle présentée dans [93] ont introduit une technique d'observateur d'intervalle LTI dans le cadre L_1/L_2 pour les systèmes LPV, mais ces solutions sont souvent trop conservatrices. De même, [94] a proposé une méthode basée sur la performance L_∞ , mais elle est limitée aux processus LTI.

En revanche, une approche novatrice proposée dans [95] se concentre sur la conception d'une estimation d'état par intervalle basée sur la matrice d'observabilité. Cette méthode

utilise la matrice d'observabilité et les mesures d'entrée-sortie disponibles pour établir des bornes garanties sur l'état réel du système, sans nécessiter une coopération parfaite au sein du système, ce qui la rend moins restrictive que les techniques précédentes.

Définition des systèmes LPV Les systèmes LPV sont des systèmes de contrôle dont la dynamique est linéaire par rapport à l'état et à l'entrée, mais dont les matrices du système dépendent de paramètres variables dans le temps. Un système LPV est dit positif si les matrices A_1, A_2, \dots, A_p sont des matrices Metzler (tous leurs éléments hors-diagonaux sont non-négatifs).

Observateurs d'intervalle pour les systèmes LPV en temps discret Dans les systèmes LPV en temps discret, les observateurs d'intervalle visent à estimer les états à l'intérieur d'un intervalle borné. Les équations des observateurs d'intervalle pour ces systèmes sont formulées en tenant compte des perturbations et du bruit de mesure. Les conditions nécessaires pour garantir que les estimations restent dans les bornes établies sont précisées dans un théorème.

Limitations des observateurs d'intervalle Les observateurs d'intervalle sont utiles pour estimer l'état des systèmes dynamiques dans une plage bornée, mais présentent des limitations notables, notamment en termes de conservatisme, de gestion des paramètres variables dans le temps, de complexité de conception, et de gestion des dynamiques d'erreur d'estimation. Ces défis soulignent le besoin de recherches continues pour améliorer leur efficacité et leur applicabilité en temps réel.

Estimation exacte en temps fini des systèmes LPV

Description du système Nous considérons les systèmes LPV décrits par les équations suivantes :

$$\begin{aligned} x_{k+1} &= \mathbb{A}(\rho_k)x_k + Bu_k \\ y_k &= Cx_k \end{aligned} \tag{B.1}$$

où $\mathbf{x}_k \in \mathbb{R}^n$ est le vecteur d'état, $\mathbf{y}_k \in \mathbb{R}^p$ est la mesure de sortie, et $\mathbf{u}_k \in \mathbb{R}^m$ est le vecteur d'entrée de contrôle. Les matrices B et C sont constantes, tandis que la matrice $\mathbb{A}(\rho_k)$ est affine en ρ_k , qui est une variable bornée et dépendante du temps.

Méthode Pour obtenir une estimation exacte en temps fini de x_k , nous utilisons une approche combinée de deux observateurs asymptotiques. Cette méthode est inspirée des techniques utilisées pour les systèmes en temps continu [100], [101]. L'idée principale est

de combiner les résultats de deux observateurs : un observateur ζ_k et un autre η_k , chacun avec des gains $\mathbb{L}(\rho_k)$ et $\mathbb{K}(\rho_k)$, respectivement.

Les équations des observateurs sont données par :

$$\zeta_{k+1} = \mathbb{A}(\rho_k)\zeta_k + Bu_k + \mathbb{L}(\rho_k)(y_k - C\zeta_k) \quad (\text{B.2a})$$

$$\eta_{k+1} = \mathbb{A}(\rho_k)\eta_k + Bu_k + \mathbb{K}(\rho_k)(y_k - C\eta_k) \quad (\text{B.2b})$$

où les matrices de gain $\mathbb{L}(\rho_k)$ et $\mathbb{K}(\rho_k)$ sont choisies pour garantir que le terme de combinaison, $\mathbb{E}_m(k)$, est inversible. Cette condition est essentielle pour assurer la convergence de l'estimateur en un temps fini $m \geq 1$. L'estimation finale \hat{x}_k est donnée par :

$$\begin{aligned} \hat{x}_k &= \mathbb{E}_m^{-1}(k) \left[\left(\prod_{j=1}^m (\mathbb{A}(\rho_{k-j}) - \mathbb{L}(\rho_{k-j})C) \right)^{-1} \zeta_k \right. \\ &\quad \left. - \left(\prod_{j=1}^m (\mathbb{A}(\rho_{k-j}) - \mathbb{K}(\rho_{k-j})C) \right)^{-1} \eta_k \right. \\ &\quad \left. + \eta_{k-m} - \zeta_{k-m} \right] \end{aligned} \quad (\text{B.3})$$

Cette formule permet d'obtenir une estimation exacte de l'état en temps fini, grâce à la convergence rapide des observateurs.

Résultats Sous certaines conditions sur les matrices de gain, notamment que tous les valeurs propres des matrices $(A_i - L_i C)$ et $(A_i - K_i C)$ soient non nulles et situées dans le cercle unité du plan complexe, l'estimateur \hat{x}_k converge en un temps fini $m \geq 1$. La méthode garantit ainsi une estimation précise et rapide de l'état du système LPV [99].

Conception d'un estimateur d'intervalle en temps fini

La conception d'observateurs pour les systèmes LPV avec des paramètres incertains, mesurés et non mesurés, est généralement complexe. Lorsque l'estimation précise de la trajectoire d'état est impossible, il devient utile d'estimer un intervalle englobant toutes les trajectoires d'état possibles du système dynamique incertain admissible. Pour les applications de surveillance des processus, cet intervalle estimé indique la plage de cas défavorables des états. Cette section présente la conception d'un observateur d'intervalle pour cette classe de systèmes LPV.

Nous considérons les systèmes LPV définis par :

$$x_{k+1} = \mathbb{A}(\rho_k)x_k + B_u u_k + B_v v_k,$$

$$y_k = Cx_k,$$

où $x_k \in \mathbb{R}^n$ est le vecteur d'état, $y_k \in \mathbb{R}^p$ est la mesure de sortie, $u_k \in \mathbb{R}^m$ est le vecteur d'entrée de commande, $\rho_k \in \Theta \subset \mathbb{R}^r$ est un paramètre mesuré variable dans le temps, et $v_k \in \Xi \subset \mathbb{R}^l$ est une incertitude non mesurable variable dans le temps.

Le lemme utilisé dans cette section suppose que les paires (A_j, C) sont observables pour tous j . Il assure que la matrice :

$$\mathbb{E}_m(k) = \left[\prod_{i=1}^m (\mathbb{A}(\rho_{k-i}) - \mathbb{L}(\rho_{k-i})C) \right]^{-1} - \left[\prod_{i=1}^m (\mathbb{A}(\rho_{k-i}) - \mathbb{K}(\rho_{k-i})C) \right]^{-1}$$

existe et est inversible pour tout $k \geq m$. En utilisant cette matrice, on peut estimer directement l'état x_k , mais comme v_k est non mesurable, cette estimation directe n'est pas possible. Il est donc nécessaire d'utiliser deux observateurs asymptotiques combinés avec les vecteurs d'état ζ_k et η_k , et l'état estimé est exprimé par :

$$\hat{x}_k = \mathbb{E}_m^{-1}(k) \left[\left(\prod_{j=1}^m (\mathbb{A}(\rho_{k-j}) - \mathbb{L}(\rho_{k-j})C) \right)^{-1} \zeta_k - \left(\prod_{j=1}^m (\mathbb{A}(\rho_{k-j}) - \mathbb{K}(\rho_{k-j})C) \right)^{-1} \eta_k \right] + \mathbb{E}_m^{-1}(k) \sum_{j=1}^m G_j(k) v_{k-j}$$

où $G_j(k)$ est calculé comme suit :

$$G_j(k) = \mathbb{E}_m^{-1}(k) \left[\left(\prod_{l=1}^m (\mathbb{A}(\rho_{k-l}) - \mathbb{L}(\rho_{k-l})C) \right)^{-1} \times \left(\prod_{i=1}^{j-1} (\mathbb{A}(\rho_{k-i}) - \mathbb{L}(\rho_{k-i})C) \right) \right. \\ \left. - \left(\prod_{l=1}^m (\mathbb{A}(\rho_{k-l}) - \mathbb{K}(\rho_{k-l})C) \right)^{-1} \times \left(\prod_{i=1}^{j-1} (\mathbb{A}(\rho_{k-i}) - \mathbb{K}(\rho_{k-i})C) \right) \right] B_V.$$

Puisque v_k est non mesurable, nous ne pouvons pas directement utiliser l'estimation obtenue. Ainsi, un observateur d'intervalle est conçu pour fournir à la fois les bornes supérieures et inférieures de l'état x_k , avec :

$$\hat{x}_k^+ = \mathbb{E}_m^{-1}(k) \left[\left(\prod_{j=1}^m (\mathbb{A}(\rho_{k-j}) - \mathbb{L}(\rho_{k-j})C) \right)^{-1} \zeta_k - \left(\prod_{j=1}^m (\mathbb{A}(\rho_{k-j}) - \mathbb{K}(\rho_{k-j})C) \right)^{-1} \eta_k + \eta_{k-m} - \zeta_{k-m} + \bar{\mathbb{G}}(k) \right]$$

$$\hat{x}_k^- = \mathbb{E}_m^{-1}(k) \left[\left(\prod_{j=1}^m (\mathbb{A}(\rho_{k-j}) - \mathbb{L}(\rho_{k-j})C) \right)^{-1} \zeta_k - \left(\prod_{j=1}^m (\mathbb{A}(\rho_{k-j}) - \mathbb{K}(\rho_{k-j})C) \right)^{-1} \eta_k + \eta_{k-m} - \zeta_{k-m} + \underline{\mathbb{G}}(k) \right]$$

où $\underline{\mathbb{G}}(k)$ et $\bar{\mathbb{G}}(k)$ sont les bornes calculées en utilisant les bornes de v_k , c'est-à-dire :

$$\underline{\mathbb{G}}(k) = \mathbb{G}^+(k)\underline{v} - \mathbb{G}^-(k)\bar{v},$$

$$\bar{\mathbb{G}}(k) = \mathbb{G}^+(k)\bar{v} - \mathbb{G}^-(k)\underline{v}.$$

Ces bornes permettent de formuler les intervalles admissibles pour l'état x_k , tel que :

$$\hat{x}_k^- \leq x_k \leq \hat{x}_k^+ \quad \forall k \geq m.$$

Conception des paramètres de l'estimateur Cette sous-section propose une caractérisation complète de l'estimateur d'intervalle en introduisant un algorithme pour calculer les valeurs des gains L_i et K_i . La conception de ces gains vise à garantir que la matrice $\mathbb{E}_m(k)$ est inversible pour un $m \geq 1$ donné et pour tous $k \geq m$.

Le théorème suivant suggère une conception des gains L_i (et K_i) qui garantit que l'erreur $\xi_k - x_k$ (et $\eta_k - x_k$) est asymptotiquement stable. Si les systèmes ξ_k et η_k partagent les mêmes dynamiques, le fait de définir les gains L_i et K_i trop proches peut entraîner des problèmes de conditionnement numérique lors de l'inversion de $\mathbb{E}_m(k)$. Les LMIs proposées prennent en compte ce problème de conditionnement numérique.

Le théorème suivant fournit les conditions LMIs à résoudre pour assurer la stabilité asymptotique des erreurs d'estimation et éviter les problèmes de conditionnement numérique.

Application de l'algorithme d'estimation développé au modèle latéral du véhicule

L'angle de dérapage a été estimé en calculant les gains L_i et K_i à l'aide d'une méthode impliquant la matrice $A_N(\rho_k)$. Cette matrice a été exprimée sous une forme spécifique, avec ξ_k^i calculé en fonction des bornes de $\rho_1(k)$ et $\rho_2(k)$ liées à la vitesse du véhicule et à son carré. Les Inégalités Linéaires sur les Matrices (LMI) ont été résolues à l'aide de l'outil Yalmip de MATLAB pour trouver les gains optimaux L_i et K_i , en veillant à ce que la matrice $\mathbb{E}_m(k)$ soit inversible pour $k \geq m$, avec $m = 2$.

Des simulations ont évalué la performance de l'estimateur sous des incertitudes de 5% et 10% dans la raideur en virage. Les variables d'état initiales ont été définies, et les résultats ont montré que l'estimateur suivait avec précision le taux de lacet r et l'angle de dérapage β . La méthode a démontré sa robustesse en gérant efficacement les incertitudes et en montrant une convergence rapide, indépendamment du niveau d'incertitude.

Une analyse comparative avec un observateur H_∞ à adhésion d'ensemble [103], testé sous 10% d'incertitude, a révélé que la méthode FLPV fournissait des estimations plus précises avec des longueurs d'intervalle significativement plus petites et une convergence plus rapide. Les métriques d'erreur quadratique moyenne (MSE) ont indiqué que la méthode FLPV atteignait des erreurs plus faibles dans l'estimation de l'angle de dérapage et du taux de lacet comparativement à l'observateur H_∞ . Cela confirme que la méthode FLPV est à la fois plus précise et plus efficace pour l'estimation des états.

Conclusion

Dans ce chapitre, nous avons conçu un observateur d'intervalle pour les systèmes discrets à paramètres variables (LPV). Nous avons développé un estimateur d'intervalle en temps

discret, combinant l'estimation exacte de l'état avec la gestion de l'incertitude. L'approche intègre des bornes calculées algébriquement, permettant d'éviter les contraintes strictes des observateurs d'intervalle traditionnels, tout en ne faisant aucune hypothèse sur l'état initial. Nous avons utilisé un modèle LPV incertain pour estimer l'angle de dérapage avec une précision accrue, tout en offrant un intervalle minimal d'estimation. Cette méthodologie améliore l'application des observateurs d'intervalle dans les systèmes de contrôle numérique et ouvre des perspectives pour des recherches futures dans ce domaine.

Chapitre 3

L'ingénierie de contrôle a largement utilisé les approximateurs de fonctions tels que les réseaux neuronaux, principalement pour l'identification des systèmes dynamiques à partir de données mesurées. Cependant, l'application des réseaux neuronaux pour l'estimation d'état dans des systèmes aux dynamiques inconnues reste encore peu explorée. Les premières recherches sur les neuro-observateurs, comme dans l'étude de [104], se basaient sur l'hypothèse de disponibilité du modèle, ce qui limitait l'utilisation des réseaux neuronaux dans un environnement contrôlé par les données.

Actuellement, l'ingénierie de contrôle s'oriente de plus en plus vers le contrôle basé sur les données, exploitant la capacité des réseaux neuronaux à apprendre et à s'adapter sans modèles préexistants. Bien que les principes de ces neuro-observateurs aient été introduits il y a près de deux décennies, la plupart des méthodes utilisent des fonctions d'activation de type fonction de base radiale, et les performances d'apprentissage ont peu évolué.

Dans ce chapitre, nous proposons une conception novatrice d'observateur basée sur l'apprentissage automatique, capable d'estimer les états et les dynamiques d'entrée inconnues de systèmes non linéaires variés. Nous utilisons la technique de Concurrent Learning (CL) pour adapter les poids en temps réel en considérant simultanément les données historiques et actuelles. L'observateur est également fondé sur des principes d'inégalités matricielles linéaires (LMI), renforçant la robustesse de l'estimation d'état. Ce travail vise à repousser les limites de l'estimation des systèmes en ingénierie de contrôle et à faire avancer les applications des neuro-observateurs dans divers domaines. Les sections principales de ce chapitre sont les suivantes :

Observateurs Neuro-Adaptatifs

Formulation du Problème Nous considérons des systèmes non linéaires modélisés par l'équation :

$$\dot{x} = Ax + \varphi(x, u), \quad y = Cx + Du.$$

où x est l'état du système, u est l'entrée de contrôle, et y les sorties mesurées. La fonction non linéaire $\varphi(x, u)$ représente les dynamiques non modélisées et est inconnue. Les matrices A , C , et D sont constantes, et le couple (A, C) est choisi pour garantir l'observabilité du système.

Observateur Neuro-Adaptatif Robuste Pour estimer à la fois l'état du système et la non-linéarité inconnue, nous proposons un observateur neuro-adaptatif. L'estimation de l'état \hat{x} et des paramètres de poids \tilde{W} est effectuée selon :

$$\begin{cases} \dot{\hat{x}} = A\hat{x} + \sum_{i=1}^n B_i \tilde{W}_i \sigma(\hat{x}, u) + L_0(y - C\hat{x}), \\ \dot{\tilde{W}}_{i,j} = L_k(y - C\hat{x}), \end{cases}$$

où \hat{x} est l'état estimé et \tilde{W} les paramètres de poids estimés. La fonction $\sigma(\hat{x}, u)$ représente les fonctions d'activation du réseau neuronal, permettant de modéliser la non-linéarité.

Observation Adaptative Basée sur l'Apprentissage Concurrent Pour les systèmes représentés en forme triangulaire :

$$\dot{x} = Ax + B[W^T \Phi(x) + g(x)u], \quad y = Cx$$

où W est un vecteur de poids constant inconnu et $\Phi(x)$ est une fonction de régression, l'observateur proposé est :

$$\begin{cases} \dot{\hat{x}} = A\hat{x} + \Gamma_1(x_1 - \hat{x}_1) + B[\hat{x}_{n+1} + g(\hat{x})u], \\ \hat{x}_{n+1} = \Gamma_2(x_1 - \hat{x}_1), \\ \bar{x}_i = M_i \rho(\hat{x}_i/M_i), \\ \dot{\hat{W}} = \Gamma_3 \Phi(\bar{x}) \left(\bar{x}_{n+1} - \hat{W}^T \Phi(\bar{x}) \right) \\ \quad + \sum_{j=1}^p \Gamma_3 \Phi(\bar{x}^j) \left(\bar{x}_{n+1}^j - \hat{W}^T \Phi(\bar{x}^j) \right). \end{cases}$$

Dans cette approche :

- \hat{x} , \hat{x}_{n+1} , et \hat{W} sont les approximations respectives de x , $x_{n+1} \triangleq W^T \Phi(x)$, et W .
- La fonction de saturation ρ est utilisée pour éviter les pics lors de la phase initiale d'apprentissage.

Cette section introduit un observateur neuro-adaptatif basé sur des Matrices d'Inégalité Linéaire (LMI) pour estimer à la fois les états et les dynamiques non linéaires inconnues d'un système dynamique.

Observateur Neuro-Adaptatif L'observateur proposé est défini par trois ensembles d'équations essentielles. L'équation principale pour l'estimation des états est :

$$\dot{\hat{x}} = A\hat{x} + LC(x - \hat{x}) + Bu + F\hat{x}_z,$$

où \hat{x} est l'estimation des états réels x , L et C sont des matrices du système, u est le contrôle appliqué, et F est une matrice associée à l'estimation des dynamiques non linéaires \hat{x}_z . Les dynamiques non linéaires sont estimées par :

$$\dot{\hat{x}}_z = KC(x - \hat{x}),$$

où \hat{x}_z est l'estimation des dynamiques non linéaires et K est une matrice de gain. Les poids du réseau neuronal utilisé pour approximer les dynamiques non linéaires sont mis à jour selon l'équation :

$$\dot{\hat{W}} = \eta_1 \sigma(\hat{x}) \left(\hat{x}_z - \hat{W}^\top \sigma(\hat{x}) \right) + \sum_{j=1}^p \eta_2 \sigma(\hat{x}^j) \left(\hat{x}_z^j - \hat{W}^\top \sigma(\hat{x}^j) \right),$$

où \hat{W} est l'estimation des poids W , $\sigma(\cdot)$ est la fonction d'activation non linéaire, et η_1 et η_2 sont des matrices de taux d'apprentissage. Cette formulation permet d'ajuster les poids du réseau neuronal en fonction des erreurs d'estimation.

Algorithme de Collecte de Données L'algorithme de collecte de données joue un rôle crucial dans la mise à jour des estimations des états et des poids. Il est conçu pour maximiser la valeur singulière minimale de la matrice historique Z . Cet algorithme fonctionne comme suit : initialement, le stack historique Z et les données correspondantes Λ sont initialisés. Lorsqu'un nouveau point de données est ajouté, l'algorithme vérifie si cette addition améliore la valeur singulière minimale de Z . Si c'est le cas, les nouvelles données sont intégrées ; sinon, les données existantes sont mises à jour pour maintenir une valeur singulière minimale élevée.

Améliorations et Remarques L'observateur neuro-adaptatif présenté améliore les méthodes antérieures de plusieurs manières. Contrairement aux méthodes précédentes qui nécessitaient une forme spécifique pour la fonction non linéaire $f(x)$, notre observateur peut gérer des systèmes non linéaires plus généraux sans connaître a priori la fonction exacte. Il utilise un approximateur neuronal pour estimer la fonction non linéaire et ses poids, ce qui rend la méthode plus flexible et applicable à un plus large éventail de systèmes.

Une autre amélioration majeure est l'approche à deux échelles temporelles, qui assure la convergence des poids du réseau neuronal même après que les états aient convergé. Les méthodes précédentes pouvaient souffrir d'une convergence inégale, où les états convergeaient rapidement mais les poids restaient imprécis. Notre méthode garantit une convergence efficace des poids en utilisant une stratégie de mise à jour des données et des poids, garantissant ainsi une performance plus cohérente.

Équations Clés

1. Estimation des États :

$$\dot{\hat{x}} = A\hat{x} + LC(x - \hat{x}) + Bu + F\hat{x}_z$$

2. Estimation des Dynamiques Non Linéaires :

$$\dot{\hat{x}}_z = KC(x - \hat{x})$$

3. Mise à Jour des Poids :

$$\dot{\hat{W}} = \eta_1 \sigma(\hat{x}) \left(\hat{x}_z - \hat{W}^\top \sigma(\hat{x}) \right) + \sum_{j=1}^p \eta_2 \sigma(\hat{x}^j) \left(\hat{x}_z^j - \hat{W}^\top \sigma(\hat{x}^j) \right)$$

4. Inégalité de Lyapunov pour les Erreurs d'Estimation des États :

$$\frac{dV_1(e)}{dt} \leq -\frac{\lambda}{\beta} V_1(e) + \frac{2\beta N_0}{\sqrt{\alpha}} \sqrt{V_1(e)}$$

5. Inégalité pour les Poids :

$$\frac{dV_2(e_W)}{dt} \leq -e_W^\top \Sigma e_W + l_1 \|e_W\|^2 + l_2 \|e_W\|$$

Ces équations et algorithmes assurent une estimation robuste et précise des états et des poids du système dynamique, tout en améliorant les méthodes précédentes avec une meilleure flexibilité et convergence.

Conclusion

Dans ce chapitre, nous avons abordé le concept des observateurs neuro-adaptatifs, qui intègrent des réseaux neuronaux pour estimer de manière adaptative les états et les dynamiques inconnues des systèmes. Nous avons examiné une méthode existante d'observateurs neuro-adaptatifs appliquée à l'estimation de l'état des véhicules, en soulignant ses points forts et ses limites. Ensuite, nous avons exploré une méthode utilisant des observateurs à apprentissage concurrent, qui améliorent la précision de l'estimation en utilisant les données enregistrées. En nous basant sur ces aperçus, nous avons proposé une approche novatrice combinant les avantages des deux méthodes pour pallier leurs inconvénients respectifs.

Notre méthode proposée est conçue pour être robuste face aux dynamiques non modélisées dans les modèles de véhicules en estimant conjointement les états et les dynamiques inconnues. L'observateur est formulé à l'aide des Inégalités de Matrices Linéaires (LMI) et utilise une technique d'apprentissage concurrent pour mettre à jour itérativement les poids de l'approximateur neuronal. Ce mécanisme de double mise à jour assure une convergence efficace à la fois des estimations d'états et des poids du réseau neuronal.

Les gains de l'observateur sont soigneusement conçus en résolvant la LMI dérivée, garantissant la convergence des états. Une fois les états convergés, les poids de l'approximateur neuronal se révèlent également convergents en pratique. Ce mécanisme de double convergence améliore la fiabilité et la précision de l'observateur, en faisant un outil puissant pour l'estimation de l'état des véhicules en présence de dynamiques non modélisées.

Nous avons ensuite réalisé des simulations sur le modèle longitudinal du véhicule pour démontrer la performance de notre méthode. Les résultats ont été comparés avec une méthode existante d'observateurs neuro-adaptatifs. Notre méthode a montré une performance supérieure, notamment en termes de contraintes de conception et de simulation réduites. Contrairement à d'autres méthodes, notre approche n'impose pas de contraintes strictes sur la fonction d'activation et ne nécessite pas une stratégie d'initialisation spécifique pour les poids. Nous avons prouvé que notre observateur converge en deux échelles temporelles : d'abord les états convergent, suivis par les poids, qui continuent de se mettre à jour même après la convergence des états grâce à l'algorithme d'enregistrement des données.

En résumé, notre observateur proposé offre une solution plus flexible et robuste pour l'estimation de l'état des véhicules, en traitant efficacement les dynamiques non modélisées tout en simplifiant les exigences de conception et d'implémentation.

Chapitre 4

Le concept d'observateur à fort gain (HGO) a été introduit au milieu du XXe siècle pour améliorer l'estimation des états d'un système dynamique avec une grande précision. Les travaux de base sur les observateurs d'état linéaires par Kalman dans les années 1960 [9] ont jeté les bases pour le développement ultérieur des observateurs non linéaires. L'HGO a été spécifiquement développé pour les systèmes nécessitant une convergence rapide des estimations d'état. Dans les années 1980 et 1990, des techniques robustes et adaptatives ont été intégrées pour traiter les incertitudes et non-linéarités [14], [111], [112].

Malgré leur efficacité, les HGO rencontrent des difficultés lorsqu'ils sont appliqués à des systèmes de haute dimension. Le gain de l'observateur est souvent déterminé par des puissances du paramètre d'ajustement (θ), ce qui pose des problèmes de mise en œuvre numérique avec des dimensions d'état élevées ou des paramètres de fort gain nécessaires pour une estimation rapide [115]. De plus, les HGO sont très sensibles au bruit de mesure, ce qui peut rendre les estimations d'état impraticables, surtout dans les systèmes non linéaires avec des constantes de Lipschitz élevées [116].

Des recherches antérieures ont intégré les HGO étendus avec le filtre de Kalman étendu (EKF) pour l'estimation des états [117] et ont proposé diverses méthodes d'adaptation des gains pour gérer les perturbations du système [118], [119]. Les avancées récentes visent à limiter la puissance du gain de l'observateur pour améliorer la performance contre le bruit de mesure [14], bien que des problèmes tels que les difficultés de mise en œuvre

numérique et les phénomènes de pic restent.

Ce chapitre se concentre sur l'analyse des problèmes de mise en œuvre des HGO dans des scénarios avec et sans bruit. Il propose des conceptions d'observateurs convergents qui utilisent des mesures supplémentaires disponibles sans modifier les équations de sortie, préservant ainsi les propriétés théoriques du système non linéaire. Deux méthodes sont proposées : la première prend en compte le bruit de mesure et introduit des conditions LMI régies par un paramètre d'ajustement, garantissant la robustesse et la stabilité en pratique. La seconde méthode combine les sorties du système avec les mesures supplémentaires pour définir une nouvelle forme de système triangulaire, assurant la faisabilité des LMI et fournissant une méthode de conception systématique pour un observateur ISS exponentiel. Les principales sections de ce chapitre sont présentées comme suit :

Résumé de la Section sur l'Observateur à Grand Gain

Cette section donne un aperçu des conditions nécessaires pour la transformation de systèmes non linéaires en formes canoniques d'observabilité, ce qui facilite la conception d'observateurs. Ces formes permettent d'utiliser des techniques de conception d'observateurs bien établies, surtout pour les systèmes non linéaires à entrée unique et sortie unique (SISO). L'extension à des systèmes multi-entrées multi-sorties (MIMO) est plus complexe.

Formes Canoniques d'Observabilité Les formes canoniques d'observabilité simplifient la modélisation des systèmes pour que les observateurs d'état puissent être conçus efficacement. Pour les systèmes non linéaires, le concept d'observabilité uniforme est crucial. Cela assure que l'observabilité des états reste constante au fil du temps, indépendamment des conditions initiales. On considère la forme canonique des systèmes linéaires avec injection de sortie pour faciliter la conception des observateurs [111].

Systèmes Autonomes Pour un système autonome à sortie unique, la transformation en une forme canonique est possible si le système est observable sur un domaine donné. Cette observabilité est caractérisée par la capacité de la sortie et ses dérivées à déterminer l'état initial. Un système est uniformément observable si une carte diffeomorphe transforme le système en une forme canonique [111].

Systèmes Non Autonomes Pour les systèmes non linéaires avec entrée, l'observabilité dépend de la capacité à maintenir l'observabilité avec des entrées universelles. Si le système autonome est uniformément observable et que le système avec entrée est observable pour toutes les entrées possibles, alors le système est uniformément observable pour toute entrée [111].

Conception d'Observateur à Grand Gain Un observateur à grand gain est conçu pour des systèmes non linéaires en forme canonique. Il utilise un paramètre de gain élevé pour garantir que l'erreur d'estimation converge rapidement vers zéro. L'observateur à grand gain est facile à ajuster mais nécessite un paramètre de gain suffisamment élevé pour assurer une convergence rapide, tout en évitant des problèmes de stabilité et d'amplification du bruit [111].

Limitations des Observateurs à Grand Gain

1. Problèmes de Mise en Œuvre

- **Charge Computationnelle** : La charge computationnelle augmente avec la dimension du vecteur d'état, et le réglage des gains est crucial pour éviter l'instabilité et l'amplification du bruit.
- **Réglage des Gains** : La sélection des paramètres de gain θ doit être suffisamment élevée pour assurer une convergence rapide, mais pas trop élevée pour éviter l'instabilité et l'amplification du bruit.
- **Complexité Algorithmique** : Les algorithmes doivent gérer les oscillations et effets transitoires potentiels induits par des gains élevés.

2. Phénomène de Pic

- **Réponse Transitoire** : Avec des gains très élevés, la réponse transitoire peut devenir excessivement grande, entraînant un pic dans l'erreur d'estimation.
- **Impact sur la Stabilité** : Le phénomène de pic peut entraîner une instabilité si l'observateur n'est pas correctement réglé.

3. Sensibilité au Bruit de Mesure

- **Amplification du Bruit** : Les grandes valeurs de la matrice de gain amplifient le bruit de mesure, réduisant ainsi la précision des estimations.
- **Impact sur l'Estimation** : Le bruit amplifié peut causer des écarts importants dans les états estimés, diminuant la précision des estimations.

4. Exigences de Forme Canonique

- **Exigence de Forme Canonique** : Le système doit être exprimé dans une forme canonique spécifique pour appliquer directement un observateur à grand gain.
- **Absence de Mesures ou Contraintes Supplémentaires** : L'observateur ne peut pas tirer parti des mesures ou contraintes supplémentaires au-delà de celles fournies par la forme canonique.

Des efforts ont été faits pour aborder les limitations des observateurs à grand gain. Par exemple, le phénomène de pic a été étudié dans les travaux [115], [116], [123], avec diverses stratégies proposées pour le réduire. La sensibilité au bruit peut être atténuée par des techniques de filtrage, des méthodes d'estimation robuste et des algorithmes de réduction du bruit [121], [128]–[130]. De plus, des méthodes avancées comme les techniques de saturation imbriquées et les observateurs LPV-LMI ont été introduites [121], [127].

Nouvelles méthodologies de conception d'observateurs

Cette partie se concentre sur les méthodologies théoriques de conception d'observateurs pour les systèmes triangulaires avec des mesures de sortie supplémentaires. La première approche est une extension directe de la méthode à gain élevé. En revanche, la seconde approche, qui sert d'alternative, utilise des techniques basées sur les LMI pour traiter certaines des limitations inhérentes à la première méthode.

Première Méthode

- **Condition LMI :**

$$A^\top P + PA - C^\top Y - Y^\top C + \lambda I < 0$$

Cette condition d'inégalité matricielle linéaire (LMI) garantit la stabilité de la conception de l'observateur. Les matrices P et Y sont liées à la fonction de Lyapunov et aux dynamiques du système, respectivement, tandis que λ est une constante positive qui aide à imposer la stabilité.

- **Contraintes sur le Gain :**

$$\theta > \max \left(1, \frac{2k_f \lambda_{\max}(P)}{\alpha \lambda} \right)$$

$$\theta < \left(\frac{(1-\alpha)\lambda}{2k_h \|M\| \lambda_{\max}(P)} \right)^{\frac{1}{n-2}}$$

Ces contraintes sur le paramètre de gain θ assurent que la performance et la robustesse de l'observateur sont maintenues. La première inégalité garantit que θ est suffisamment grand pour répondre aux critères de stabilité, tandis que la seconde veille à ce qu'il ne soit pas excessivement grand, équilibrant performance et robustesse.

- **Dynamiques d'Erreur :**

$$\dot{\hat{e}} = \theta (A - KC) \hat{e} + \frac{1}{\theta} B \Delta f + T^{-1} M \Delta h$$

Cette équation décrit la dynamique de l'erreur d'estimation \hat{e} . Le terme $\theta(A - KC)$ régit comment les erreurs évoluent, avec des termes supplémentaires tenant compte des incertitudes ou des perturbations dans f et h .

- **Dérivée de la Fonction de Lyapunov :**

$$\dot{V}(\hat{e}) \leq (-\theta\lambda + 2k_f \lambda_{\max}(P) + 2\theta^{n-1} k_h \|M\| \lambda_{\max}(P)) \|\hat{e}\|^2$$

Cette inégalité fournit une borne sur la dérivée de la fonction de Lyapunov $V(\hat{e})$, utilisée pour montrer que l'erreur d'estimation \hat{e} diminue avec le temps. Elle garantit que l'erreur converge vers zéro.

- **Condition pour Convergence Exponentielle :**

$$\theta > \frac{2k_f \lambda_{\max}(P)}{\lambda} + \frac{2\theta^{n-1} k_h \|M\| \lambda_{\max}(P)}{\lambda}$$

Cette condition assure la convergence exponentielle de l'erreur d'estimation. Elle définit une borne inférieure pour θ en fonction des paramètres du système et du taux désiré de convergence.

- **Contrainte sur la Matrice M :**

$$\|M\| \leq \frac{(1-\alpha)\lambda}{2k_h \lambda_{\max}(P) \theta^{n-2}}$$

Cette contrainte sur la matrice M garantit que l'amplitude de M est contrôlée, ce qui impacte la robustesse de l'observateur face aux incertitudes du modèle.

Deuxième Méthode

- **Condition LMI pour l'Approche LPV/LMI :**

$$A^\top P + PA - C^\top Y - Y^\top C - \Sigma^\top(\sigma, w)Z - Z^\top \Sigma(\sigma, w) + \lambda I < 0 \quad \forall w \in \mathcal{W}$$

Cette condition LMI est utilisée dans les systèmes linéaires variant en paramètres (LPV) pour garantir la stabilité tout en tenant compte des variations de paramètres. Les termes impliquant $\Sigma(\sigma, w)$ et Z prennent en compte les variations de paramètres et les incertitudes.

- **Contraintes sur le Gain :**

$$\frac{2k_f \lambda_{\max}(P)}{\lambda} < \theta \leq \sigma$$

Ceci fixe la plage pour le paramètre de gain θ dans le contexte LPV/LMI, assurant qu'il est suffisamment grand pour maintenir la stabilité mais pas trop grand pour dégrader la performance.

- **Dynamiques d'Erreur avec LPV/LMI :**

$$\dot{\tilde{e}} = \theta (A - KC - \bar{M}\Sigma(\theta, \Psi)) \tilde{e} + B[f(x) - f(\hat{x})]$$

Cette équation décrit la dynamique de l'erreur \tilde{e} dans un système LPV, incluant les effets des paramètres variables $\Sigma(\theta, \Psi)$ et des incertitudes.

- **Dynamiques d'Erreur Simplifiées :**

$$\dot{\varepsilon} = \theta \left(A + \mathcal{N}\mathcal{A}(\Psi^\theta) - KC \right) \varepsilon + \frac{1}{\theta^n} B \Delta f - K_w$$

Une forme simplifiée des dynamiques d'erreur utilisée pour l'analyse et la conception dans les systèmes LPV, prenant en compte l'influence des variations de paramètres et

des perturbations.

Observer Grand Gain Généralisé avec Bornes ISS

- **Dynamiques de l'Observateur Généralisé :**

$$\dot{\tilde{e}} = (A - LC)\tilde{e} + B[f(x) - f(\hat{x})] - \mathcal{M}[h(x) - h(\hat{x})] - Lw$$

Cela décrit les dynamiques de l'erreur de l'observateur \tilde{e} lorsqu'on utilise des observateurs grand gain. Cela prend en compte les dynamiques du système, les perturbations et le bruit de mesure.

- **Dynamiques d'Erreur Transformées :**

$$\dot{\varepsilon} = \theta(A - KC)\varepsilon + \frac{1}{\theta^n}B\Delta f - \mathcal{N}_\theta\Delta h - Kw$$

Ces dynamiques d'erreur transformées considèrent l'impact du paramètre grand gain θ sur la réponse en erreur du système, avec des termes pour les perturbations et le bruit.

- **Dynamiques d'Erreur Simplifiées Transformées :**

$$\dot{\varepsilon} = \theta\left(A + \mathcal{N}\mathcal{A}(\Psi^\theta) - KC\right)\varepsilon + \frac{1}{\theta^n}B\Delta f - Kw$$

Une version simplifiée des dynamiques d'erreur transformées utilisée pour analyser et concevoir des observateurs grand gain en présence de variations de paramètres et de perturbations.

- **Condition LMI pour le Grand Gain Généralisé :**

$$\begin{bmatrix} \mathcal{H}e\left\{\mathcal{P}A - \mathcal{Y}^\top C + \mathcal{Z}^\top \mathcal{A}(\xi)\right\} + \lambda \mathbb{I}_n & \mathcal{Y}^\top \\ \mathcal{Y} & -\mathcal{X} \end{bmatrix} < 0, \quad \forall \xi \in \mathcal{V}^\sigma$$

Cette condition LMI assure la stabilité dans le contexte des observateurs Grand gain généralisés. Elle prend en compte les variations de paramètres et les incertitudes du système.

- **Condition pour une Borne ISS Exponentielle :**

$$\|\tilde{e}(t)\| \leq \theta^{n-1} \sqrt{\frac{\lambda_{\max}(\mathcal{P})}{\lambda_{\min}(\mathcal{P})}} \|\tilde{e}_0\| e^{-\frac{\kappa}{2}t} + \frac{\theta^{n-\frac{1}{2}}}{\sqrt{\kappa}} \sqrt{\frac{\lambda_{\max}(\mathcal{S})}{\lambda_{\min}(\mathcal{P})}} \sup_{s \in [0,t]} \|w(s)\|$$

Cette borne assure que l'erreur d'estimation décroît de manière exponentielle au fil du temps, en tenant compte de l'erreur initiale, des perturbations et du bruit. Elle établit les conditions pour la stabilité exponentielle et la robustesse.

Extension dynamique basée sur la sortie pour l'observateur High-Gain

Dans cette section, nous proposons une méthode pour concevoir un observateur High-Gain (SHGO) adapté aux systèmes non linéaires avec des sorties supplémentaires non triangulaires. Cette méthode repose sur une transformation dynamique du système pour intégrer ces sorties dans l'observateur, permettant ainsi de surmonter les limitations de la méthode SHGO classique.

Méthode proposée

1. **Transformation du Système :** Nous introduisons une nouvelle sortie y_{new} , combinant les sorties initiales y et z , et transformons le système en une forme adaptée pour l'application de l'observateur.
2. **Conception de l'Observateur :** Nous définissons un observateur d'état pour estimer l'état \hat{x} du système transformé. L'objectif est de faire converger l'erreur d'estimation $\tilde{\xi}$ vers zéro en ajustant les paramètres α , β , θ , et la matrice K .
3. **Analyse de l'Erreur :** Nous dérivons les dynamiques de l'erreur d'estimation et montrons que, sous certaines conditions, les termes non linéaires peuvent être rendus négligeables en augmentant θ , garantissant ainsi la convergence de l'estimation.

Contributions

- Cette méthode étend l'application de SHGO à des systèmes avec des sorties non linéaires.
- Elle permet d'intégrer des sorties supplémentaires dans la conception de l'observateur, améliorant ainsi la précision de l'estimation.

Conclusion

Dans ce chapitre, nous avons exploré en détail la théorie des observateurs Grand Gain et ses applications. Nous avons commencé par une présentation approfondie de l'observateur Grand Gain, en exposant ses principes fondamentaux et sa théorie sous-jacente. Nous avons également mis en évidence les limites intrinsèques de cet observateur, notamment lorsqu'il est appliqué à des systèmes où les mesures supplémentaires ne peuvent pas être efficacement utilisées.

Conscients de ces limites, nous avons introduit une nouvelle méthodologie visant à intégrer des mesures ou contraintes supplémentaires dans le système. Cette approche novatrice permet d'incorporer des données supplémentaires que le cadre traditionnel des observateurs Grand Gain ne pouvait pas gérer. Nous avons fourni des preuves rigoureuses de la convergence de cet observateur amélioré, démontrant son efficacité à l'aide d'une borne de Stabilité d'Entrée à État (ISS). Nos preuves ont combiné les méthodologies des observateurs Grand Gain et LPV/LMI.

De plus, nous avons étendu notre discussion aux formes de systèmes plus complexes et aux sorties non linéaires. En augmentant les états du système avec une sortie étendue, nous avons proposé une stratégie plus générale pour gérer diverses configurations de systèmes. Cette approche élargit non seulement l'applicabilité de notre conception d'observateur, mais améliore également sa robustesse au bruit de mesure, assurant une performance fiable dans des scénarios pratiques.

En somme, ce chapitre a établi un cadre complet pour la conception et l'implémentation des observateurs Grand Gain, en abordant à la fois les défis traditionnels et les nouvelles opportunités pour intégrer des mesures supplémentaires. Nos contributions offrent une base solide pour des recherches futures et des applications pratiques, faisant avancer l'état de l'art dans la conception d'observateurs pour des systèmes complexes.

Chapitre 5

Le suivi précis et robuste des dynamiques des véhicules joue un rôle crucial dans diverses technologies automobiles, allant des systèmes d'assistance au conducteur à la conduite autonome [15], [16]. Cependant, atteindre un suivi précis et fiable des véhicules pose de nombreux défis nécessitant des solutions sophistiquées. Les systèmes de véhicules sont intrinsèquement complexes et non linéaires, avec des dynamiques influencées par des facteurs externes tels que le bruit des capteurs, les pannes d'actionneurs et les perturbations environnementales. Ces incertitudes peuvent perturber considérablement l'exactitude du suivi, rendant difficile la prédiction et la reconstruction de l'état réel du véhicule. Bien que les capteurs fournissent des mesures précieuses [15], ils offrent intrinsèquement des informations incomplètes sur l'état du véhicule. Les limitations des capteurs, telles que le bruit, les délais et les contraintes de bande passante, aggravent encore le défi de obtenir une image précise du comportement du véhicule.

Les méthodes de suivi traditionnelles reposent souvent sur des modèles linéaires, malgré la nature intrinsèquement non linéaire du mouvement des véhicules. Les approches précédentes ont tenté de traiter cette complexité par une linéarisation par morceaux, introduisant des modèles séparés pour des manœuvres spécifiques [17]. Ces méthodes utilisaient généralement des filtres à modèles multiples interactifs (IMM), tels que les filtres Kalman IMM [18], [133], pour l'estimation d'état. Cependant, les méthodes basées sur la linéarisation présentent plusieurs limitations :

- **Absence de Preuves de Stabilité** : Ces méthodes manquent souvent de garanties formelles de stabilité, suscitant des préoccupations quant à leur performance dans des conditions de conduite réelles.
- **Couverture Limitée des Manœuvres** : Les modèles linéaires choisis peuvent ne pas couvrir l'ensemble des manœuvres possibles du véhicule, ce qui peut entraîner un suivi inexact lors de mouvements plus complexes.

- **Exigences Computationnelles :** L'implémentation des filtres IMM peut être coûteuse en termes de calcul, nécessitant une évaluation en temps réel des probabilités associées à chaque modèle individuel, ce qui peut solliciter les ressources des systèmes embarqués.

Il est donc crucial d'explorer des approches alternatives capables de gérer efficacement les non-linéarités inhérentes au mouvement des véhicules sans sacrifier la stabilité, la maniabilité ou l'efficacité computationnelle.

Notre approche commence par le suivi du mouvement longitudinal d'autres véhicules. Initialement, des simulations Matlab ont été utilisées pour valider l'efficacité de notre algorithme développé au Chapitre 4 dans un environnement contrôlé. Par la suite, le scénario a été reproduit dans le simulateur CARLA, offrant un terrain d'essai plus dynamique et réaliste. La performance cohérente dans les deux environnements a démontré la robustesse de notre algorithme de conception à grand gain.

De plus, nous avons étendu l'application de notre algorithme pour estimer le mouvement du véhicule en utilisant un modèle cinématique. Cette phase a impliqué des tests Matlab, qui ont ensuite été validés à l'aide du jeu de données KITTI, une collection complète de données de conduite réelles. Ces étapes ont été cruciales pour évaluer la viabilité pratique et la précision de l'algorithme. Dans certains scénarios, nous avons comparé notre algorithme au Filtre de Kalman Étendu (EKF) et avons démontré que nos algorithmes (Chapitre 4) peuvent offrir de meilleures performances, notamment en cas de perte de données.

Ce chapitre s'appuie sur les discussions précédentes concernant l'observateur à grand gain et les modèles de véhicules. Les principales sections de ce chapitre sont présentées comme suit :

Suivi Longitudinal des Véhicules

La section sur le suivi longitudinal des véhicules est cruciale pour le développement des systèmes d'assistance à la conduite avancés (ADAS) et des technologies de conduite autonome. Elle traite de la surveillance et du contrôle de la vitesse du véhicule et de sa distance par rapport aux autres véhicules sur la même voie pour garantir une conduite sûre et efficace. Le suivi longitudinal est essentiel pour des tâches comme le régulateur de vitesse adaptatif et l'évitement des collisions.

Cette section explore l'application de la conception à fort gain pour le suivi longitudinal, avec des simulations MATLAB pour valider l'approche avant de passer à des scénarios plus dynamiques dans le simulateur CARLA. Le modèle dynamique longitudinal du véhicule est présenté, utilisant la loi de Newton pour établir les équations du système. La section détaille également les résultats des simulations MATLAB, comparant les performances des observateurs à fort gain standard avec ceux utilisant des mesures supplémentaires de vitesse. Les résultats des simulations montrent que l'utilisation de la mesure de vitesse améliore la précision des estimations d'état du véhicule, en particulier pour l'accélération. En outre, les

scénarios de simulation basés sur CARLA confirment que la méthode proposée est efficace pour suivre les états du véhicule dans des conditions réalistes, même en présence de bruit et de défaillances de capteurs. La comparaison avec l'observateur à fort gain standard met en évidence une meilleure performance en termes de vitesse de convergence, précision et rejet du bruit lorsque la mesure de vitesse est utilisée.

Estimation de Trajectoire du Véhicule

Cette section traite de l'estimation du mouvement du véhicule en utilisant un modèle cinématique triangulaire. Le modèle cinématique du véhicule est présenté avec des équations qui relient les positions et les angles aux vitesses et aux angles de braquage. Le modèle est simplifié pour des manœuvres douces et un rayon de courbure plus grand que la longueur du véhicule. La transformation non linéaire est appliquée au modèle pour le rendre plus adapté à l'utilisation d'un observateur à fort gain, permettant ainsi une estimation précise de la trajectoire du véhicule malgré les bruits de mesure.

Un observateur à fort gain est conçu en transformant le modèle en une forme triangulaire, ce qui permet de résoudre des inégalités matricielles linéaires (LMI) pour déterminer les gains de l'observateur. Les performances de l'observateur sont validées à l'aide de simulations avec différentes conditions de conduite (droite ou virage à gauche) et avec des données du dataset KITTI pour évaluer l'exactitude de l'estimation du mouvement du véhicule.

Les résultats expérimentaux montrent que l'observateur propose des estimations précises même en cas de perte de données. En comparaison avec un filtre de Kalman étendu (EKF), l'observateur à fort gain converge plus rapidement et est plus robuste face aux lacunes de données, bien que l'EKF puisse parfois offrir des estimations plus précises de l'angle de lacet dans certains cas. La fusion de capteurs avec EKF est également explorée pour améliorer la performance en utilisant des mesures supplémentaires comme le taux de lacet.

Conclusion

Dans ce chapitre, nous avons évalué de manière approfondie notre observateur à fort gain en utilisant des simulations et des données réelles du dataset KITTI. Les résultats montrent la robustesse et la précision de notre observateur dans les tâches de localisation du véhicule, même en présence de lacunes importantes dans les données et de bruit.

Les expériences réalisées avec le dataset KITTI ont démontré que l'observateur à fort gain estime efficacement les états du véhicule, y compris la position, la vitesse et l'angle de lacet, avec une grande précision. Sa performance a été particulièrement remarquable dans des scénarios impliquant des vitesses variables et des trajectoires complexes, en maintenant précision et vitesse de convergence même avec jusqu'à 40% de perte de données. Nos résultats ont montré que notre observateur surpassait le Filtre de Kalman Étendu (EKF) traditionnel en termes de taux de convergence et de précision d'estimation globale,

notamment pour l'estimation de la position. Toutefois, bien que la stabilité de l'observateur soit assurée, la méthode proposée rencontre des difficultés avec le bruit de mesure, ce qui entraîne des estimations bruitées.

Nous avons également exploré les avantages d'incorporer des mesures supplémentaires telles que le taux de lacet, soulignant l'adaptabilité de l'observateur et sa performance améliorée dans les applications de fusion de capteurs. Les gains de l'observateur ont été ajustés pour donner la priorité à ces mesures supplémentaires, améliorant ainsi l'estimation des états dans des conditions bruyantes.

Dans l'ensemble, nos résultats valident l'efficacité et la résilience de l'observateur à fort gain, suggérant son potentiel pour des applications réelles dans la navigation des véhicules autonomes et d'autres systèmes dynamiques nécessitant une estimation précise des états.